Influence of Climatic Factors on Water and Heat Transfer Within Subgrades

Kerwin G. Modeste

A Dissertation Submitted to
The Faculty of Graduate Studies
In Partial Fulfillment of the Requirements
for the Degree of Doctor of Philosophy

Graduate Program in Civil Engineering
York University
Toronto, Ontario

July 2023

Abstract

The Enhanced Integrated Climate Model (EICM) is incorporated into the Mechanistic Empirical Pavement Design Guide (MEPDG) to account for the influence of the environment and climate on water contents, and resilient modulus (M_R) of each unbound material. EICM consists of four model components including the Precipitation (Precp) model, Infiltration and Drainage (ID) model, Cold Region Research Engineering Laboratory (CRREL) frost heave and thaw settlement model and Climate Material Structural (CMS) model. The primary EICM output is the depth and time dependent composite environmental adjustment factor (F_{env}) which accounts for the influence of the environment on the resilient modulus. F_{env} consists of an adjustment factor for the frozen condition (F_F), thaw recovery condition (F_R), and unfrozen condition (F_U) which are influenced by volumetric water contents within the unbound materials. F_{env} is multiplied by the optimum resilient modulus (M_{Ropt}) (at optimum water content, maximum dry density and the stress state) to obtain the resilient modulus of the subgrade at a specific volumetric water content.

There are limitations in the climatic boundary conditions in EICM. EICM neglects the impact of land climate interaction (LCI) on the water and heat transfer within subgrades. EICM accounts only for infiltration through cracks on the pavement surface and neglects the influence of evapotranspiration on water and heat transfer. EICM accounts only for liquid water transfer and neglects water vapour transfer. These limitations in EICM result in inaccuracies in predicting in-situ volumetric water contents due to inaccuracies in predicting in-situ suction and in-situ soil water characteristic curve (SWCC). EICM assumes a constant and uniform subgrade temperature and neglects the influence of climatic factors on fluctuations in water and heat transfer. EICM accounts for water transfer influence by the depth of shallow groundwater table but neglects the influence of the water table at significant depths. These limitations in EICM result in inaccuracies in predicting in-situ volumetric water contents and in-situ resilient moduli of subgrades that forms the basis for the pavement mechanistic response. The inaccuracies in predicting the water and heat transfer and in-situ resilient modulus of each unbound material result in inaccuracies in predicting the pavement distress. Hence, these limitations in EICM result in inaccurate prediction of the pavement performance, service life, and implementing uneconomical pavement structures.

The objective is to investigate the impact of precipitation, air temperature, net solar radiation, relative humidity, wind speed, and evapotranspiration (climatic factors) on volumetric water contents within subgrades. The investigation focuses on the impact of LCI on water and heat transfer which is achieved through the development of a Quantitative Empirical Model (QE Model). The QE Model represents a LCI surface boundary condition to account for the impact of climatic factors on in-situ volumetric water contents within subgrades. It is intended that the QE Model would be incorporated into

EICM for improving EICM and MEPDG to account for the impact of climatic factors on in-situ volumetric water contents and resilient moduli of subgrades.

The methodology included one-dimensional (1-D) and two-dimensional (2-D) water and heat transfer finite element analyses (FEA) modeling using two rigid pavements in a wet freeze climate. Nonlinear regression analyses were conducted using climatic factors, in-situ volumetric water contents and 2-D FEA volumetric water contents output to develop correlation functions. Mathematical computations were used to incorporate liquid water and water vapour properties, initial degree of saturation, hydraulic properties of subgrades and wearing courses, and integration to develop the QE Model. The accuracy of the QE Model and EICM were evaluated by comparing the output of the models to in-situ volumetric water contents, F_{env} and M_R using four independent pavement section in wet freeze and wet no-freeze climates. The QE Model is incorporated into EICM by incorporating the QE Model into the F_{env} to develop the modified composite environmental adjustment factor (the F_{envCF} model). The modified M_R (M_{RCF}) model was also developed by using the product of the M_{ROpt} and F_{envCF} values.

The water and heat transfer within subgrades is influenced by transient water transfer, saturated/unsaturated conditions, heat conduction and forced convection with water transfer. The influence of these processes on water and heat transfer was evident in continual fluctuations in the water transfer in response to climatic factors. Continual fluctuations in volumetric water contents indicate that climatic factors influence water and heat transfer within subgrades with hysteresis. The QE Model accounts for the influence of climatic factors on water and heat transfer within subgrades. The QE Model accurately predicts the influence of climatic factors on fluctuations in volumetric water contents within subgrades in wet freeze and wet no-freeze climates. The QE Model also has a higher accuracy than EICM in predicting in-situ water and heat transfer within subgrades. The volumetric water contents predicted using the QE Model is more suitable for calculating in-situ M_R of subgrades than volumetric water contents predicted using EICM.

The QE Model represents an in-situ SWCC which accounts for the impact of climatic factors on volumetric water contents within subgrades. The QE Model mitigates the primary limitations in EICM by incorporating the impact of climatic factors and LCI on water and heat transfer within subgrades which are neglected by EICM. The QE Model accounts for liquid water and water vapour transfer. But EICM accounts only for liquid water and neglects water vapour transfer. Unlike EICM, the QE Model accurately predicts in-situ volumetric water contents without site-specific calibration. The F_{envCF} and M_{RCF} models developed as part of this study, account for the impact of climatic factors on volumetric water contents and resilient moduli of subgrades. Incorporating the QE Model into EICM and MEPDG facilitates the design and construction of economical pavement structures. A model was also proposed for predicting the site-specific net evapotranspiration (the Net ET) which applies the Penman-Monteith method to predict changes in Net ET as a nonlinear function of changes in climatic factors {Net ET (ΔA)}.

Table of Contents

List of Figures

List of Tables

List of Notations

Acronym	Definition
AASHTO	The American Association of State Highway and Transportation Officials
ACHM	Asphalt concrete hot mix
AC wearing course	Asphalt concrete wearing course
AEV	Air entry value
BC	Boundary condition
CI	Intermediate plasticity Clay
CL	Low plasticity Clay
CMS model	Climate Material Structural model
CRREL model	Cold Region Research and Engineering Laboratory model
D_{60}	Effective grain size
1-D	One-dimensional
2-D	Two-dimensional
3-D	Three-dimensional
EICM	Enhanced Integrated Climate Model
$\theta_{tn} = \theta_{CF}$	Volumetric water content predicted using the quantitative empirical model which accounts for climatic factors
F_{envCF}	F_{envCF} = Modified unfrozen composite environmental adjustment factor for the material layer under consideration which accounts for climatic factors
F_{env}	Composite environmental adjustment factor
F_F	Frozen environmental adjustment factor
F_R	Thaw recovery environmental adjustment factor
F_u	Unfrozen environmental adjustment factor
F_{uCF}	F_{UCF} = Modified unfrozen environmental adjustment factor (accounts for climatic factors)
f-function	Function incorporating the system dependent properties of the subgrades
FEA	Finite element analysis
FHWA	Federal Highway Administration
FWD.	Falling Weight Deflectors
GC	Ground cover
GIS	Geographic information system
HCC	Hydraulic cement concrete
HD material	Heavy Duty binder course
ICM	Integrated climate model
ID model	Infiltration and Drainage model
IPCC	Intergovernmental Panel on Climate Change
IRI	International roughness index
LAI	Leaf area index
LCI	Land climate interaction
LTPP	Long Term Pavement Performance
MEPDG	Mechanistic Empirical Pavement Design Guide
M_{RCF}	M_{RCF} = Modified resilient modulus (depth and time specific: accounts for climatic factors)
M_R	Resilient modulus
M_{ROPT}	Resilient modulus at optimum water content
MTO	Ministry of Transportation Ontario
NCHRP	National Cooperative Highway Research Program

Acronym	Definition
OGDL	Open graded drainage layer
P_{200}	Percent passing No. 200 sieve
PLCA	Pavement life cycle assessment
PLCCA	Pavement life cycle cost assessment
Precp	Precipitation
PCC wearing course	Portland cement concrete wearing course
PI	Plasticity Index
P_1, P_2, P_3	Nonlinear regression parameters
R-value	Pearson correlation coefficient
RMSE	Root mean square error
S_{CF}	Degree of saturation calculated using the volumetric water content predicted using the quantitative empirical model which accounts for climatic factors
SEEP/W	Seepage analysis finite element analysis program
SMP	Seasonal Monitoring Program
SM	silty Sand
SP materials	Superior Performing Asphalt Pavements (Superpave) materials
SP FC	Superpave Friction course
SPMDD	Standard proctor maximum dry density
SWCC	Soil water characteristic curve
SPR site	Pack River site
TEMP/W	Heat transfer finite element analysis program
TDR	Time domain reflectometers
TMI	Thornthwaite Moisture Index

List of Symbols

Equation No.	Symbol	Unit	Definition
Eq. 2.1 and Eq. 2.3	θ_w	Unitless	Volumetric water content
	θ_s	Unitless	Saturated volumetric water content
	ψ	kPa	Soil matric suction
	a	kPa	Soil parameter related to air-entry value of soil;
	n	Unitless	Soil parameter related to slope at inflection point on SWCC
	m	Unitless	Soil parameter related to residual water content of soil
	C_r	kPa	Parameter related to the residual matric suction.
	e	Unitless	Base for natural logarithm (2.71828)
Eq. 2.4	q_P	mm / day	Rainfall
	q_M	mm / day	Snowmelt
	α	Degrees	Angle for converting q_p and q_m to a normal to interface
	q_E	mm / day	Evaporation
	q_R	mm / day	Runoff
	q_I	mm / day	infiltration
Eq. 2.5 to Eq. 2.7	q_{PET}	mm / day	Potential evapotranspiration
	h_{fg}	MJ / kg	Latent heat of vaporization
	q_n	MJ / (m^2 day)	Net radiation
	q_g	MJ / (m^2 day)	Ground heat flux
	ρ_a	kg / m^3	Mean air density in the atmosphere
	C_{sa}	MJ / (kg ^oC)	Specific heat of moist air
	P^a_{v0}	kPa	Saturated vapour pressure at mean air temperature
	p^a_v	kPa	Actual vapour pressure of air at referenced height
	r_c	S / m	Crop canopy bulk surface resistance
	r_a	S / m	Aerodynamic resistance
	γ	kPa / ^oC	Psychrometric constant
	Γ	kPa / ^oC	Slope of saturation vapour pressure vs. temperature curve
	u	m / s	Wind speed
	k	Unitless	von Karman’s constant
	Z_{ref}	m	Measured height of wind, humidity, and temperature
	d	m	Zero-plane displacement height of wind profile
	Z_{om}	m	Surface roughness height for momentum flux
	Z_{oh}	m	Surface roughness height for heat and vapour flux
	Z_c	m	Crop height
	r_l	m / s	Bulk stomatal resistance of well-illuminated leaf
Eq. 3.1 to Eq. 3.4	$M_{r\text{-}OPT}$	MPa	Resilient modulus at optimum water content
	M_R	MPa	Resilient modulus at a specific water content
	θ_b	MPa	Bulk stress
	τ_{oct}	MPa	Octahedral shear stress
	p_a	MPa	Atmospheric pressure
	k_1, k_2, and k_3	Unitless	Fitting parameters
	S_{op}	Decimals	Degree of saturation at optimum water content
	S	In decimals	Degree of saturation at a specific water content
	a	Unitless	Minimum of log $\{M_R / M_{R\text{-}opt}\}$
	b	Unitless	Maximum of log $\{M_R / M_{R\text{-}opt}\}$

Equation No.	Symbol	Unit	Definition
	k_m	Unitless	Regression parameter
	h	kPa	Matric suction model for subgrades
	α, β, γ, δ	Unitless	Regression constants associate
	TMI	Unitless	Modified Thornthwaite Moisture Index
	w	Decimal	Decimal form of P_{200}
	P	cm	Annual precipitation
	PE	cm	Potential evapotranspiration
Eq. 5.1	ΔA	MJ ^oC / (s^2 day)	The change in the climatic factors
	ΔT_{Air}	^oC	The change in air temperature
	ΔR_s	MJ / (s m^2)	The change in net solar radiation
	ΔRH	Decimal	The change in relative humidity
	V_w	m / s	The change in wind speed
	$\Delta Precp$	m / day	The change in precipitation
	ΔET	m^3 / (day m^2)	The change in evapotranspiration
	ΔE_{wa}	m^3 / (day $m^{2)}$)	The change in evaporation through surface to atmosphere
Eq. 5.2 to Eq. 5.4	$\Delta\theta$ (ΔA)	Unitless	The change in volumetric water content due to change ΔA
	ΔA	MJ ^oC / (s^2 day)	The change in the climatic factors
	e	Unitless	The exponential constant with a value of 2.71828
	π	Unitless	The mathematical constant pi with a value of 3.14159
	P_1, P_2, P_3,	Unitless	Nonlinear regression parameters
	P_a, P_b, P_c	Unitless	Nonlinear regression parameters
	P_{r1}, P_{r2}, P_{r3}	Unitless	Nonlinear regression parameters
Eq. 5.5	RMSE	Unitless	Root mean square error
	S	Unitless	Predicted values
	O	Unitless	Observed values
	n	Unitless	Number of observed values
Eq. 6.1 to Eq. 6.28	θ_{th}	Unitless	The total volumetric water content at the end of time "n"
	θ_{to}	Unitless	The initial volumetric water content at end of construction
	$\Delta\theta_{th}$	Unitless	Sum of changes in volumetric water content at time "n"
	ΔA	MJ ^oC / (s^2 day)	The change in climatic factors
	X_1	Unitless	System dependent property which form part of f-functions
	X_2	day s^2 / (MJ ^oC)	System dependent property which form part of f-functions
	X_3	Unitless	System dependent property which form part of f-functions
	Cp	MJ / (kg ^oC)	Specific heat capacity of liquid water at 25.0 ^oC
	$\Delta Hvap$	MJ / kg	Heat of vaporization of liquid water
	ρ_w	kg / m^3	Density of liquid water at 25.0 ^oC
	g	m / s^2	Gravitational acceleration
	P_v	Kg / m^2	Vapour pressure of water (equilibrium vapour pressure
	α_w	m^2 / day	Thermal diffusivity of liquid water at 25.0 ^oC
	ρ_v	Kg / m^3	Density of water vapour at 20.0 ^oC
	α_v	m^2 / day	Thermal diffusivity of water vapour at 1.0 atm and 100.0 ^oC
	D_{swt}	m	Depth from subgrade surface to static water table
	k_{sat}	m / s	Saturated hydraulic conductivity of subgrade
	k_{res}	m / s	Residual hydraulic conductivity of subgrade
	θ_{sat}	Unitless	Saturated volumetric water content within subgrades
	θ_{res}	Unitless	Residual volumetric water content within subgrades

Equation No.	Symbol	Unit	Definition
	t	day	Time
	t	day	The total time ⇒ $t_i + t_{lag}$
	t_i	day	Any time "t"
	t_{lag}	day	The lag time
	f_1	Unitless	Function parameter
	f_2	day s^2 / (MJ ^oC)	Function parameter
	f_3	Unitless	Function parameter
	e	Unitless	The exponential constant with a value of 2.71828

Chapter 1 Introduction

1.1 Introduction

Chapter 1 provides an overview of the primary strengths of the Mechanistic Empirical Pavement Design Guide (MEPDG) and Enhanced Integrated Climate Model (EICM) in predicting the in-situ water and heat transfer, and performance of pavement structures. Chapter 1 also provides background details on the MEPDG including the pertinent features of the current version of MEPDG and EICM. The Chapter provides an overview of the Long-term Pavement Performance (LTPP) program and the Seasonal Monitoring Program (SMP) implemented to support the development and the local calibration of MEPDG.

Chapter 1 provides details of the problems caused by the limitations in EICM in predicting the in-situ water and heat transfer within subgrades. The Chapter provides details of the significance of the research and contribution made by the research to the engineering practice. The Chapter also provides details of the research objectives and research hypothesis. Chapter 1 concludes by providing an overview of the research methodology, analyses and results, by providing a list of research deliverables and by providing a summary of the organization of the dissertation.

1.2 Background on MEPDG

This section provides an overview of the primary strengths, pertinent features and framework of EICM and MEPDG. The overview of MEPDG is provided in this section to highlight the significant contribution EICM and MEPDG make to the design and implementation of pavement structures. This section also provides a summary of the primary limitations in EICM and MEPDG in predicting the in-situ water and heat transfer which cause long-term reduction in the pavement performance. These limitations are also used for developing the problem statement.

1.2.1 Overview of the Primary Strengths of EICM and MEPDG

The Mechanistic Empirical Pavement Design Guide (MEPDG) was developed through the National Cooperative Highway Research Program (NCHRP) to facilitate an improved and detailed process for the design and analysis of new and rehabilitated pavement structures. The MEPDG was developed to replace the American Association of State Highway and Transportation Official (ASSHTO) 1993 Guide for the design of pavement structures (Applied Research Associates Inc., 2004; AASHTO 2020).

The development and local calibration of MEPDG were supported by the Long-term Pavement Performance (LTPP) and Seasonal Monitoring Program (SMP) implemented over a 2-year period from 1984 using over 800 in-service pavement sections in the United States of America and Canada. The LTPP program was implemented using various pavement materials, geological conditions, traffic loading, climates, and environments (Kim, et al. 2011; AASHTO 2010). The LTPP and SMP are intended to investigate the long-term performance of various pavement structure design and rehabilitation options to improve the pavement life and performance (LTPP, and SMP database 2020; AASHTO 2010).

The MEPDG provides an innovative and iterative approach for designing and evaluating the performance of pavement structures. The primary design features of the MEPDG include incorporating climatic factors and traffic loading in the characterization of materials, pavement design and performance. MEPDG uses input data which include pavement materials properties, traffic and climatic data (AASHTO 2020 and 2010; Applied Research Associates Inc. 2004). The MEPDG also accounts for the influence of the pavement structure on the performance of rigid, flexible and composite pavements. The MEPDG incorporates the mechanical analysis to predict the stress, strain and deflection within pavement structures (the pavement response). MEPDG also incorporates the empirical analysis to predict the pavement distress which is used to evaluate the pavement life cycle and the associated life cycle cost analysis (AASHTO 2020 and 2008).

1.2.2 Overview of the Pertinent Features and Framework of EICM and MEPDG

The MEPDG incorporates the principles of engineering mechanics based on an integrated analyses approach to predict the time dependent pavement conditions including fatigue, rutting, and thermal cracking in flexible pavements (AASHTO 2020 and 2008). The rutting occurs under the wheel paths and is associated with stress induced permanent deformation of flexible pavement subgrades and/or the asphalt concrete wearing course under traffic loading. The rutting is directly influenced by the resilient modulus of each material layer, particularly by the resilient modulus of the subgrade. The rutting results in reduced pavement reliability and causes traffic safety problems associated with hydroplaning due to ponding within ruts during rainfall events (Kim, et al. 2011). The MEPDG is also used to predict cracking and faulting in rigid pavements and to facilitate the evaluation of design alternatives, reliability, and the implementation of cost-effective pavement designs. Transverse cracking is the primary distress in rigid pavements and is due to weak subgrades subjected to heavy traffic loading which result in differential settlement (Mu, et al. 2012; Perera, and Kohn 2001). The MEPDG also evaluates other distress within pavement structures such as the international roughness index (IRI). The IRI is measured along longitudinal profiles of pavement structures to characterize the extent of the smoothness of pavement surfaces. The IRI also characterizes the quality of the ride users experience while traveling in vehicles. The IRI is influenced by the traffic loading, the thickness of each pavement material layer, subgrade type and performance, environment conditions and climatic factors. The IRI also has a direct impact on the user costs and maintenance costs of pavement structures (Mu, et al. 2012; Perera, and Kohn 2001, TAC 1997). A flow chart showing the various processes in the MEPDG is shown in Figure 1.1.

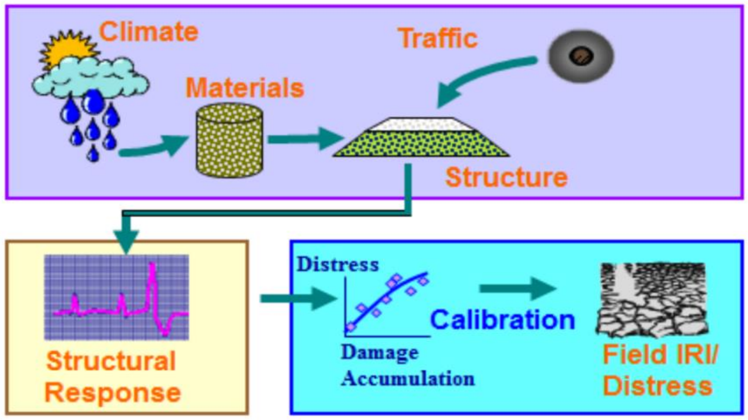

Figure 1.1: The flow chart of the MEPDG process (Goldbaum 2022)

The three stages which are used in MEPDG to implement the analysis and design of pavement structures are shown in Figure 1.2. Stage One supports the evaluation of data input, trial design strategies and foundation analysis. The trial pavement design cross section is used for predicting the pavement response due to the influence of climatic factors and traffic loading. Stage One also facilitates the evaluation of various options for data input depending on the project complexity and resources available for sourcing input data. The options which are used for sourcing input data include Level One input data obtained from laboratory and in-situ testing. Level One input data provide the highest level of accuracy and are used for the design of pavement structures subjected to heavy traffic loading. Level Two input data are typically obtained from limited laboratory and in-situ testing or they are estimated using empirical correlations. Level Two input data provide an intermediate level of accuracy. Level Three input data are based on average parameters for similar regional materials and conditions. Level Three input data also provide the lowest level of accuracy and are used for the design of pavement structures where the consequence of early failure is minimal. Level Three input data are available as the default values in MEPDG. Stage Two is used to implement the analysis stage which incorporates the trial design cross section. The trial design cross section is analyzed incrementally using a pavement response and distress prediction model. The pavement response is used to predict the accumulated damage which is then related to the pavement distress and smoothness over time. The efficacy of the trial design cross section is evaluated by comparing the distress and smoothness output of the trial design cross section to limiting design criteria using sensitivity analyses. The sensitivity analyses are conducted until an acceptable design cross section is achieved. Stage Three is used for implementing the selection strategy which is used for evaluating design alternatives based on limiting engineering, constructability and life cycle cost analysis criteria (AASHTO, 2020 and 2008; Li, et al. 2011).

The MEPDG accounts for the influence of the climate and environment by incorporating the Enhanced Integrated Climate Model (EICM). EICM consists of four model components which include the Precipitation (Precp) model, Infiltration and Drainage (ID) model, Climate Material Structural (CMS) model, and Cold Region Research and Engineering Laboratory (CRREL) frost heave and thaw settlement model (Bulut, and Javid 2019; Bulut, et al. 2014; Li, et al. 2011; McCartney, et al. 2010).

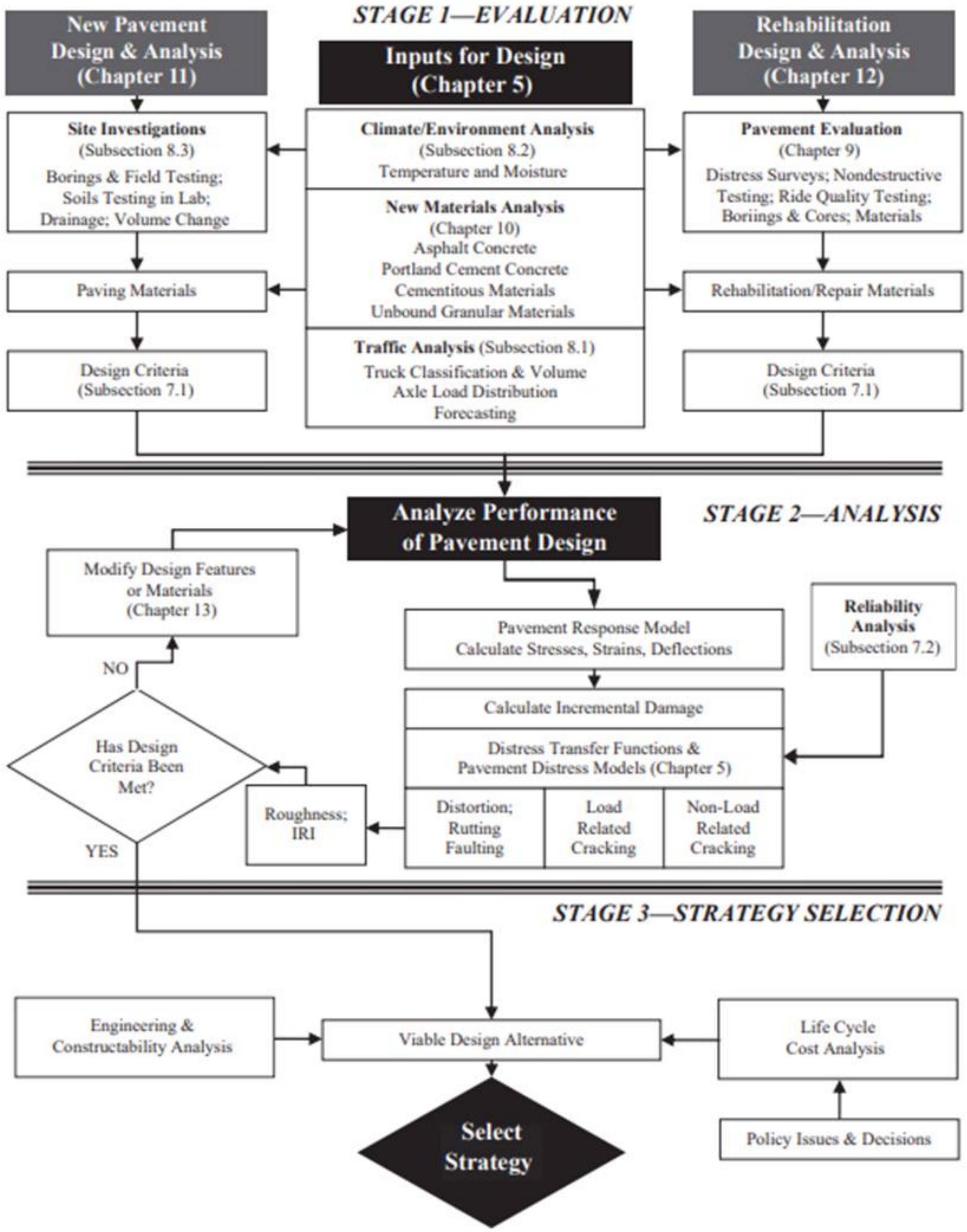

Figure 1.2: Flowchart for three-stage design process of MEPDG (AASHTO 2020)

1.2.3 Primary Limitations in EICM in Predicting Pavement Performance

This section provides details of the limitations in EICM in predicting the in-situ water contents and the impact on the inaccurate prediction of resilient moduli of subgrades. The limitations in EICM are provided to highlight the cause of the problems associated with EICM and MEPDG which form the basis of the problem statement.

Although MEPDG has useful features for evaluating and designing pavement structures, most of these features require improving particularly the water contents and the distress prediction models (Hall, et al. 2013; McCartney, et al. 2010). The current version of EICM predicts the convective cooling poorly during high air temperature which contributes to EICM predicting water contents poorly (Bryce, et al. 2021).

The water contents prediction model used in EICM has inaccuracies in predicting the in-situ water and heat transfer. EICM predicting water and heat transfer poorly results in the inaccurate prediction of the resilient modulus because EICM inaccurately accounts for the impact of climatic factors. The inaccuracies in predicting resilient moduli of unbound materials also contribute to the inaccurate prediction of the pavement distress (Bulut, and Javid 2019; Bulut, et al. 2014; Hall, et al. 2013; Bulut, et al. 2013; McCartney, et al. 2010). The MEPDG also neglects the site specific design and construction specifications and maintenance strategies. The MEPDG requires site specific calibration and validation to produce acceptable distress prediction limits. The MEPDG should be improved to facilitate implementing more economical pavement design and construction (Yuan, and Nemtsov 2017 and 2018; Hall, et al. 2013; Qin, and Hiller 2013; Kim, et al. 2011; Houston, et al. 2006; Bayomy, and Salem 2005; Ahmed, et al. 2005).

The MEPDG has limitations in predicting longitudinal cracking, alligator cracking, thermal cracking, International Roughness Index (IRI) and rutting (flexible pavement distress). The MEPDG also has limitations in predicting faulting, cracking and IRI (rigid pavement distress). The MEPDG distress prediction models were initially calibrated using national averages of material input data which lead to the use of global calibration factors. The global calibration factors are not suitable for local application due to variation in climatic factors and pavement materials properties. Variations in climatic factors and pavement materials properties result in MEPDG inaccurately predicting pavement distress (Mu, et al. 2012; Perera, and Kohn 2001; Kim, et al. 2011; Li, et al. 2011; AASHTO 2010). The use of global calibration factors in the current version of MEPDG distress prediction model result in inaccuracies in predicting the site-specific pavement distress. The distress prediction models in MEPDG should be re-calibrated locally to account for local material properties, construction methods, environmental conditions, and for improving the distress prediction (Yuan, and Nemtsov 2017; Huang, et al. 2016; Yut, et al. 2014; Kim, et al. 2011).

The alligator cracking and rutting are the primary distress which impact the performance of flexible pavement structure. The alligator cracking is primarily due to inadequate thickness of the asphalt concrete (AC) wearing course, and unstable base course and subgrade layer. The total rutting is primarily due to permanent deformation of the AC wearing course, base course and subgrade layer. Figure 1.3 shows the alligator cracking and Figure 1.4 shows the total rutting and poor performance of pavement structures which were designed using MEPDG version 1.1 (University of Arkansas 2022; Blow 2021; Farashah, et al. 2021; Yut, et al. 2014).

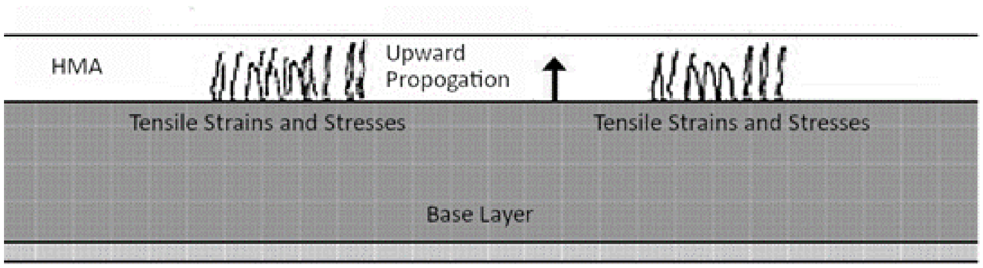

(a)

(b)

Figure 1.3: (a) Schematic of alligator cracking, and (b) Alligator cracking of a pavement structure designed using MEPDG version 1.1 (Yut, et al. 2014)

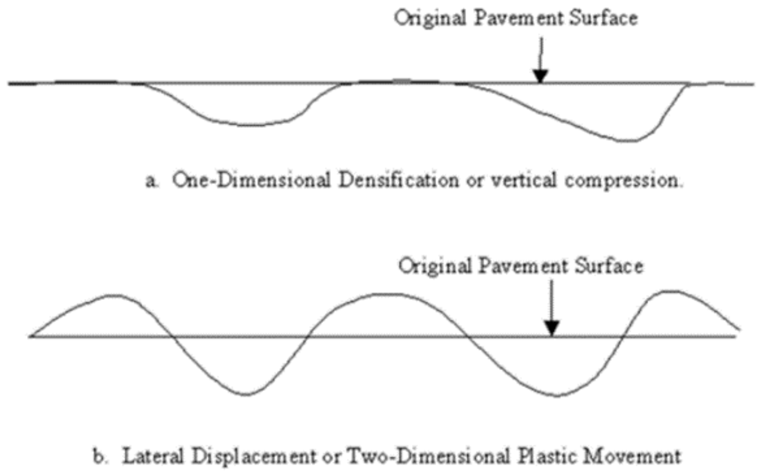

(a)

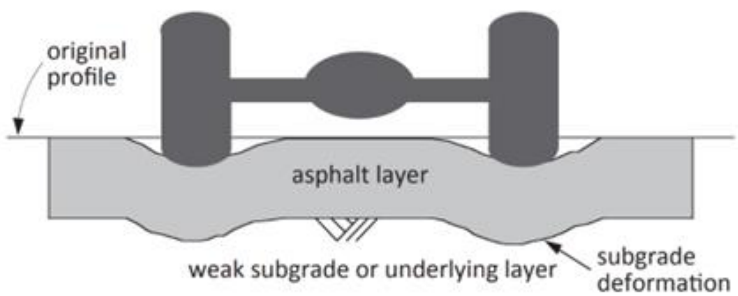

(b)

(c)

Figure 1.4: Schematic of rutting: (a) (Yut, et al. 2014); (b) (Asphalt Institute 2014); and (c) Total rutting of a pavement structure designed using MEPDG (University of Arkansas 2022)

1.2.4 Studies Highlighting Primary Limitations in MEPDG in Predicting Flexible Pavement Distress

<u>*A Study Conducted in Ontario, Canada: (Yuan, and Nemtsov 2017)*</u>

An Ontario, Canada study evaluated the impact of the local calibration of rutting (rut depth), cracking and international roughness index (IRI) prediction models in EICM version 3.2 (the current version of EICM) in a wet freeze climate. The summary of this study presented below focuses on the calibration of the rut depth prediction model in the current version of EICM and the influence of the rut depth on the pavement design and performance. The rut depth is associated with the permanent deformation of the subgrade and/or the asphalt concrete wearing course of flexible pavement structures under traffic loading (Yuan, and Nemtsov 2017). The pavement cross section details and the subgrade classification for the sites investigated in this study are presented in Table 1.1 and Table 1.2 respectively.

Table 1.1: Pavement cross section details (Yuan, and Nemtsov 2017)

Material Layer	Pavement Section ID				
	114 (Arterial)	698 (Arterial)	835 (Collector)	1217 (Freeway)	1260 (Freeway)
	Material layer thickness (mm)				
SP 12.5 FC 1	40	40	40	40	40
SP 19	50	50	100	120	40
Pulverised	-	200	-	-	-
SP 25	-	-	-	180	-
Old HD 8	-	-	-	-	200
Old SP 19	50	-	-		-
Granular Type A	225	190	150	550	300
Granular Type B	-	150	-	-	300
Granular Type B 1	-	-	450	-	-
Subgrade layer	-	-	-	-	-

Table 1.2: Subgrade material classification (Yuan, and Nemtsov 2017)

Material Layer	Pavement section ID				
	114	698	835	1217	1260
	Material classification				
Subgrade	SM	SM	CL	CL-ML	CI

silty Sand (SM), low plasticity Clay (CL), low plasticity Silt (ML), intermediate plasticity Clay (CI)

The analyses of data presented in this study indicated that for sites where the current version of EICM overestimates in-situ water contents, the current version of EICM predicts in-situ resilient moduli which are lower than the actual in-situ resilient moduli. This results in pavement structures which are over-designed to mitigate the consequences of underestimating in-situ resilient moduli. Pavement structures which are over-designed are subjected to lower distress including lower rut depths under traffic loading than the distress predicted by the current version of EICM/MEPDG as shown in Figure 1.5. Pavement structures which are over-designed have higher design and initial construction cost and increased life cycle cost. The analysis presented in Figure 1.6 shows that the distress prediction model in EICM/MEPDG can be improved through local calibration. Although the local calibration improves the distress prediction in EICM/MEPDG, the analysis shows that the locally calibrated distress model also underestimates and overestimates rut depths particularly in the higher range of rut depths (Yuan, and Nemtsov 2017).

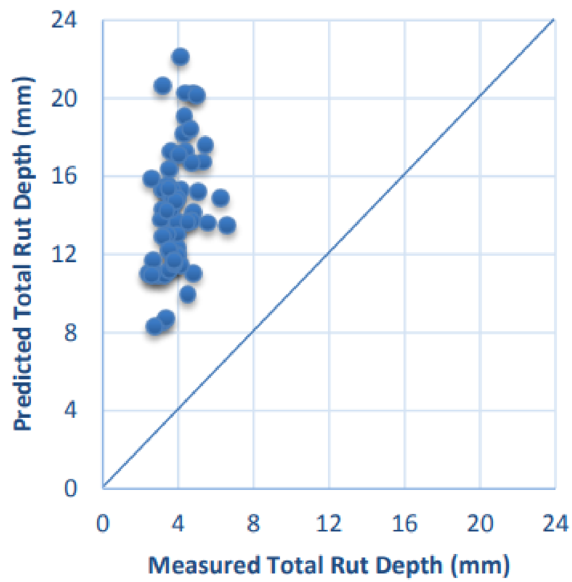

Figure 1.5: Measured vs predicted total rut depths using the current version of MEPDG using global calibration factors (Yuan and Nemtsov 2017)

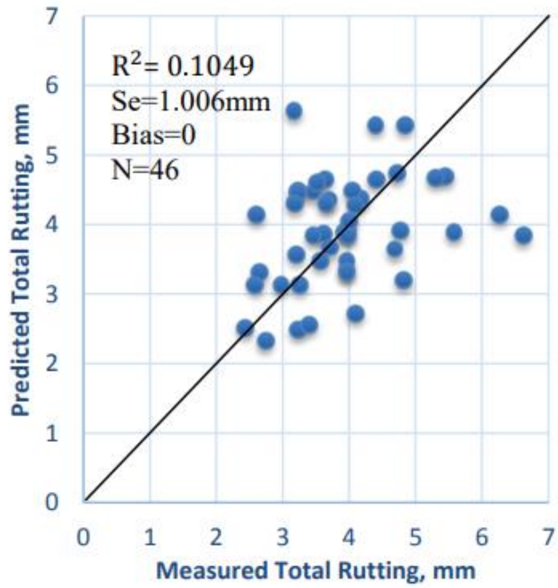

Figure 1.6: Measured vs predicted total rut depths using the current version of MEPDG after local calibration (Yuan, and Nemtsov 2017)

A Study Conducted in Connecticut, United States: (Yut, et al. 2014)

A study was conducted in Connecticut, United States on Highway Route No.2 (the Connecticut study) for the local calibration of the distress prediction models used in MEPDG. This analysis summary focuses on the rutting predicting model used in MEPDG. The pavement cross section details and classification of the subgrade material used in this study are provided in Table 1.3 and Table 1.4 respectively.

Table 1.3: Pavement cross section details (Yut, et al. 2014)

Material Layer	Average material Layer Thickness (mm)
AC wearing course	338.0
Stabilized base course	100.0
Subbase course	250.0
Subgrade	-

Table 1.4: Subgrade material classification (Yut, et al. 2014)

Material Layer	Material Classification	Description
Subgrade	A-3	fine Sand

The analysis of the data presented in the Connecticut study indicated that the rutting is primarily impacted by the traffic loading and the strength of the subgrade. The rutting is also impacted by changes in climatic factors. The analysis indicated that the strength of the base course has minimal impact on rut depths.

The analysis of the data presented in Figure 1.7 indicated that for sites where the current version of EICM underestimates in-situ water contents, the current version of EICM predicts in-situ resilient moduli which are higher than the actual in-situ resilient moduli. This results in pavement structures which are subjected to higher distress and damage under traffic loading. Subjecting pavement structures to higher distress result in a lower performance, reduced service life, and higher maintenance and life cycle cost.

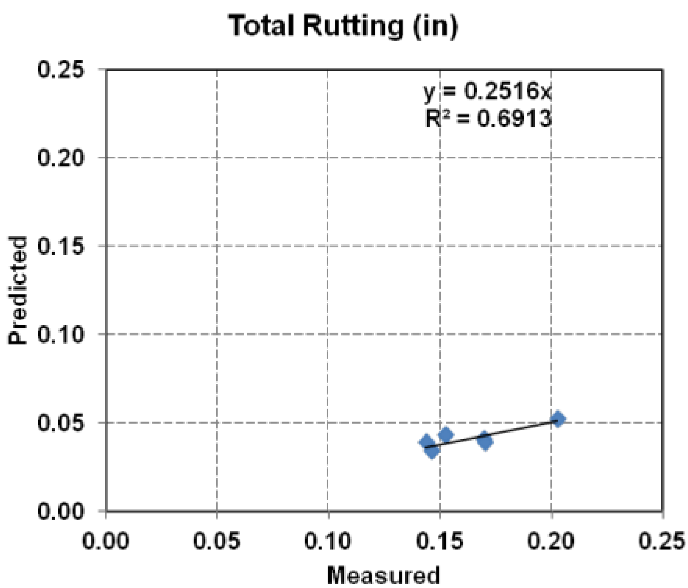

Figure 1.7: Measured vs predicted total rut depths using EICM ver. 3.2 (Yut, et al. 2014)

1.2.5 Summary of the Primary Limitations in the Current Version of EICM

A summary of the primary limitations in the current version of EICM in predicting water and heat transfer in flexible and rigid pavement structures is presented in Table 1.5.

Table 1.5: Summary of primary limitations in EICM model components

Primary limitations in EICM model component	Studies highlighting the limitation
EICM version 3.2 (the current EICM) neglects the impact of climatic factors on fluctuations in water contents within subgrades.	Bulut, and Javid (2019); Bulut, et al. (2014); Bulut, et al. (2013); McCartney, et al. (2010).
The current EICM water contents prediction model (the Fredlund, and Xing 1994 model) predicts in-situ water contents and SWCC poorly.	Hall, et al. (2013); Zapata, and Houston (2008).
The ID model assumes water transfer is primarily via surface cracks. The ID model also assumes that the base course is free draining and drains horizontally, and that no water is transferred to the subgrade.	Zapata, and Houston (2008); Bayomy, and Salem (2005); Drumm, and Meier (2003).
The ID model neglects increase in water transfer due to an increase in infiltration. It accounts for shallow groundwater table and neglects the groundwater table at significant depth.	Zapata, and Houston (2008); Drumm, and Meier (2003); Witczak, et al. (2000).
The current EICM neglects the impact of increased precipitation in evaluating water contents due to its reliance on surface cracks.	Zapata, and Houston (2008); Drumm, and Meier (2003).
The current EICM inaccurately predicts the convective cooling during high air temperature.	Bryce, et al. (2021).
The current EICM neglects the impact of increased wind speed on convective cooling and has an overreliance on minimal natural convection in the absence of wind.	Bryce, et al. (2021); Qin, and Hiller (2013); Jiji (2009).
The current EICM accounts only for liquid water transfer and neglects water vapour transfer.	McCartney, et al. (2010); Zapata, and Houston (2008); Dempsey, et al. (1986).
The CRREL model neglects water transfer through advection, accounts for liquid water transfer and neglects water vapour transfer.	Bulut, et al. (2014); McCartney, et al. (2010).
The CRREL model has an overreliance on capillary rise from shallow water tables.	Bulut, et al. (2014); McCartney, et al. (2010).
The CMS model neglects condensation and evaporation. It assumes a water equilibrium influenced by the water table and neglects fluctuations in water contents due to climatic factors.	Bulut, and Javid (2019); Applied Research Associates Inc. (2004); Dempsey, et al. (1986).
The CMS model also neglects surface water transfer into subgrades through infiltration, neglects horizontal flow to and/or from adjacent soils and assumes a constant pavement temperature above freezing.	Bulut, and Javid (2019); Applied Research Associates Inc. (2004); Dempsey, et al. (1986).

Primary limitations in EICM model component	Studies highlighting the limitation
The current version of EICM and MEPDG inaccurately predict rutting in flexible pavements.	Yuan, and Nemtsov (2017; Kim, et al. 2011).
The composite environmental adjustment factor (F_{env}) neglects the impact of the climate on the degree of saturation and resilient modulus.	Zapata, and Houston (2008); Zapata, et al. (2007).

1.3 Summary

A major challenge in managing pavement structures is that these pavement structures have been subjected to more severe climatic factors relative to the climatic factors accounted for in their design (Sultana 2017; Sultana, et al. 2014; Gaspard, et al. 2007). The impact of the climate and environmental factors is accounted for in MEPDG by incorporating EICM. Many studies have been conducted in the United States and Canada to evaluate, calibrate and validate EICM in predicting the impact of the climate and environment on water and heat transfer within pavement structures. In addition, MEPDG and the associated EICM model components have been updated many times between 2005 and 2012 to improve the water and heat transfer and the distress prediction models. However, the current version of EICM has inaccuracies in the climatic boundary conditions. EICM should be improved to accurately account for the impact of climatic factors and LCI boundary conditions on water and heat transfer, the resilient modulus and the pavement distress prediction. Previous studies show that the volumetric water contents prediction model used in EICM is not accurate. The model should be improved to account for the impact of climatic factors on the water and heat transfer within subgrades.

Improving EICM requires an understanding of the computational framework and delineating strengths and limitations in EICM to support optimizing pavement designs, performance and life cycle cost. The equations in EICM which are used for calculating the composite environmental adjustment factor (F_{env}), unfrozen environmental adjustment factor (F_U), and resilient modulus (M_R) should be improved to account for climatic factors. The F_{env}, F_U, and M_R may be improved by incorporating climatic factors into the equation used in EICM for calculating the degree of saturation (S). The equation used for calculating "S" should be improved because "S" is the primary input parameter which is used for calculating the F_{env}, F_U, and M_R.

1.4 The Problem Statement

There are limitations in the climatic boundary conditions used in EICM. EICM neglects the impact of land climate interaction (LCI) (on vegetated or bare ground areas in the vicinity of pavement structures) on water and heat transfer within subgrades. EICM accounts for only infiltration through cracks on the pavement surface and neglects the influence of evapotranspiration on the water and heat transfer. EICM accounts for only liquid water transfer and neglects water vapour transfer. These limitations in EICM result in inaccuracies in predicting in-situ volumetric water contents due to inaccuracies in predicting in-situ suction and in-situ soil water characteristic curve (SWCC) (Hall, et al. 2013; McCartney, et al. 2010; Zapata, and Houston 2008; Zapata, et al. 2007; Ahmed, et al. 2005; Bayomy, and Salem 2005; Drumm, and Meier 2003; Witczak, et al. 2000; Zapata, et al. 1999).

EICM assumes a constant and uniform subgrade temperature, only accounts for water transfer influence by the depth of shallow groundwater table, neglects the influence of the water table at significant depth and neglects the influence of climatic factors on fluctuations in the in-situ water and heat transfer within subgrades. These limitations result in inaccurate prediction of in-situ water contents for cases with low groundwater table elevations (Bayomy, and Salem 2005; Drumm, and Meier 2003; Witczak, et al. 2000).

These limitations in EICM also result in inaccuracies in predicting in-situ volumetric water contents and in-situ resilient moduli of subgrades that form the basis for the pavement mechanistic response. The inaccuracies in predicting the water and heat transfer and in-situ resilient moduli of unbound materials result in inaccuracies in predicting the pavement performance (Hall, et al. 2013; Kim, et al. 2011; Kim, and Siddiki 2006; Ovik et al 2000). These limitations in EICM lead to inaccurate prediction of the pavement performance and service life and result in the implementation of uneconomical pavement structures (University of Arkansas 2022; Farashah, et al. 2021; Yuan, and Nemtsov 2017; Yut, et al. 2014).

1.5 The Significance of the Research

The research includes the development of a Quantitative Empirical Model (the QE Model) using a comprehensive water balance approach. The QE Model accounts for the impact of climatic factors on fluctuations in in-situ volumetric water contents and associated fluctuations in resilient moduli of subgrades. The QE Model represents an in-situ soil water characteristic curve (the in-situ SWCC) which is influenced by climatic factors (the energy state). The in-situ SWCC accounts for the impact of climatic factors on fluctuations in volumetric water contents of fine and coarse grained subgrades in a wet freeze and wet no-freeze climates.

The research also includes the development of a model for predicting the site-specific net evapotranspiration (Net ET) which uses the Penman-Monteith method. The proposed model predicts the Net ET as a nonlinear function of climatic factors. The Net ET model accounts for both condensation and evapotranspiration.

The QE Model may be incorporated into EICM and MEPDG to account for the impact of climatic factors on water and heat transfer, and the resilient moduli of subgrades. Incorporating the QE Model into

EICM and MEPDG facilitates the design and construction of more economical pavement structures with improved performance and increased service life.

The QE Model, Net ET Model and the frameworks used for the development of the models are applicable for use in unsaturated geotechnics which include pavement geotechnics and geotechnical engineering applications for roadway and railway engineering, and analyses of soil cover systems. The QE Model also makes a significant and innovative contribution to the overall engineering practice.

1.6 Research Objective

The primary objective of this research is to investigate the influence of changes in climatic factors on changes in water transfer and volumetric water contents within subgrades. The investigation focuses on the impact of land climate interaction (LCI) on water and heat transfer within subgrades. The specific objective is achieved by developing a Quantitative Empirical Model (the QE Model) which represents an LCI surface boundary condition. The QE Model account for the impact of changes in precipitation, air temperature, net solar radiation, wind speed, relative humidity, and evapotranspiration on changes in volumetric water contents within subgrades.

It is intended that the QE Model would be incorporated into EICM for improving EICM and MEPDG to account for the impact of climatic factors on in-situ volumetric water contents and resilient moduli of subgrades.

1.7 Research Hypotheses

It is assumed that LCI influences changes in volumetric water contents within subgrades including for cases where wearing courses (on traffic lanes and shoulders) are impervious (or have no cracks) and the static water table is at significant depth. It is also assumed that changes in volumetric water contents within subgrades are influenced by changes in precipitation, air temperature, net solar radiation, wind speed, relative humidity, and evapotranspiration (climatic factors). It is also assumed that changes in volumetric water contents within subgrades are primarily influenced by changes in precipitation and air temperature.

It is assumed that a Quantitative Empirical Model (the QE Model) representing LCI surface boundary conditions can be developed to account for the influence of changes in climatic factors on changes in volumetric water content within subgrades. It is also assumed that the QE Model is more accurate than EICM in simulating in-situ volumetric water contents for use in calculating the time and depth dependent composite environmental adjustment factor (F_{env}). It is also assumed that the QE Model can be incorporated into EICM and MEPDG to facilitate EICM and MEPDG accounting for climatic factors.

Research hypotheses were tested by simulating changes in in-situ volumetric water contents within subgrades using the QE Model. The simulated in-situ volumetric water contents were superimposed against the measured in-situ volumetric water contents to verify the accuracy of the QE Model in predicting in-situ water and heat transfer within subgrades. The accuracy of the QE Model was also verified using the coefficient of determination (R^2) analysis between the simulated in-situ volumetric water contents and the measured in-situ volumetric water contents.

The research hypotheses were also tested by incorporating the QE Model into the modified F_{env} and M_R equations developed as part of this research. The F_{env} and M_R values were calculated using in-situ volumetric water contents simulated using the QE Model and EICM (the simulated F_{env} and M_R values). F_{env} and M_R values were also calculated using the measured in-situ volumetric water contents (the measured F_{env} and M_R values). The simulated F_{env} and M_R values were compared to the measured F_{env} and M_R values to verify the accuracy of the QE Model and EICM in simulating the influence of changes in climatic factors on fluctuations in F_{env} and resilient moduli of subgrades.

A Two-tailed F-test was conducted to evaluate the accuracy of the QE Model against the accuracy of EICM. The Two-tailed F-test was also conducted to evaluate the suitability of the in-situ volumetric water contents simulated using the QE Model and EICM for calculating the F_{env} and the in-situ M_R of subgrades. The Two-tailed F-test was conducted using the simulated F_{env} values obtained using the QE Model output and the simulated F_{env} values obtained using the EICM output.

1.8 Overview of the Research Methodology, Results and Analyses

The research investigates the impact of water and heat transfer on volumetric water contents within subgrades by incorporating a water balance approach which is influenced by climatic factors. The research also investigates the impact of climate-induced fluctuations in in-situ water contents on fluctuations in in-situ resilient moduli of subgrades.

The research uses finite element analysis (FEA) modeling, statistical analyses and mathematical computations to develop a Quantitative Empirical Model (the QE Model) which accounts for the influence of climatic factors on water and heat transfer within subgrades. The research also develops modifications to the existing equations which are used in the current version of EICM and MEPDG which include the composite environmental adjustment factor (F_{env}) and resilient modulus (M_R) of the subgrade. The modifications to the F_{env} and M_R equations are achieved by incorporating the QE Model into the F_{env} and M_R equations to account for the influence of climatic factors on water contents and resilient moduli of subgrades. The research also proposes a model for predicting the site-specific net evapotranspiration (Net ET) which applies the Penman-Monteith method. The proposed model predicts changes in Net ET as a nonlinear function of changes in climatic factors {Net ET (ΔA)}

The research uses statistical analyses for evaluating the accuracy of the QE Model in predicting the influence of climatic factors on volumetric water contents within fine-grained and coarse-grained subgrades in various climates. The research also verifies the accuracy of the QE Model by comparing the volumetric water contents which are predicted using the QE Model (the simulated volumetric water contents) to the measured in-situ volumetric water contents. The accuracy of the QE Model was also verified by comparing the F_{env} and M_R values which are calculated using the simulated in-situ volumetric water contents, to the F_{env} and M_R values calculated using the measured in-situ volumetric water contents for sites in various climates.

The research findings show that resilient moduli of subgrades are influenced by fluctuations in in-situ water contents. An increase in the in-situ water content causes a decrease in the in-situ resilient modulus of the subgrade. The reduction in resilient moduli of subgrades results in higher deformation, more distress, lower performance and shorter service life of pavement structures. The results of the evaluation processes indicate that the QE Model accurately predicts the influence of climatic factors on fluctuations in the water and heat transfer within subgrades. The data also show that the QE Model is more accurate than the current version of EICM and MEPDG in predicting the impact of climatic factors on in-situ volumetric water contents within fine-grained and coarse-grained subgrades in different climates. The data also show that in-situ volumetric water contents predicted using the QE Model are more suitable for calculating the impact of climatic factors on the F_{env} and M_R of subgrades than the in-situ volumetric water contents predicted using the current version of EICM and MEPDG.

1.9 Research Deliverables

The research deliverables include a Ph.D dissertation and up to four journal papers as listed below:

1. An in-depth review of limitations in EICM and MEPDG in predicting the impact of climatic factors and LCI on water and heat transfer within subgrades;
2. The influence of climatic factors on water and heat transfer within subgrades using LCI-based numerical modeling;
3. A Quantitative Empirical Model incorporating the influence of climatic factors on water and heat transfer within subgrades in various climates; and
4. Incorporating a Quantitative Empirical Model into EICM and MEPDG to account for the influence of climatic factors on water and heat transfer, and resilient moduli of subgrades.

1.10 Organization of the Dissertation

This dissertation comprises eight chapters. Chapter 1 provides an overview of the primary strength of the Mechanistic Empirical Pavement Design Guide (MEPDG) and the Enhanced Integrated Climate Model (EICM) in predicting the in-situ water and heat transfer and performance of pavement structures. Chapter 1 also provides background details on the MEPDG which include the pertinent features of the current version of MEPDG and the EICM. Chapter 1 also provides an overview of the Long-term Pavement Performance (LTPP) program and the Seasonal Monitoring Program (SMP) implemented to support the development and local calibration of MEPDG. Chapter 1 also provides details of problems caused by EICM predicting the in-situ water and heat transfer within subgrades poorly. The Chapter provides details of the significance of the research and contribution made by the research to the engineering practice. The Chapter also provides details of the research objectives and research hypothesis. The Chapter concludes by providing an overview of the research methodology, analyses and results, by providing a list of research deliverables and by providing a summary of the organization of the dissertation.

Chapter 2 presents an overview of unsaturated soil mechanics and its application in the compacted fill materials used for the design and construction of pavement structures. The Chapter also provides details of the pertinent principles governing water and heat transfer in unsaturated subgrades (one of the objectives of this study). The Chapter also provides details of the principles governing the influence of climatic factors on in-situ water and heat transfer, the resilient modulus and pavement performance. The Chapter also provides details of the primary differences between seasonal changes in climatic factors and climate change. Chapter 2 also provides details of principles governing the finite element analysis (FEA) modeling of water and heat transfer in unsaturated subgrades. The Chapter also provides details of the application of the surface mass balance and LCI (a primary component of this study). Chapter 2 also provides details of the primary LCI processes which include details of evapotranspiration (which is represented by the Penman-Monteith equation), heat conduction, and heat convection (natural and forced convection with water transfer). This chapter also provides details of the principles governing the boundary conditions used in the FEA modeling of water and heat transfer which form part of this study.

Chapter 3 provides an overview of the procedures used for designing and constructing traditional flexible and rigid pavement structures, and the framework used for designing economical and sustainable pavement structures. Chapter 3 also provides details on the primary features of MEPDG and EICM. The Chapter provides a discussion of the application of the composite environmental adjustment factor (F_{env}) incorporated into EICM. The F_{env} account for the influence of the climate and environment on resilient moduli of subgrades. The Chapter also provides an overview of the impact of changes in volumetric water contents and stress state within pavement materials on resilient moduli and shear strengths of pavement materials, and their impact on pavement performance. Chapter 3 also presents the primary features of the current version of EICM and include the model components which form part of EICM. Chapter 3 also provides details of the primary limitations in EICM in predicting in-situ water and heat transfer within subgrades. The Chapter also provides a summary of studies conducted to evaluate, calibrate and validate EICM in predicting in-situ water and heat transfer within subgrades in different climates. The Chapter also provides detailed analyses of the studies conducted to calibrate and validate EICM which are also used for evaluating the accuracy of the QE Model in predicting in-situ water and heat transfer within subgrades at selected sites in different climates. Chapter 3 also provides a detailed analytical summary of studies highlighting the primary limitations in EICM. The Chapter also provides a summary of EICM's primary limitations which are mitigated by the QE Model.

Chapter 4 presents a flow chart showing tasks conducted for the development and for evaluating the accuracy of the transient water and heat transfer models of the two pavement sections. The Chapter presents details of sources of the in-situ monitoring data including pavement cross sections, material properties, in-situ volumetric water contents, and depths to the water table. The Chapter also provides the input parameters used for the water and heat transfer FEA modeling. Chapter 4 also presents the methodology used for the development of the LCI boundary conditions used in the FEA modeling. Chapter 4 also provides the methodology used for the development, calibrating and for evaluating the accuracy of the 1-D and 2-D transient water and heat transfer FEA models. The 1-D and 2-D transient water and heat transfer FEA modeling was conducted to investigate the influence of changes in climatic factors and LCI on water and heat transfer within unsaturated subgrades. The Chapter provides analyses of the 1-D and 2-D water and heat transfer FEA modeling output. The Chapter also provides analyses of the spatial distribution of volumetric water contents. Chapter 4 also provides details of the analysis of the impact of changes in climatic factors on lag times. Lag times are associated with changes in climatic factors and the response time of changes in volumetric water contents within subgrades.

Chapter 5 provides details of statistical analyses conducted to evaluate the accuracy of the FEA models, to evaluate the relationship between in-situ climatic factors and volumetric water contents, to formulate the general form equation for the QE Model and to evaluate the accuracy of the QE Model. The statistical analyses were conducted using XLSTAT statistical software. The software was published by ADDINSOFT which is located in Paris, France. The Chapter presents statistical analyses including correlation testing used to evaluate the inter-relationships between climatic factors. The correlation testing was also used to determine the extent to which changes in climatic factors influence changes in in-situ volumetric water contents within subgrades. The statistical correlation testing was conducted using the correlation coefficient (R) value. The "R" values are used for evaluating the relationship between changes in climatic factors and changes in in-situ volumetric water contents to determine the influence of changes in climatic factors on water and heat transfer within subgrades. Chapter 5 also presents the correlation of determination (R^2) analysis conducted to determine the correlation between in-situ volumetric water contents and volumetric water contents obtained from the 1-D and 2-D water and heat transfer FEA modeling output. The "R^2" analysis is used for calibrating and for evaluating the accuracy of the 1-D and 2-D FEA models. The Chapter also presents the R^2 analysis conducted to evaluate the accuracy of the QE Model and EICM in predicting in-situ volumetric water contents, and their suitability for use in calculating the F_{env}. The analysis was conducted by comparing the F_{env} values calculated using volumetric water contents obtained from the QE Model and EICM with F_{env} values calculated using the measured in-situ volumetric water contents. The Chapter also provides details of the two-tailed F-test statistics used to determine which climatic factors produced the best fitting climatic factors dataset for developing the QE Model. The statistical analysis was conducted using the partial F-test. Chapter 5 also provides details of the F-test statistics used for conducting a comparison between the exponential, sin and power functions to determine the best fitting function for use as the general form equation for the QE Model. The Chapter also provides the F-test statistics used for evaluating statistical correlations and statistical significance between the function parameters (P_i) and the system dependent properties of the subgrade (X_i) which are represented by P_1 and X_1, P_2 and X_2, and P_3 and X_3.

Chapter 6 provides an overview of the inter-relationships between climatic factors and volumetric water contents within subgrades. The Chapter provides a background on the hydrological cycle and the pertinent climatic processes that impact changes in water and heat transfer within subgrades. The Chapter also provides a discussion of the background on climatic factors and LCI. The Chapter also provides a background on nonlinear regression and its application in the development of models used for predicting the impact of climatic factors on water and heat transfer within subgrades. Chapter 6 also provides the methodology used for the development of the QE Model for predicting the impact of changes in climatic factors on changes in water and heat transfer within subgrades. The details provided include the method used for formulating the pertinent climatic factors incorporated into the QE Model. The Chapter also provides details of the nonlinear regression conducted to evaluate the statistical relationship between volumetric water contents within subgrades and climatic factors. The Chapter also provides the methodology used for the development and selection of the general form of the equation used for the formulation of the QE Model. Chapter 6 also provides details of the mathematical formulations which include the integration used for the development of the QE Model. The Chapter also provides the methodology used for incorporating the system dependent properties of subgrades into the *f-functions* incorporated into the QE Model. Chapter 6 also provides a summary of the QE Model and input parameters. Chapter 6 also provides details of the application of the QE Model in the engineering practice. The Chapter also provides details of the modified composite environmental adjustment factor (the F_{envCF} model). The F_{envCF} model is developed for incorporating the impact of climatic factors into resilient moduli and performance evaluation of subgrades. Chapter 6 also provides details of the modified resilient modulus of the subgrade (M_{RCF}) which is developed to account for the impact of climatic factors on the pavement response and performance.

Chapter 7 provides background on the methodology used for developing the QE Model, the primary features and application of the model. Chapter 7 also provides the strategy implemented for evaluating the accuracy of the QE Model. The Chapter provides details of data sources, locations of the sites, and details of the pavement sections used for evaluating the accuracy of the model. The Chapter also provides details of the nine tasks conducted for evaluating the accuracy of the QE Model (determined input data, obtained input climatic factors, calculate and review the accuracy of the measured in-situ volumetric water contents, predict in-situ volumetric water contents using the QE Model, evaluate the accuracy of the QE Model, compared the QE Model output to the EICM output, compared the Fenv calculated using the QE Model output to the Fenv calculated using the measured in-situ volumetric water contents, evaluated the trends in volumetric water contents and evaluated the accuracy of the QE Model and EICM using statistical analyses). The accuracy of the QE Model was evaluated by comparing predicted volumetric water contents calculated using the model to the measured in-situ volumetric water contents. The accuracy of the QE Model was also evaluated against EICM by comparing F_{env} values calculated using the predicted volumetric water contents which were calculated using the model and EICM to F_{env} values calculated using the measured in-situ volumetric water contents. The accuracy of the QE Model was also evaluated against EICM by comparing resilient moduli values which were calculated using the F_{env} values calculated using volumetric water contents predicted using the QE Model (M_{RCF}) to the resilient moduli values which were calculated using the F_{env} values calculated using volumetric water contents predicted using EICM (M_R). The M_{RCF} and M_R values were compared to the measured in-situ resilient moduli values. Chapter 7 also provides a summary of the evaluation process, limitations in EICM mitigated by the QE Model, and details of primary features of the QE Model. The Chapter also provides details of the contribution of the QE Model to improving EICM and MEPDG to account for the impact of climatic factors on water and heat transfer, resilient moduli of subgrades, pavement performance and service life.

Chapter 8 provides background details of the literature review which was conducted to delineate limitations in EICM in predicting the in-situ water and heat transfer within subgrades. The Chapter provides a brief summary of the study's problem statement, research objectives, and research methodology used for conducting the FEA modeling and the development of the QE Model. The Chapter also provides a summary of the methodology used for the verification of the QE Model.

Chapter 8 also provides a summary of tasks conducted for verifying the accuracy of the QE Model in predicting in-situ water and heat transfer within subgrades due to climatic factors. The Chapter also provides a summary of tasks conducted for verifying the accuracy of the QE Model vs the accuracy of EICM in predicting in-situ water and heat transfer and in-situ resilient moduli of subgrades.

The Chapter also provides a conclusion which includes the potential for incorporating the QE Model into EICM and MEPDG. The conclusion includes the contribution of the QE Model in improving EICM and MEPDG for the design and construction of more economical pavement structures. The conclusion also includes the primary research findings, the primary features of and accuracy of the QE Model in predicting the impact of climatic factors on the in-situ water and heat transfer within subgrades. The conclusion also provides a summary of the primary limitations in EICM which are mitigated by the QE Model.

The Chapter also provides recommendations for further research to investigate the impact of climatic factors on the in-situ water and heat transfer within different types of subgrades and in different climates. Chapter 8 also provides recommendation for improving the water contents prediction model used in EICM.

Chapter 2 The Impact of Climatic Factors on Water and Heat Transfer Processes in Unsaturated Subgrades

2.1 Introduction

Chapter 2 provides an overview of unsaturated soil mechanics which form the governing principles for the compacted fill materials used in the design and construction of pavement structures. The Chapter also provides an overview of the climate and the impact of climatic factors on water and heat transfer, the resilient modulus and performance of pavement structures (one of the objectives of this study). Chapter 2 also provides details which describe the primary differences between variations in seasonal climatic factors and climate change.

Chapter 2 also provides pertinent details of the principles governing the finite element analysis (FEA) modeling of water and heat transfer in unsaturated subgrades including the application of the surface mass balance and the land climate interaction (LCI) which form a primary component of this study. The primary LCI processes presented in this chapter are the details of water and heat transfer processes including evapotranspiration (which is represented by the Penman-Monteith equation), heat conduction, and heat convection including natural and forced convection with water transfer. This Chapter also provides details of the principles governing the boundary conditions used in the FEA modeling of water and heat transfer within pavement structures which form part of this study.

2.2 Mechanism of Water Transfer in Unsaturated Subgrades

The seepage, shear strength and volume change are the primary constitutive characteristics of saturated soil mechanics. These constitutive relationships form the basis for unsaturated soil mechanics in addition to the matric suction which is a stress state associated with unsaturated soils (Han, et al. 2016; Laloui 2013; Vanapalli, and Oh 2011; Ravichandran, and Krishnapillai 2011; Fredlund 2006; Nimmo 2005; Vanapalli, et al. 1999; Vanapalli, et al. 1998; Sillers 1997; Fredlund, and Xing 1994; Alonso, and Delage 1996). The constitutive characteristics of saturated and unsaturated soil mechanics are also applicable to the mechanisms which influence water and heat transfer in pavement materials. The water transfer within pavement structures is also influenced by the water characteristics curve (SWCC) which represents the relationship between the matric suction and the water content of the material (Han, and Vanapalli 2015; Vanapalli, and Han 2014; Rosenbalm, and Zapata 2013; Khoury, et al. 2011; Khoury, et al. 2010; Kim, and Siddiki 2006; Oloo, et al. 1997). The SWCC is typically used to describe the pavement response in various environments and water contents. The SWCC also accounts for the influence of increased water content on the resilient modulus, shear strength and bearing capacity of pavement subgrades (Han, et al. 2016; Han, and Vanapalli 2015; Vanapalli, and Han 2014; Rosenbalm, and Zapata 2013; Khoury, et al. 2011; Khoury, et al. 2010; Kim, and Siddiki 2006; Oloo, et al. 1997).

The most commonly used SWCC models include the Gardner's (1958) model which is assessed as continuous and simplistic. Gardner's model consists of parameters *a* and *n* which represent the inverse of the air entry value (AEV) and pore size respectively. The primary limitation of the Gardner model is that it inaccurately represents the SWCC at or near the saturation condition (Song, et al. 2013).

The Brooks and Cory (1964) model is based on a power function with parameters h_b and λ which are associated with the AEV and pore size distribution respectively. The primary limitation of the Brooks and Corey (1964) model is that the mathematical function is not continuous over the entire soil suction range which is typically assessed as 0 to 10^6 kPa.

The van Genuchten (1980) model is based on parameters α, *n* and *m* which are associated with the inverse of the AEV, the pore size distribution and the model asymmetry respectively. The primary advantages of the van Genuchten (1980) model are that the model facilitates a continuous relationship for unsaturated conditions and accurately characterizes the SWCC. The van Genuchten (1980) model presented in Eq. 2.1 and Eq. 2.2 was used for conducting the water and heat transfer finite element analysis (FEA) modeling which forms part of this study (GeoSlope 2020; van Genuchten 1980).

The Fredlund, and Xing (1994) model presented in Eq. 2.3 and Eq. 2.4 represents a wide range of soil types particularly in the high suction ranges. This model addresses the primary limitations of the Brooks, and Corey (1964) model which does not represent soils over the full range of soil matric suction. The Brooks, and Corey (1964) model also neglects soil water contents at soil matric suction values less than the air-entry value. In Eq. 2.3, the relationship represented by the function in Eq. 2.4 is a correction function which results in the SWCC accounting for a soil matric suction value of $1\text{x}10^6$ kPa which corresponds to a water content value of zero. Eq. 2.3 and Eq. 2.4 are incorporated into EICM and are used in MEPDG to determine the volumetric water contents within subgrades. The Fredlund, and Xing (1994) model has limitations which result in the model predicting in-situ water contents poorly. The limitations in the Fredlund, and Xing (1994) model include the model neglecting the impact of climatic factors on water and heat transfer, neglects fluctuations in the in-situ water contents and predicts the in-situ SWCC poorly (Hall, et al. 2013, McCartney, et al. 2010; Drumm and Meier 2003).

$$\theta_{\mathrm{w}} = \theta_{\mathrm{res}} + \left(\frac{\theta_{\mathrm{sat}} - \theta_{\mathrm{res}}}{\{1+(\mathrm{a}*\psi)^{\mathrm{n}}\}^{\mathrm{m}}}\right) \tag{2.1}$$

$$\mathrm{m} = \left(1-\frac{1}{\mathrm{n}}\right) \tag{2.2}$$

θ_w = Volumetric water content; θ_{res} = Residual volumetric water content; θ_{sat} = Saturated volumetric water content; ψ = Soil suction; $a' \Rightarrow 1/a$ = Parameter related to shape of SWCC and air-entry value (a); n = Parameter related to the slope at inflection point on SWCC; m = Parameter related to shape of SWCC and residual water content.

$$\theta_w = \theta_s \left(1 - \frac{\ln\left(1+\frac{\psi}{C_r}\right)}{\ln\left(1+\frac{10^6}{C_r}\right)}\right)\left(\frac{1}{\ln\left(e+\left(\frac{\psi}{a}\right)^n\right)^m}\right) \quad (2.3)$$

$$C(\psi) = \left(1 - \frac{\ln\left(1+\frac{\psi}{C_r}\right)}{\ln\left(1+\frac{10^6}{C_r}\right)}\right) \quad (2.4)$$

θ_w = Volumetric water content; θ_s = Saturated volumetric water content; ψ = *Soil suction;* a = Soil parameter related to air-entry value of soil; n = Soil parameter related to slope at inflection point on SWCC; m = Soil parameter related to residual water content of soil; e = Natural number which equals to 2.71828; and C_r = Residual matric suction.

Pavement structures are typically constructed within the unsaturated zone located above the groundwater table. Within the unsaturated zone, the water transfer is influenced by the soil texture, soil structure and transient water contents which result in variations in water contents within pavement structures over time. The variations in water contents result in changes in the hydraulic conductivity of the pavement materials (Han, and Vanapalli 2015; Vanapalli, and Han 2014; Rosenbalm, and Zapata 2013; Price, et al. 2000; Vanapalli, et al. 1999; Khoury, et al. 2011; Khoury, et al. 2010; Kim, and Siddiki 2006; Oloo, et al. 1997). One of the primary characteristics of unsaturated pavement materials is the air entry value which is the matric suction value corresponding to the water content below which the materials start to desaturate (Khoury, et al. 2010; Nimmo 2005; Drumm and Meier 2003). The water and heat transfer within pavement structures is influenced by capillary rise due to shallow groundwater table which is the primary mechanism of water transfer accounted for in EICM (Khoury, et al. 2010; McCartney, et al. 2010; Drumm and Meier 2003).

The water transfer in unsaturated pavement material layers consists of liquid water and water vapour transfer. The water vapour transfer is influenced by diffusion due to a temperature gradient, while the liquid water transfer is influenced by adsorbed water and isothermal water transfer (McCartney, et al. 2010; Tuller, and Or 2002; Ovik, et al. 2000; Kosmas, et al. 1998; Philip 1958; Philip 1957b and 1957h). The thermal properties of the pavement materials including the thermal conductivity, volumetric heat capacity and thermal diffusivity are influenced by the volumetric water content (Roxy, et al. 2014; O'Donnell, et al. 2009; Kasubuchi 1975). The FEA modeling which forms part of this study incorporated these relationships to improve the accuracy of the water and heat transfer FEA modeling of the pavement sections (GeoSlope 2020; GeoSlope 2012).

The performance of unsaturated subgrades is influenced by changes in the post construction water contents due to variations in climatic factors (Perez-Garcia, et al. 2016). These changes in water contents are associated with changes in water contents from the initial compaction water content, variations in water contents due to freezing and thawing, fluctuations in water contents due to infiltration through the surface cracks and fluctuations in the groundwater elevation (Perez-Garcia, et al. 2016; Houston, et al. 2006; Witczak, et al. 2006). Changes in water contents from the initial compaction water content to the equilibrium water content, and freezing and thawing have the most influence on resilient moduli of subgrades (Houston, et al. 2006; Witczak, et al. 2000).

Although the current version of EICM has an overreliance on infiltration through surface cracks, studies have indicated that the infiltration through surface cracks has minimal influence on seasonal fluctuations in water contents and resilient moduli of subgrades (Houston, et al. 2006; Witczak, et al. 2006). Studies have also indicated that the infiltration of water through pavement structures is complex and that the use of edge drainage systems has proven unsuccessful in mitigating the impact of infiltration on the changes in the water content and resilient modulus of subgrades (Perez-Garcia, et al. 2016; Houston, et al. 2006; Birgisson, and Roberson 2000; Basma, and Al-Suleiman 1991).

The water contents within soil structures are typically evaluated using state variables including soil water contents, soil suction, and seepage analyses. Water contents and seepage analyses are used in this study due to the simplicity in measuring and simulating changes in water contents and seepage over time (Marr, et al. 2004; Briaud, et al. 2003). The assessment of water contents is based on the movement of the wetting front which is influenced by changes in climatic factors which are represented by LCI boundary conditions. LCI boundary conditions account for precipitation, infiltration, surface water runoff and ponding, actual evaporation, and transpiration (Bulut, and Javid 2019; Thode, and Gitiriana 2008; Overton, et al. 2006; Fredlund, and Gitirana Jr. 2005; Marr, et al. 2004; Briaud, et al. 2003; Tuller, and Or 2002; Fredlund, and Hang 2001; Pufahl, and Lytton 1991).

2.3 Impact of Climatic Factors on Water and Heat Transfer and the Resilient Modulus

The climate is associated with the average of climatic factors including precipitation, air temperature, humidity, sunshine and wind speed (climatic factors) in a specific region over a long-term period. Climate change is associated with the long-term changes in the climatic factors sustained over a long time period. Climate change may be due to natural factors including long-term changes in the solar cycle or may be induced by human activities including the use of fossil fuels which generate greenhouse gas emission including carbon dioxide, methane and water vapour. An increase in the greenhouse gas emissions creates a blanketing effect of the earth's atmosphere which traps heat near the land surface resulting in increased air temperatures, increased land surface temperatures and associated changes in the hydrological cycle (IPCC 2007; NASA 2005).

The performance of pavement structures is directly influenced by the resilient modulus of each unbound material and forms the basis for characterizing the strength of subgrades. The resilient moduli of subgrades are influenced by seasonal changes in climatic factors and typically fluctuate seasonally due to changes in subgrades water contents (Perez-Garcia, et al. 2016; Bulut, et al. 2013; Khoury, et al. 2011; Khoury, et al. 2010). Climatic factors directly impact infiltration characteristics, water contents and associated material properties, mechanistic response and performance of subgrades (Perez-Garcia, et al. 2016; Modeste, et al. 2015; Khoury, et al. 2010; Zapata, and Houston 2008; Zapata, et al. 2007, Ovik, et al 2000). To improve the climate resilience of pavement structures, it has been deemed necessary to better understand the climatic factors which influence the mechanical response of pavement structures (Perez-Garcia, et al. 2016; United Nations Economic Commission for Europe 2013; Khoury, et al. 2010; Zapata, and Houston 2008; Zapata, et al. 2007, Ovik, et al 2000).

Studies have indicated that the impact of climatic factors on the performance of transportation infrastructure have a direct impact on the economy. There are significant costs for upgrading existing and for implementing new infrastructure so that the infrastructure can safely withstand and mitigate the impact of climatic factors. Hence, the impact of climatic factors should be incorporated in the short-term and long-term investment decisions for implementing transportation infrastructure (Todd 2014; Weisbrod, and Reno 2009; National Research Council 2008). It is necessary to consider the cost of implementing climate resilient infrastructure relative to the cost of reduced performance or failure of infrastructure inundated by events induced by changes in climatic factors (Li, et al. 2011; National Research Council 2008).

Studies have indicated that climatic factors directly impact the water and heat transfer and resilient moduli of subgrades (one of the primary objectives of this study). These climatic factors and the environmental conditions have a direct impact on water and heat transfer, the resilient modulus of the unbound materials and the performance of pavement structures. In addition to the climate and environment, the resilient modulus of each unbound material is influenced by the soil type, compaction method, stress state, and water contents. Precipitation induced increase in water contents of unbound layers results in a decrease in resilient moduli of subgrades (Gudipudi, et al. 2017; Han, et al 2016; Li, et al. 2011; Bayomy, and Salem 2005; Ovik, et al. 2000; Hein, and Jung 1994; Benson, and Othman 1993; Mahoney, et al. 1988; Lary, and Mahoney 1984).

Studies have noted that fluctuations in precipitation result in corresponding fluctuations in water contents of Clay subgrades as shown in Figure 2.1. The analysis of the data shown in Figure 2.1 also indicated that changes in water contents of subgrades at shallow depths respond more quickly to changes in precipitation (shorter lag times) relative to the response of changes in water contents of subgrades at lower depths to changes in precipitation (Thiam, et al. 2013). Irrespective of the reference depth within subgrades, studies have shown that lag times between precipitation event and changes in water contents of subgrades. During unfrozen conditions, reductions in resilient moduli of Silt and clayey Sand subgrades are primarily due to increases in precipitation induced water contents as shown in Figure 2.2. The analysis of the data presented in Figure 2.2 indicated that the impact of precipitation on changes in water contents and resilient moduli of unbound materials is influenced by the rate of infiltration. The rate of infiltration is influenced by the time and depth dependent hydraulic properties of materials which vary with the soil type (Bayomy, and Salem 2005).

Studies have also indicated that the impact of climatic factors and the environment on the water and heat transfer within pavement structures is also influenced by the geometric design characteristics and drainage system in pavement structures (Mohammad 2021; Guyer 2018; Vanek, et al. 2014; Ovik, et al. 2000; Lytton, et al. 1993).

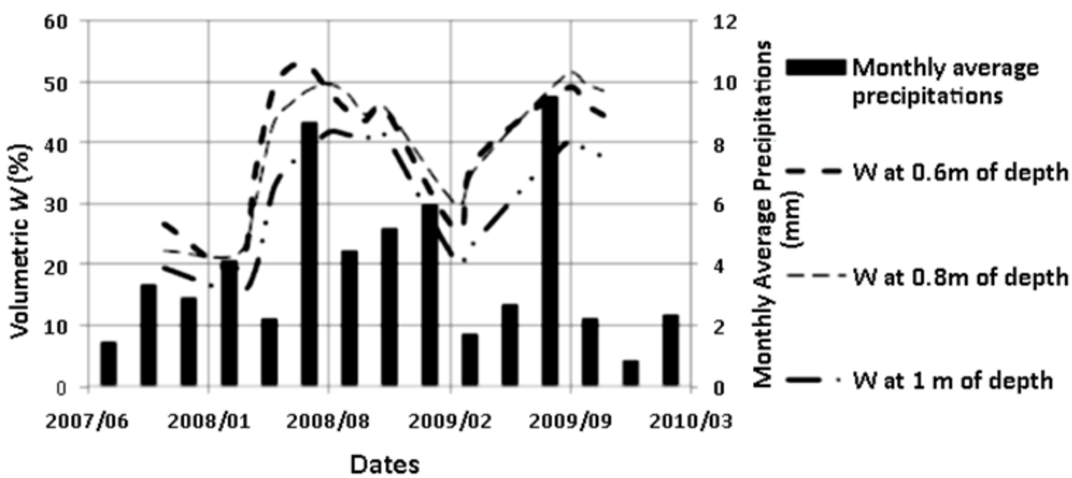

Figure 2.1: Precipitation vs. volumetric water content within Clay subgrade (Thiam, et al. 2013)

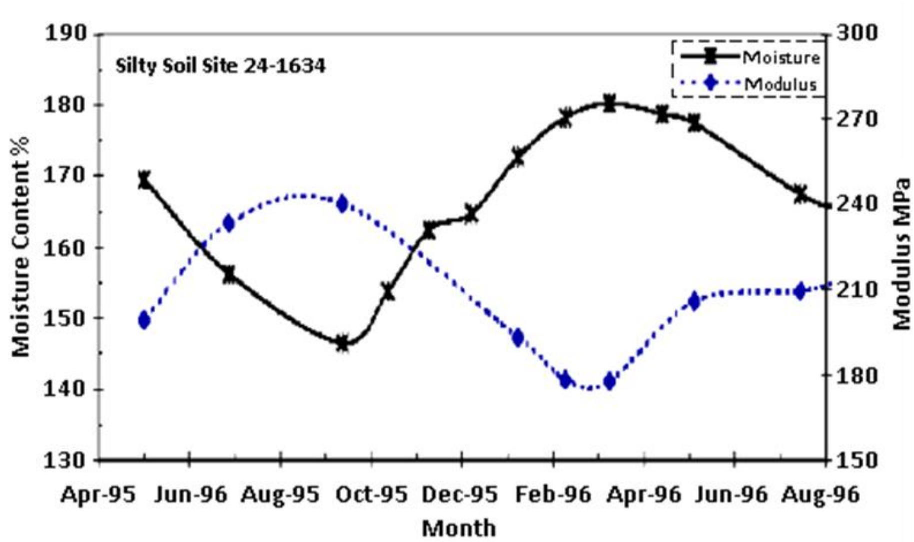

(a). Flexible pavement with fine Silt (A-4) subgrade

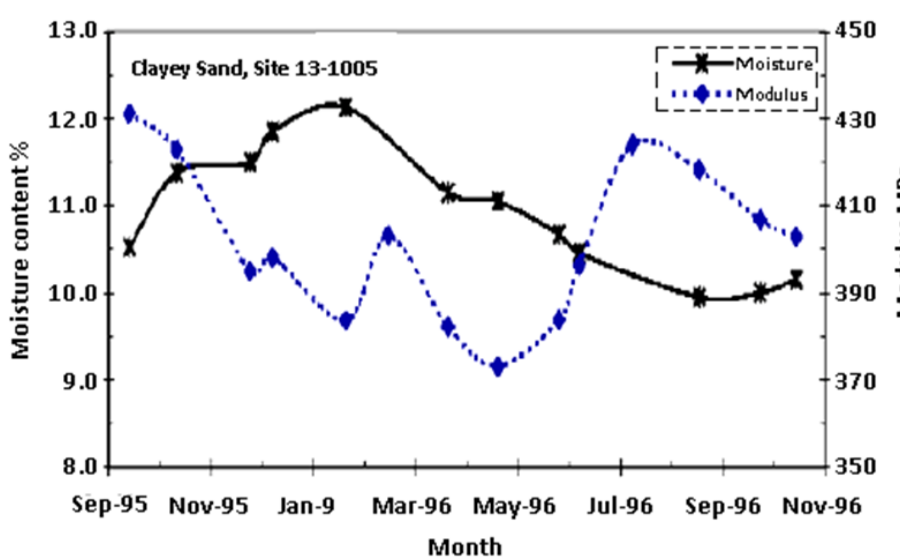

(b). Flexible pavement with fine clayey Sand (A-6) subgrade

Figure 2.2: Water content vs. resilient modulus of the subgrade (Bayomy, and Salem 2005)

Studies have indicated that air temperature influences the temperature profile within the pavement structure which impacts water contents, the hydraulic and mechanical properties of unbound materials. Temperature changes result in unfrozen conditions during the summer, fall and spring, and frozen conditions during the winter. The resilient moduli of unbound materials are highest during freezing conditions, while resilient moduli of unbound materials decrease significantly during thawing due to increased water contents during thaw conditions (Gudipudi, et al. 2017; Ovik, et al. 2000; Lary, and Mahoney 1984). Hydraulic and mechanical properties of unbound materials are further impacted by freeze and thaw cycles due to temperature fluctuations. Freeze and thaw cycles result in micro-fissures which develop in unbound materials resulting in an increase in hydraulic conductivity and increases water contents (Domitrović, et al. 2019; Badeli, et al. 2018; McCartney, et al. 2010; Henry, et al. 2005; Houston, et al. 2006; Lary, and Mahoney 1984).

Studies have indicated that an increase in the air temperature and precipitation result in increased pavement distress. Asphalt concrete (AC) wearing courses used in flexible pavement structures are more sensitive to changes in air temperature. Changes in air temperature also impact the stability of AC wearing courses and rut depths within AC wearing courses. Resilient moduli of AC wearing courses are at minimum values during the summer when air temperatures are highest, and are at maximum values during freezing conditions as shown in Figure 2.3 (Domitrović, et al. 2019; Badeli, et al. 2018; Ovik, et al. 2000).

Temperature gradients between the surface and bottom of Portland cement concrete (PCC) wearing courses used in rigid pavement structures result in curling stress in PCC wearing courses. The curling stress is due to compression at the cooler surface and expansion at the warmer bottom section of the PCC wearing course. An increase in precipitation may result in the presence of excess pore water at the interface of PCC wearing courses and underlying base courses. This excess pore water causes pumping, faulting and structural failure of PCC wearing courses. The structural failure of PCC wearing courses is also due to frost heaving caused by freeze and thaw cycles (Luo, et al. 2022; Gudipudi, et al. 2017; Ovik et al. 2000).

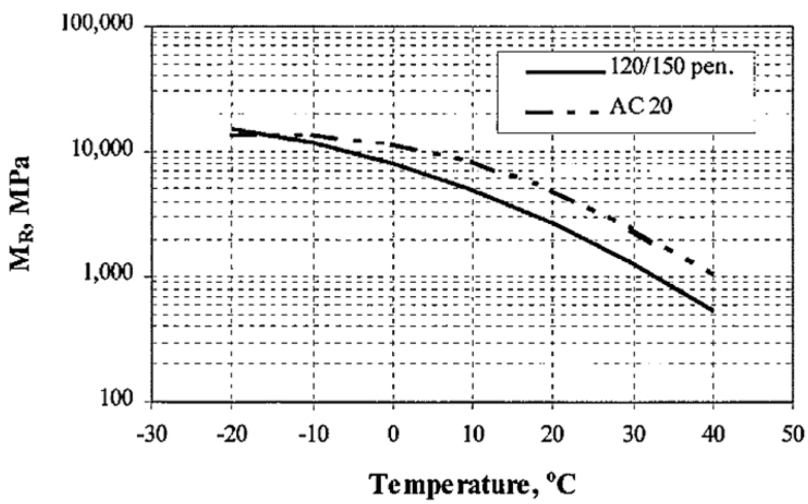

Figure 2.3: Resilient modulus of AC wearing course vs temperature (Ovik et al. 2000)

2.4 Modeling the Impact of LCI on Water and Heat Transfer in Unsaturated Subgrades

As discussed previously, water and heat transfer FEA modeling were conducted as part of this study to investigate the impact of climatic factors on water and heat transfer within subgrades and the impact on resilient moduli of subgrades. The impact of climatic factors was represented by LCI boundary conditions in the FEA modeling.

LCI boundary conditions represent precipitation, air temperature, net solar radiation, and evapotranspiration in addition to infiltration and runoff. LCI boundary conditions incorporated in the 2-D FEA modeling were represented by the net infiltration and the surface temperature. LCI boundary conditions incorporated in this study are based on the surface mass balance equation presented in Eq. 2.5 (Bryce, et al. 2021; GeoSlope 2020; Rivera-Hernandez, et al. 2019; Huang, et al. 2015; Bulut, et al. 2014; Jiji 2009; Incropera, et al. 2007; Gitirana Jr, et al. 2006; Gitirana Jr, et al. 2005; Yang, et al. 1998; Newman 1995; Farouki 1987; de Vries 1975). The FEA modeling accounted for liquid water and water vapour transfer, and the influence of changes in water contents on the hydraulic conductivity of the subgrade. The FEA modeling also accounted for the heat transfer due to heat conduction, heat radiation, heat convection consisting of natural and forced convection with water transfer, evaporation, and condensation (Bryce, et al. 2021; GeoSlope 2020; Bulut, et al. 2014; Bulut, et al. 2013; Ravichandran, and Krishnapillai 2011; Jiji 2009; Incropera, et al. 2007; Gitirana Jr, et al. 2006; Yang, et al. 1998; Newman 1995; Farouki 1981; Johansen 1975; de Vries 1975).

$$(q_P + q_M)\ cos\alpha + q_E + q_R = q_I \qquad (2.5)$$

q_p = Rainfall flux, q_M = Snowmelt flux, $Cos\ \alpha$ = Angle for converting q_p and q_m to a normal to the interface boundary, q_E = Evaporation flux, q_R = Runoff flux, and q_I = infiltration flux.

The FEA modeling incorporated potential evapotranspiration using the Penman-Monteith equation presented in Eq. 2.6 to Eq. 2.8 (Allen, et al. 1998). These equations account for the energy balance which is represented by radiation, aerodynamic processes and water vapour transfer to the atmosphere above the crop canopy which is influence by the aerodynamic resistance. The evapotranspiration controls the water transfer from the pavement structure and adjacent vegetation to the atmosphere through evaporation and transpiration (GeoSlope 2020; Vinnikov, et al. 1999; Allen, et al. 1998; van den Honert 1948).

$$q_{PET} = q_{\underset{PET}{rad}} + q_{\underset{PET}{aero}} = \left(\frac{1}{h_{fg}}\right)\left[\left\{\frac{\Gamma\left(q_n - q_g\right)}{\Gamma+\gamma\left(1+\frac{r_c}{r_a}\right)}\right\} + \left\{\frac{\rho_\alpha C_{S\alpha}\left(\frac{p_{\alpha_{v0}} - p_{\alpha_v}}{r_a}\right)}{\Gamma+\gamma\left(1+\frac{r_c}{r_a}\right)}\right\}\right] \qquad (2.6)$$

$$r_a = \frac{1}{uk^2}\left[ln\left(\frac{Z_{ref}-d}{Z_{om}}\right)\right]\left[ln\left(\frac{Z_{ref-d}}{Z_{oh}}\right)\right] \qquad (2.7)$$

$$r_c = \left(\frac{r_l}{0.5LAI}\right) = \left(\frac{200.0}{0.5LAI}\right) \quad (2.8)$$

q_{PET} = Potential evapotranspiration flux (mm/day); h_{fg} = Latent heat of vaporization (MJ/kg); q_n = Net radiation (MJ/m^2/day); q_g = Ground heat flux (MJ/m^2/day); ρ_a = Mean air density in the atmosphere (kg/m^3); C_{sa} = Specific heat of moist air (MJ/kg ^{o}C); $P^a_{v0} - p^a_v$ = Vapour pressure deficit (kPa); P^a_{v0} = Saturated vapour pressure at mean air temperature (kPa); p^a_v = Actual vapour pressure of air at referenced height (kPa); r_c = Crop canopy bulk surface resistance (sec/m); r_a = Aerodynamic resistance (sec/m); γ = Psychrometric constant ⇒ 0.0665 (kPa/^{o}C); Γ = Slope of the saturation vapour pressure vs. temperature curve (kPa/^{o}C); u = Wind speed (m/sec); k = von Karman's constant ⇒ 0.41; Z_{ref} = Measured height of wind, humidity, and temperature; d = Zero-plane displacement height of wind profile ⇒ (0.6666 x Z_c); Z_{Om} = Surface roughness height for momentum flux ⇒ (0.123 x Z_c); Z_{Oh} = Surface roughness height for heat and vapour flux ⇒ (0.1 x Z_{Om}); Z_c = Crop height; r_l = Bulk stomatal resistance of well-illuminated leaf ⇒ 100.

2.4.1 Boundary Conditions used in the Water and Heat Transfer FEA Modeling

This study consists of investigating the impact of climatic factors on water and heat transfer using FEA modeling which was conducted using various boundary conditions. The land climate interaction (LCI) based finite element analyses (FEA) modeling is dependent on the boundary conditions assigned to the FEA model. The simulation of LCI was represented by LCI boundary conditions which consists of two components: evaluating the net infiltration at ground surface and evaluating the root water uptake (GeoSlope 2020; Franke, et al. 1987). The water transfer is simulated using natural boundary conditions and/or essential boundary conditions which are further characterized as system dependent or system independent (GeoSlope 2020; Bulut, and Javid 2019; Franke, et al. 1987; Bear 1979; Neuman, et al. 1974).

LCI is assessed as a system dependent boundary condition where the potential fluxes are influenced by the precipitation and evaporation, while the actual fluxes are dependent on the soil's transient water content. The surface runoff or surface water accumulation is produced when the rate of precipitation exceeds the infiltration capacity of the soil. For such cases, the infiltration rate is dependent on the infiltration capacity of the soils rather than the rate of precipitation. Natural boundary conditions are satisfied after the problem solution is achieved, while the essential boundary conditions are applied explicitly on the domain. Natural boundary conditions are typically used to simulate liquid water transfer influenced by LCI and groundwater flow. The Neuman boundary conditions are natural boundary conditions which are represented by the specified flux boundary conditions or the zero-flow boundary conditions. The specified flux boundary condition represents the water flow rate across specified boundaries. The water flux boundary condition represents a specific discharge of water into or out of the system and is applied normal to the system. The infiltration flux is a natural boundary condition which is typically applied to the surface in the two dimensional (2-D) and three dimensional (3-D) FEA models (GeoSlope 2020; Rivera-Hernandez, et al. 2019; Bulut, and Javid 2019; Huang, et al. 2015; Franke, et al. 1987; Bear 1979; Neuman, et al. 1974). In one dimensional (1-D) liquid water transfer modeling, it is assumed that infiltration through the ground surface is eventually transferred to the deep groundwater system and is assessed as net percolation. For such cases, the unit gradient boundary condition is used to represent the condition where the net percolation is equal to the hydraulic conductivity at a constant negative porewater pressure. Hence, a unit gradient boundary condition is typically applied at the bottom of 1-D FEA models (GeoSlope 2020; Geo-Slope 2015).

A zero-flow boundary condition is used for cases where the net flow rate is zero. It is assumed that a zero-flow boundary condition applies where no boundary condition is applied (GeoSlope 2020; Rivera-Hernandez, et al. 2019).

The essential boundary conditions are used for liquid water transfer influenced by the total head of water on a system with a static water table and are associated with steady state flow. Dirichlet boundary conditions are essential boundary conditions based on the constant head used in groundwater modeling. The use of the essential boundary conditions are based on the assumption that the groundwater regime is independent of the surface water flow (Bulut, and Javid 2019; Franke, et al. 1987; Bear 1979).

2.5 Summary

The current version of EICM incorporated in the Mechanistic Empirical Pavement Design Guide (MEPDG) accounts for only liquid water and neglects water vapour transfer within the pavement structure. In addition, the current version of EICM accounts for infiltration only through surface cracks and neglects LCI beyond the pavement surface.

Chapter 3 Pavement Design Processes and the Mechanistic Empirical Pavement Design Guide (MEPDG)

3.1 Introduction

Chapter 3 presents an overview of the procedures used for the design and construction of traditional flexible and rigid pavement structures. Chapter 3 also presents the framework for the design of economical and sustainable pavement structures. Chapter 3 also provides details on the primary features of the Mechanistic Empirical Pavement Design Guide (MEPDG) and the Enhanced Integrated Climate Model (EICM). The discussion includes the environmental adjustment factor incorporated in EICM to account for the influence of the climate and environment on the resilient modulus of subgrades. The Chapter also provides an overview of the impact of changes in volumetric water contents and stress state within the pavement materials on resilient moduli and shear strengths of pavement materials, and their impact on pavement performance.

Chapter 3 presents the primary features of the current version of EICM including the model components which form part of EICM and the primary limitations in EICM in predicting water and heat transfer within subgrades. It provides a summary of studies conducted to evaluate, calibrate and validate EICM in predicting water and heat transfer within subgrades in various climates.

The Chapter also provides detailed analyses of the studies conducted to calibrate and validate EICM which are also used for evaluating the accuracy of the Quantitative Empirical Model (QE Model) in predicting water and heat transfer within subgrades at selected sites in various climates. Chapter 3 also provides a detailed analytical summary of studies highlighting the primary limitations in EICM. The Chapter also provides a summary of EICM's primary limitations which are mitigated by the QE Model.

3.2 Overview

Pavement structures are categorized as flexible or rigid. A flexible pavement typically consists of an asphalt concrete (AC) layer as the wearing course underlain by a compacted granular base course, a granular subbase and a subgrade layer. A rigid pavement typically consists of a Portland cement concrete (PCC) or hydraulic cement concrete (HCC) layer as the wearing course placed on a compacted open graded drainage layer (OGDL) or a granular base course. The base course or OGDL is underlain by a compacted granular subbase layer placed over a compacted subgrade. The material layers are typically compacted in accordance with the design specifications based on 95.0 % to 100.0 % of the standard proctor maximum dry density (SPMDD). A typical cross section detail of a flexible pavement structure and a rigid pavement structure is presented in Figure 3.1a and Figure 3.1b respectively (MTO 2013; TAC 1997).

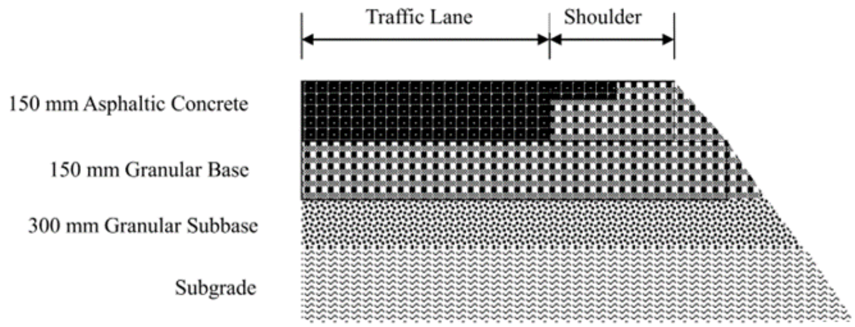

(a)

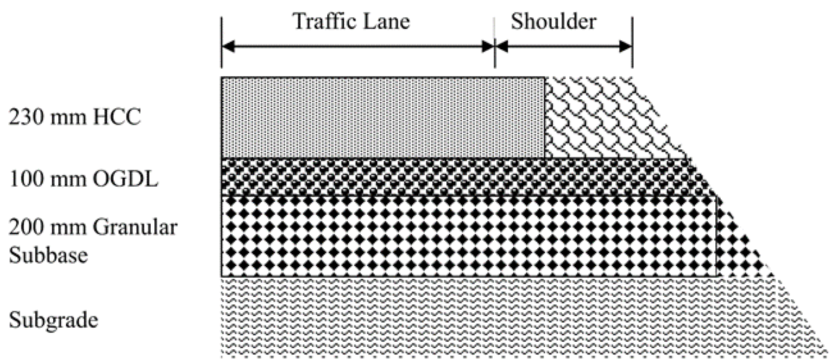

(b)

Figure 3.1: Conventional cross section details of: (a) flexible and (b) rigid pavement structures (MTO 2013)

The pavement design process is typically implemented using project implementation criteria that include defining the project scope, design specifications, construction and maintenance strategies. The primary objective of the pavement design process is to develop an economical pavement cross section to meet the expected serviceability and performance criteria (MTO 2013; TAC 1997). The design criteria used to develop a design pavement cross section include evaluating site geology, engineering properties of pavement materials, climatic factors, expected traffic loading, pavement performance, and economic factors. The design criteria include the functional classification of road systems consisting of the following:

- Freeways: Consist of multiple lanes to facilitate free flow of traffic;
- Arterial roads: Consist of two or more lanes with restricted access;
- Collectors: Typically consist of two lanes to facilitate the flow of traffic and access to adjacent properties; and

- Local roads: Typically consist of two lanes of traffic primarily to facilitate access to adjacent properties and services within an adjacent community.

The functional classification of highways also includes differentiating between divided and undivided highways. In divided highways, the directions of travel are typically separated by a median as shown in Figure 3.2. Unlike a divided highway, the pavement structure in each direction of travel in an undivided highway is not physically separated. The median on a divided highway may provide operational benefits including providing areas for the storage of snow and for future lane expansion (Chiu, et al. 2017; Vanek, et al. 2014; Gulliver, et al. 2014; Banks 2002). Although the pavement surface is relatively impervious and facilitates minimal infiltration of water into the pavement structure, the median and ditches (on a divided highway) may facilitate ponding and water transfer into the pavement structure (Gulliver, et al. 2014; Banks 2002). The water and heat transfer finite element analysis (FEA) modeling which forms part of this study was conducted using two divided highway sections.

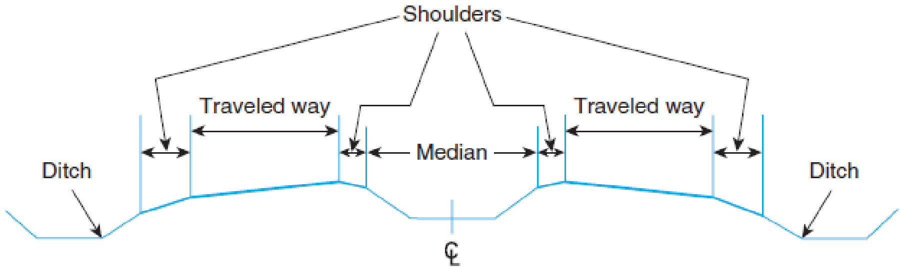

(a)

(b)

Figure 3.2: A typical divided highway ((a) Vanek, et al. 2014; (b) Highway No.2, in the north of Calgary, AB, Canada: Google Earth 2023)

The pavement design criteria incorporates the geometric characteristics of the pavement structure and are influenced by the traffic volume, design speed and existing site conditions (Vanek, et al. 2014; MTO 2013; TAC 1997). The surface and internal drainage design form an integral component of the pavement design criteria. The drainage system is intended to mitigate the impact of surface water infiltration and groundwater flow on the resilient moduli of pavement materials and pavement performance. The approach used in MEPDG version 1.1 for designing pavement structures is provided below (Yut, et al. 2014; TAC 2014; TAC 1997; AASHTO 1998).

- A trial pavement design cross section is developed using initial input data;
- The performance prediction of the trial pavement design cross section is evaluated against the limiting distress criteria; and
- If the predicted distress for the trial pavement design cross section exceeds the limiting distress criteria, the trial pavement design cross section is revised.

The conventional pavement design framework used in Ontario; Canada is shown in Figure 3.3.

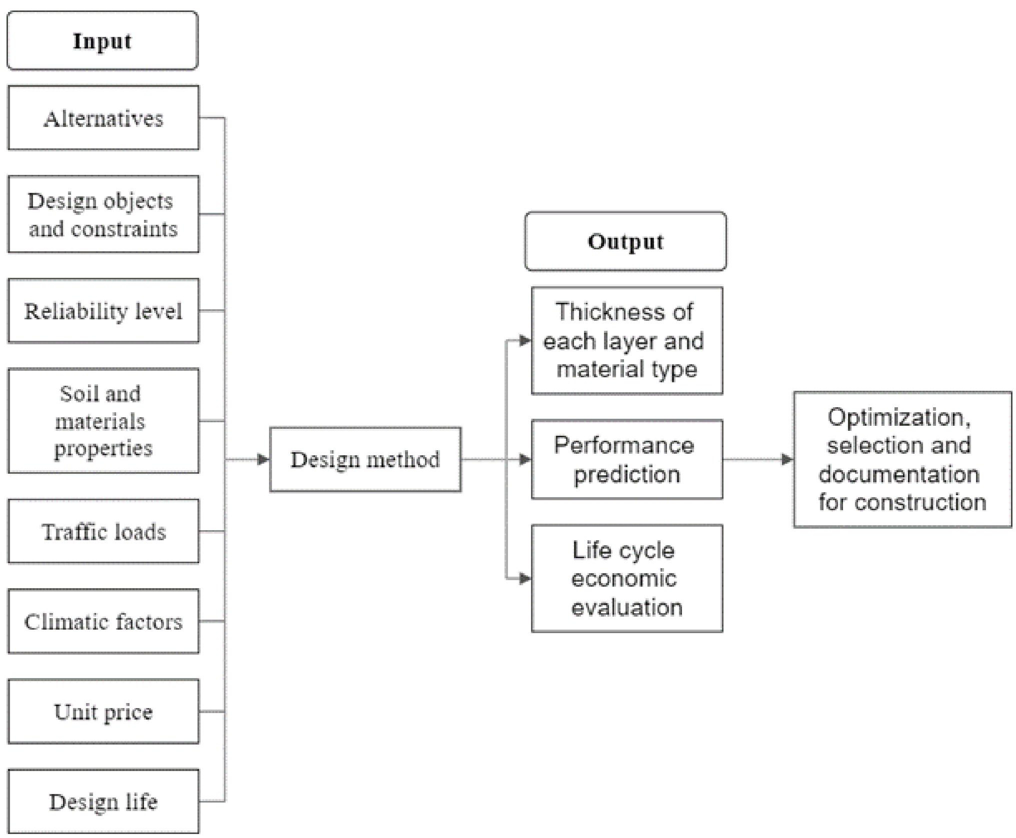

Figure 3.3: The conventional pavement design framework used in Ontario, Canada (TAC 2014)

Studies have shown that the convectional pavement design approach for flexible pavements is not adequate for mitigating the impact of climatic factors on pavement performance. Hence, many highway agencies implement a sustainable pavement design system which includes evaluating long-term pavement performance by incorporating the pavement life cycle assessment (PLCA) and the pavement life cycle cost assessment (PLCCA) as shown in Figure 3.4 (Asres, et al. 2022).

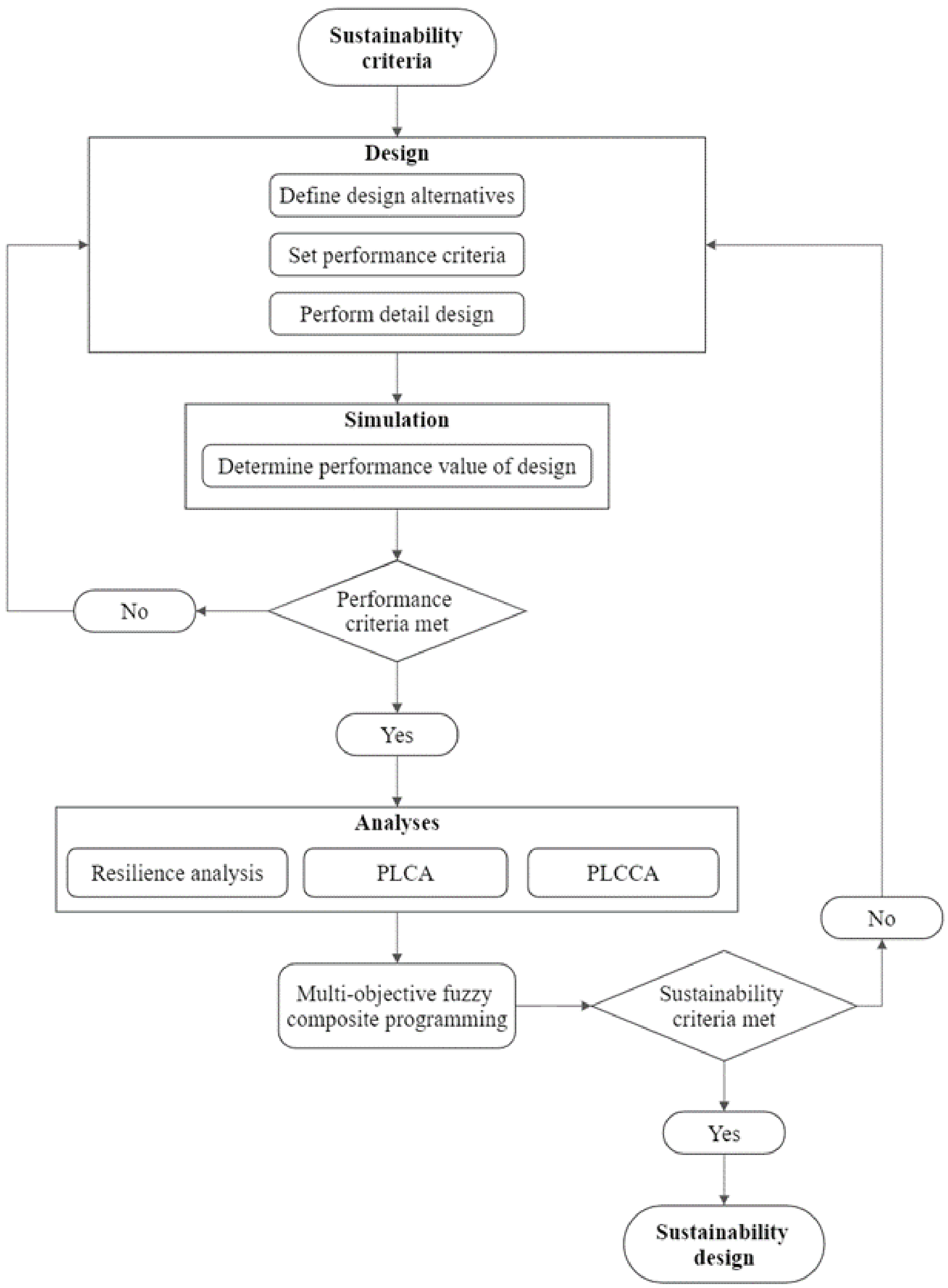

Figure 3.4: The design framework for sustainable flexible pavements (Asres, et al. 2022)

3.3 The Pertinent Features of MEPDG

The AASHTO Road Test carried out from 1958 to 1961 facilitated the development of the AASHTO 1962 Design Guide which was updated in 1972 (The AASHTO 1972 Design Guide). The AASHTO 1972 Design Guide was updated from 1981 to 1993 and incorporated improved criteria for Portland cement concrete pavements and an empirical design approach (Applied Research Associates Inc. 2004; AASHTO 1993). Due to limitations in the empirical design method, the National Corporative Highway Research Program (NCHRP) implemented a mechanistic design approach which resulted in the development of the Mechanistic Empirical Pavement Design Guide (MEPDG) version 0.7 to the current MEPDG version 1.1 developed through NCHRP 1-37A Project to NCHRP 1-40D Project (AASHTO 2010; Witczak 2007; Applied Research Associates Inc. 2004). MEPDG was developed to facilitate sensitivity analyses in pavement design including performance evaluation throughout the pavement service life. The intention was to simulate the impact of climatic factors and drainage on the material properties. MEPDG consists of three major design components: materials, structural response, and performance prediction criteria. MEPDG consists of a set of input data (modules) used for simulating pavement distress. The modules include traffic datasets, climate and environment datasets used as input in the Enhanced Integrated Climate Model (EICM). The modules also include materials characterization, pavement response (based on finite element analyses), distress prediction, and a smoothness prediction model (McCartney, et al. 2010; Applied Research Associates Inc. 2004).

EICM consists of internal output data which include the volumetric water content, pore water pressure, temperature at each node over time; and the degree of saturation. The degree of saturation is assessed as being in equilibrium when the groundwater table is static and there is an absence of surface cracks so no infiltration occurs through the wearing courses. The external output data from EICM includes the composite environmental adjustment factors (F_{env}) as shown in Eq. 3.1. The depth and time dependent F_{env} is the primary output in EICM, and it is used in the structural analysis of the unbound material layers in flexible and rigid pavements when the analysis is conducted using the linear elastic theory. F_{env} accounts for the influence of the environmental factors including water, freeze and thaw, and thaw recovery conditions on the unbound materials properties. F_{env} consists of an environmental adjustment factor for the frozen condition (F_F), an adjustment factor for the thaw recovery condition (F_R) and an adjustment factor for the fully thawed condition (F_U). F_{env} is influenced by the predicted volumetric water contents which form part of the internal output of EICM. F_{env} is multiplied by the resilient modulus of the material layer at optimum water content, maximum dry density and at any stress state (M_{ROpt}) to obtain the depth and time dependent resilient modulus of the material layer (M_R). The calculated M_R forms part of the external output of EICM. The evaluation of M_R also incorporates the influence of the stress state and water-density relationship (Bulut, and Javid 2019; Bulut, et al. 2014; Applied Research Associates Inc. 2004; Dempsey, et al. 1985).

$$F_{env} = \frac{\{h_{total} * t_{total}\}}{\sum_{t=1}^{total} \left\{ \sum_{node=1}^{n} \left(\frac{h_{node}}{F_{node,t}} \right) \right\}} \tag{3.1}$$

F_{env} = Composite environmental adjustment factor for the material layer under consideration; F_{node},t = Environmental adjustment factor at a specific node and time calculated using F_F, F_R or F_U based on whether the material is in a frozen, thawed or unfrozen condition respectively; t = time; t_{total} = Total number of time increments for which the resilient modulus is being calculated; h_{node} = Length of the spring assigned to the node; and h_{total} = Total height of the material layer.

Previous studies have indicated that the resilient modulus of each unbound material layer is influenced by seasonal changes in in-situ volumetric water contents and the associated changes in in-situ degree of saturation (Perez-Garcia, et al. 2016; Modeste, et al. 2015; Khoury, et al. 2011; Khoury, et al. 2010; Zapata, and Houston 2008; Zapata, et al. 2007; Ovik, et al. 1999; Drumm, et al. 1997). EICM incorporates the relationships between the ratio of the in-situ resilient modulus and resilient modulus at the optimum water content and maximum dry density (M_r / M_{ropt}) and the difference between the in-situ degree of saturation and the degree of saturation at optimum water content (S - S_{opt}) as shown in Figure 3.5. The relationships between "M_r / M_{ropt}" and "S - S_{opt}" are used in EICM and MEPDG to calculate the unfrozen environmental adjustment factor (F_U). The F_U value is used as input for calculating the unfrozen composite environmental adjustment factor (F_{env}) which is used for calculating the in-situ resilient modulus (Applied Research Associates Inc. 2004).

The analyses of data presented in Figure 3.5 show that changes in in-situ resilient moduli of subgrades are influenced by changes in the in-situ degree of saturation. The analyses of data presented in Figure 3.5 also show that the "S - S_{opt}" values have a higher impact on the "M_r / M_{ropt}" values at dry of the optimum water content (when S is less than S_{opt}) relative to the impact of the "S - S_{opt}" values on the "M_r / M_{ropt}" values at wet of the optimum water content (when S is more than S_{opt}). The data presented in Figure 3.5 also show that for water contents dry of the optimum water content, "S - S_{opt}" values have a higher impact on the "M_r / M_{ropt}" values of fine-grained subgrades. For water contents wet of the optimum water content, the "S - S_{opt}" values have a higher impact on the "M_r / M_{ropt}" values of coarse-grained subgrades. For water contents significantly dry of the optimum water content (near the residual water content), changes in "S - S_{opt}" values induce minimal changes in the "M_r / M_{ropt}" values for both fine-grained and coarse-grained subgrades. Similarly, for water contents significantly wet of the optimum water content (near the saturated water content), changes in "S - S_{opt}" values induce minimal changes in the "M_r / M_{ropt}" values for both fine-grained and coarse-grained subgrades.

This implies that resilient moduli of fine grained subgrades are influenced primarily by the subgrade type, degree of saturation and compacted density. But resilient moduli of coarse grained subgrades are influenced primarily by the degree of saturation and compacted density (Kim, and Siddiki 2006; Li, and Seilg 1994). The data presented in Figure 3.5 also show that at water contents wet of the optimum water content, both fine-grained and coarse-grained subgrades are subjected to a smaller rate of change in the resilient modulus. This observation implies that the smaller rate of change in the resilient modulus occur because both fine-grained and coarse grained subgrades are subjected to lower volume change when compacted at wet of optimum water content.

The resilient moduli of expansive fine-grained subgrades and subgrades consisting of Sand generally have a low sensitivity to changes in water contents up to the saturated water content. The resilient moduli of expansive fine-grained subgrades are impacted by the extent of the swelling and shrinkage due to variations in the degree of saturation. Hence, expansive fine-grained subgrades are typically compacted at water contents wet of the optimum water content to control the extent of the volume change (Gautam, et al. 2019; Fredlund, and Hung 2001). However, resilient moduli of expansive fine-grained subgrades have a high sensitivity to changes in water contents which are significantly wet of the optimum water content. Expansive fine-grained subgrades are subjected to high permanent strain at water contents wet of the optimum water content (Soliman, and Shalaby 2010).

Previous studies also show that EICM both underestimates and overestimates the in-situ degree of saturation (Quintero 2007; Bayomy, and Salem 2005). These studies also show that EICM primarily underestimates the in-situ degree of saturation (Hall, et al. 2013; Quintero, 2007; Bayomy, and Salem 2005). The data presented in Figure 3.5 imply that the primary reason for EICM overestimating in-situ resilient moduli of subgrades is because EICM underestimates the in-situ degree of saturation. EICM overestimating in-situ resilient moduli of subgrades results in pavement structures designed using EICM and MEPDG having subgrades with actual in-situ resilient moduli that are lower than resilient moduli predicted using EICM. Hence, EICM overestimating resilient moduli of subgrades results in pavement structures being subjected to higher rutting and lower performance under traffic loading.

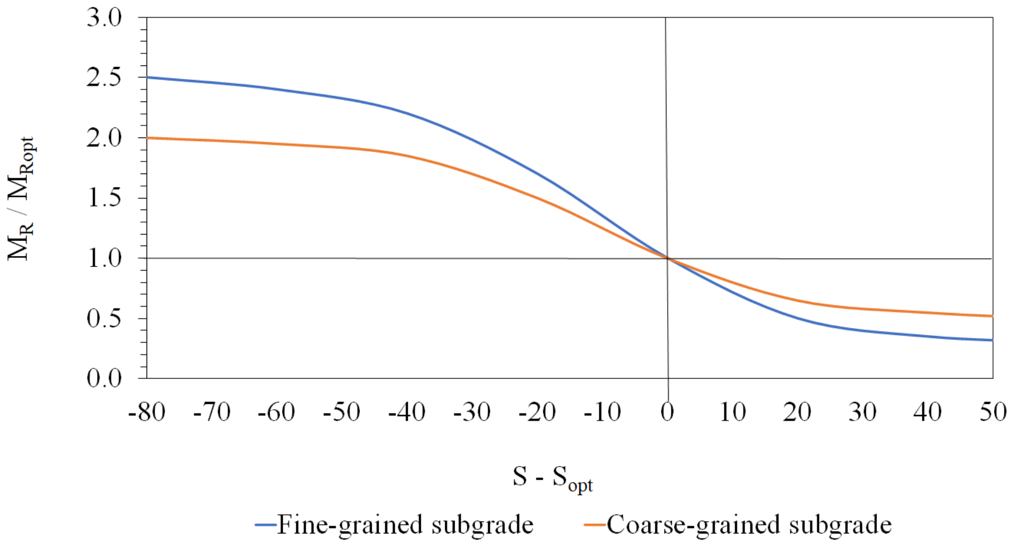

Figure 3.5: The impact of changes in in-situ degree of saturation on the ratio of the in-situ and optimum resilient moduli (Applied Research Associates Inc. 2004)

The 2007 version of MEPDG accounts for the relationships between "M_r / M_{ropt}" and "S - S_{opt}" presented in Figure 3.5 to account for the impact of variations in in-situ water contents on the predicted in-situ M_R of subgrades by incorporating Eq. 3.2. Eq. 3.2 incorporates the M_{Ropt} of the subgrade because MEPDG assumes that subgrades are initially compacted at approximately the optimum water content and maximum dry density (Zapata, et al. 2007; Witczak, et al. 2000). The M_{Ropt} and the M_R values overtime are impacted by the subgrade type, initial compaction effort, degree of saturation and freeze thaw cycles (Kim, and Siddiki 2006; Ovik, et al. 2000; Applied Research Associates Inc. 2004).

Eq. 3.2 is an empirical relationship used in the current version of EICM to compute the environmental adjustment factor for the unfrozen or fully recovered materials (F_U). The model accounts for the influence of the degree of saturation on seasonal variations in the resilient modulus of subgrades. This approach is widely used because the parameters do not require calibrating as they require specific values of the M_{ROpt}, S_{opt} and "S". The model is based on empirical regression constants and neglects the stress state of subgrades. The 2004 and 2007 versions of MEPDG also neglect the influence of climatic factors on the seasonal fluctuations in the resilient modulus (Zapata, et al. 2007, Witczak, et al. 2000). Further analysis indicated that the F_U factor also neglects the impact of climatic factors on the degree of saturation. The F_U factor inaccurately accounts for the impact of climatic factors on the resilient modus of the subgrade.

$$log\{F_U\} = log\left\{\frac{M_R}{M_{ROpt}}\right\} = a + \frac{\{b-a\}}{1+EXP\left\{ln\left(\frac{-b}{a}\right)+k_m(S-S_{opt})\right\}} \qquad (3.2)$$

M_R = Resilient modulus at a specific water content or at a specific degree of saturation; M_{ROpt} = Resilient modulus at the optimum water content and at the maximum dry density; S_{opt} = Degree of saturation at the optimum water content (in decimals); S = Degree of saturation at a specific water content (in decimals); a = Minimum of log $\{M_R/M_{R\text{-}opt}\}$. For fine grained soils, a = -0.5934, and for coarse grain soils, a = -0.3123; b = Maximum of log $\{M_R/M_{R\text{-}opt}\}$. For fine grained soils b = 0.4, and for coarse grain soils, b = 0.3; k_m = Regression parameter. For fine grained soils k_m = 6.1324, and for coarse grained soils k_m = 6.8157.

The 2004 version of MEPDG also incorporates the M_{Ropt} of subgrades and accounts for the influence of applied shear stress as shown in Eq. 3.3. Eq. 3.3 neglects the influence of variations in water contents on the resilient moduli of subgrades (Applied Research Associates Inc. 2004; Uzan 1985). Eq. 3.3 also neglects the impact of climatic factors on the resilient modulus. Neglecting the impact of climatic factors in the design of pavement structures and on the pavement life cycle result in the implementation of uneconomical and unsustainable pavement structures (Asres, et al. 2022).

The predicted resilient modulus over time (M_R) which incorporates the impact of the environmental factors is calculated using Eq. 3.4 (Zapata, et al. 2007; Applied Research Associates Inc. 2004). The M_R and the associated pavement performance evaluated in MEPDG may be improved by incorporating climatic factors in F_U and F_{env} (Zapata, et al. 2007; Drumm, and Meier 2003).

$$M_{ROpt} = \left\{k_1 p_a * \left\{\frac{\theta_b}{p_a}\right\}^{k_2} * \left\{\frac{\tau_{oct}}{p_a} + 1\right\}^{k_3}\right\} \qquad (3.3)$$

M_{ROpt} = Resilient modulus at the optimum water content; θ_b = Bulk stress; τ_{oct} = Octahedral shear stress; p_a = Atmospheric pressure; and k_1, k_2, and k_3 = Fitting parameters.

$$M_R = F_{env} * M_{ROpt} \qquad (3.4)$$

M_R = Resilient modulus at a specific depth and time; F_{env} = Composite environmental adjustment factor for the material layer under consideration; and M_{ROpt} = Resilient modulus at optimum conditions (optimum water content and maximum dry density).

The analyses of data presented in Figure 3.6 show that the resilient modulus decreases due to an increase in the unfrozen water content (Kim, and Siddiki 2006; Ovik, et al 2000). The data presented in Figure 3.6 also show that changes in resilient moduli of subgrades are more sensitive to changes in water contents relative to the sensitivity of resilient moduli of aggregate base courses to changes in water contents. The data presented in Figure 3.6 also show that resilient moduli of aggregate base courses and subgrades generally fluctuate in response to changes in water contents. The analyses of data presented in Figure 3.6

also show that the resilient modulus of both materials is generally at a minimum during the thaw period. The data also show that the aggregate base course thaws earlier than the subgrade which is highlighted by the aggregate base course reaching its maximum water content before the subgrade. However, the resilient modulus of both materials remain relatively low and unchanged during the summer as shown in Figure 3.6 (Ovik, et al 2000).

The extent of changes in the resilient modulus due to changes in volumetric water contents is dependent on the soil type and the dry density. The dry density is influenced by the external stress applied during compaction and by whether material layers were compacted dry or wet of the optimum water content (Kim, and Siddiki 2006; Ovik, et al 2000; Vanapalli, et al 1996). The shear strength and resilient modulus of the subgrade generally increase with an increase in the external stress. An increase in the external stress results in an increase in the air entry value (AEV) of the subgrade, an increase in the dry density and a reduction in the void ratio. An increase in the external stress also causes a reduction in the hydraulic conductivity, reduced infiltration capacity and an increase in the water storage capacity. The increase in shear strength and resilient modulus of the subgrade are higher for subgrades which are compacted wet of the optimum water content. The relationship between the stress state and shear strength is shown in Figure 3.7 (Vanapalli, et al 1996).

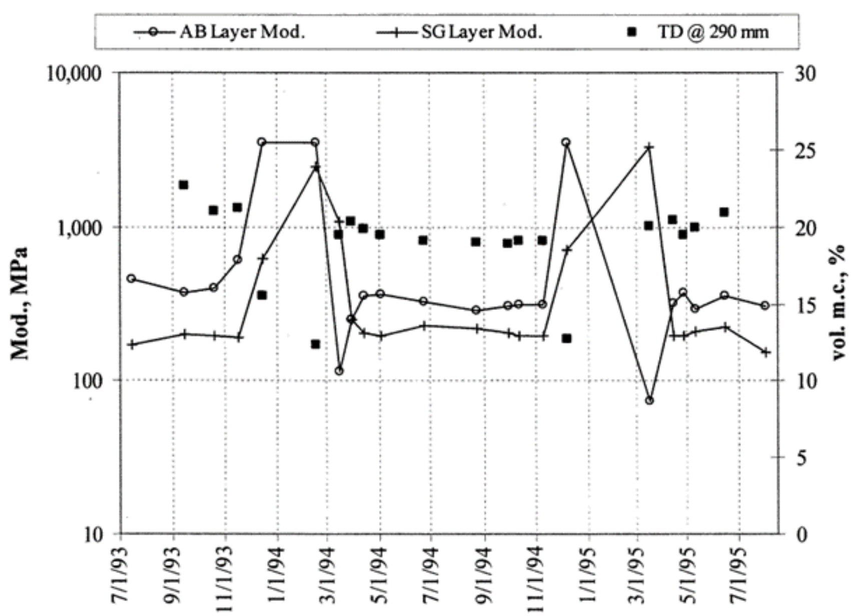

Figure 3.6: Resilient modulus vs post construction water content for a compacted aggregate base (AB) and subgrade (SG) at a depth of 290 mm (Ovik, et al 2000)

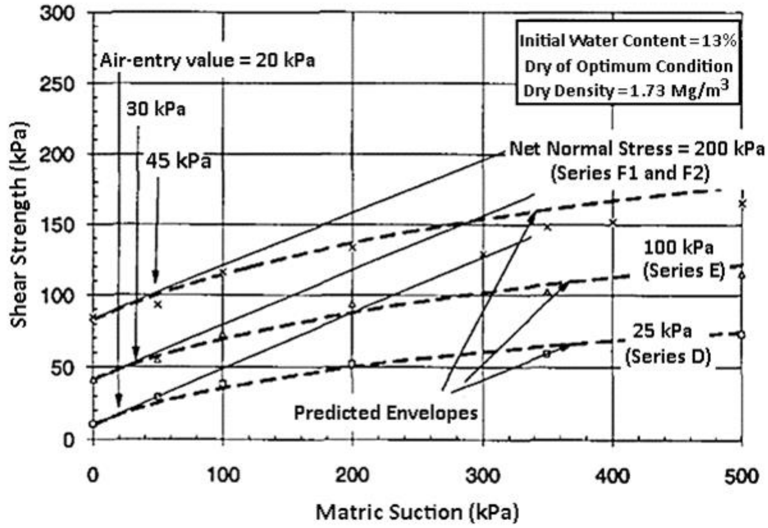

(a) Subgrades compacted dry of optimum

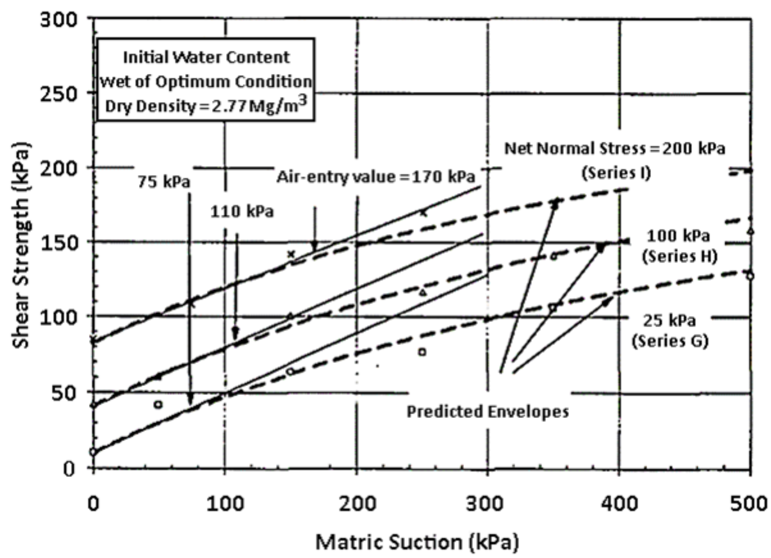

(b) Subgrades compacted wet of optimum

Figure 3.7: Relationship between the stress states and shear strength of subgrades (Vanapalli, et al 1996)

3.3.1 Background and Applicable Features of EICM

The initial Integrated Climate Model (the Initial ICM) was first developed for the Federal Highway Administration (FHWA) by Texas A and M University and the Texas Transportation Institute. The initial ICM was developed by integrating the Infiltration and Drainage (ID) model developed through FHWA, the Climate Material Structural (CMS) model previously developed at the University of Illinois, and the Frost Heave and Thaw Settlement model developed through the US Army Cold Regions Research Experimental

Laboratory (CRREL) model. The initial ICM has gone through numerous improvements which have resulted in the development of the ICM version currently known as the Enhanced Integrated Climate Model (EICM) version 2.6 (Witczak, et al. 2000; Zapata, et al. 1999; Larson, and Dempsey 1997; Liang, and Lytton 1989; Lytton, et al. 1989; Guymond, et al. 1986; Liu, and Lytton 1985; Dempsey, et al. 1985). EICM consists of four model components (the PRECIP, ID, CRREL and CMS models) as shown in Figure 3.8.

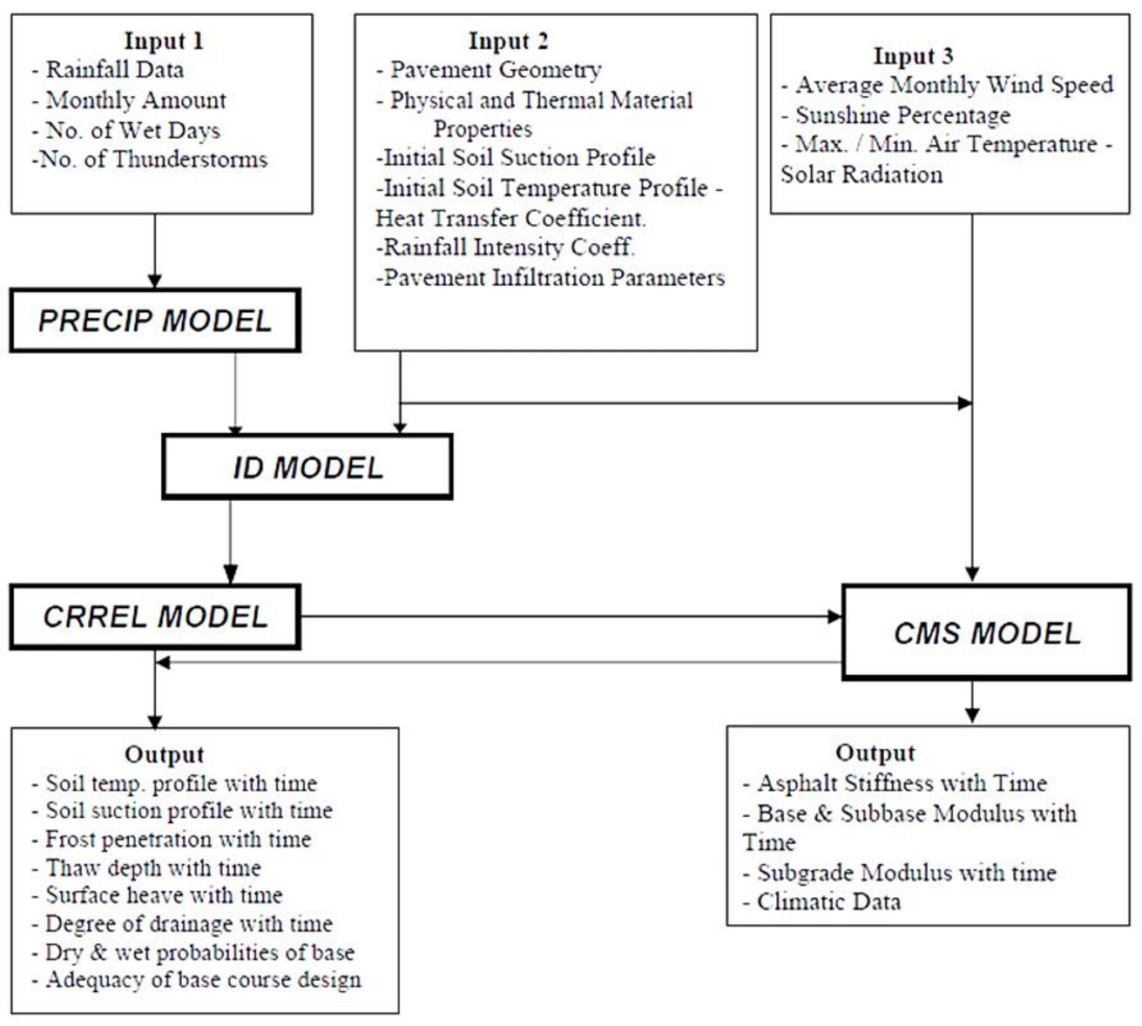

Figure 3.8: Flow chart of EICM model computation components (Birgisson, et al. 2000)

EICM version 2.6 was developed under NCHRP 1-37A Project which includes improvements to the volumetric water content prediction model and capabilities for predicting SWCC using soil index properties. EICM version 2.6 also includes improvements to the saturated and unsaturated hydraulic conductivity functions using SWCC, and the inclusion of default soil parameters governed by the AASHTO soil classification system. EICM version 2.6 is a 1-D coupled water and heat transfer model which facilitates input, collection, characterization, and analyses of climatic data and unbound pavement materials properties to predict pavement response and performance (Zapata, and Houston 2008; Houston, et al. 2006; Applied Research Associates 2004; Witczak, et al. 2000). Improvements incorporated into EICM version 2.6 consist of the following components:

- Replaced the SWCC model proposed by Gardner (1958) with the model proposed by Fredlund and Xing (1994) to obtain a better fitting SWCC;
- Improved the prediction of SWCC, saturated hydraulic conductivity and specific gravity using soil index properties and grain size distribution including Plasticity Index (PI), percent passing No. 200 sieve (P_{200}) and effective grain size (D_{60});
- Incorporated the model proposed by Fredlund and Xing (1994) for predicting unsaturated hydraulic conductivity based on the SWCC; and
- Incorporated climatic datasets from 800 weather stations in the USA. The climatic data include precipitation, percent sunshine, wind speed, air temperature and relative humidity.

Improvements were made to EICM version 2.6 in developing EICM version 3.0 to EICM version 3.2 incorporated into MEPDG version 0.7 to MEPDG version 1.1. MEPDG version 1.1 was developed under NCHRP 9-23 Project, NCHRP 1-40A Project and NCHRP 1-40D Project (McCartney, et al. 2010; Zapata, et al. 2009; Zapata, and Houston 2008; Witczak, et al. 2007; Brown, et al. 2006; Darter, et al. 2006; Houston, et al. 2006; Larson, and Dempsey 2003). The primary improvements incorporated into EICM version 3.2 consist of the following:

- Incorporated the modified Thornthwaite Moisture Index (the modified TMI) proposed by Witczak, et al. (2006) presented in Eq. 3.5 to develop the TMI-P_{200}/wPI relationship. This relationship is used for predicting the suction profile represented by Eq. 3.6;
- Incorporated improvements in the SWCC model parameters;
- Incorporated improvements in the saturated hydraulic conductivity and specific gravity models,
- Incorporated improvements in the compaction model based on the grain size-index properties relationship; and
- Incorporated updated rehabilitation analyses and the inclusion of the distress and performance prediction analysis.

$$\text{TMI} = 75\left\{\left(\frac{\text{P}}{\text{PE}}\right) - 1\right\} + 10 \qquad (3.5)$$

$$h = \alpha \left[e^{\left\{\frac{\beta}{(TMII+\gamma)}\right\}} + \delta \right] \quad (3.6)$$

h = Matric suction model for subgrades; $\alpha, \beta, \gamma,$ and δ = Regression constants associate with $TMI\text{-}P_{200}/wPI$ relationship; *TMI* = Modified Thornthwaite Moisture Index (Witczak, et al. 2006); *w* = Decimal form of P_{200}; *P* = Annual precipitation (cm); *PE* = Potential evapotranspiration (cm), and if predicted *TMI* value is > 100, set *TMI* =100.

3.3.2 Pertinent Features of the Enhanced Integrated Climate Model

The EICM is incorporated into the MEPDG to account for the influence of climatic factors and environmental conditions on the water and heat transfer within pavements, the resilient moduli of subgrades and the associated pavement performance (Bulut, and Javid 2019; Bulut, et al. 2014; Zapata, et al. 2007; McCarthey, et al. 2010).

The first EICM model component is the Precipitation (PRECIP) model which accounts for the impact of variations in precipitation on pavement performance. The PRECIP model is based on a deterministic algorithm (for a specific input, it computes the same output using the same model framework) which uses the average climatic datasets and a probabilistic analysis for simulating rainfall intensity. The PRECIP model is used when actual precipitation data are not provided (Bulut, and Javid 2019; Bulut, et al. 2014; Liang, and Lytton (1989).

The second EICM model component is the Climate Material Structural (CMS) model which accounts for the influence of climatic factors on the heat transfer. The CMS model uses estimates of the heat flux at the pavement surface for predicting the temperature profile within asphalt layers. The CMS model uses the thermal conductivity and specific heat capacity of pavement materials to estimate the temperature profile within asphalt layers. The model uses the predicted temperature profile within asphalt layers to predict the temperature profile within the pavement structure. The asphalt surface and top of the base course temperature boundary conditions are determine using the equation proposed by Dempsey, et al. (1985). The time dependent variations in asphalt temperatures are determined using a 1-D partial differential equation for heat transfer through conduction based on Fourier’s Law (Bulut, and Javid 2019; Bulut, et al. 2014; McCartney, et al. 2010; Dempsey, et al. 1985).

The third EICM model component is the U.S Army Cold Region Research and Engineering Laboratory (CRREL) frost heave and thaw settlement model. The CRREL model is based on a 1-D coupled heat and water transfer model used to evaluate the influence of freezing on the subgrade performance. The CRREL model simulates time and depth dependent variations in the temperature and water transfer within subbases and subgrades. This is done using finite element analyses based on Richard’s equation which governs water transfer in unsaturated subgrade, and Fourier’s equation which governs heat transfer. The temperature at the bottom of the asphalt layer predicted by the CMS model is used as input in the frost heave and thaw settlement model for predicting the temperature profile. The CRREL model subsequently uses the temperature profile through the asphalt wearing courses predicted by the CMS model to simulate changes in the material temperature for each layer. The CRREL model uses a time and depth dependent 1-D diffusion analysis to simulate variations in the matric suction profile within subgrades. The matric suction boundary condition at the subgrade surface in the CRREL model is controlled by the ID Model. The other boundary conditions in the CRREL model are sourced from the CMS model. The CRREL model requires the input of thermal soil properties including thermal conductivity and specific heat capacity, and soil hydraulic properties including hydraulic conductivity and SWCC (Bulut, and Javid 2019; Bulut, et al. 2014; McCartney, et al. 2010; Guymon, et al. 1986).

The fourth EICM model component is the Infiltration and Drainage (ID) model which is used to simulate gravity drainage of the base course, to simulate infiltration, and to evaluate pavement design options. The infiltration component of the ID model is implemented using four categories of rainfall intensity: none, minor, moderate, and extreme. The rainfall categories are based on the percentage of precipitation entering the pavement structure, and on the pavement shoulder type. The ID model assumes that cracks on the pavement surface and pavement shoulders are the primary locations for water transfer into pavement structures. For infiltration analyses, the ID model uses the Ridgeway (1976) model in the presence of cracking, or the Dempsey, and Robnett (1979) model in the absence of cracking (Bulut, and Javid 2019; Bulut, et al. 2014; McCartney, et al. 2010; Lytton, et al. 1993; Liu, and Lytton 1985). The model uses a numerical approach for predicting the extent of drainage used for the durability analyses of the base courses (Lytton, et al. 1993). The ID model is critical to the water transfer process as it controls the hydraulic boundary condition at the subgrade surface. The ID model output consists of the degree of saturation of the base course, the extent of drainage during dry periods, and a probabilistic assessment of whether the base course is in a dry or wet condition (Bulut, and Javid 2019; Bulut, et al. 2014; McCartney, et al. 2010; Lytton, et al. 1993; Liu, and Lytton 1985).

3.4 Previous Studies Conducted to Evaluate, Calibrate and Validate EICM

3.4.1 Background

The MEPDG was developed through the National Cooperative Highway Research Program (NCHRP) Project 1-37A. MEPDG uses global input parameters which are not applicable for the local implementation of MEPDG (Yuan, and Nemtsov 2017; Huang, et al. 2016; Yut, et al. 2014; Kim, et al. 2011; AASHTO 2010). NCHRP Project 1-40B which was released in 2010 provides a guide (the steps) for the local calibration of the distress prediction models in the current version of MEPDG (AASHTO 2010). NCHRP

Project 1-40D (released in 2007) is supported by a technical document released in 2020 which provides a user manual and local calibration guide for MEPDG and the associated software (AASHTO 2020).

Studies were conducted throughout the United States to evaluate the accuracy and to calibrate the validity of EICM version 3.2 (the current EICM version). These studies were conducted to determine the accuracy of the current version of EICM in predicting the influence of climatic factors on water and heat transfer within pavements, resilient moduli of materials and the pavement performance. These studies were conducted in the various climatic zones used to categorize regions in the Long-Term Pavement Performance (LTPP) and Seasonal Monitoring Program (SMP) database. The climatic zones in LTPP and SMP were classified using logical regression analyses and classification of monthly and annual air temperature, precipitation, snowfall, relative humidity, and freeze and thaw cycles (climatic factors) using multivariate analyses. The multivariate analyses included principal component analyses, factor analyses, cluster analyses and geographic information system (GIS) (climatic factors analyses). Climatic factors analyses were conducted to classify climatic factors into various groups depending on optimal characteristics common to climatic factors. Fisher's discriminant analyses and artificial neural networks analyses were then conducted to create climatic zones based on similar climatic patterns. The climatic zones were subsequently presented on a GIS map. The four climatic zones developed for use in LTPP and SMP are Wet Freeze, Wet No-Freeze, Dry Freeze, and Dry No-Freeze (Dong, et al. 2021; Wang 2005).

3.4.2 Introduction

Selected studies conducted to evaluate, calibrate and validate EICM in various climatic zones are presented in Section 3.4.3 to Section 3.4.5. These studies were conducted to investigate limitations in the current version of EICM in predicting water and heat transfer within pavement structures in various climates.

3.4.3 Previous Studies Conducted in a Wet Freeze Climatic Zone in the United States

Studies conducted in Indiana indicated that EICM version 3.2 computational output are primarily influenced by gravimetric water contents. These studies also noted that seasonal changes in resilient moduli of subgrades are independent of the water table elevation in the state of Indiana. The resilient moduli of subgrades are independent of the water table (in Indiana) because of the climatic conditions and the associated in-situ degree of saturation of subgrades which are typically more that 95.0 %. This results in EICM version 3.2 inaccurately predicting seasonal changes in water transfer and resilient moduli of subgrades. This is because EICM version 3.2 has an overreliance on the water table elevation in predicting water transfer within subgrades (El Howayek, et al. 2016).

Studies conducted in Minnesota indicated that EICM version 3.2 predicts heat transfer poorly, and that EICM version 3.2 heat transfer model is highly sensitive to changes in the thermal conductivity of each material (Johanneck, et al. 2011).

Studies conducted in New Jersey also indicated that EICM version 3.2 water and temperature prediction models are sensitive to changes in climatic factors and the interaction between the climatic condition and the traffic (Zaghloul, et al. 2006).

3.4.4 Previous Studies Conducted in a Wet No-Freeze Climatic Zone in the United States

Studies conducted in Oklahoma indicated that pavement materials properties are influenced by changes in climatic factors. These studies also indicated that boundary conditions within the pavement profile in EICM version 3.2 are controlled by the depth to water table and TMI. These studies also indicated that EICM version 3.2 predicts water transfer poorly particularly near the surface. This implies that EICM version 3.2 has a poor water balance model (Bulut, and Javid 2019; Bulut, et al. 2014).

Studies conducted in Arkansas highlighted that EICM version 3.2 accurately predicts temperature profiles, but water contents and associated seasonal fluctuations in matric suction are poorly predicted. EICM version 3.2 neglects climate pavement interaction and its influence on water transfer (McCartney, and Khosravi 2013; McCartney, et al. 2010). EICM version 3.2 also predicts pore water pressure within subgrades poorly (McCartney, et al. 2010).

3.4.5 Previous Studies Conducted in a Dry Freeze Climatic Zone in the United States

Studies conducted in Wyoming indicated that inaccuracies in MEPDG version 1.1 are also due to the limited availability of field performance data. These studies also indicated that the use of climatic data over limited analysis periods may lead to unrealistic performance prediction due to the impact of anomalies and short-term weather extremes. The studies recommended using climatic data recorded over longer periods (Dzotepe, and Ksaibati 2010).

Studies conducted in Utah found that MEPDG generally predicts low to medium distress levels for specific climatic conditions accurately, but rut depths are an exception. These studies also found that moderate to severe distress are not simulated due to a lack of field performance data relating to moderate to severe distress (Darter, et al. 2009).

3.5 Previous Studies Conducted to Validate EICM and used to Validate the Quantitative Empirical Model

3.5.1 Introduction

Studies were conducted in various climates to validate the accuracy of EICM in predicting water and heat transfer within subgrades. These selected studies were also used for validating the Quantitative Empirical Model. The specific studies are summarized in Section 3.5.2 and Section 3.5.3.

3.5.2 Study Conducted in Ohio in the United States: Quintero (2007)

Quintero (2007) conducted a study to validate the volumetric water contents prediction model in EICM for flexible and rigid pavement sites in Ohio (the Ohio study) in a wet freeze climate. The sites formed part of the LTPP and SMP. The in-situ volumetric water contents were measured from 1996 to 2002 using time domain reflectometers (TDR) which were installed at varying depths within the pavement. The cross-section details and materials properties for site 390108 and site 390203 are shown in Table 3.1 and Table 3.2, respectively.

Table 3.1: Pavement structure cross-section details (LTPP and SMP 2020).

Material	Layer Thickness (mm)	
	Site 390108	Site 390203
AC wearing course	168	-
PCC wearing course	-	285
Unbound granular base course	205	155
Treated granular	100	
Compacted subgrade	-	-

Table 3.2: Pavement materials properties (LTPP and SMP 2020).

Material	Site 390108	Site 390203
Compacted subgrade classification	A-6 Silty Clay	A-6 Silty Clay

The pavement section for site 390203 is similar to the pavement sections for the sites used in developing the Quantitative Empirical Model (the QE Model), and the sites are in a similar climate. Hence, site 390108 and site 390203 are used for evaluating the accuracy of the QE Model although site 390108 consists of AC wearing course. The in-situ volumetric water contents measured at site 390108 and site 390203 are used for evaluating the accuracy of the QE Model. The volumetric water contents predicted using the QE Model and EICM for the two sites are compared for evaluating the accuracy of the QE Model against EICM in predicting the in-situ volumetric water contents within the subgrade.

This Section presents an analysis summary of the Ohio study and focuses on the comparison of the in-situ and EICM predicted volumetric water contents for site 390108 and site 390203. This study noted that EICM generally predicts a constant volumetric water content during the analysis period and underestimates the in-situ volumetric water contents as shown in Figure 3.9 and Figure 3.10. The constant volumetric water content predicted by EICM does not reflect the seasonal fluctuations in volumetric water contents observed in the in-situ volumetric water contents. This observation may be due to EICM neglecting the influence of changes in climatic factors on the fluctuations in water and heat transfer within the pavement structure. The volumetric water content value referred to as the saturated volumetric water content in this study may not actually be the saturated volumetric water content. EICM neglects the influence of increased precipitation induced infiltration on volumetric water contents, and the study provides no basis for the assumed saturated volumetric water content. The differences between the in-situ and EICM predicted volumetric water contents are lower for pavement structures with stabilized base courses relative to unbound base courses. EICM also neglects the cyclic variations (fluctuations) observed in in-situ volumetric water contents for these pavement sections. This may contribute to EICM inaccurately predicting in-situ volumetric water contents.

The analyses of data presented in the Ohio study indicated that EICM generally underestimates volumetric water contents within subgrades which results in EICM overestimating resilient moduli of subgrades. This results in subgrades that have higher volumetric water contents, lower resilient moduli, lower performance and shorter services life during the operations period. The analyses indicated a closer correlation between the in-situ and EICM predicted volumetric water contents for subgrades classified as A-4 (A-4 subgrades) relative to subgrades classified as A-6 (A-6 subgrades). Water vapour transfer is the primary form of water transfer in fine-grained subgrades, while liquid water transfer is the primary form of water transfer in coarse-grained subgrades. Hence, water vapour transfer may be higher for A-6 subgrades relative to A-4 subgrades. EICM accounts for only liquid water and neglects water vapour transfer. This may contribute to the closer correlation between the in-situ and EICM predicted volumetric water contents for A-4 subgrade relative to the A-6 subgrade presented in the Ohio study. In the Ohio study, it may also be possible that liquid water transfer was higher in the A-4 subgrade, while water vapour transfer was higher in the A-6 subgrades.

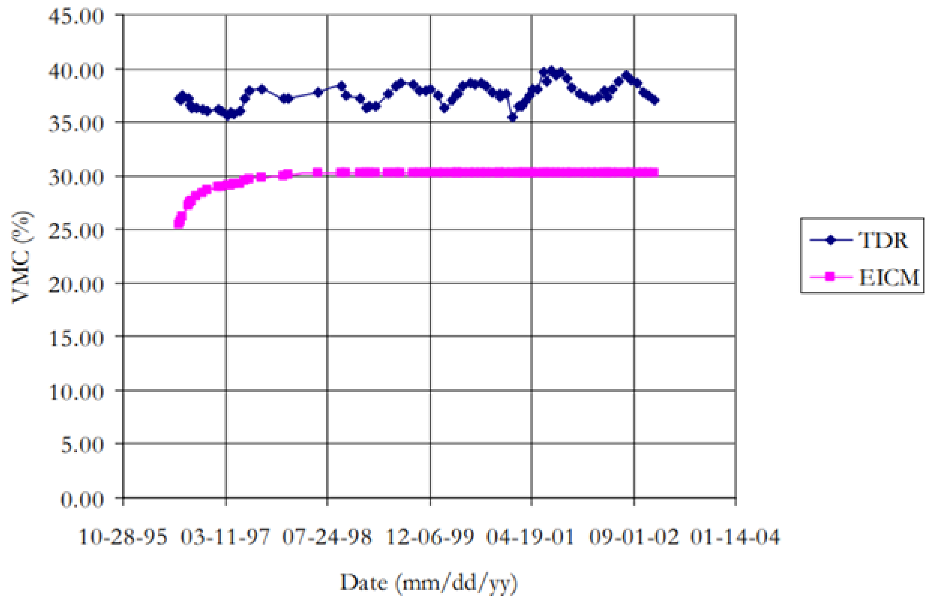

(a.)

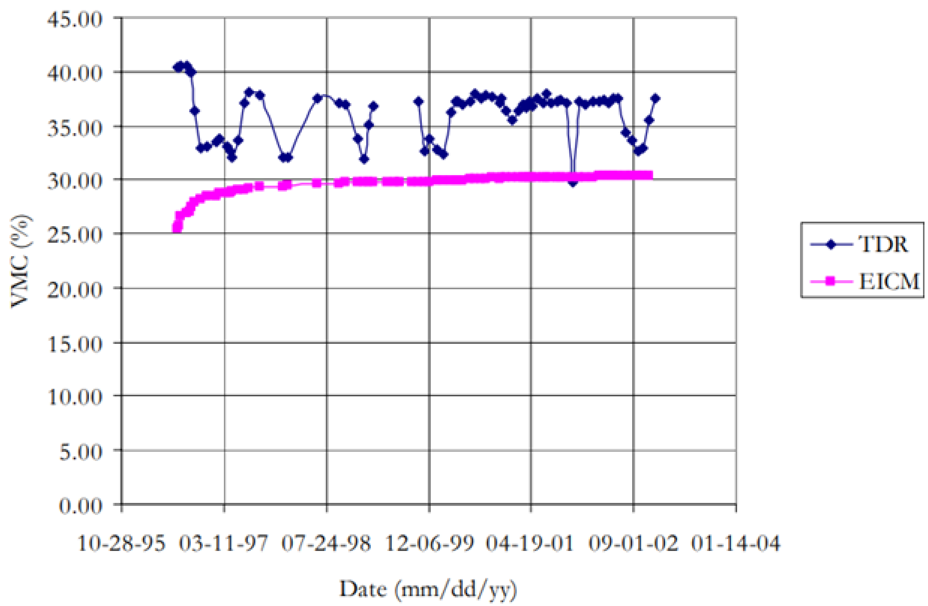

(b)

Figure 3.9: Measured vs. EICM predicted volumetric water content: site 390108 at 175 mm (a) and 1.2 m (b) below the subgrade surface (Quintero, 2007)

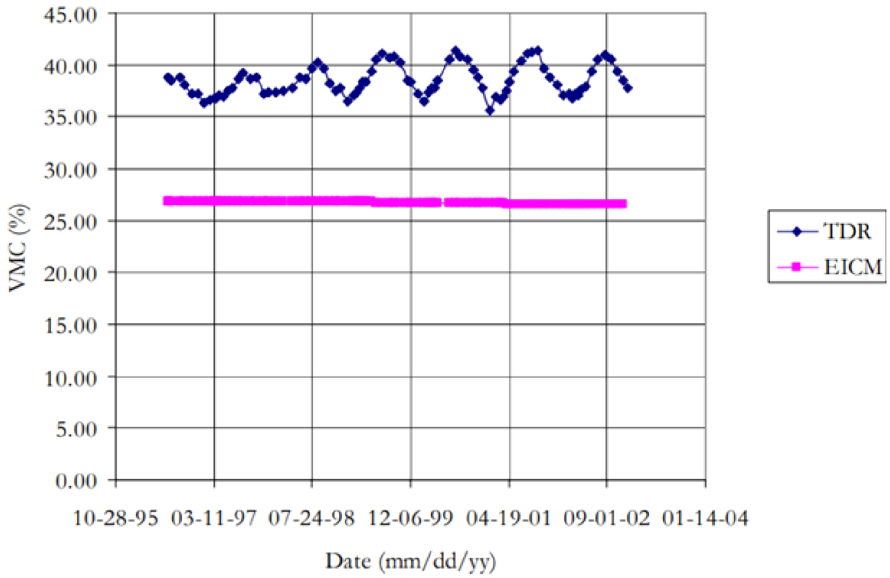

(a)

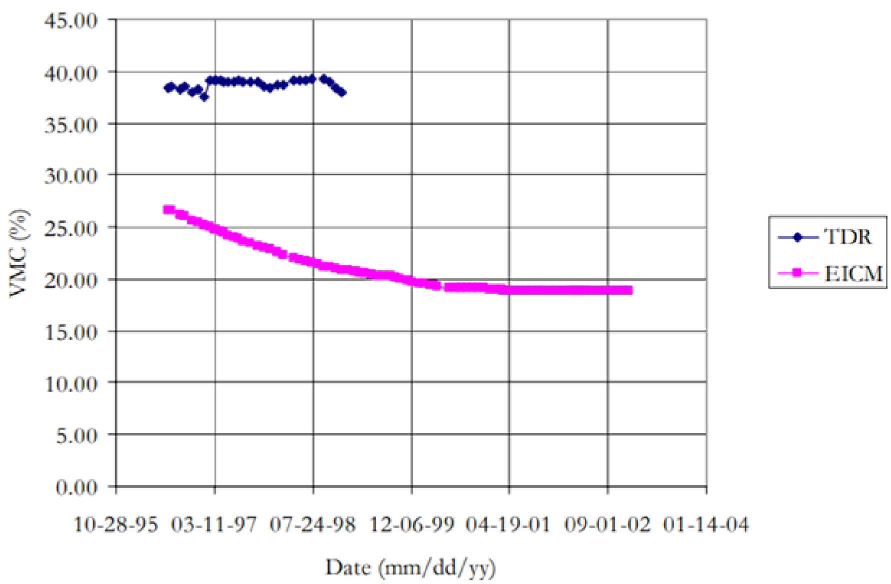

(b)

Figure 3.10: Measured vs. EICM predicted water content: site 390203 at 400 mm (a) and 1.18 m (b) below the subgrade surface (Quintero, 2007)

The Ohio study included measurements of in-situ temperature profiles within pavement structures obtained using thermistors. The analyses of data presented in the study generally indicated a good correlation between the in-situ and EICM predicted temperature profiles within subgrades as shown in Figure 3.11. However, there was a poor correlation between the in-situ and EICM predicted temperature profile for periods of high air temperature as shown in Figure 3.11 and Figure 3.12. The observed discrepancies between the in-situ and EICM predicted temperature profiles indicate that EICM predicts temperature profiles poorly during periods of high air temperature due to the limitations in the heat transfer model incorporated in EICM.

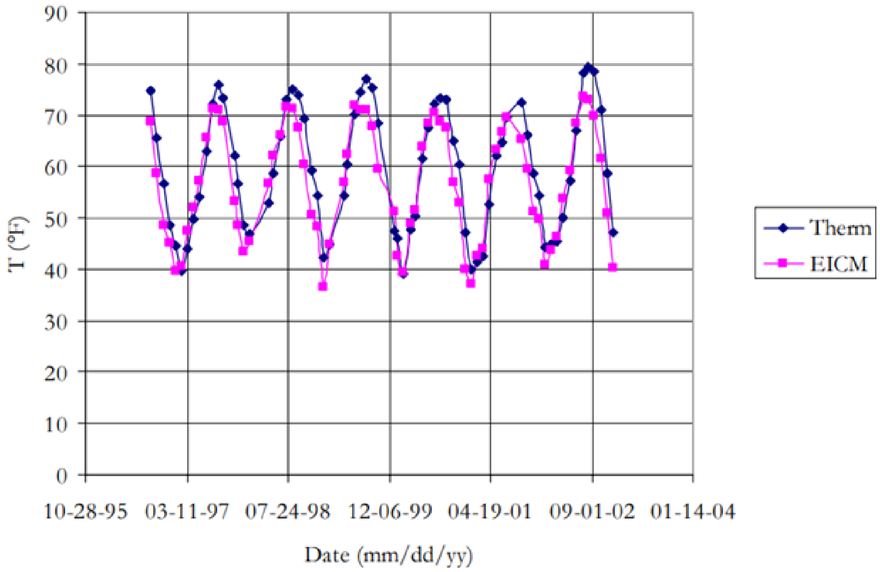

(a.)

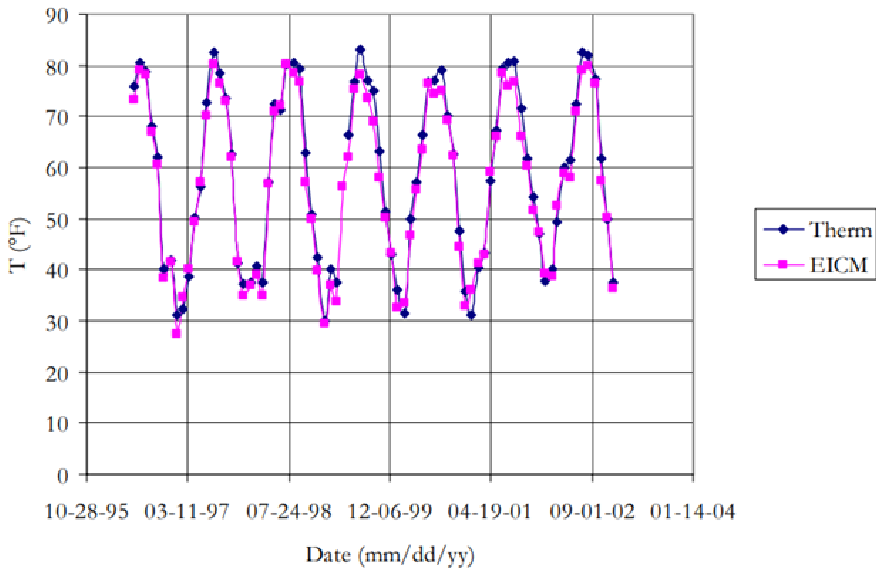

(b)

Figure 3.11: Measured vs. EICM predicted temperature profile: site 390108 at 675 mm (a) and site 390203 at 400 mm (b) below the subgrade surface (Quintero, 2007)

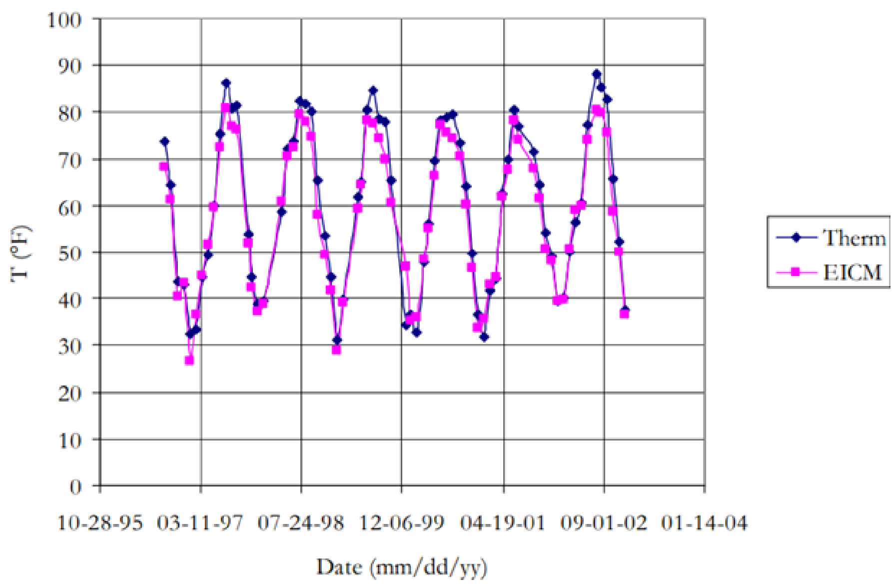

Figure 3.12: Measured vs. EICM predicted temperature profile: site 390108 at 400 mm below the pavement surface (Quintero, 2007)

3.5.3 Study Conducted in Arkansas in the United States: Hall et al. (2013)

Hall et al. (2013) conducted a study to evaluate the permeability of asphalt concrete hot mix (ACHM) for Superior Performing Asphalt Concrete Pavements (Superpave). The study was conducted to develop a correlation between the in-situ measurements and laboratory testing of permeability of the ACHM for sites in Arkansas which is in a wet no-freeze climate (the Arkansas study). The Arkansas study also evaluated the prediction of water transfer within flexible pavements and validated the prediction of volumetric water contents using EICM version 3.2. The summary of the analysis of the Arkansas study presented in this section focuses on the prediction of water transfer within pavements, and the validation of EICM version 3.2 in predicting volumetric water contents within subgrades for sites in Arkansas. The summary also focuses on the Fort Smith site as this site is used for evaluating the accuracy of the Quantitative Empirical Model. The cross-section details and materials properties for the Fort Smith site are shown in Table 3.3 and Table 3.4 respectively.

Table 3.3: Pavement structure cross-section details (LTPP and SMP 2020)

Material	Layer Thickness (mm)
	Fort Smith site
AC wearing course	230
Unbound granular base course	100
Compacted subgrade	-

Table 3.4: Pavement materials properties (LTPP and SMP 2020)

Material	Fort Smith site
Compacted subgrade classification	A-6 (clayey Gravel with sand)

The analysis of the Arkansas study indicated that a weak correlation was observed between the in-situ measured and laboratory testing permeability for the ACHM. The analysis indicated that the permeability of the ACHM is time dependent, is influenced by post construction pavement condition, and changes seasonally due to changes in climatic factors. The analysis also indicated that the permeability of the ACHM is influenced by the percentage of in-situ air voids and the void ratio.

The analysis of the Arkansas study also indicated that volumetric water contents and resilient moduli of subgrades change seasonally and are independent of changes in precipitation. However, the authors of the Arkansas study made no mention of the influence of the intensity and duration of precipitation on volumetric water contents within subgrades.

Studies have indicated that the rate of infiltration of water within soils is influenced by the intensity and duration of the rainfall. These studies found that a low-intensity rainfall with a longer duration has a higher influence on the rate of infiltration and the slope stability relative to a high-intensity rainfall with a shorter duration. This is due to a low-intensity rainfall with a longer duration resulting in the wetting front advancing to deeper depths. Multiple rainfall events induce many wetting fronts and each rainfall event induces a wetting front which advances due to increased infiltration. Water contents are influenced by the characteristics and location of wetting fronts (Hou, et al 2019; Li, et al. 2016; Zhang, et al 2014)

The authors of the Arkansas study noted that the Fredlund and Xing (1994) model incorporated into EICM version 2.6 to version 3.2 (the Fredlund and Xing 1994 model) may predict SWCC developed from laboratory testing within acceptable limits. However, the authors noted that the Fredlund and Xing (1994) model predicts in-situ SWCC poorly which results in EICM version 3.2 predicting seasonal changes in the in-situ water transfer poorly. Figure 3.13 shows that temperature profiles for the Fort Smith site predicted by EICM version 3.2 correlate well with measured temperature profiles, except for measured summer temperatures. This confirms limitations in EICM version 3.2 in predicting pavement temperatures during periods of high air temperatures because EICM version 3.2 neglects the influence of convective cooling.

Water contents predicted using EICM version 3.2 for the base and subbase layers correlate poorly with measured water contents. EICM version 3.2 underpredicts water contents within the base and subbase layers by up to 100%. EICM version 3.2 also underpredicts water contents within subgrades in the summer by up to 50% and overpredicts water contents within subgrades in the winter by up to 50%. A comparison between the in-situ and EICM predicted water contents within the subgrade for the Fort Smith site is shown in Figure 3.14.

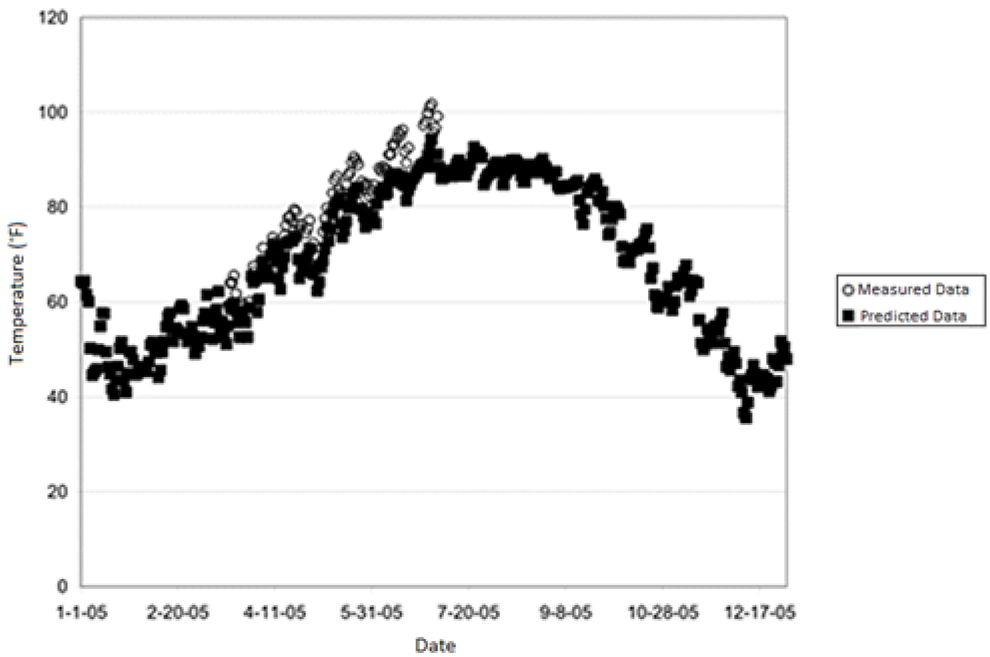

(a)

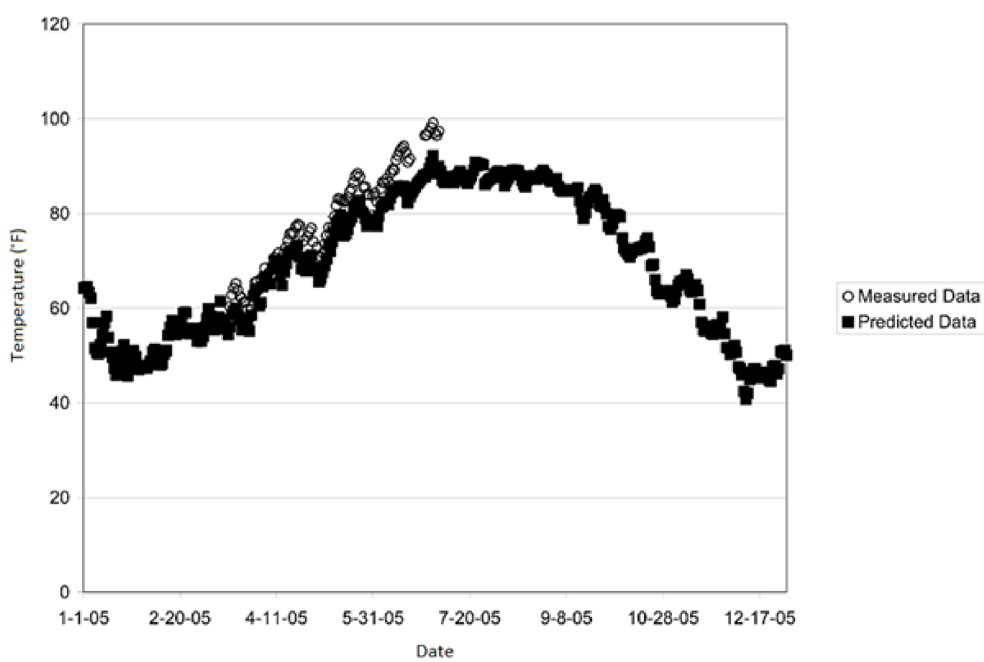

(b)

Figure 3.13: Measured vs. EICM predicted temperature profiles: Fort Smith site at 50 mm (a) and 250 mm (b) below the subgrade surface (Hall, et al. 2013)

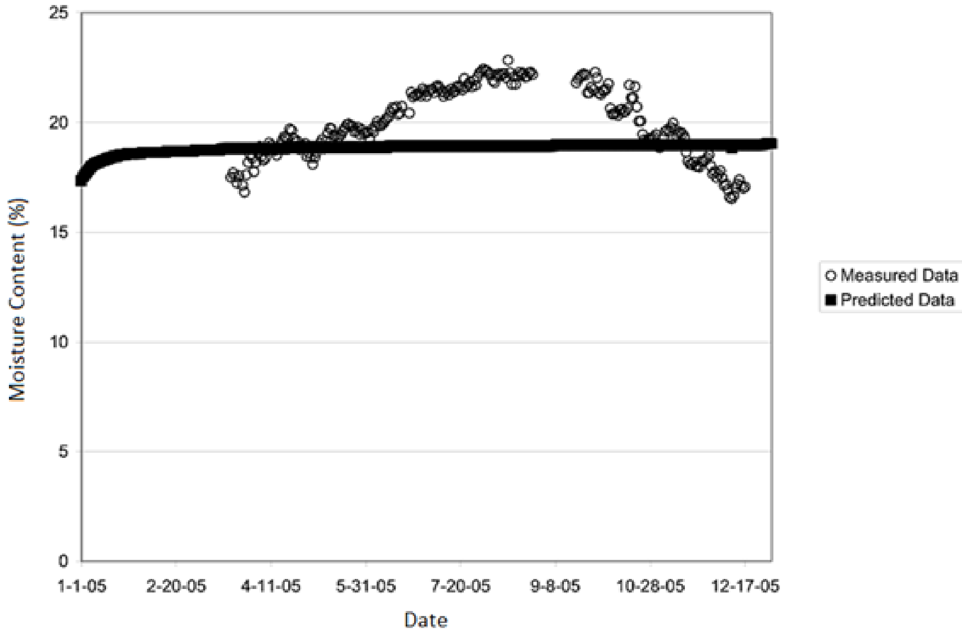

(a)

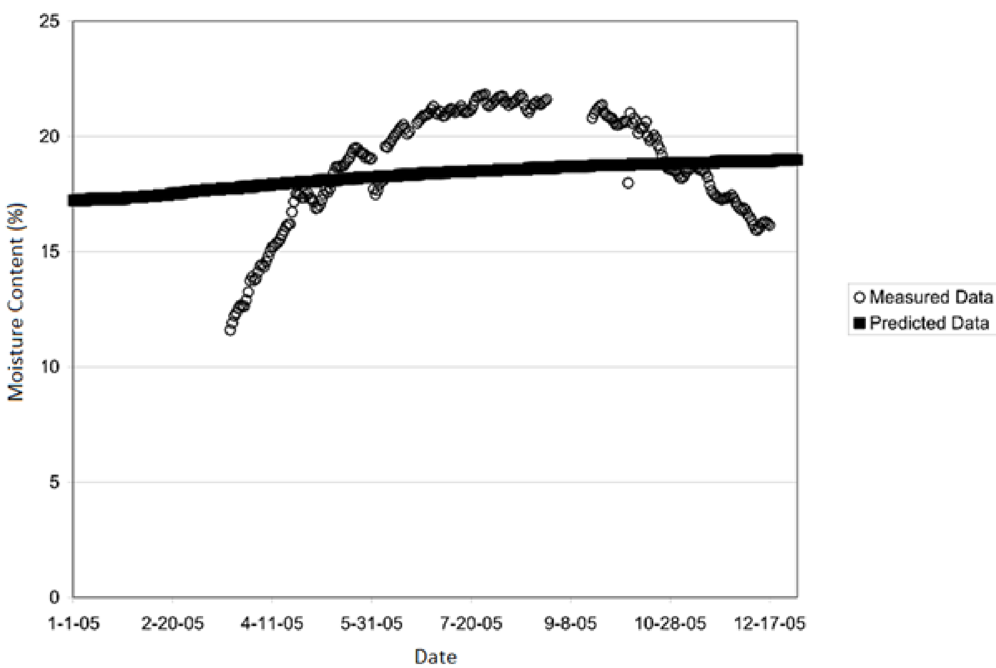

(b)

Figure 3.14: Measured vs. EICM predicted water contents profiles: Fort Smith site at 50 mm (a) and 250 mm (b) below the subgrade surface (Hall, et al. 2013)

3.6 Studies Highlighting the Primary Limitations of the Current Version of EICM

3.6.1 Introduction

Section 3.6.2 presents a detailed analysis of a study conducted by Ahmed et al. (2005) in New Jersey, United States using LTPP section 5E and 9C (the New Jersey study). Section 3.6.3 presents the analysis of a study conducted by Bayomy and Salem (2005) in Idaho, United States (the Idaho study). The New Jersey and Idaho studies were in a wet freeze climate. These studies presented the primary limitations in EICM version 3.0 including limitations in predicting the in-situ water and heat transfer and the associated impact on the pavement performance. The limitations in EICM version 3.0 are included in the analysis summary for the current version of EICM because the limitations in EICM version 3.0 noted in these studies also exist in the current version of EICM.

3.6.2 Studies Conducted in New Jersey in the United States: Ahmed, et al. (2005)

The New Jersey study was conducted to validate the EICM version 3.0 in predicting seasonal fluctuations in the in-situ water and heat transfer and to conduct material characterization. The study focused on investigating the primary climatic and environmental parameters which influence pavement performance. The study compared the in-situ and EICM predicted temperature profiles and water contents within subgrades. The comparison between the in-situ and EICM predicted data was conducted to evaluate the accuracy of EICM in predicting in-situ temperature and water contents within subgrades. TDR water probes were used to measure the in-situ water contents within the unbound material layers, and thermistors were used to measure the in-situ temperature profiles within subgrades. The in-situ water contents and temperature profiles within pavement structures were monitored continuously and measured daily. The data presented in the study are summarized in Table 3.5 to Table 3.7. The material thickness is presented in Table 3.5. A comparison between measured and predicted temperatures and water contents are presented in Table 3.6 and Table 3.7 respectively.

The study found that EICM overestimates temperatures from late spring to late fall. The higher temperatures result in inaccuracies associated with high evaporation which result in an underestimation of the stored water within subgrades. During the winter, EICM underestimates the temperature profiles within subgrades. Where the underestimated winter temperatures are negative, inaccuracies appear to be associated with higher predicted accumulation of surface water and overestimated evaporation which results in underestimated stored water within subgrades. Where underestimated winter temperatures are positive, inaccuracies appear to be associated with lower predicted accumulation of surface water and underestimated evaporation which results in overestimated stored water. EICM poorly predicts the depth and time dependent fluctuations in water contents within subgrades as shown in Figure 3.15 and Figure 3.16.

Table 3.5: Pavement details for Site 5E and Site 9C (Ahmed, et al. 2005)

Material Layer	LTPP Site 5E		LTPP Site 9C	
	Thickness (mm)	Material description	Thickness (mm)	Material description
Base layer	97	Coarse stone with sand	241	Sandy Gravel
Subbase layer	343	Coarse sandy Gravel	660	Silty Sand with gravel
Subgrade layer	-	Silty Sand	-	Silty Sand, trace of clay

Table 3.6: Measured vs. predicted temperature (ºC), LTPP Sites 5E and 9C (Ahmed et al. 2005)

Material	Data: Asphalt concrete (AC); % sunshine (SS); Wind speed (WS, km/hr).	LTPP Site 5E				LTPP Site 9C			
		2002				2002			
		Apr	Jul	Sept.	Dec.	Apr	Jul	Sept.	Dec.
AC	Field data	17.5	30.2	27.9	0.9	17.8	29.3	27.1	-2.0
	EICM (56 SS, 16 WS)	20.8	33.5	30.1	-1.3	20.9	33.9	30.0	1.1
Base	Field data	14.6	28.8	26.6	3.3	14.6	28.7	26.4	3.3
	EICM (56 SS, 16 WS)	18.4	32.0	27.4	-1.0	18.4	31.8	27.1	-1.1
Subbase	Field data	14.1	28.8	26.5	5.0	13.3	28.1	26.0	5.8
	EICM (56 SS, 16 WS)	18.5	32.4	27.7	-1.0	18.6	32.1	27.8	-1.0
Subgrade	Field data	12.2	26.4	25.4	8.8	11.6	25.4	24.8	9.5
	EICM (56 SS, 16 WS)	19.4	31.7	28.2	-1.0	20.5	31.8	29.0	-2.1
		2003				2003			
AC	Field data	8.9	24.8	23.9	5.5	18.9	25.0	23.7	1.3
	EICM (56 SS, 16 WS)	11.6	31.4	25.7	4.8	24.4	31.2	25.9	0.7
Base	Field data	6.9	27.8	24.2	5.4	15.6	27.8	24.1	4.3
	EICM (56 SS, 16 WS)	8.9	30.5	23.9	1.9	22.2	30.0	24.0	0.0
Subbase	Field data	7.6	27.8	24.7	6.3	14.5	26.9	24.4	6.9
	EICM (56 SS, 16 WS)	9.6	30.0	24.5	2.4	23.4	28.8	24.9	0.4
Subgrade	Field data	9.2	24.6	24.2	9.7	12.5	23.4	23.5	10.8
	EICM (56 SS, 16 WS)	10.5	25.4	24.5	4.4	24.3	24.2	25.0	-0.2

Table 3.7: Measured vs. predicted water contents, LTPP sites 5E and 9C (Ahmed et al. 2005)

Material	Data Source	LTPP Site 5E				LTPP Site 9C			
		2002				2002			
		April	July	Sept.	Dec.	April	July	Sept.	Dec.
Base	Field Data	41.0	41.0	34.8	-	18.0	22.9	18.0	34.8
	EICM	18.3	15.9	16.2	3.1	18.7	16.0	18.1	9.6
Subbase	Field Data	24.2	33.7	20.4	29.4	38.0	34.8	35.9	34.8
	EICM	21.5	18.8	19.1	26.1	24.9	21.6	24.1	12.6
Subgrade	Field Data	40.0	39.1	38.0	38.3	48.0	48.7	49.5	48.7
	EICM	33.3	30.2	30.8	12.5	35.6	31.9	34.8	18.3
		2003				2003			
Base	Field Data	45.5	43.8	43.8	45.5	29.0	31.4	31.4	22.9
	EICM	19.5	19.6	16.4	19.2	18.5	19.6	18.7	18.9
Subbase	Field Data	29.0	31.4	29.0	43.8	46.4	42.1	42.9	38.0
	EICM	22.8	22.9	19.4	22.5	24.7	25.9	24.8	25.1
Subgrade	Field Data	54.8	50.0	53.3	29.0	48.7	49.5	50.3	48.0
	EICM	34.7	34.8	31.0	34.3	35.4	36.6	35.6	35.9

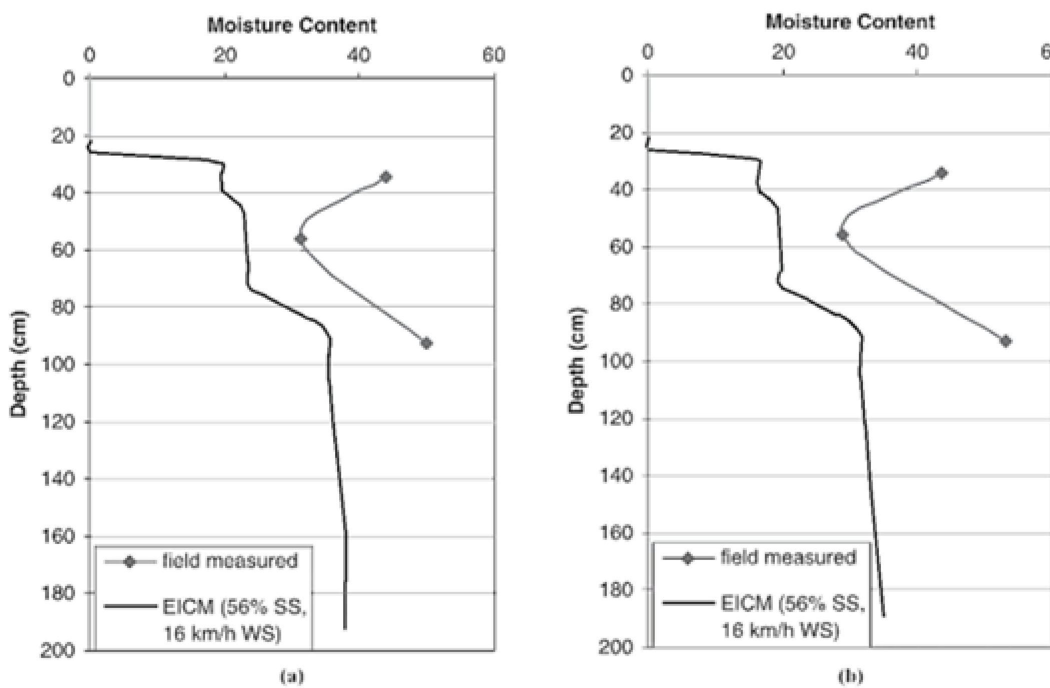

Figure 3.15: In-situ vs EICM predicted water content profiles within subgrades for site 5E: July 2003 (a.) and September 2003 (b) (Ahmed, et al. 2005)

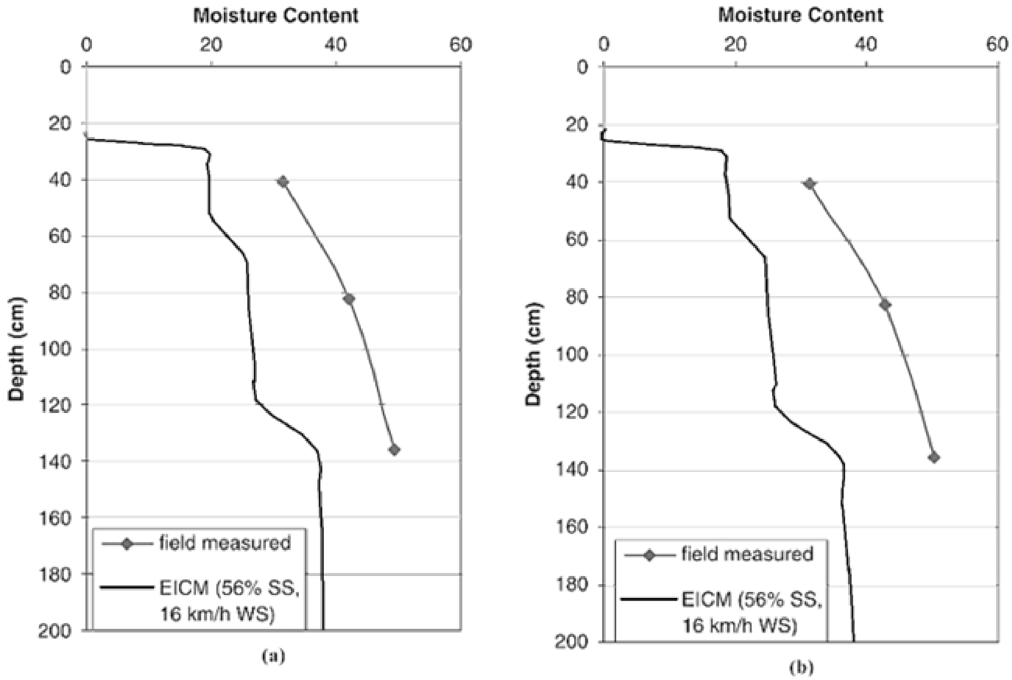

Figure 3.16: In-situ vs EICM predicted water content profiles within subgrades for site 9C: July 2003 (a) and September 2003 (b) (Ahmed, et al. 2005)

3.6.3 Study Conducted in Idaho in the United States: Bayomy, and Salem (2005)

The Idaho study included sites in Pack River, Worley, Moscow, Lewiston and Weiser. The analyses of the study focused on the Moscow site A, Moscow site B and Pack River site 4A (the SPR site). The Idaho study was conducted to evaluate the accuracy of EICM version 3.0 in predicting the impact of the climate and the environment on the water and heat transfer within pavement structures. The objectives of the study also included an evaluation of the impact of the climate and environment on changes in subgrade volumetric water contents, changes in the asphalt concrete wearing course temperature and the associated pavement performance.

The in-situ volumetric water content data were collected daily, weekly and monthly using time domain reflectometers (TDR) probes installed at various depths within the pavement structure. The temperature profiles at various depths within the pavement structure were measured using thermistors. The frost depths were measured using resistivity probes, and the groundwater table was measured using piezometers. The structural capacity of pavement structures was measured annually using Falling Weight Deflectors (FWD). Historical climatic data were also collected from the nearest weather station.

The pavement cross-section details for the Moscow sites and the SPR site are presented in Table 3.8. The material classification and the depth to the groundwater table at the three sites are presented in Table 3.9 and Table 3.10 respectively.

Table 3.8: Pavement cross-section details (Bayomy, and Salem 2005)

Material Layer	Moscow site A	Moscow site B	Park River site 4A (SPR)
	Material layer thickness (mm)		
AC wearing course	120	120	150
Base course	150	690	-
Rock cap layer	540	-	600
Subgrade layer	-	-	-

Table 3.9: Subgrade material classification (Bayomy, and Salem 2005)

Material Layer	Moscow site B	Moscow site B	SPR site
	Material description and classification		
Subgrade	Low plasticity Clay A-4	Low plasticity Clay A-4	silt and silty Gravel A-2-4

Table 3.10: Range of in-situ groundwater table elevation (Bayomy, and Salem 2005)

Moscow site A	Moscow site B	Park River site 4A (SPR)
July 2000 to March 2002	July 2000 to March 2002	December 2000 to May 2003
Groundwater table (m below pavement surface)		
2.62 to 3.38	No groundwater was encountered	1.40 to 2.32

The study found that the rock cap layer consisting of crushed rock was placed between the base course and the subgrade at the Moscow site A. The use of the rock cap resulted in higher volumetric water contents within the subgrade at the Moscow site A relative to volumetric water contents within the subgrade at the Moscow site B which did not include the rock cap. The use of the rock cap facilitated an increase in the infiltration and water storage at the interface of the rock cap and the subgrade. This resulted in an increase in the infiltration and volumetric water contents within the subgrade at the Moscow site A. Although the rock cap provides a layer with a high bearing capacity within the pavement structure, the rock cap causes increased volumetric water contents within the subgrade. The use of the rock cap also causes a reduction in the resilient modulus of the subgrade.

The analysis of the data presented in the Idaho study indicated that EICM version 3.0 generally overestimates the depth and time dependent volumetric water contents within the subgrade for the Moscow sites as shown in Figure 3.17. EICM version 3.0 generally underestimates the depth and time dependent volumetric water contents within the subgrade at the SPR site as shown in Figure 3.18. The study noted that the groundwater table fluctuated from a depth of approximately 2.62 m to 3.38 m and 1.40 m to 2.32 m below the pavement surface at the Moscow site A and SPR site respectively. The analysis of the data presented in the Idaho study indicated that changes in the groundwater elevation impacted changes in volumetric water contents within the subgrade at the Moscow site A and SPR site. However, no groundwater was encountered at the Moscow site B within the maximum depth investigated which was approximately 3.50 m below the pavement surface (the maximum termination depth). The study noted that fluctuations in volumetric water contents within the subgrade were observed at the Moscow site B despite the absence of groundwater within the maximum termination depth. This observation implies that the groundwater table had no impact on changes in volumetric water contents within the subgrade at the Moscow site B. Hence, it is likely that changes in climatic factors influence changes in volumetric water contents within subgrades at these sites.

The analysis of the data presented in the Idaho study indicated that the contribution of capillary rise to volumetric water contents within the subgrade was higher for the Moscow site A which consisted of a low plasticity Clay subgrade relative to the SPR site which consisted of a silty Gravel subgrade. The Idaho study confirms that EICM version 3.0 has an overreliance on capillary rise in predicting volumetric water contents within subgrades. The overreliance on capillary rise contributed to EICM version 3.0 overestimating volumetric water contents within the subgrade at the Moscow site A. However, EICM version 3.0 overreliance on capillary rise also resulted in EICM underestimating volumetric water contents within the subgrade in the absence of high capillary rise at the SPR site. The study also indicated that EICM version 3.0 inaccurately accounts for the impact of changes in climatic factors on changes in volumetric water contents within subgrades.

The study noted that volumetric water contents predicted using EICM version 3.0 correlates poorly with depth dependent fluctuations in in-situ volumetric water contents within subgrades. This is because EICM version 3.0 neglects the influence of climatic factors on the water and heat transfer. EICM version 3.0 predicted an apparent equilibrium water content from approximately 4.5 feet as shown in Figure 3.17 and Figure 3.18. This shows that EICM version 3.0 output misrepresents the in-situ water contents within subgrades.

The study noted that incorporating the influence of climatic factors into the pavement analysis and design result in lower pavement performance and shorter service life.

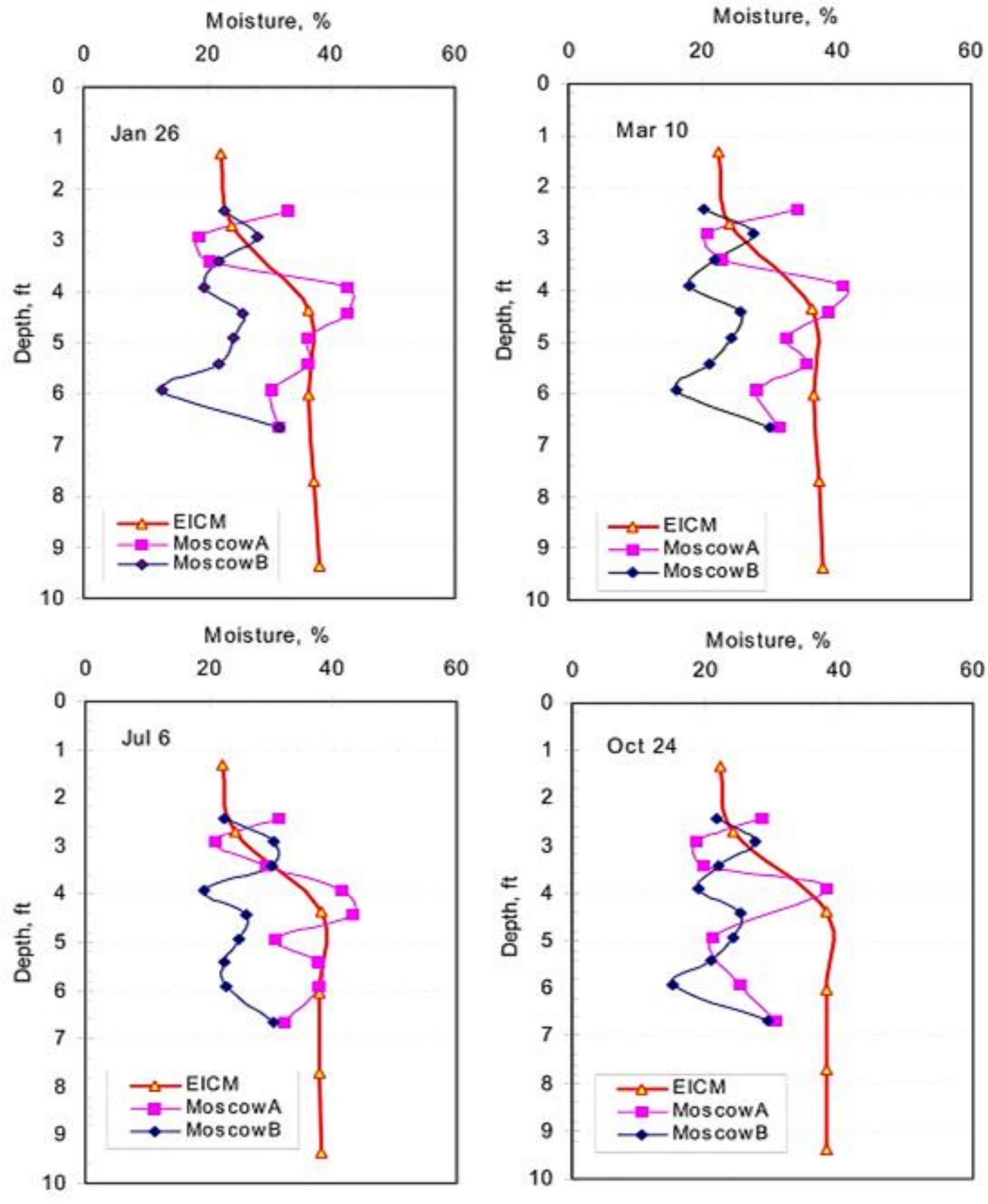

Figure 3.17: EICM output vs in-situ water contents: Moscow site A and Moscow site B (Bayomy, and Salem 2005)

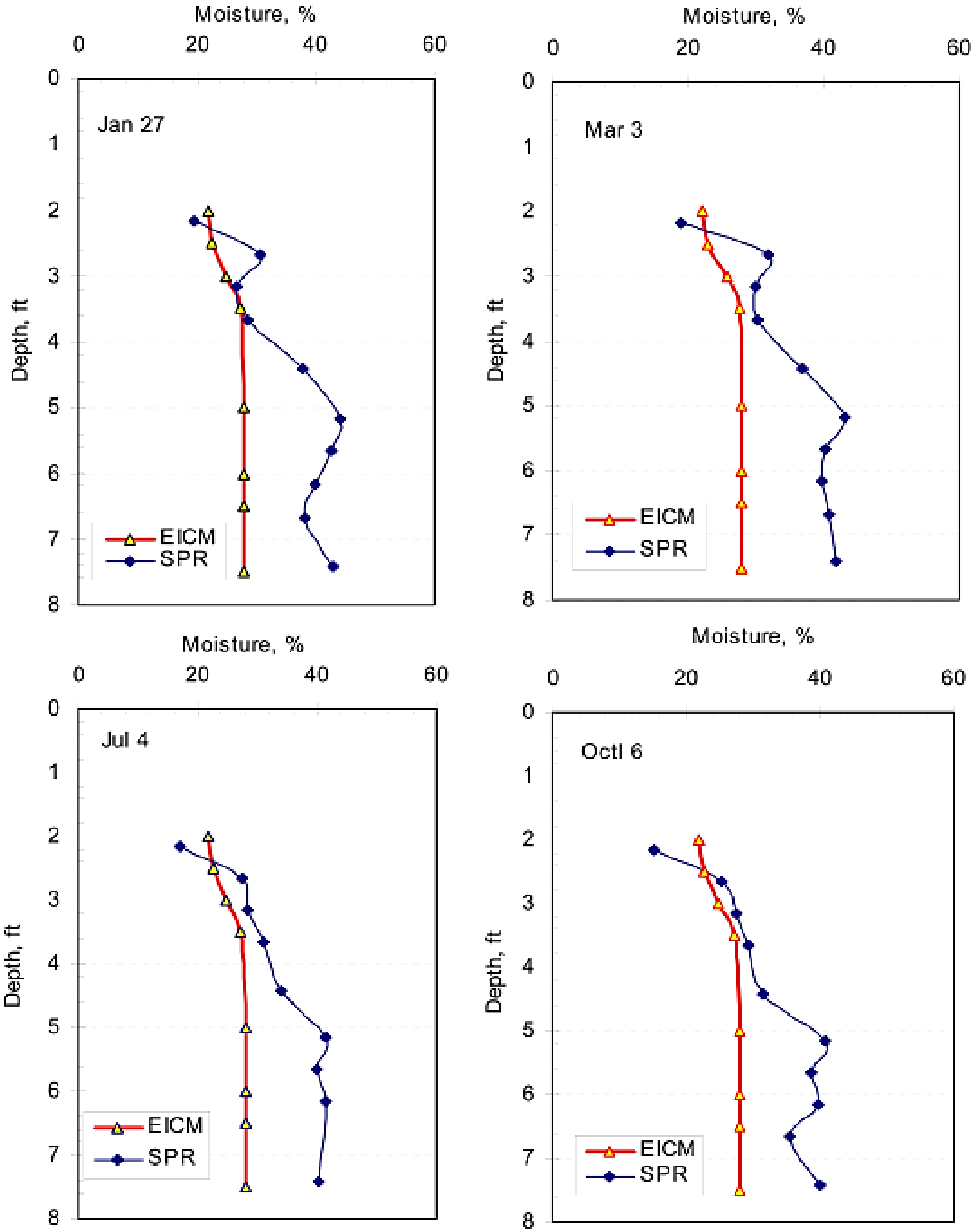

Figure 3.18: EICM output vs in-situ water contents: SPR site (Bayomy, and Salem 2005)

3.7 Limitations in the Current Version of EICM Mitigated by the Quantitative Empirical Model

The primary objective of this dissertation is to investigate the impact of climatic factors on water and heat transfer within pavement structures. The main deliverable of this dissertation is to develop a Quantitative Empirical Model (the QE Model) which is an LCI boundary condition, to predict volumetric water contents within subgrades. The development of the QE Model is intended to mitigate the primary limitations in the current version of EICM. The primary limitations of the current version of EICM mitigated by the QE Model are shown in Table 3.11.

Table 3.11: Limitations in current version of EICM mitigated by the Quantitative Empirical Model

Primary features of the Quantitative Empirical Model (QE Model)	Limitations in the current version of EICM (current EICM) mitigated by features in the Quantitative Empirical Model (QE Model)
Incorporates the impact of climatic factors on water and heat transfer within subgrades.	Current EICM produces uneconomical pavement structures because it neglects climatic factors. Current EICM neglects the impact of climatic factors on fluctuations in water and heat transfer and the associated resilient moduli of subgrades.
Accounts for the LCI beyond the pavement surface.	Current EICM accounts for only minimal infiltration through cracks on pavement surfaces.
Incorporates the net infiltration beyond the pavement surface which accounts for precipitation induced infiltration, evapotranspiration and runoff.	Current EICM has an overreliance on the water table and inaccurately accounts for increases in precipitation induced infiltration.
Accounts for both liquid water and water vapour transfer within subgrades.	Current EICM accounts for only liquid water and neglects water vapour transfer.
Incorporates the evapotranspiration.	Current EICM neglects the evapotranspiration.
Incorporates the relative humidity.	Current EICM neglects the impact of relative humidity on the evapotranspiration.
Accounts for changes in the temperature profile within subgrades.	Current EICM assumes a constant subgrade temperature.
Incorporates the wind speed.	Current EICM has an inaccurate heat transfer boundary condition. Current EICM has an inaccurate convective cooling during high air temperatures because it neglects wind speed.
The QE Model accurately predicts site specific volumetric water contents within subgrades and does not require local calibration.	Current EICM requires site specific calibration of the volumetric water contents prediction model.

Chapter 4 Development and Verification of Transient Water and Heat Transfer Models of Pavement Structures

4.1 Introduction

Chapter 4 provides a flow chart describing the tasks conducted for developing and calibrating the transient water and heat transfer models. Chapter 4 also provides details of sources of in-situ monitoring data, pavement cross-section, material properties, in-situ water contents, and depths to the water table. The Chapter provides input parameters for the water and heat transfer finite element analysis (FEA) modeling including site-specific climatic factors, vegetation data, volumetric water contents, hydraulic conductivity function parameters, and initial groundwater condition parameters.

Chapter 4 presents the methodology used for developing the one-dimensional (1-D) and two-dimensional (2-D) transient water and heat transfer FEA modeling (1-D and 2-D FEA modeling) within subgrades. The 1-D and 2-D FEA modeling was conducted to investigate the influence of changes in climatic factors and land climate interaction (LCI) on water and heat transfer within unsaturated subgrades.

Chapter 4 also presents the methodology used for developing LCI boundary conditions and details of the calibration and verification of the 1-D and 2-D FEA models. The Chapter provides analyses of the 1-D and 2-D water and heat transfer FEA modeling output including the 1-D FEA net infiltration output, 2-D FEA volumetric water contents output and 1-D FEA evapotranspiration output. The Chapter also provides analyses of the spatial distribution of volumetric water contents. The Chapter also provides details of the impact of changes in climatic factors on lag times. Lag times are associated with the response times of changes in volumetric water contents to changes in climatic factors.

4.2 Summary of Tasks Conducted to Develop and Verify 1-D and 2-D FEA Models

Chapter 4 focuses on the development and verification of the 1-D and 2-D water and heat transfer FEA (1-D and 2-D FEA) modeling of two pavement structures. The Chapter also focuses on analyses of the 1-D and 2-D FEA modeling output and include the net infiltration flux, volumetric water contents, and evapotranspiration. The eight tasks conducted to develop, verify and analyze the 1-D and 2-D FEA modeling output presented in Chapter 4 are summarized in Figure 4.1.

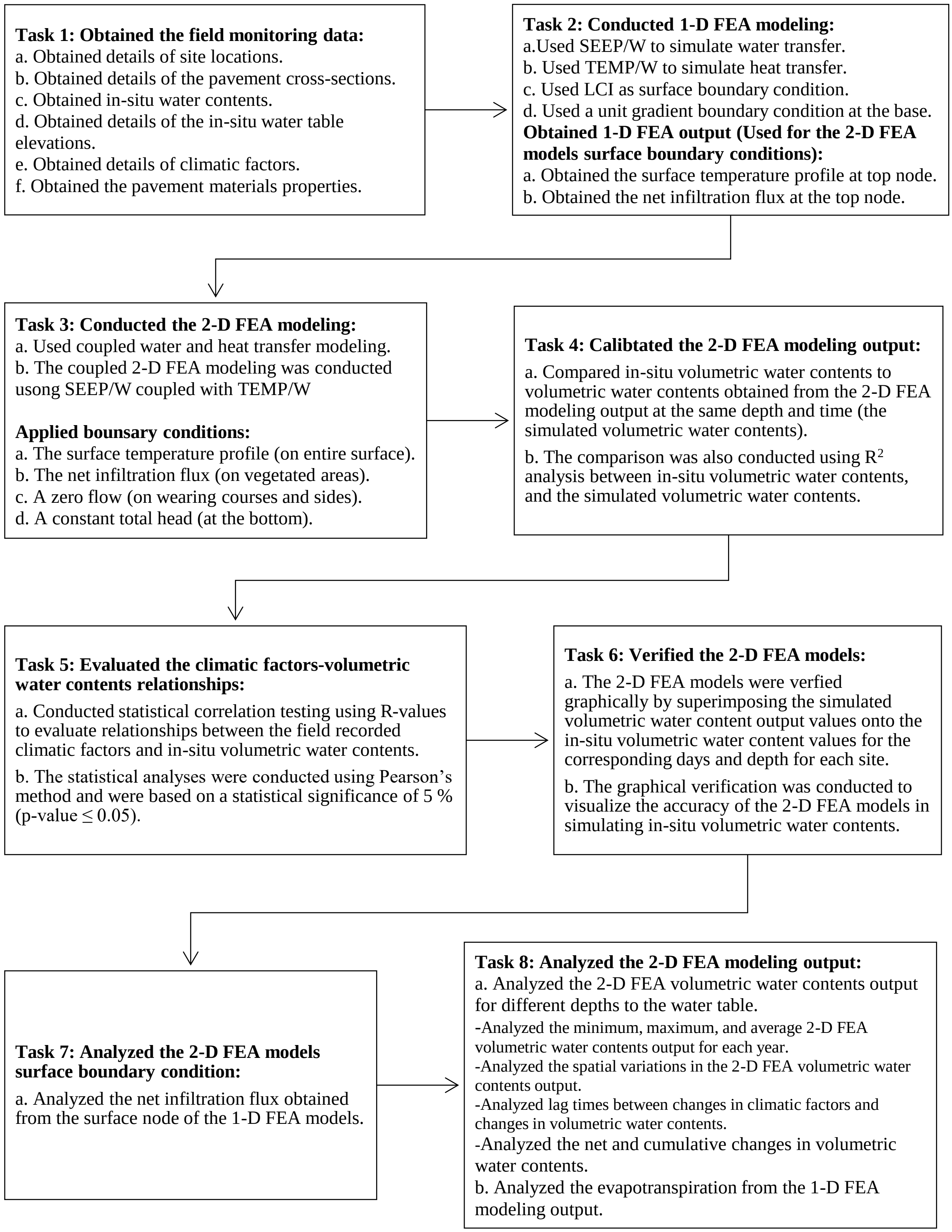

Figure 4.1: Flow chart summarizing tasks conducted to develop and verify FEA models

4.3 Field Monitoring Data Sources

The two research sites used for the 1-D and 2-D FEA modeling form part of the Long-Term Pavement Performance (LTPP) and Seasonal Monitoring Program (SMP) implemented through the Federal Highway Administration (FHWA). The 1-D and 2-D FEA modeling was conducted using one rigid pavement section located on US Highway 2/Minnesota Highway 6 in Minnesota with LTPP-SMP State Code 27 and SHRP ID 4040; 47.3088N, 93.7167W as shown in Figure 4.2 (Research Site No. 1). The second rigid pavement section was located on US Highway 41 in Indiana with LTPP-SMP State Code 18 and SHRP ID 3002; 40.5972N, 87.3803W as shown in Figure 4.3 (Research Site No. 2). The two research sites are in a wet freeze climatic zone. The wet freeze climatic zone includes 18 states in the United States (Minnesota, Indiana, New York, North Dakota, Illinois, South Dakota, Washington, Iowa, Connecticut, Idaho, Kansas, Pennsylvania, Michigan, Montana, Virginia, Colorado, New Hampshire and Ohio) and 10 provinces in Canada (Alberta, Manitoba, Ontario, Quebec, British Columbia, Saskatchewan, New Brunswick, Prince Edward Island, Newfoundland and Nova Scotia).

A summary of the cross-section details and material properties of the two research sites is presented in Table 4.1 and Table 4.2 respectively. The thickness of the granular base course below the traffic lanes was similar for both sites. The thickness of the granular base course below the shoulder at Research Site No.1 was more than twice the thickness of the granular base course below the shoulder at Research Site No. 2. The subgrade at both sites consisted of compacted sandy lean Clay which is clasified as A-6. Materials properties used in the 1-D and 2-D FEA modeling were obtained from field and laboratory testing from the LTPP and SMP, and were also calculated from published data.

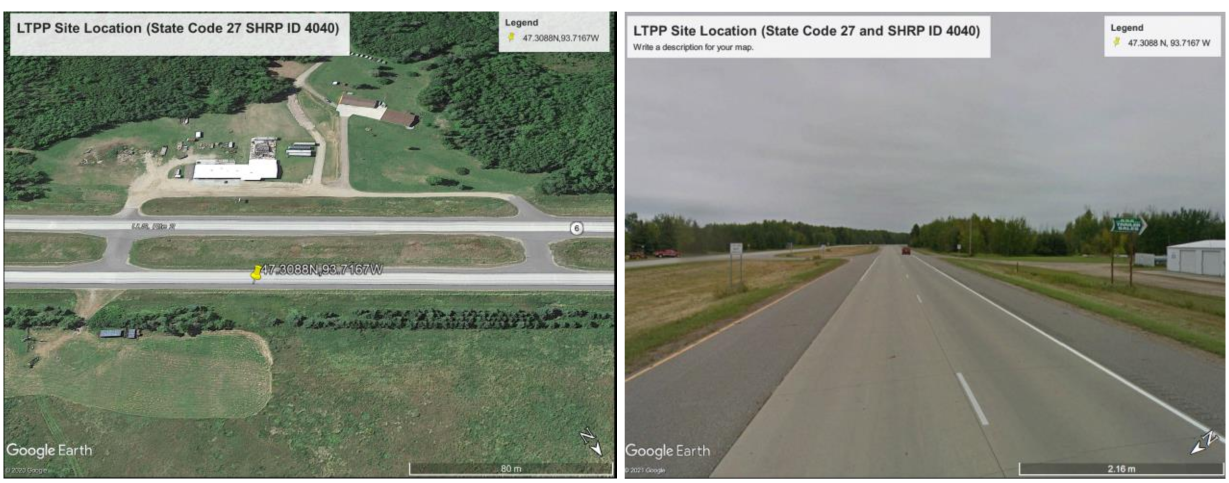

Figure 4.2: Research Site No. 1, US HWY 2/Minnesota HWY 6 (Google Earth, 2020)

Figure 4.3: Research Site No. 2, US HWY 41, Indiana (Google Earth, 2020)

Table 4.1: Pavement structures cross-section details used in the FEA modeling for the two sites (LTPP and SMP 2020)

Materials	Location	Layer Thickness (mm)			
		Research Site No. 1		Research Site No. 2	
		Within traffic lanes	Within Shoulders	Within traffic lanes	Within Shoulders
Granular base course	Below the wearing course	150.0	292.0	150.0	140.0
Compacted subgrade	Below the granular base course	400.0	-	400.0	-

Table 4.2: Pavement materials properties used in the FEA modeling for the two sites (LTPP and SMP 2020)

Materials Layer	Location	Material Description	Condition used in the FEA Models
Granular base course	Below wearing course in traffic lanes	A-1-b: Granular: Unbound	Compacted
Granular base course	Below wearing course in shoulders	A-1-b: Granular: Unbound	Compacted
Compacted subgrade	Below granular base course in traffic lanes	A-6: sandy lean Clay	Compacted
Native soil cover	Median, side slopes and ditches	A-6: sandy lean Clay	Grass, shrubs, and trees
Native soil top layer	Top layer of subsurface soil	A-6: sandy lean Clay	In-situ condition
Native soil bottom layer	Bottom layer of subsurface soil	A-6: sandy lean Clay	In-situ condition

The pavement cross-section details and summary of depths to the water table for Research Site No.1 and Research Site No.2 are shown in Figure 4.4 and Figure 4.5 respectively. Research Site No.1 is in Minnesota within a lake region and is adjacent to many lakes and shallow ponds with the bottom elevation of these shallow ponds located above the subgrade surface. Research Site No.2 is in Indiana in a region characterized by grassland and farmland. The two sites are located approximately 1,200.0 km apart in different environments including different surface water conditions. The depths to the piezometric surface for the two pavement sections were obtained from the LTPP and SMP (2020) database and are presented graphically in Figure 4.6. The analysis of the data presented in Figure 4.6 shows fluctuations in the depth to the piezometric surface at the two sites due to changes in climatic factors and environmental conditions. The water table elevation at Research Site No.1 was also influenced by the surface water conditions including the adjacent lakes and shallow ponds. The water table at Research Site No.1 was at shallower depths than the water table at Research Site No.2.

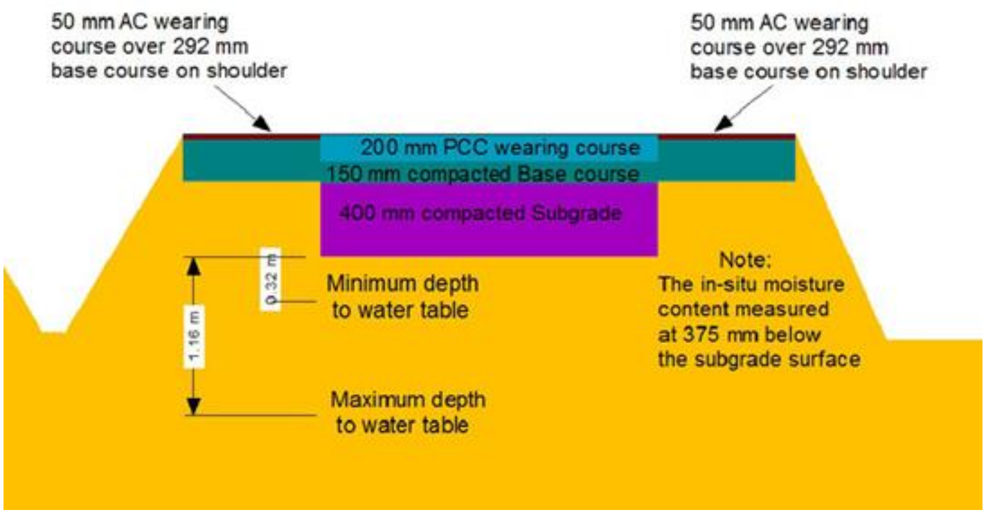

Figure 4.4: Pavement cross-section details for Research Site No. 1

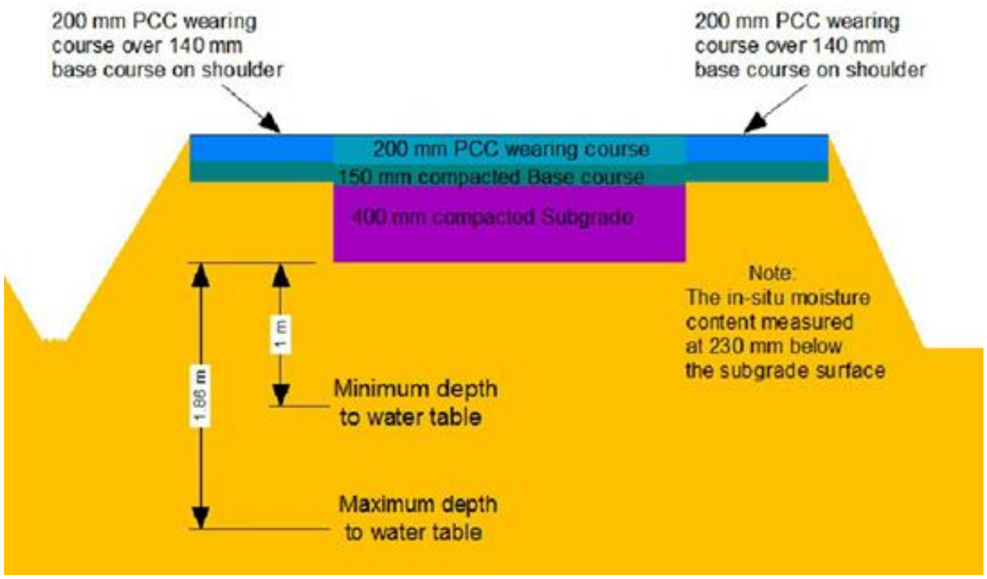

Figure 4.5: Pavement cross-section details for Research Site No. 2

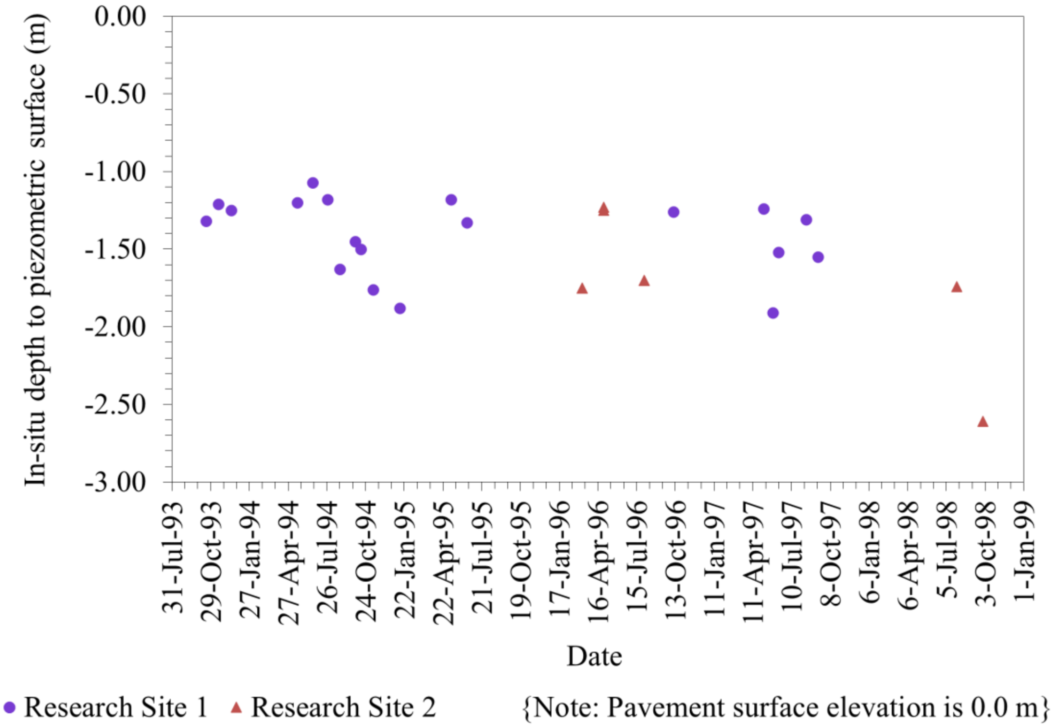

Figure 4.6: In-situ depth to the piezometric surface for Research Site No.1 and Research Site No. 2

In-situ volumetric water contents measured at Research Site No. 1 and Research Site No. 2 were used for calibrating the 2-D FEA models and are presented in Figure 4.7. The analysis of the data presented in Figure 4.7 indicated seasonal fluctuations in volumetric water contents at both sites. The analysis also indicated that the fluctuations in the unfrozen volumetric water contents were influenced by fluctuations in the depths to the piezometric surface during unfrozen conditions. Shallower depths to the piezometric surface resulted in higher volumetric water contents. The analysis also indicated that volumetric water contents at both sites fluctuated seasonally in response to seasonal changes in climatic factors and environmental conditions.

The measured in-situ volumetric water contents: Research Site No. 1 and Research Site No.2

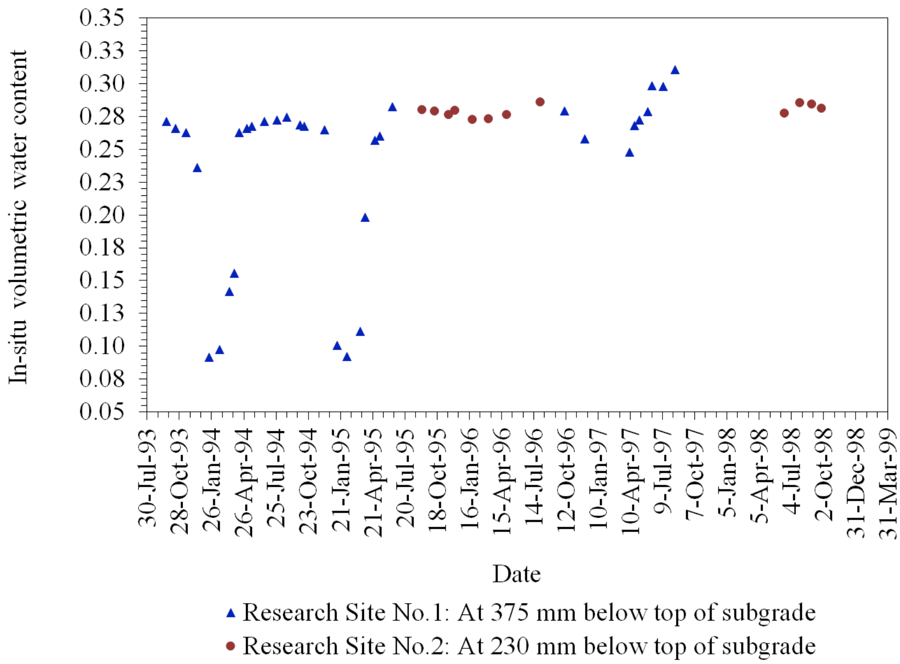

Figure 4.7: The measured in-situ volumetric water contents (LTPP and SMP, 2020)

4.3.1 Climatic Factors used as Input in the 1-D FEA Modeling

Table 4.3 shows the six climatic factors used as input for the 1-D FEA modeling. The six climatic factors are also presented graphically in Figure 4.8 to Figure 4.19. The daily 24-hour datasets used for each climatic factor were recorded from 01st October 1979 (construction completion date) to 20th September 2017 (38-years analysis period) for Research Site No. 1, and from 01st August 1976 (construction completion date) to 21st July 2014 (38-years analysis period) for Research Site No. 2.

The analyses of the air temperature data presented in Figure 4.8 show that significant freezing temperature (approximately -40 ^{o}C) measured during the winter of 1994 and 1995 for Research Site No.1, induced significant reduction in the measured in-situ water contents within the subgrade. The data also show that warmer winter temperatures (which cause thawing of the subgrade and more unfrozen pore water) and lower summer temperatures (which are associated with reduced evapotranspiration) measured in 1997 induced increased water contents within the subgrade for Research Site No.1 as shown in Figure 4.7. The analyses of the precipitation data presented in Figure 4.10 show that the increased precipitation measured in the summer of 1997 also contributed to the increased water contents within the subgrade for Research Site No.1 in the summer of 1997.

Table 4.3: Summary of climatic factors used as input for the 1-D FEA modeling

Climatic factor	Primary application in the 1-D FEA modeling
Air temperature	For heat conduction, coupled convective-thermal modeling, forced convection and natural convection processes.
Precipitation	For primary source of water, liquid water transfer and to support forced convection with water transfer.
Net solar radiation	For net solar radiation-air temperature-evapotranspiration processes.
Relative humidity	For evapotranspiration-relative humidity process.
Wind speed	For air temperature-wind speed-evapotranspiration process.
Snow depth	For contribution to total precipitation.

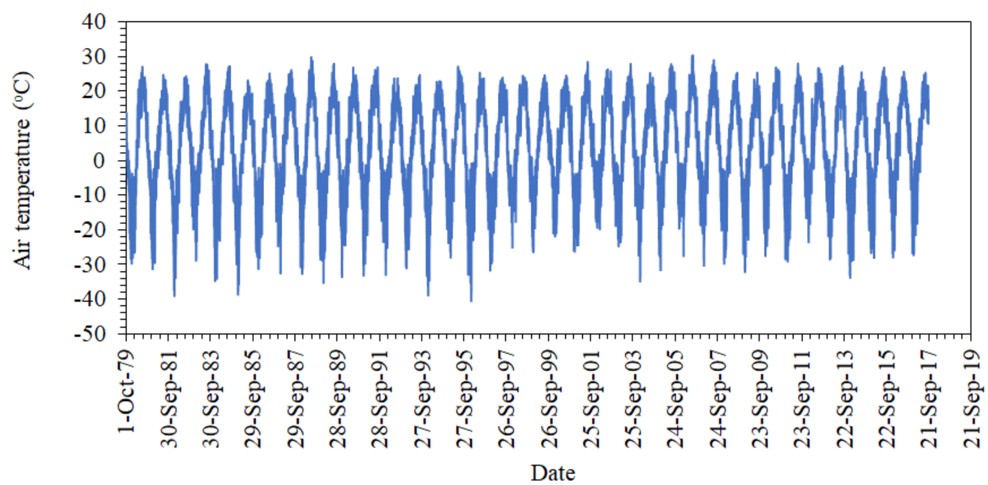

Figure 4.8: Daily air temperature vs. time for Research Site No. 1 (LTPP and SMP, 2020)

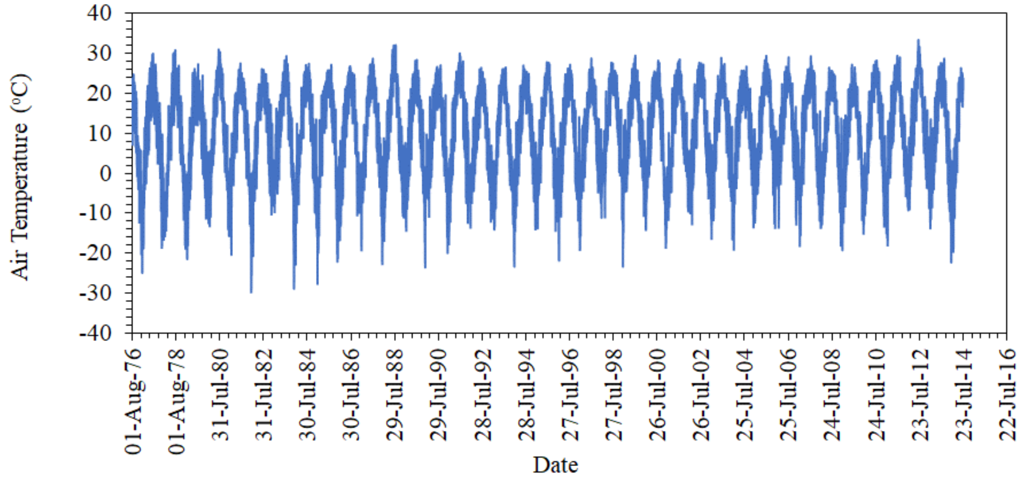

Figure 4.9: Daily air temperature vs. time for Research Site No. 2 (LTPP and SMP, 2020)

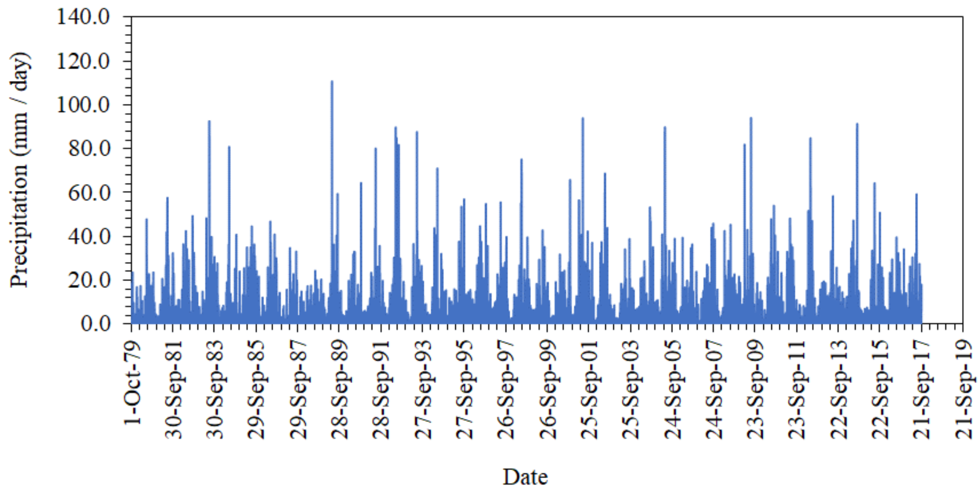

Figure 4.10: Daily precipitation vs. time for Research Site No. 1 (LTPP and SMP, 2020)

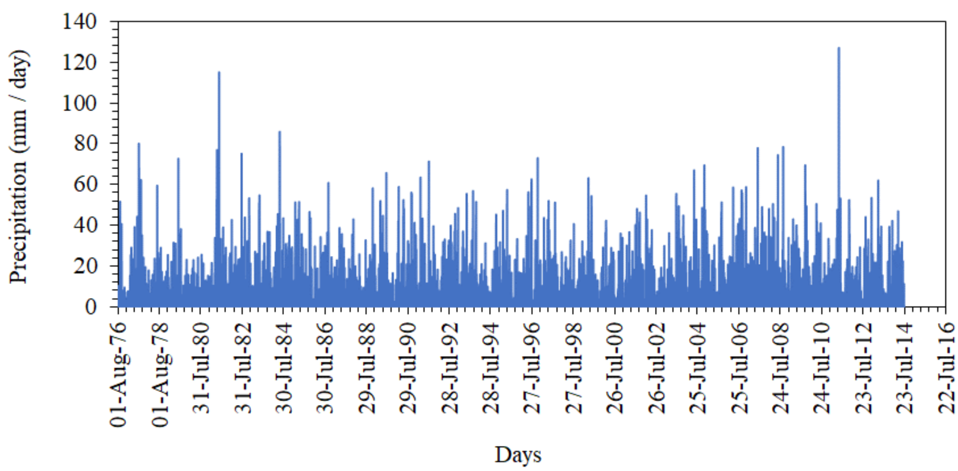

Figure 4.11: Daily precipitation vs. time for Research Site No. 2 (LTPP and SMP, 2020)

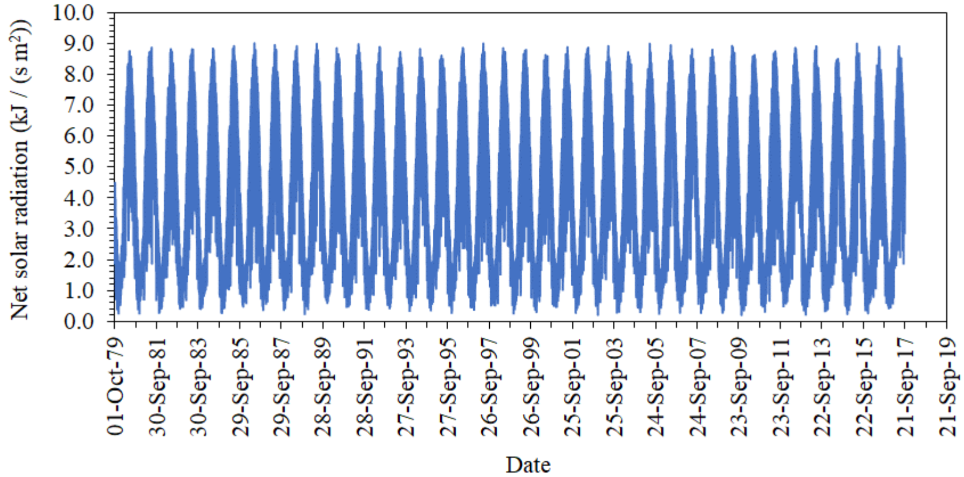

Figure 4.12: Daily net solar radiation vs. time for Research Site No.1 (LTPP and SMP, 2020)

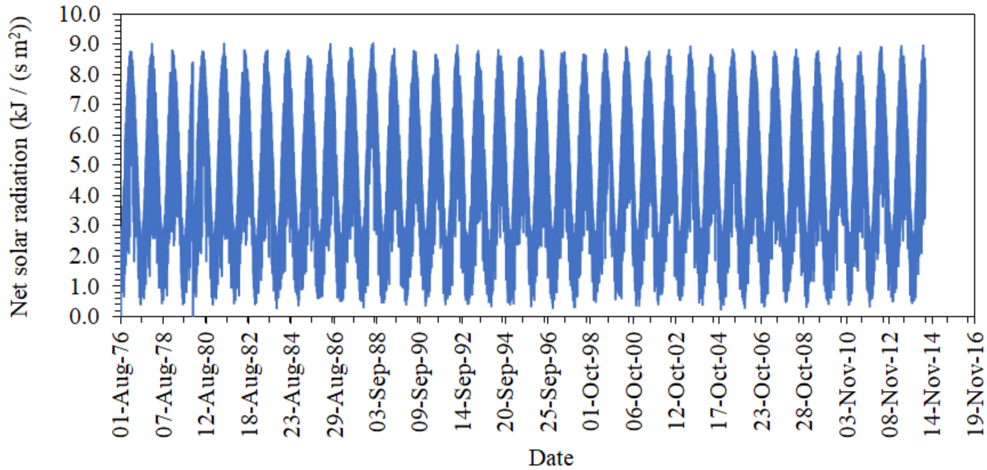

Figure 4.13: Daily net solar radiation vs. time for Research Site No.2 (LTPP and SMP, 2020)

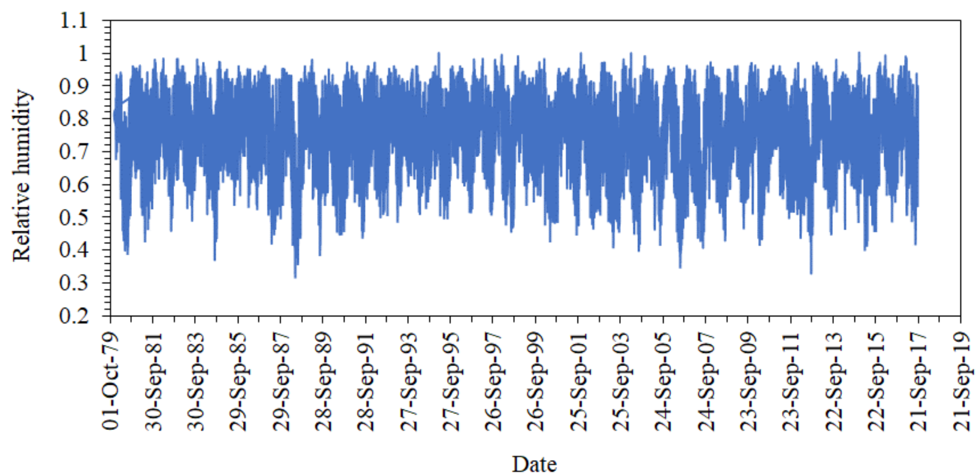

Figure 4.14: Daily relative humidity vs. time for Research Site No.1 (LTPP and SMP, 2020)

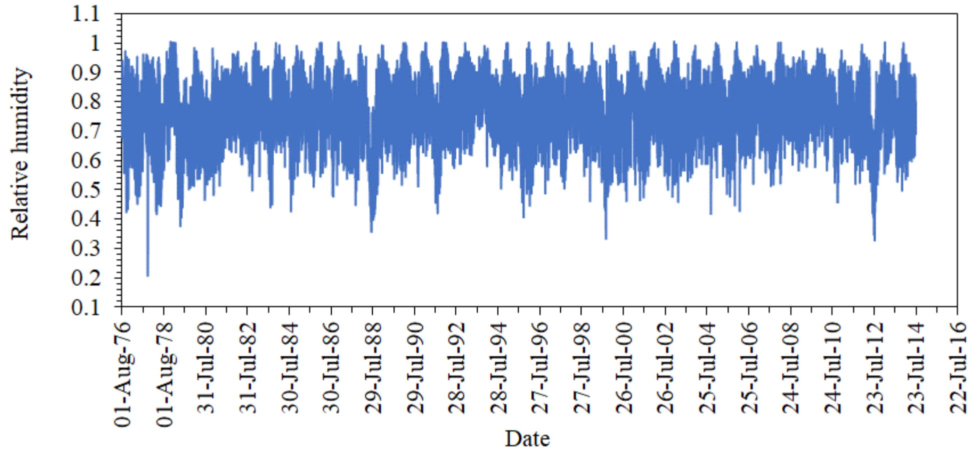

Figure 4.15: Daily relative humidity vs. time for Research Site No.2 (LTPP and SMP, 2020)

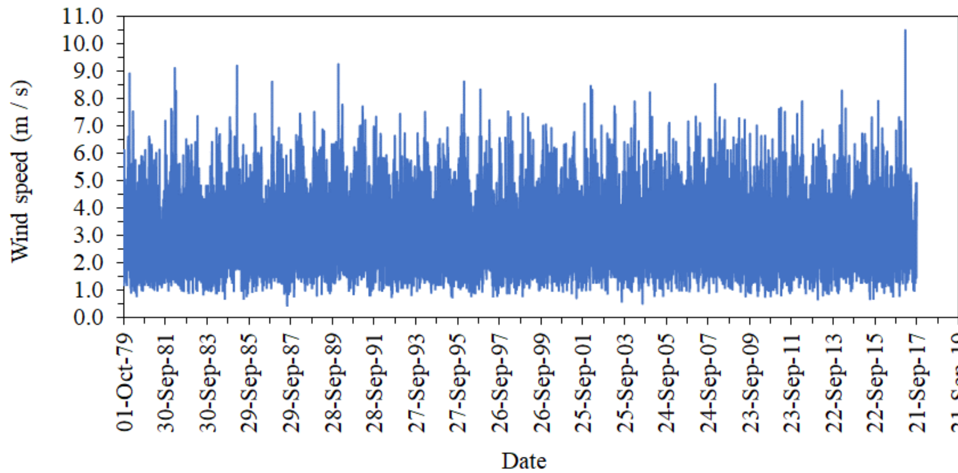

Figure 4.16: Daily wind speed vs. time for Research Site No.1 (LTPP and SMP, 2020)

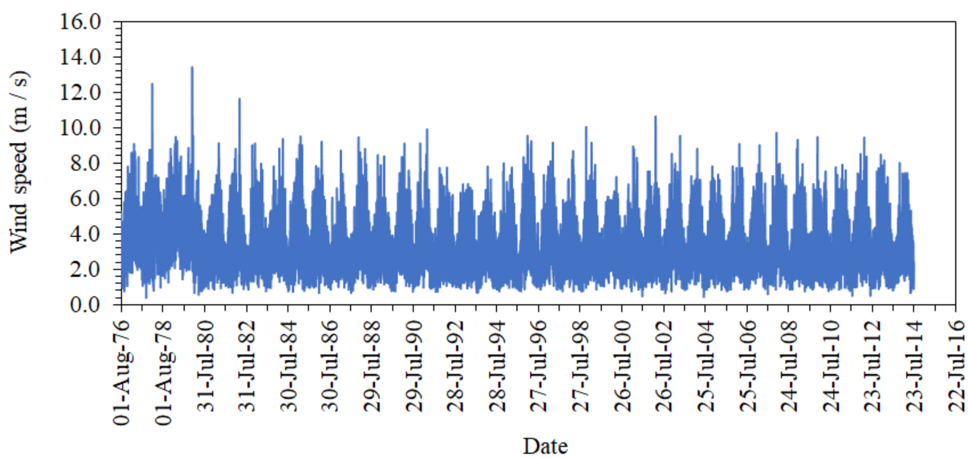

Figure 4.17: Daily wind speed vs. time for Research Site No.2 (LTPP and SMP, 2020)

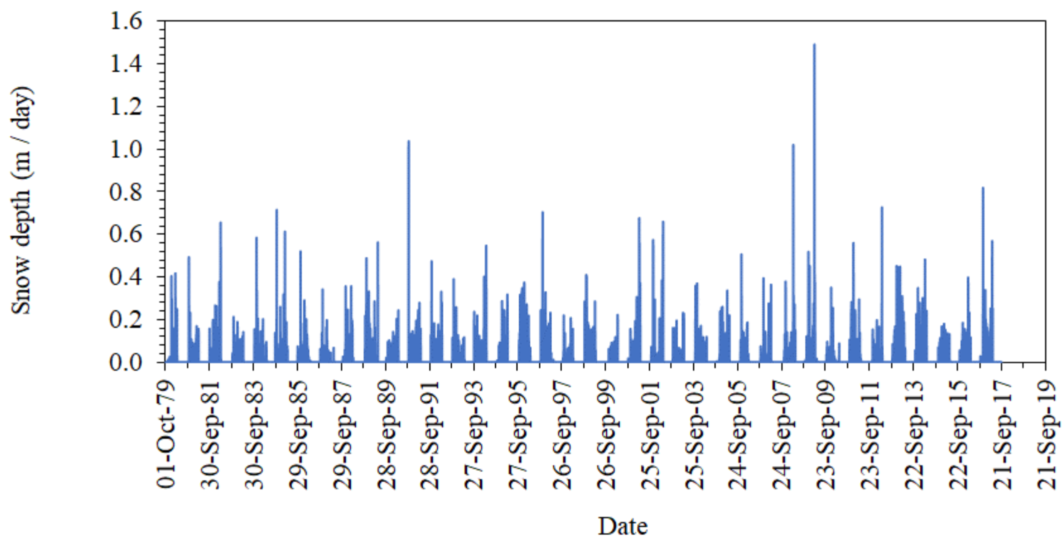

Figure 4.18: Daily snow depth vs. time for Research Site No.1 (LTPP and SMP, 2020)

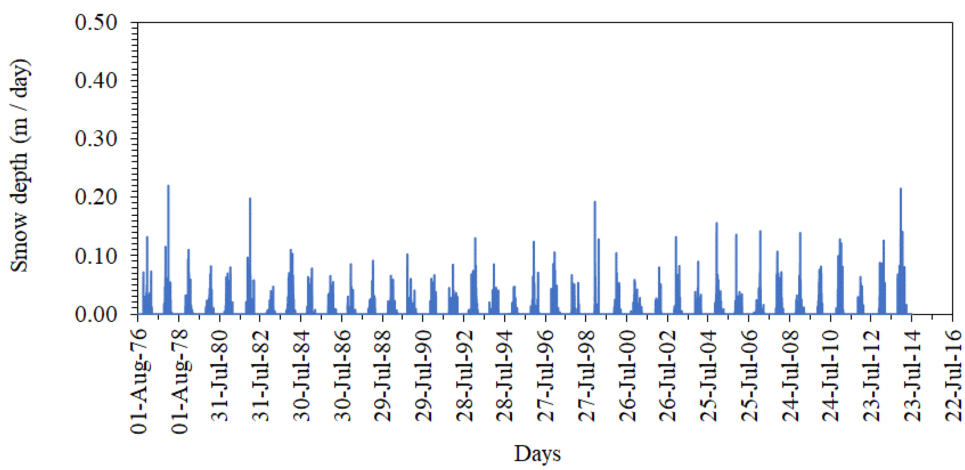

Figure 4.19: Daily snow depth vs. time for Research Site No.2 (LTPP and SMP, 2020)

4.3.2 Vegetation Function Parameters Obtained from Previous Studies

The 1-D FEA models use the soil-water-plant relationships as input to evaluate the soil water retention characteristics and the impact of the soil-water-plant relationships on evapotranspiration (GeoSlope 2020; Ramirez-Garcia, et al. 2012; Mullan, and Reynolds 2010; Thorup-Kristensen, et al. 2009; Evans, et al. 1996). The vegetation function parameters used as input for the 1-D FEA modeling for vegetated areas were obtained from previous studies. The vegetation function parameters obtained from previous studies include the leaf area index function, the ground cover-leaf area index relationship and the root depth function.

The Leaf Area Index Function

The leaf area index (LAI) vs time function (the LAI function) is used to characterize the crop canopy. The LAI function is the ratio of the sum of the projected area of the leaves and the unit of ground surface covered. The LAI changes seasonally due to changes in climatic factors and the environmental conditions. The LAI function varies during the development stages of crops and vegetation throughout the growing season (Dong, et al. 2021; Anapalli, et al. 2005).

The areas adjacent to the pavement section at the Research Site No.1 in Minnesota (as shown in Figure 4.2) consist primarily of corn and wheat crops (United States Department of Agriculture 2017).The areas in the vicinity of the pavement section at the Research Site No.2 consist primarily of corn as shown in Figure 4.3. Hence, an average of the LAI function for the wheat and corn crops is used for Research Site No. 1, while an LAI function for corn is used for Research Sire No.2. The LAI functions for wheat and corn were obtained from studies completed by Dong, et al. (2021); Papanikolaou, and Sakellariou-Makrantonaki (2020); Anapalli, et al. 2005. The LAI function datasets were exported to Excel where the graphical relationships were developed as shown in Figure 4.20.

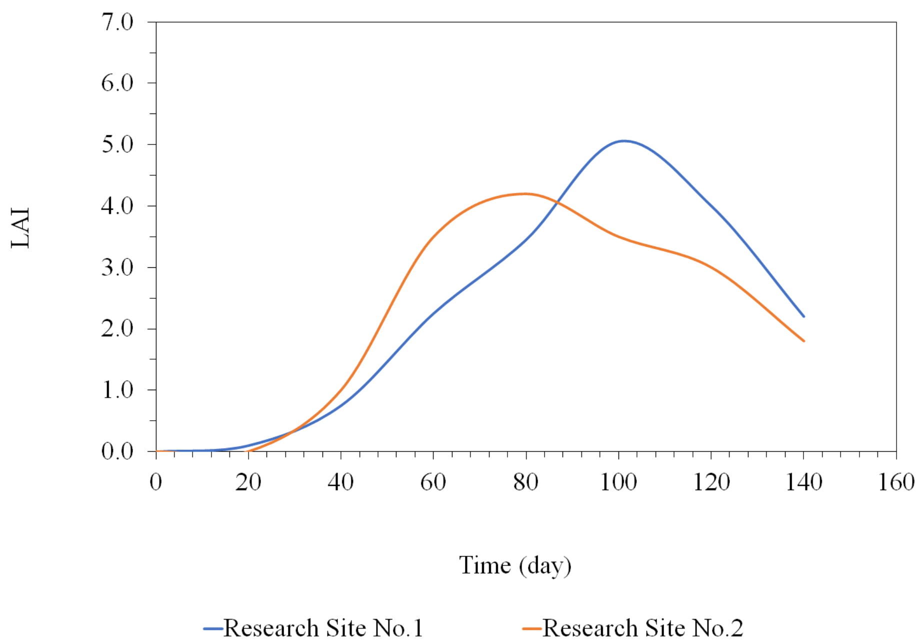

Figure 4.20: Leaf area index function for Research Site No. 1 and Research Site No. 2

The Ground Cover-Leaf Area Index Function

The ground cover (GC) represents the percentage of the ground surface which is covered by crops and/or the vegetation. A higher GC contributes to a lower rate of evaporation of the water within soils and the GC increases with an increase in LAI. The ground cover-leaf area index (the GC-LAI function) used in this study represents the crop canopy characteristics for the respective crop and vegetation (Ramirez-Garcia, et al. 2012; Mullan, and Reynolds 2010). The GC-LAI function for the combined wheat and corn crops (for Research Site No.1) and for the corn crop (for Research Site No.2) used as input in the 1-D FEA modeling were obtained from previous studies conducted by Nielsen, et al. (2012). The GC-LAI datasets were exported to Excel and the relationship were developed graphically as shown in Figure 4.21.

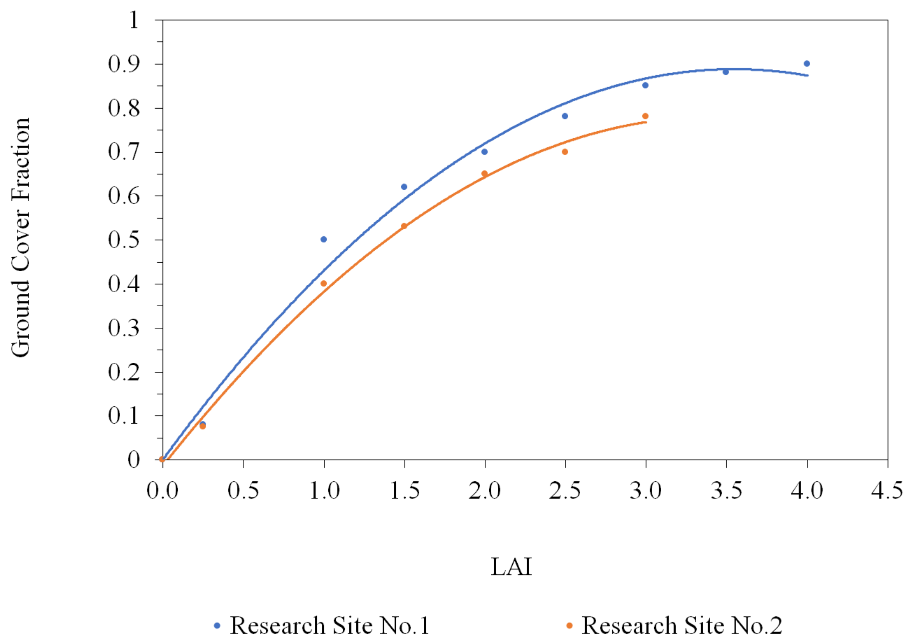

Figure 4.21: Ground cover-leaf area index function for Research Site No. 1 and Research Site No. 2

<u>The Root Depth Function</u>

The root depth vs time relationship (the root depth function) is influenced by the plant species, soil type, the crop and vegetation development stages, the seasonal climatic factors and environmental conditions. The root depth function accounts for the maximum potential root depth and the time that the maximum root depth is achieved (Thorup-Kristensen, et al. 2009; Evans, et al. 1996).

An average root depth function for wheat and corn crops was used for Research Site No.1, while the root depth function for corm was used for Research Site No.2. The root depth function for corn was obtained from a study completed by Evans, et al. (1996), while the root depth function for wheat was obtained from a study completed by Thorup-Kristensen, et al. (2009). The datasets were exported to Excel and the root depth-time relationships were developed as shown in Figure 4.22.

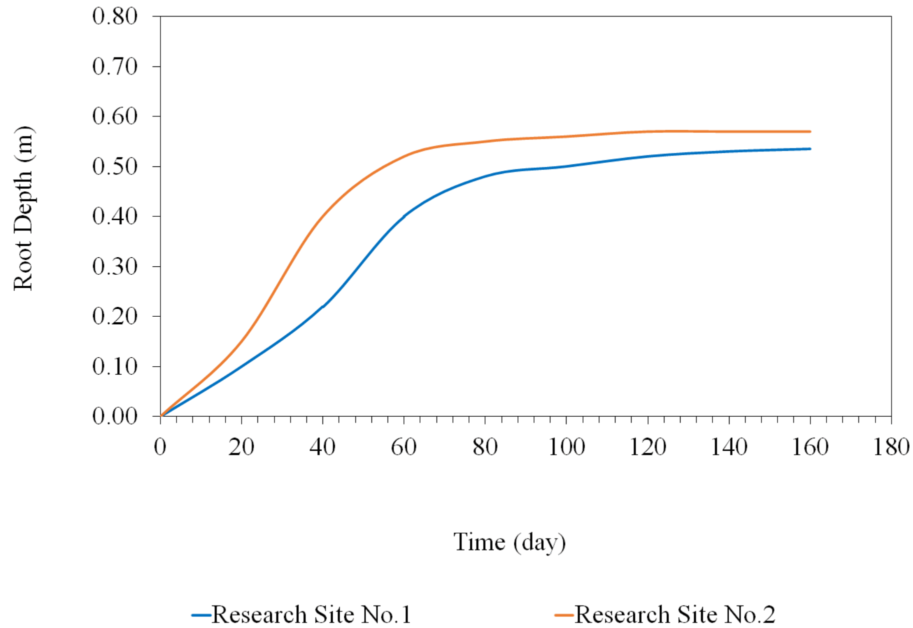

Figure 4.22: Root depth function for Research Site No. 1 and Research Site No. 2

4.3.3 Vegetation Function Parameters Calculated Using Empirical Relationships Provided in Previous Studies

The vegetation function parameters used as input for the 1-D water and heat transfer FEA modeling for vegetated areas were also calculated from empirical equations provided in previous studies. The vegetation function parameters calculated using empirical equation from previous studies include the root density distribution function and the plant water limit function.

The Root Density Distribution Function

Studies have indicated that root depths typically increase over the growing season. These studies also show that the normalized root density characterizes the root characteristics-plant water uptake relationship. Hence, the root density distribution is represented by the normalized root density vs the normalized root depth to account for the influence of the maximum root depth on the root distribution (the normalized root density function). The input parameters for this function include variations of root length due to changes in the relative soil depth. This relationship incorporates the plant root characteristics which are influenced by the soil depth and the maximum root depth (Wu, et al. 1999). The analysis was completed in Excel and is presented in Figure 4.23.

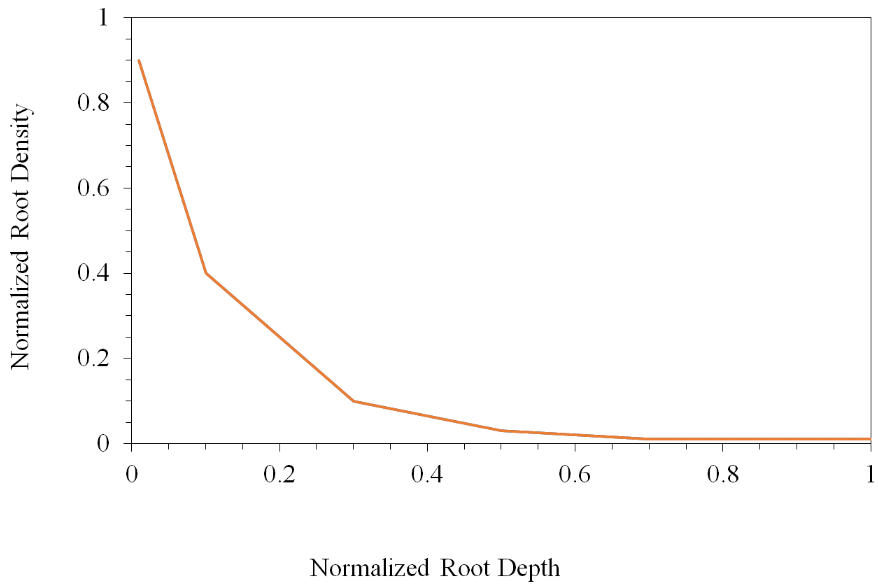

Figure 4.23: Normalized root density function for Research Site No. 1 and Research Site No. 2

<u>The Plant Water Limit Function</u>

The plant water limit is represented by the limiting factor-matric suction relationship. The plant water limit represents the influence of atmospheric conditions on the relationship between the maximum root water uptake, root density and rate of transpiration. The relationship also accounts for changes in the maximum root water uptake due to changes in the soil water pressure. This is achieved by incorporating a reduction coefficient for root water uptake. The limiting factor-matric suction relationship was determined by calculating the actual root water flux density and the maximum root water uptake. The reduction coefficient for the root water uptake-soil water pressure relationship was determined by using varying values of the actual root water flux density to calculate the ratio of the actual root water flux density and the maximum root water uptake, while neglecting the salinity reduction factor. The matric suction was calculated using the relationship between the reduction coefficient for root water uptake and the soil water pressure (Feddes, et al. 2001; Wesseling, 1991; Feddes, et al. 1978). The analysis was conducted in Excel and is presented in Figure 3.24.

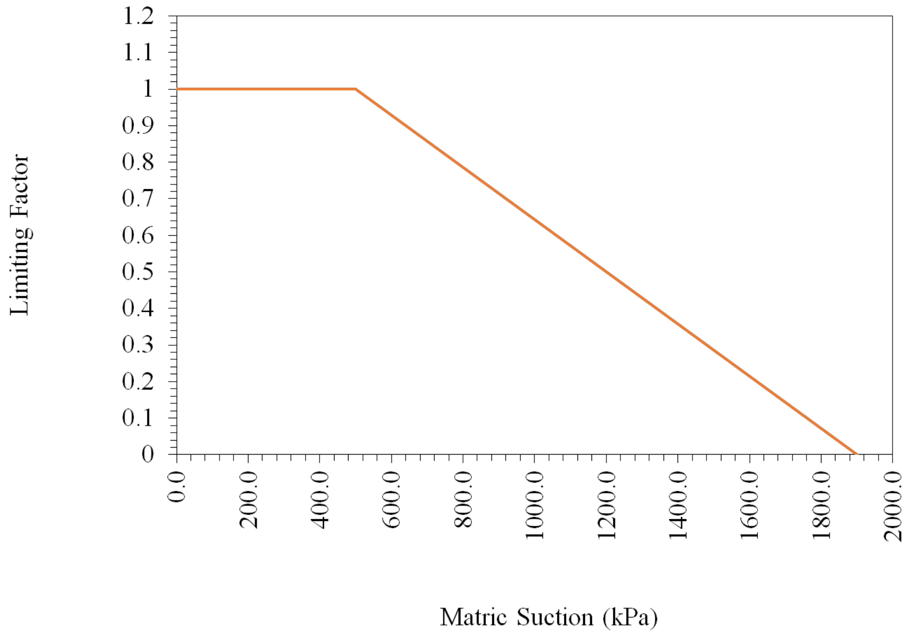

Figure 4.24: Plant water limit function for Research Site No. 1 and Research Site No. 2

Summary of the Crop and Vegetation Functions

The analysis of the vegetation function shown in Figure 4.21 indicated that the corn crop has a higher rate of increase of the LAI than the combined wheat and corn crops within the first 80.0 days after planting. The data also show that the corn crop develops its maximum LAI at approximately 80.0 days after planting. However, beyond 80.0 days after planting, the LAI of the corn crop decreases with time. Although the combined wheat and corn crops have a lower rate of increase of the LAI within the first 80.0 days after planting, the combined wheat and corn crops develop a higher LAI at approximately 100.0 days after planting. The LAI of the combined wheat and corn crops also decrease after approximately 100.0 days after planting. These observations indicate that the corn crop produces a lower ground coverage which contributes to an increase in the evaporation of the water within soils throughout the growing season.

The wheat crop has a higher GC and a higher LAI than that of the corn crop which imply that the wheat crop provides a higher ground coverage than the corn crop. This indicates that the wheat crop contributes to a lower rate of evaporation of the water within soils than the corn crop. The corn crop also has a higher root depth than the wheat crop which implies that the corn crop has a higher root water uptake and facilitates higher transpiration than the wheat crop.

4.3.4 Water Contents, Hydraulic Properties and Water Table Details Used in the FEA Modeling

The volumetric water contents function parameters used in the FEA modeling for each material are presented in Table 4.4. The volumetric water contents function parameters were estimated from the subgrade laboratory testing results and material classification provided in the LTPP and SMP (2020) database. The estimated volumetric water contents function parameters were verified by comparing them to the van Genuchten function parameters for similar soils presented in a study conducted by Wösten, et al. (1999).

The data indicate that the saturated volumetric water content and the air entry value are higher for fine-grained materials, and that the air entry value increases as the material became finer. A compressibility value of zero is used for each material in the FEA modeling because the water within each material is assumed to be incompressible.

Table 4.4: Volumetric water contents function parameters used in the FEA modeling (Wösten, et al. 1999)

Materials: Soil classification	Volumetric water content parameters		Van Genuchten parameters		Ky/kx Ratio	Compressibility (/kPa)
	Saturated water content	Residual water content	a (AEV) (kPa)	n		
Granular base layer (A-1-b)	0.30 to 0.35	0.02 to 0.03	5 to 10	1.3 to 1.6	1.0	0
Subgrade layer (A-6)	0.40 to 0.60	0.04 to 0.05	100 to 150	1.2 to 1.3	1.0	0
Native soil layers (A-6)	0.45 to 0.65	0.05 to 0.06	200 to 300	1.1 to 1.2	1.0	0

The hydraulic conductivity function parameters used in the FEA modeling are presented in Table 4.5. The hydraulic conductivity function parameters were estimated from the subgrade laboratory testing results and material classification provided in the LTPP and SMP (2020) database. The estimated material hydraulic conductivity function parameters were also verified by comparing them to the hydraulic conductivity function parameters for similar soils presented in a study conducted by Wösten, et al. (1999).

The data indicate that saturated hydraulic conductivity decreased as the material became finer. The analyses were based on vertical and horizontal hydraulic conductivity being equal.

Table 4.5: Hydraulic conductivity function parameters used in the FEA modeling (Wösten, et al. 1999)

Materials (Soil Classification)	Hydraulic conductivity point function		
	Saturated k_x (m/sec)	Maximum suction (kPa)	Anisotropy (k_y/k_x)
Granular base layer (A-1-b)	$2.0x10^{-5}$ to $5.0x10^{-5}$	$1.0x10^{4}$	1.0
Compacted Subgrade layer (A-6)	$3.0x10^{-8}$ to $6.0x10^{-8}$	$1.0x10^{6}$	1.0
Native soil layers (A-6)	$3.0x10^{-9}$ to $8.0x10^{-9}$	$1.0x10^{6}$	1.0

The thermal properties of the pavement materials were estimated from data presented in a studies conducted by Applied Research Associates Inc. (2004) and Pahud (2002). The data indicate that the thermal conductivity decreases as the material become finer, while the volumetric heat capacity increases as the material become finer. A summary of thermal properties of each material are shown in Table 4.6 and Table 4.7.

Table 4.6: Materials thermal property parameters used in the FEA modeling: Research Site No.1 (Applied Research Associates Inc. 2004; Pahud 2002)

Materials (Soil Classification).	Thermal properties parameters	
	Thermal conductivity (kJ / (m s ºC))	Volumetric heat capacity (kJ / (m^3 ºC))
Granular base (A-1-b)	$6.5x10^{-4}$ to $13.5x10^{-4}$	$1.75x10^{3}$ to $3.25x10^{3}$
Compacted Subgrade (A-6)	$2.5x10^{-4}$ to $8.0x10^{-4}$	$2.25x10^{3}$ to $4.70x10^{3}$
Native soil (A-6)	$1.5x10^{-4}$ to $6.5x10^{-4}$	$2.50x10^{3}$ to $5.25x10^{3}$

Table 4.7: Materials thermal property parameters used in the FEA modeling: Research Site No.2 (Applied Research Associates Inc. 2004; Pahud 2002)

Materials (Soil Classification).	Thermal properties parameters	
	Thermal conductivity (kJ / (s m ºC))	Volumetric heat capacity (kJ / (m^3 ºC))
Granular base (A-1-b)	$6.5x10^{-4}$ to $13.5x10^{-4}$	$1.15x10^{3}$ to $2.45x10^{3}$
Compacted Subgrade (A-6)	$3.0x10^{-4}$ to $8.5x10^{-4}$	$1.50x10^{3}$ to $3.60x10^{3}$
Native soil (A-6)	$1.8x10^{-4}$ to $7.0x10^{-4}$	$1.75x10^{3}$ to $4.25x10^{3}$

Table 4.8 presents activated pore water pressures and activated temperatures data. Activated pore water pressure values increase as the material become finer. Activated pore water pressures were used to

simulate the initial pore water pressure and the corresponding initial volumetric water content. Activated material temperatures were chosen to simulate the in-situ temperature of the respective material layer at the completion of pavement construction. Activated material temperatures were increased with depth relative to activated temperature of the top material layer.

Table 4.8: Initial groundwater conditions parameters used in the FEA (LTPP and SMP, 2020)

Research site ID	Activation porewater pressure (kPa)		
	Materials (Soil Classification)		
	Granular base layer (A-1-b)	Compacted subgrade layer (A-6)	Native soil layer (A-6)
Research Site No.1	-10.0 to -5.0	-1,200.0 to -1,000.0	-2,500.0 to -2,100.0
Research Site No.2	-10.0 to -5.0	-1,000.0 to -800.0	-2,000.0 to -1,800.0
	Activation Temperature (°C)		
Research Site No.1	5.0 to 7.0	6.0 to 8.0	5.0 to 10.0
Research Site No.2	5.0 to 10.0	10.0 to 15.0	10.0 to 15.0

The plots of material property functions presented in Figure 4.25 to Figure 4.28 were developed using the volumetric water content and hydraulic conductivity function parameters presented in Table 4.4 and Table 4.5 respectively. The volumetric water content and hydraulic conductivity function parameters presented in Table 4.4 and Table 4.5 respectively were used as input in the respective van Genuchten (1980) model to develop the SWCC for each material and presented graphically in Excel. A sensitivity analysis was conducted using varying values of the saturated volumetric water content (θ_{sat}), residual volumetric water content (θ_r) and the parameter a′, n and m within the established range for each parameter to generate the best fitting SWCC curves which were developed graphically in Excel.

The thermal property function parameters presented in Table 4.6 and Table 4.7 and the varying volumetric water content values were used as input in the Johansen (1975) and De Vries (1975) models to develop the thermal conductivity-volumetric water content relationship curves as shown in Figure 4.29 and Figure 4.30. The volumetric heat capacity-volumetric water content relationship curves were also developed as shown in Figure 4.31 and Figure 4.32 respectively for each material. The analysis and development of these Figures were conducted in Excel. A sensitivity analysis was conducted using varying values of the thermal property function parameters within the established range for each parameter to generate the best fitting curves.

The data indicate that matric suction is zero at the saturated volumetric water content. The volumetric water content remains constant at the saturated condition with an increase in matric suction up to a matric suction corresponding to the air entry value. Beyond the air entry value, the volumetric water content decreases gradually with an increase in matric suction to a volumetric water content corresponding to the residual water content. The rate of change in volumetric water contents beyond the residual water content is relatively minimal.

Desaturation starts at a volumetric water content value corresponding to a matric suction value which is more than the air entry value and takes place in the transition zone. The air entry value also represents the matric suction value at which air starts to enter the large pores in the soil. The slope of the desaturation section of the volumetric water content vs. matric suction curve is lower for finer materials. This pattern indicates that the rate of change of the volumetric water content due to a unit change in matric suction is lower for finer materials. The relationship shows the basis for the granular base course having a higher rate of desaturation and a lower water storage capacity than the subgrade and native soil. The rate of desaturation is influenced by the grain size distribution of the material and is represented by the parameter "n" in the van Genuchten (1980) model.

A similar pattern was observed for the relationship between hydraulic conductivity and matric suction. The data indicate that the thermal properties increase with an increase in the volumetric water content up to the saturated volumetric water content and are constant beyond the saturated condition. Coarse materials have higher thermal conductivity, and finer materials have higher volumetric heat capacity. The relationship between changes in thermal properties and volumetric water contents of materials was used to facilitate coupled convective-thermal material modeling.

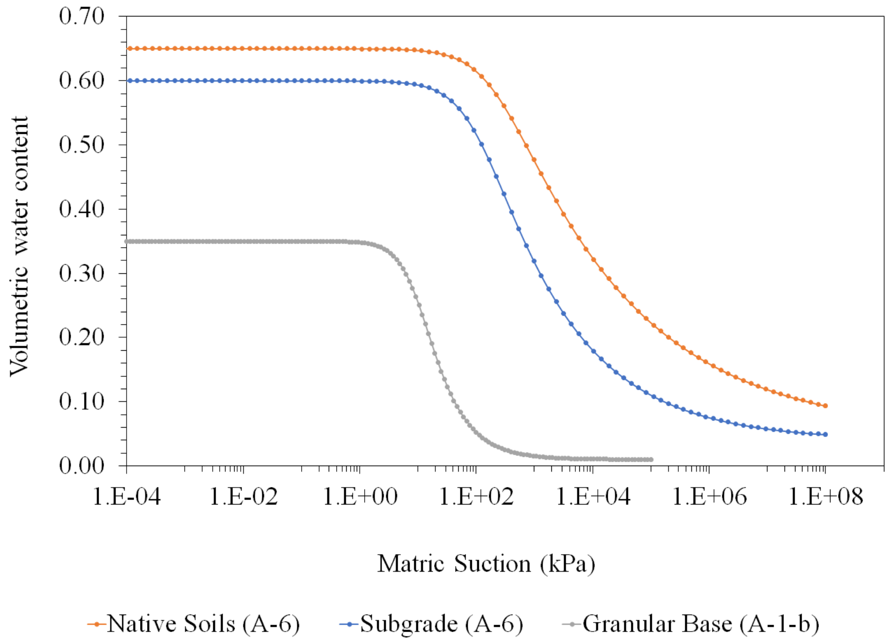

Figure 4.25: SWCC for pavement layer materials for Research Site No. 1

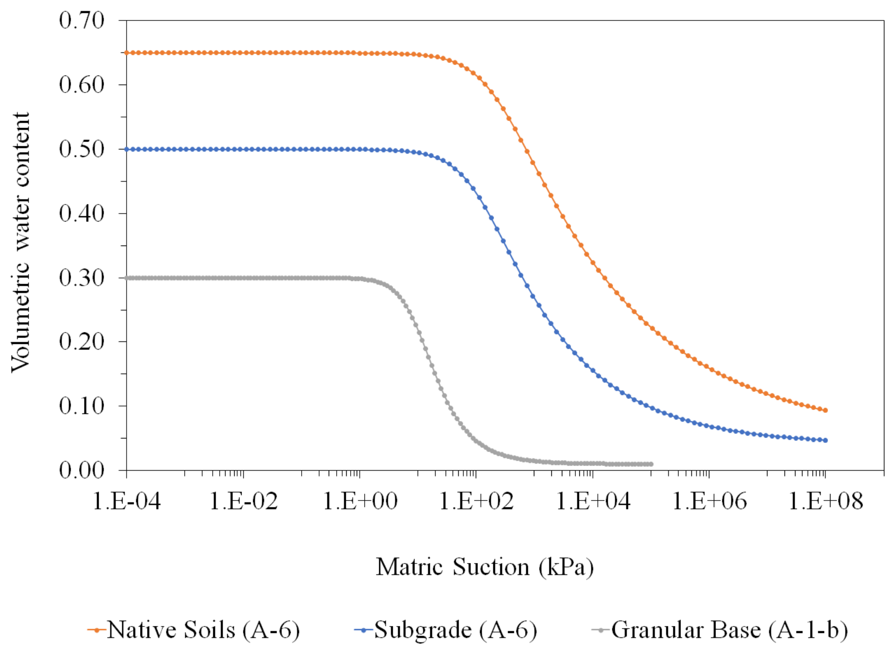

Figure 4.26: SWCC for pavement layer materials for Research Site No. 2

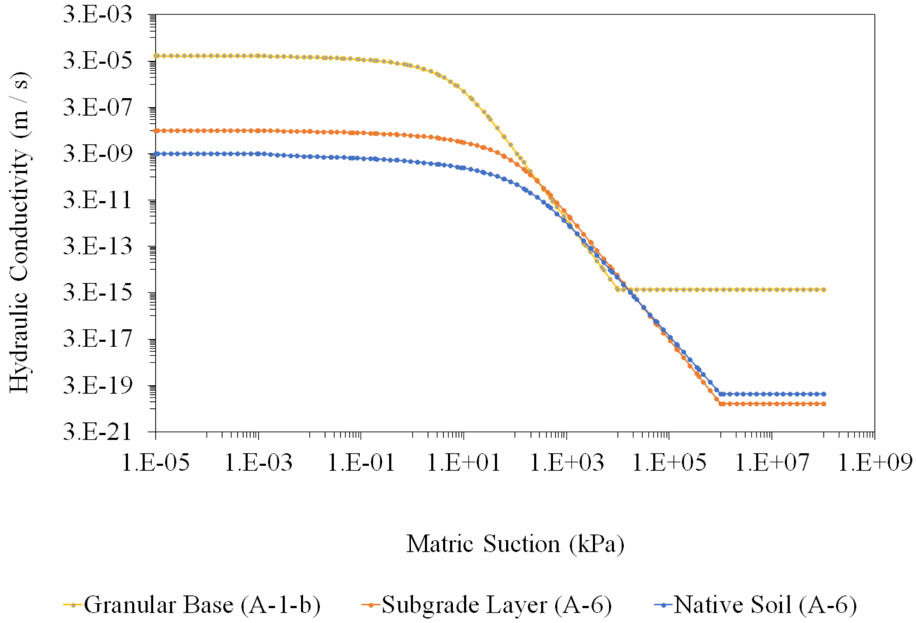

Figure 4.27: Hydraulic conductivity function for pavement layer materials for Research Site No. 1

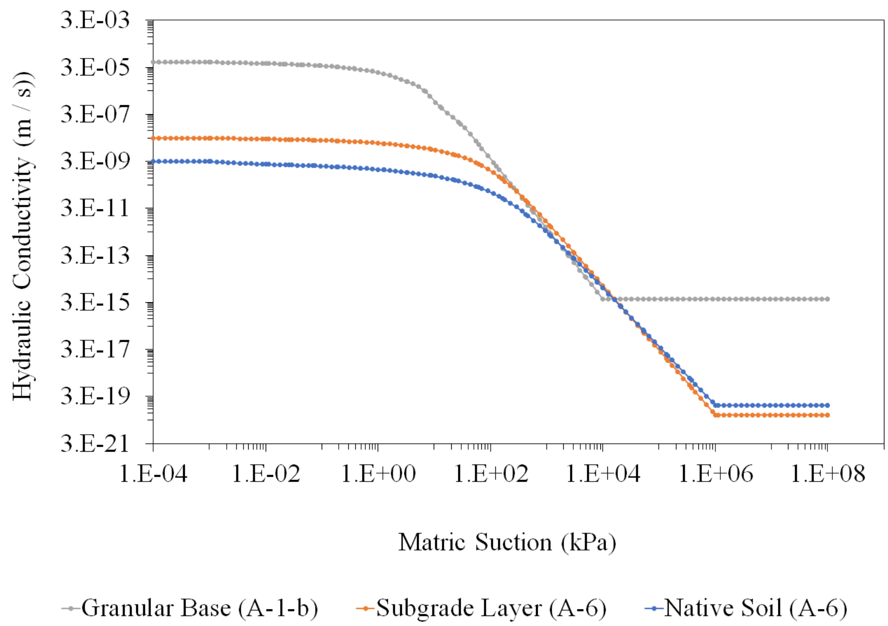

Figure 4.28: Hydraulic conductivity function for pavement layer materials for Research Site No. 2

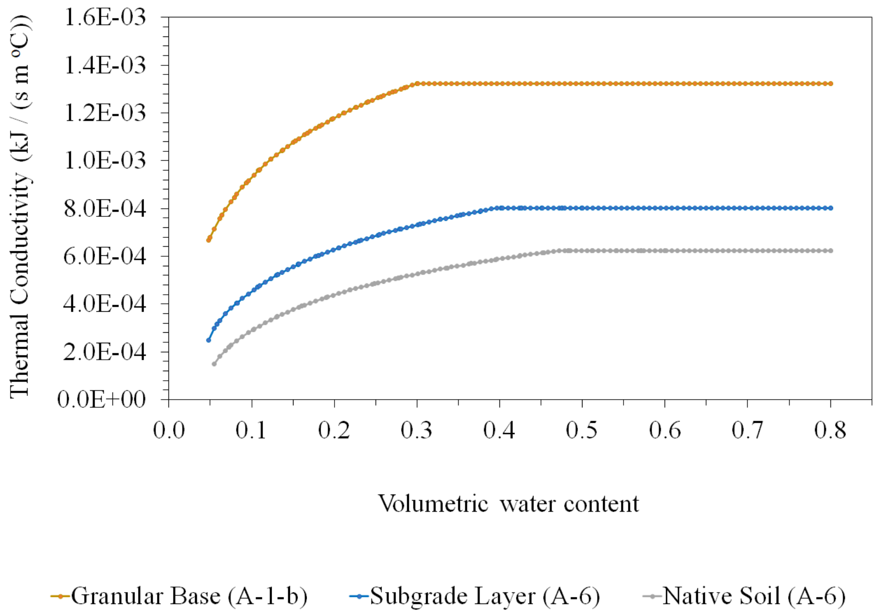

Figure 4.29: Thermal conductivity function for pavement layer materials for Research Site No.1

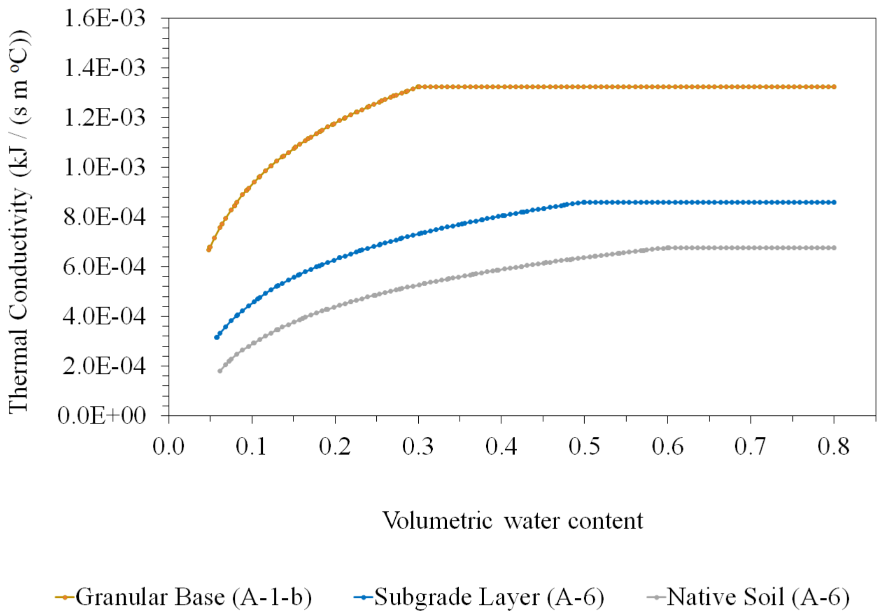

Figure 4.30: Thermal conductivity function for pavement layer materials for Research Site No.2

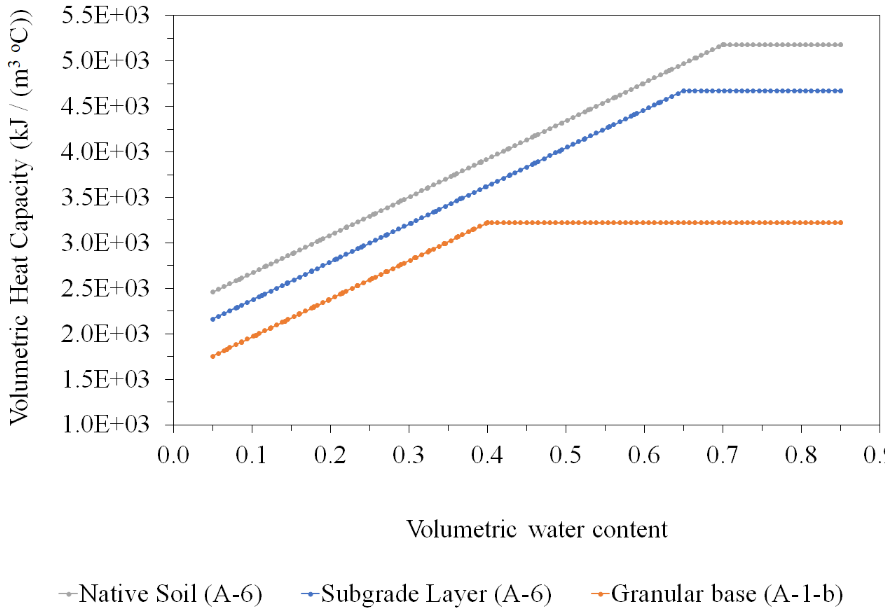

Figure 4.31: Volumetric heat capacity function for pavement layer materials for Research Site No.1

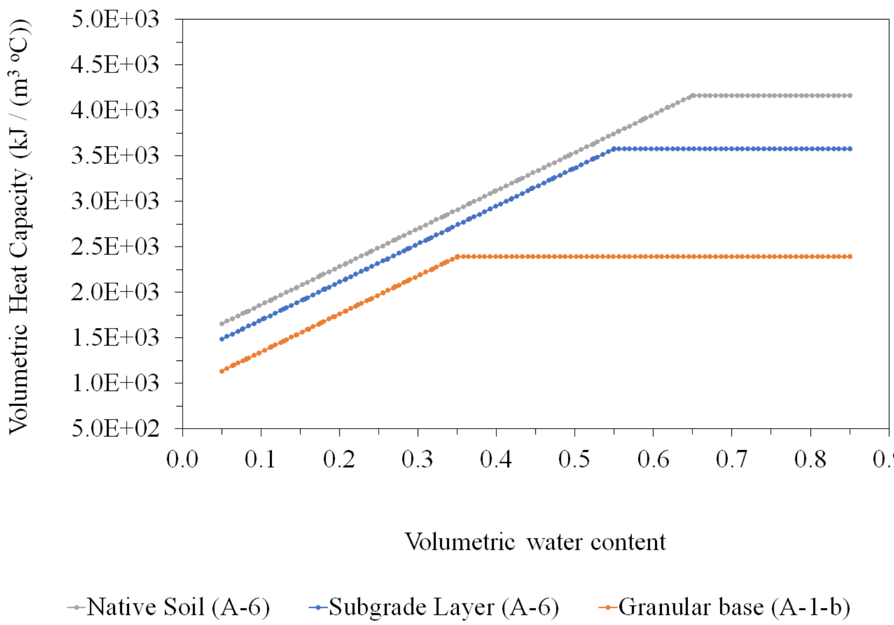

Figure 4.32: Volumetric heat capacity function for pavement layer materials for Research Site No.2

4.4 Methodology for Conducting the Land Climate Interaction Modeling

The FEA modeling was conducted using SEEP/W to simulate water transfer and using TEMP/W to simulate heat transfer within subgrades. SEEP/W and TEMP/W form part of the GeoStudio software package developed by GeoSlope International Ltd. which is part of Seequent and is based in Calgary, Alberta, Canada.

1-D heat transfer FEA modeling followed by 2-D heat transfer FEA modeling were conducted using transient heat transfer and forced convection with liquid water transfer and water vapour transfer. The heat transfer modeling was integrated with the water transfer modeling which consisted of natural (free) convection and water vapour transfer based on thermal and isothermal conditions. The heat transfer modeling and water transfer modeling were integrated using coupled convective-thermal material modeling. In the coupled convective-thermal material modeling approach, thermal properties of materials are represented as a function of volumetric water contents for the unfrozen condition as shown below:

- Thermal conductivity vs. volumetric water content function;
- Volumetric heat capacity vs. volumetric water content function;
- Unfrozen water content vs. temperature function estimated based on soil classification; and
- Water density vs. temperature function.

The 1-D water transfer FEA modeling was conducted followed by 2-D water transfer FEA modeling. The FEA modeling for liquid water transfer was based on gravity flow, pore water pressure gradients and water density gradients. The FEA modeling for water vapour transfer was due to water vapour pressure gradients. The FEA modeling for water transfer was conducted using transient conditions and consisted of coupling water transfer and heat transfer modeling. Hydraulic material modeling was based on saturated/unsaturated conditions as follows:

- Volumetric water content vs. matric suction function (SWCC) estimated using Van Genuchten function parameters, the saturated water content, and the residual water content;
- Hydraulic conductivity vs. matric suction function estimated using Van Genuchten function parameters, saturated hydraulic conductivity, and SWCC including the residual water content; and
- Water density vs. temperature function.

The 2-D water transfer FEA modeling was conducted using initial groundwater conditions based on the activation pore water pressure, and the activation temperature for each material layer. It was assumed that the hydraulic conductivity of materials decreased during freezing conditions. The water and heat transfer FEA modeling was conducted using a representative pavement structure profile for each research site. The 2-D water and heat transfer FEA modeling sensitivity analyses were conducted using a global mesh size of 0.5 m to 2.5 m. The 1-D water and heat transfer FEA modeling were conducted using 48 time-steps per day over a total of 13,870 days which represented the 38-year analysis period. The 2-D water and heat transfer FEA modeling were conducted using one time-step per day over a total of 13,870 days.

The 2-D FEA modeling was conducted using Constant Total-head Boundary Condition values of 4.0 m, 3.0 m, -5.0 m, -10.0 m, and -20.0 m (FEA Case No.1 to FEA Case No.5) which represent static water table elevation of 1.65 m, 2.65 m, 10.65 m, 15.65 m and 25.65 m below the subgrade surface. The domain elevations were referenced from a datum (elevation 0.0 m) located at 6.0 m below the pavement surface.

4.4.1 Boundary Conditions used for 1-D and 2-D Water and Heat Transfer FEA Modeling

The land climate interaction (LCI) surface boundary conditions for the 1-D water and heat transfer FEA modeling were developed using climatic data including precipitation, air temperature, relative humidity, net solar radiation, wind speed, and snow depth. The vegetation data including leaf area index, plant water limit, root depth, normalized root density, ground cover, and vegetation height functions were used to simulate evapotranspiration based on the Penman-Monteith method (LCI Surface Boundary Condition). The initial Surface Temperature Boundary Condition was developed by conducting 1-D heat transfer FEA modeling using the surface energy balance boundary condition. The surface energy balance boundary condition consisted of air temperature, net solar radiation, wind speed and relative humidity. Subsequently, 1-D water and heat transfer FEA modeling were conducted using the LCI Surface Boundary Condition and the initial Surface Temperature Boundary Condition based on coupling SEEP/W and TEMP/W. A Unit Gradient Boundary Condition was used at the bottom of the domain for the 1-D water and heat transfer FEA modeling.

The net infiltration flux from the 1-D water and heat transfer FEA modeling, and the surface temperature from the 1-D heat transfer FEA modeling were used for the Net Infiltration Flux Boundary Condition and Surface Temperature Boundary Condition respectively, for the coupled 2-D water and heat transfer FEA modeling. For the 2-D water and heat transfer FEA modeling, the Net Infiltration Flux Surface Boundary Condition was applied on the entire surface of the domain except the wearing courses on traffic lanes and shoulders. The Net Infiltration Flux Boundary Condition was not applied on the wearing courses because the wearing courses were assessed as impervious. The Surface Temperature Boundary Condition was applied on the entire surface on the domain. The Zero-flow Boundary Condition was applied on the surface of the base course as it was assumed that there was no infiltration of water through the wearing courses because the wearing courses were assumed impervious. This assumption also implied that no water infiltrated the interface of the wearing courses and the base course. The Zero-flow Boundary Condition was also applied on the sides of the domain as it was assumed that there was no migration of water along the vertical boundary. It was also assumed that the water flow condition outside the vertical boundary did not influence the water flow within the domain because the domain extended 100.0 m on each side of the centreline of the median. The Constant Total-head Boundary Condition with values ranging from 4.0 m to -20.0 m which represented static water table elevation of 1.65 m to 25.65 m below the subgrade surface, was used at the bottom of the domain. The water table elevation with values ranging from 1.65 m to 25.65 m below the subgrade surface was used for conducting the sensitivity analyses of the coupled 2-D water and heat transfer FEA modeling. The bottom of the domain was set at 26.0 m below the pavement surface, and the lateral limit of the domain was set at 100.0 m offset from the centreline of the median. A summary of the boundary conditions used for the 1-D and 2-D water and heat transfer FEA modeling is presented in Figure 4.33 and Figure 4.34 respectively.

Color	Name	Model	Model
	1-Native Soil Top Layer (A-6)	Coupled Convective Thermal	Saturated / Unsaturated
	2-Native Soil Bottom Layer (A-6)	Coupled Convective Thermal	Saturated / Unsaturated

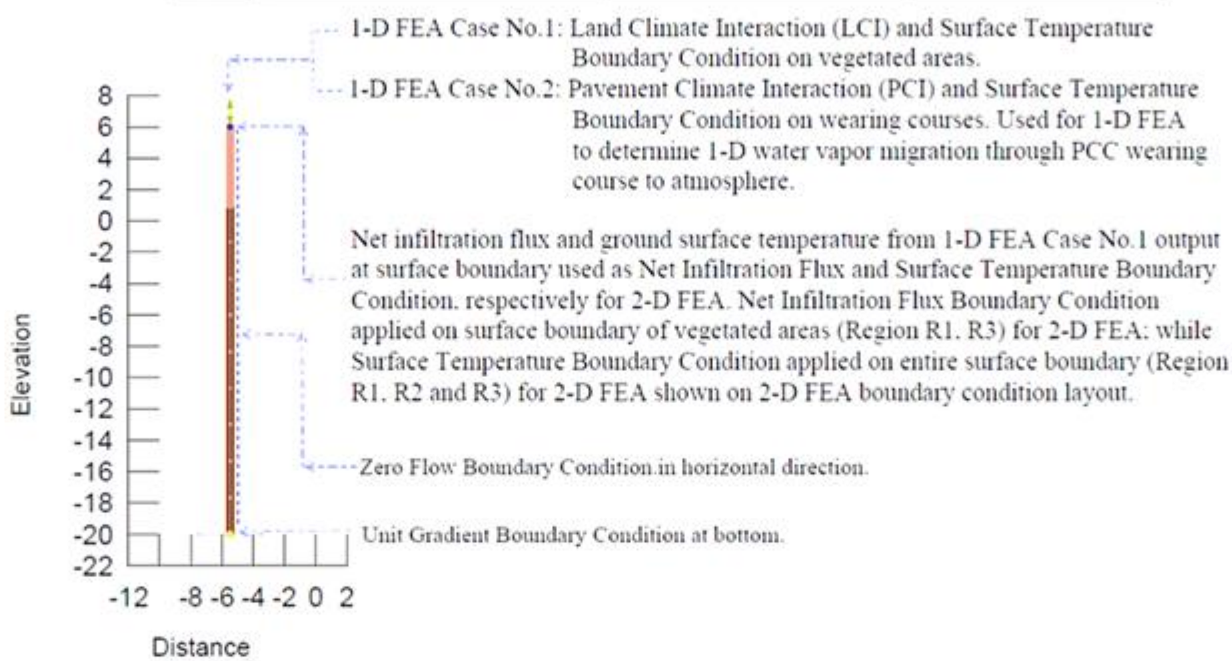

Figure 4.33: Summary of boundary conditions used for I-D water and heat transfer FEA modeling

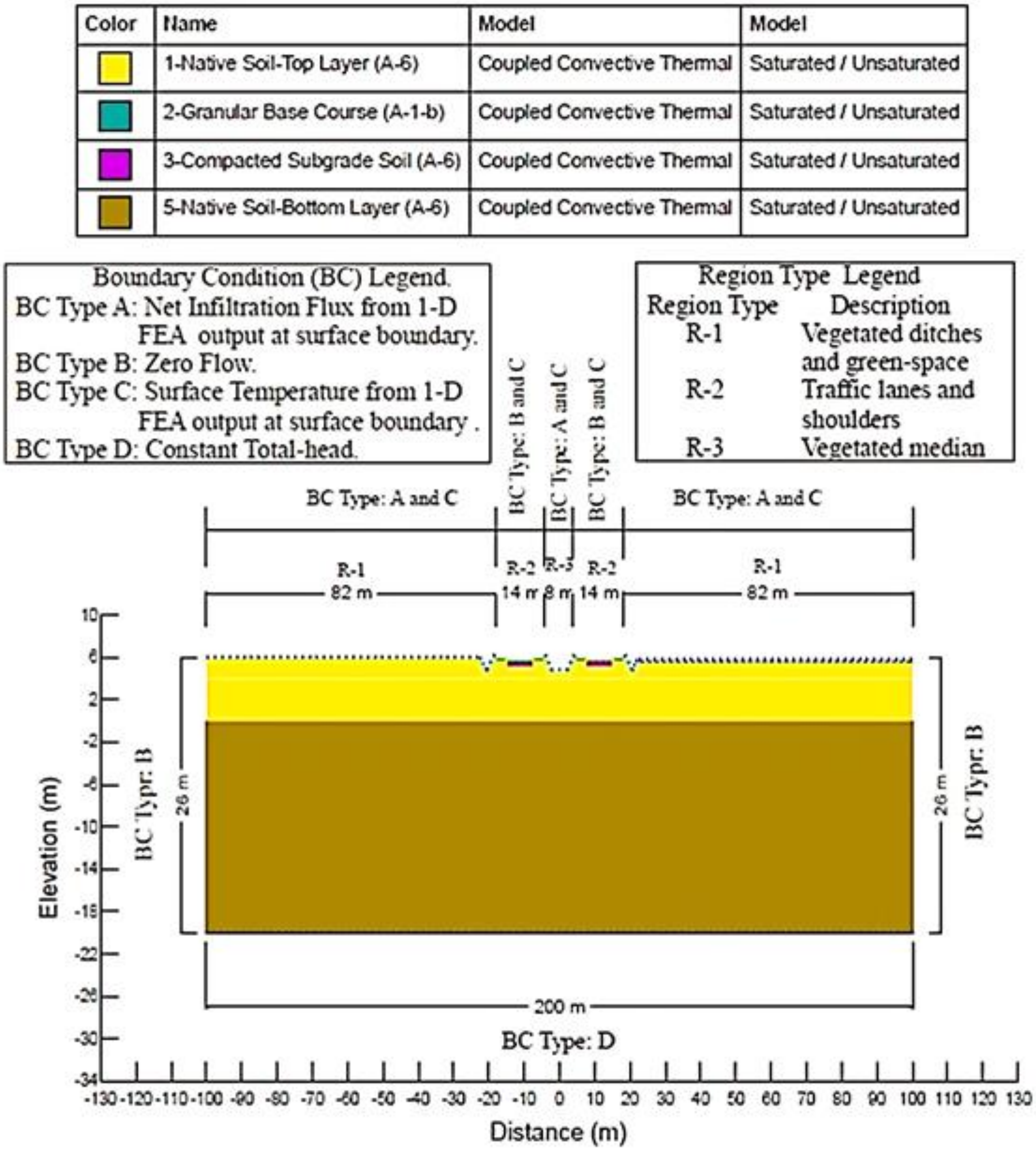

Figure 4.34: Summary of boundary conditions used for 2-D water and heat transfer FEA modeling

4.4.2 Details of SEEP/W and TEMP/W used for 1-D and 2-D Water and Heat Transfer Modeling

The pavement section geometry was drawn in SEEP/W and TEMP/W using the site-specific cross-section details provided in Table 4.1. Each material layer in the pavement structure was drawn as an independent region. The material properties database, including the hydraulic and thermal properties for each material layer in the pavement structure which includes the base course, subgrade, and native soil was created in SEEP/W and TEMP/W. The respective material properties for each material layer were assigned to each corresponding region in SEEP/W and TEMP/W. The water and heat transfer conditions in SEEP/W and

TEMP/W were applied and included water transfer modeling based on liquid water transfer due to gravity flow and water vapour transfer due to thermal and isothermal conditions. The water and heat transfer conditions also included convective-thermal conditions, hydraulic conductivity as a function of volumetric water content, decreased hydraulic conductivity during freezing conditions and evapotranspiration modeling using the Penman-Monteith equation. The mesh size, time steps, and boundary conditions were applied in SEEP/W and TEMP/W and each model in SEEP/W and TEMP/W was run to generate the water and heat transfer output. The output include the volumetric water content and temperature profile within the respective pavement material layer.

The heat transfer FEA modeling consisted of the TEMP/W solver converting the uniformly distributed and time dependent heat flux from the surface temperature boundary condition to the total heat flow at each node. The TEMP/W solver conducted the heat conversion by integrating the heat transfer equations and utilizing the temperature gradients along the edge of the mesh. The converted total heat flow at each node was then used to calculate the rate of change of the thermal energy stored in the pavement structure based on the conservation of energy. The heat transfer FEA modeling included forced convection with liquid water and water vapour transfer, and coupled convective-thermal material modeling (hydro-thermal coupling). The hydro-thermal coupling was conducted using the water flux output obtained from the water transfer FEA modeling which was coupled with the heat flux output obtained from the heat transfer FEA modeling. The hydro-thermal coupling consists of the soil's thermal properties analyzed as a function of changes in volumetric water contents.

SEEP/W used the specified net infiltration flux obtained from the net infiltration surface boundary condition to conduct the analyses of water transfer. The water transfer solver triggered a positive surface water pressure which is associated with ponding to induce water transfer for cases where the specified net infiltration flux exceeded the saturated hydraulic conductivity. The water transfer process at each node in the 2-D FEA modeling was also influenced by the time steps and the length of the mesh edges used in the SEEP/W analyses.

4.5 Calibration and Analysis of Water and Heat Transfer FEA Modeling Output

This section presents details of the approach used for verifying the 2-D FEA models. The section also presents the findings of the analyses of the 1-D and 2-D water and heat transfer FEA modeling output for subgrades for the two pavement sections analyzed. The section also provides details of the sensitivity analyses conducted to evaluate the influence of varying static water table elevations on volumetric water contents within subgrades. The section also provides details of the analyses of: net infiltration and evapotranspiration; the influence of changes in climatic factors on changes in volumetric water contents within subgrades; and the impact of seasonal minimum, maximum and average volumetric water contents on changes in the resilient modulus and changes in pavement performance.

4.5.1 Calibration and Verification of FEA Models

The 1-D and 2-D water and heat transfer FEA models were calibrated visually by superimposing the measured in-situ volumetric water contents within subgrades (the measured in-situ datasets) onto the in-situ volumetric water contents obtained from the water and heat transfer FEA modeling output (the FEA volumetric water contents output) at corresponding time periods, depths, and locations within subgrades.

The 2-D water and heat transfer FEA models were also calibrated using the coefficient of determination (R^2) analysis between the measured in-situ datasets and the 2-D FEA volumetric water contents output. The 2-D FEA water and heat transfer modeling and R^2 analysis were conducted until the R^2 value between the measured in-situ datasets and the 2-D FEA volumetric water contents output was at least 0.8.

In-situ volumetric water contents within subgrades were recorded at an offset of positive 0.76 m from the interface of the outside traffic lane and shoulder (an offset of positive 0.76 m). In-situ volumetric water contents recorded at depths of 375.0 mm and 230.0 mm below the subgrade surface using time-domain reflectometer (TDR) water sensors were used for calibrating the FEA models for Research Site No. 1 and Research Site No. 2 respectively. The typical TDR sensor layout plan used for the Long Term Pavement Performance (LTPP) and Seasonal Monitoring Program (SMP) is shown in Figure 4.35.

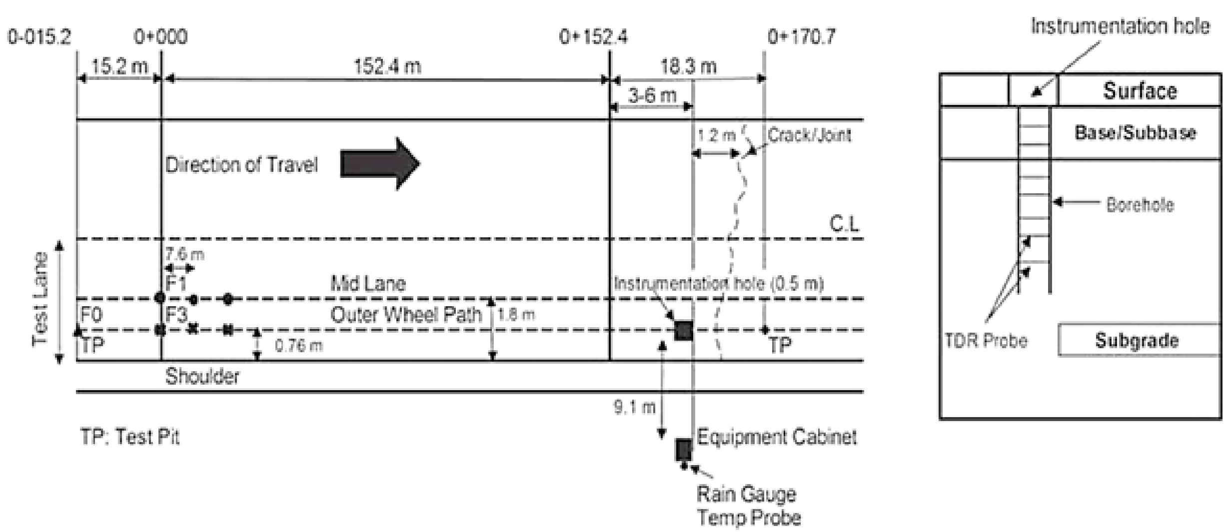

(a)

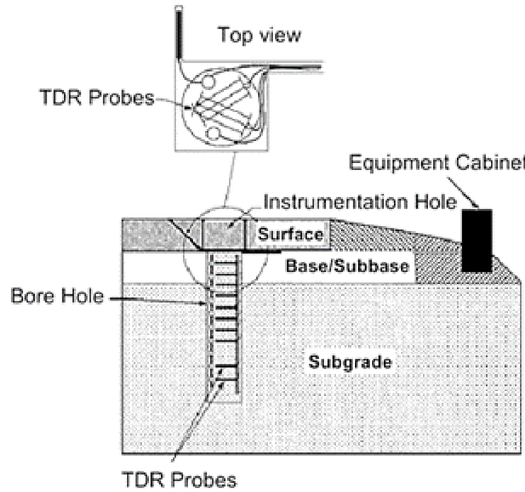

(b)

Figure 4.35: Summary of typical TDR sensor installation layout plan used in the LTPP and SMP (Zollinger, et al 2008; Rada, et al. 1995)

Studies have shown that water contents within subgrades are time and location dependent. However, the 2-D FEA volumetric water contents output were obtained at approximately an offset of positive 0.76 m and at a depth of 375.0 mm and 230.0 mm below subgrade surface for Research Site No. 1 and Research Site No. 2 respectively. The locations of the 2-D FEA volumetric water contents output correspond to the in-situ installation layout of the TDR water probes used in the LTPP and SMP as shown in Figure 4.35. The 2-D FEA volumetric water contents output were obtained at locations corresponding to the locations of the installed TDR sensors for the respective site. This approach was used to facilitate a comparison between the 2-D FEA volumetric water contents output and the in-situ volumetric water contents measured using the TDR. This comparison was conducted to evaluate the accuracy of the 2-D FEA volumetric water contents output.

During the calibration of the 1-D and 2-D water and heat transfer FEA modeling, the Van Genuchten function parameters, the saturated water content, the residual water content, the saturated hydraulic conductivity, thermal properties and activation parameters for materials that were used as input values were adjusted within an established range. The Constant total-head Boundary Condition values were also adjusted within the established range as shown in Table 4.4 to Table 4.8. The range for each parameter provided in Table 4.4 to Table 4.8 was obtained by calculating the average minimum and maximum values for each parameter provided in previous studies. The thickness of pavement material layers, thickness of in-situ soil layers, the LCI Surface Boundary Condition and the Surface Temperature Boundary Condition were not adjusted during the calibration of the 2-D FEA models.

4.5.2 Evaluating In-situ Climatic Factors-Volumetric Water Contents Relationship

The analysis of the data presented in Table 4.9 indicated that a higher correlation coefficient value (r-value) is an indication of a stronger inter-relationship between changes in climatic factors. The data also show that a higher r-value represents a stronger influence of changes in climatic factors on changes in in-situ volumetric water contents and depths to water table. The statistical analyses show a negative relationship between changes in wind speed and the in-situ volumetric water contents. This implies that an increase in the wind speed results in a decrease in the in-situ volumetric water contents within subgrades. The analysis also indicated a strong negative correlation between changes in measured wind speeds and air temperatures. This indicates that an increase in the measured wind speed results in a cooling effect near the ground surface.

The analysis also indicated a weak negative correlation between changes in wind speeds and precipitation, and a moderate negative correlation between changes in evaporation and precipitation. These results imply that an increase in the measured wind speed and evaporation are associated with a reduction in the precipitation measured near the ground surface. These observations may be due to inaccurate measurements of precipitation using rain gauges during periods of high wind speeds and high rates of evaporation. Studies show that an increase in the wind speed causes disturbances in conditions near rain gauges. These disturbances result in a lower quantity of rainfall being caught within rain gauges relative to the amount of rainfall which reaches the ground surface (the wind-induced under-catch). The wind-induced under-catch contributes to errors in the measured rainfall. The wind-induced under-catch also contributes to the negative relationship between wind speed and precipitation (World Meteorological Organization 2014).

Previous studies indicate that during periods of higher relative humidity, increased precipitation is associated with high wind speeds measured near the ground surface. These studies also indicate that an increase in the wind speed induces an increase in evaporation which facilitates an increase in precipitation (Back, and Bretherton 2005; Raymond, et al. 2003). This implies that the interaction between climatic factors measured near the ground surface may be different from the inter-relationship between climatic factors in the hydrological cycle in the lower atmosphere.

The analysis of climatic factors and in-situ volumetric water contents data indicated that an increase in in-situ volumetric water contents within the subgrade is primarily influenced by an increase in the air temperature, net infiltration and precipitation. The data presented in Table 4.9 show a negative relationship between the relative humidity and evaporation. This implies that an increase in the relative humidity results in a decrease in evaporation. This also implies that an increase in the relative humidity results in an increase in the in-situ volumetric water contents within subgrades. This observation is supported by the positive relationship between relative humidity and the in-situ volumetric water contents. An increase in the in-situ volumetric water contents within subgrades is also influenced by an increase in the depth to water table, but to a lesser extent. The data presented in Figure 4.9 show that the positive relationship between changes in the depth to water table and changes in the in-situ volumetric water contents is associated with a negative relationship between changes in the depth to water table and evaporation. The relationships between climatic factors and water contents shown in the statistical analyses are also reflected in the 2-D FEA water contents output except for the statistical relationship between wind speed and precipitation as mentioned previously.

Shallow depths to the water table result in higher capillary rise which contributes to increased liquid water transfer within subgrades. Shallow depths to the water table also result in lower water vapour transfer within subgrades. This implies that shallow depths to the water table result in increased liquid water transfer within subgrades due primarily to higher capillary rise associated with liquid water transfer. Hence, shallow depths to the water table primarily contribute to an increase in liquid water transfer within subgrades.

Deep water tables result in minimal capillary rise to subgrades and lower degree of saturation (resulting in minimal contribution of the capillary rise and liquid water transfer to volumetric water contents). The minimal capillary rise and lower degree of saturation facilitate an increase in the water vapour transfer within subgrades (the primary mechanism of water transfer within fine-grained subgrades). The increase in water vapour transfer results in an increase in volumetric water contents within subgrades (due to diffusion and subsequent condensation). These observations confirm a positive relationship between changes in depths to the water table and volumetric water contents within fine-grained subgrades (Arunkumar 2021; Zhang, et al. 2016).

It was observed that an increase in net infiltration flux is primarily due to an increase in precipitation as precipitation is the primary source of water. An increase in the net infiltration flux is also due to an increase in the relative humidity, depth to water table, in-situ volumetric water contents of subgrades, and increased air temperature. It was also observed that a reduction in net infiltration is influenced by an increase in the net solar radiation, evaporation and wind speed. An increase in evaporation is primarily influenced by an increase in the net solar radiation and air temperature, while a reduction in evaporation is associated with an increase in depth to water table, precipitation, net infiltration and relative humidity.

The analysis indicated strong inter-relationships between changes in volumetric water contents within subgrades and changes in air temperature, net infiltration, precipitation, and evaporation. These observations support the assessment that water and heat transfer within subgrades is influenced by thermal processes including forced convection with liquid water and water vapour transfer, and evapotranspiration. The analysis also indicated a good correlation between changes in volumetric water contents within subgrades and depth to water table confirming that the water table elevation impacts water and heat transfer within subgrades. The analysis also shows that the impact of the water table elevation on water and heat transfer within subgrades is influenced by system dependent characteristics of subgrades.

The analysis also confirms that land climate interaction (LCI) is a system dependent boundary condition which is influenced by changes in volumetric water contents within the subsurface soils. The strong statistical correlation between changes in net infiltration, climatic factors, volumetric water contents within subgrades, and depth to water table confirm that net infiltration is a LCI boundary condition which is influenced by the system dependent characteristics of subgrades. It is also observed that the net infiltration is influenced by changes in volumetric water contents within subgrades and by changes in climatic factors.

The analysis indicated that changes in volumetric water contents are due to temperature gradients, relative humidity gradients, changes in infiltration, changes in evaporation, and changes in groundwater elevations. Changes in depth to water table are influenced by changes in precipitation, net infiltration, soil water content, and relative humidity. Changes in depth to water table influence the capillary fringe zone and capillary rise to the soil above the water table. The analyses indicate that inter-relationships among climatic factors are influenced by changes in climatic factors and seasonal climatic conditions. The analysis also shows that inter-relationships among climatic factors are stronger during spring and summer conditions than during winter conditions. Days with changes in climatic factors with a value of zero result in weaker inter-relationships among climatic factors. The analyses indicate that changes in volumetric water contents within subgrades are influenced by changes in climatic factors, LCI and system dependent characteristics of subsurface soils.

These observations indicate that climatic factors should be incorporated in models developed for predicting the impact of climatic factors on water and heat transfer within subgrades. The analysis indicated that changes in precipitation and air temperature have a higher impact on changes in net infiltration and volumetric water contents within subgrades relative to the impact of other climatic factors. The analysis presented here and various previous studies indicate that the interactions between climatic factors are continuous and interrelated processes (Shrestha, et al. 2019; Farhat 2018; Liuzzo, et al. 2016; IPCC 2013; Wang, and Dickinson 2013; Kousari, and Ahani 2012; Dinpashoh, et al. 2011; IPCC 2001). The interrelationships between climatic factors and between climatic factors and water contents within subgrades are evaluated further in Section 6.2. Hence, both the stronger and weaker interrelationships between climatic factors should be incorporated in the Quantitative Empirical Model.

A summary of the statistical analyses conducted between climatic factors, and between climatic factors and volumetric water contents is presented in Table 4.9.

Table 4.9: Analyses of climatic data and in-situ water content for the pavement section in Minnesota from May to November 1994

Variables	Change in precipitation (m/s)	Change in net infiltration (m/s)	Change in volumetric water content	Change in air temperature (^{0}C)	Change in net solar radiation (kJ/s m^2)	Change in evaporation (m^3/s m^2)	Change in relative humidity (%)	Change in wind speed (m/s)	Change in depth to water table (m)
Change in precipitation (m/s)	1.00	0.98	0.75	0.52	-0.75	-0.43	0.77	-0.12	0.89
Change in net infiltration (m/s)	0.98	1.00	0.79	0.60	-0.70	-0.29	0.85	-0.30	0.80
Change in volumetric water content	0.75	0.79	1.00	0.95	-0.13	-0.19	0.48	-0.44	0.39
Change in air temperature (^{0}C)	0.52	0.60	0.95	1.00	0.16	0.50	0.35	-0.62	0.08
Change in net solar radiation (kJ/s m^2)	-0.75	-0.70	-0.13	0.16	1.00	0.81	-0.72	-0.20	-0.93
Change in evaporation (m^3/s m^2)	-0.43	-0.29	0.19	0.50	0.81	1.00	-0.18	-0.74	-0.80
Change in relative humidity (%)	0.77	0.85	0.48	0.35	-0.72	-0.18	1.00	-0.53	0.63
Change in wind speed (m/s)	-0.12	-0.30	-0.44	-0.62	-0.20	-0.74	-0.53	1.00	0.28
Change in depth to water table (m)	0.89	0.80	0.39	0.08	-0.93	-0.80	0.63	0.28	1.00

4.5.3 Lag Times Between Changes in Climatic Factors and Changes in Volumetric Water Contents

Studies have indicated that the influence of climatic factors on volumetric water contents within subgrades is impacted by seasonal variations in climatic factors, the environment and subgrades properties. These factors include the rainfall intensity and duration, evapotranspiration, environment condition, transient water and heat transfer, hydraulic properties of subgrades, and characteristics of the vegetation. Variations in climatic factors, environment condition and subgrade properties influence response times (lag times) of changes in volumetric water contents within subgrades to changes in climatic factors. Studies have also indicated that the impact of variations in climatic factors on lag times is depth dependent. Studies have also indicated that lag times from precipitation events to changes in volumetric water contents within subgrades are generally minimal within shallow depths (up to 600.0 mm below the pavement surface). Lag times from precipitation events to changes in volumetric water contents within subgrades are longer for depths greater than 600.0 mm below the pavement surface. Studies have also indicated that increased lag times are associated with corresponding increased surface and subsurface runoff. The runoff results in a reduction in the impact of increased precipitation on volumetric water contents within subgrades. In addition, increased lag times result in corresponding increase in the impact of positive changes in air temperature on evapotranspiration and associated reduction in volumetric water contents within subgrades (Ding, et al. 2021; Cheng, et al. 2020; Scaife, et al. 2020; Feki, et al. 2018; Su, and Shangguan 2018; Jia, et al. 2017; Wang, et al. 2013).

Figure 4.36 to Figure 4.41 show the inter-relationships between climatic factors and between climatic factors and water contents within the subgrade for Research Site No.1. The analyses of data presented in Figure 4.36 to Figure 4.41 confirm that lag times are impacted by changes in climatic factors including changes in precipitation and air temperature. The data also show that changes in air temperature have a higher impact on lag times relative to the impact of changes in precipitation. The data presented in Figure 4.36 to Figure 4.41 also show that changes in air temperature are reflected more quickly in lag times relative to the response of lag times to changes in precipitation. This observation implies that changes in water vapour transfer have a higher impact on lag times relative to the impact of changes in liquid water transfer particularly within fine-grained subgrades. These analyses also shows that the impact of changes in precipitation on lag times is impacted by the extent of changes in precipitation which are associated with the rainfall intensity. The analysis of data presented in Figure 4.36 indicates that during periods of low to medium changes in precipitation, lag times are primarily impacted by changes in precipitation and the low to medium rainfall intensity. For periods of low to medium changes in precipitation, positive changes in precipitation result in shorter lag times, while negative changes in precipitation result in longer lag times. The analysis of data presented in Figure 4.36 also indicated that consecutive positive changes in precipitation due to consecutive precipitation events result in further reductions in lag times. However, these analyses indicated that very large positive changes in precipitation as shown on 27th June 1980, do not have significantly higher impact on lag times. It appears that during periods of very large positive changes in precipitation, lag times are impacted primarily by infiltration capacities of subgrades rather than by high rainfall intensities. This observation indicates that lower rainfall intensities over longer periods cause higher infiltration within subgrades. This observation also implies that lag times are impacted by the hydraulic conductivity (as a function of water contents) of subgrades.

The analysis of data presented in Figure 4.37 shows a general trend where positive changes in air temperatures result in corresponding negative changes in volumetric water contents, while negative changes in air temperatures result in corresponding positive changes in volumetric water contents within subgrades. This analysis also shows that larger positive and negative changes in air temperatures, as seen on 27th June and 28th February 1980 respectively, have a higher impact on lag times relative to the impact of smaller changes in air temperature on lag times. This analysis also shows that larger positive and negative changes in air temperatures result in shorter lag times, while smaller positive and negative changes in air temperatures result in longer lag times. Despite large positive changes in precipitation, on 27th June 1980 (highlighted in Figure 4.36), the subgrade desaturated during this period due to large positive changes in air temperatures. The subgrade desaturated from August to September 1980 despite minimal negative changes in precipitation. The desaturation of the subgrade during this period was due primarily to large positive changes in air temperature. These observations confirm that changes in air temperature have a higher impact on lag times relative to the impact of changes in precipitation. The general trend indicates that lag times were up to 1.0 day during unfrozen and frozen conditions. The data presented in Figure 4.36 and Figure 4.37 show that lag times are influenced both by changes in precipitation and changes in air temperatures during unfrozen conditions. The data also show that lag times are influenced primarily by changes in air temperatures during frozen conditions. This analysis also indicated that models, including the Quantitative Empirical Model (the QE Model), developed in this study to predict the impact of climatic factors on water and heat transfer within subgrades should incorporate the impact of climatic factors (including the impact of precipitation and air temperature) on lag times.

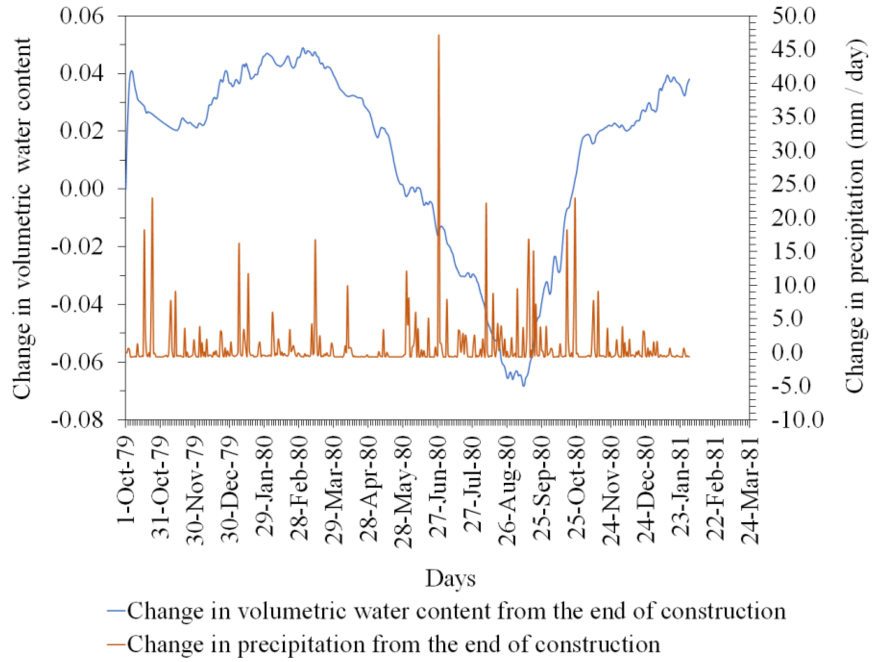

Figure 4.36: Change in precipitation vs change in volumetric water content

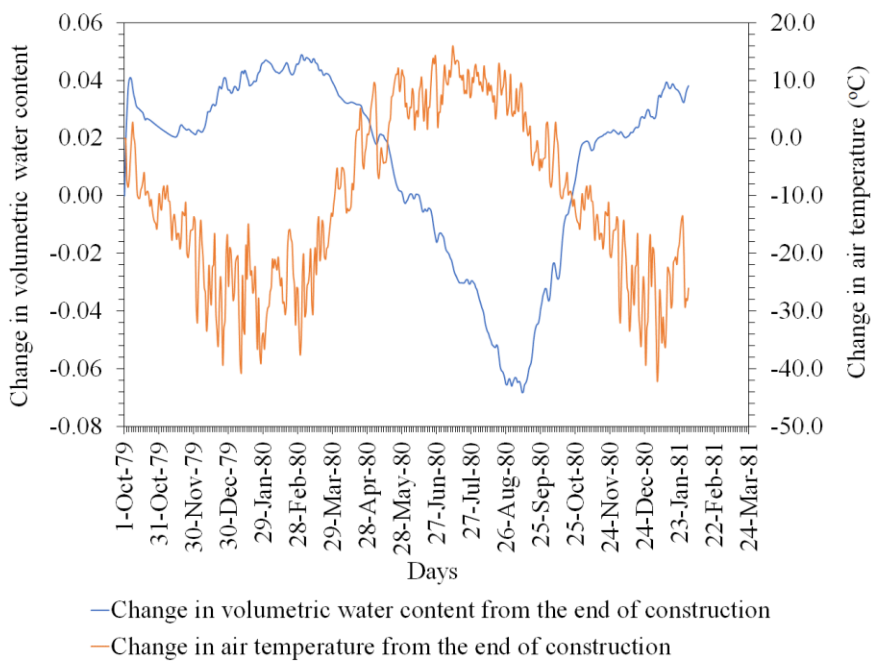

Figure 4.37: Change in air temperature vs change in volumetric water content

The analysis of data presented in Figure 4.38 indicated that positive changes in air temperatures result in increased evapotranspiration and corresponding negative changes in volumetric water contents within subgrades. The analysis of data presented in Figure 4.39 indicated that positive changes in relative humidity are associated with positive changes in volumetric water contents. The data also show that negative changes in relative humidity correspond to negative changes in volumetric water contents. The analysis of data presented in Figure 4.40 indicated that positive changes in air temperatures correspond to negative changes in relative humidity. The data presented in Figure 4.40 also show that negative changes in air temperatures correspond to positive changes in relative humidity. The analysis of data presented in Figure 4.41 show that an increase in the relative humidity results in a decrease in evapotranspiration. This dataset also show that a decrease in the relative humidity results in an increase in the evapotranspiration. These observations also confirm that an increase in the relative humidity results in a corresponding increase in volumetric water contents within subgrades.

The analysis of data presented in Figure 4.39 also show lag times between changes in relative humidity and changes in volumetric water contents within subgrades. These observations indicate that the impact of changes in precipitation, air temperature, relative humidity and evapotranspiration on lag times and volumetric water contents within subgrades should be accounted for in the QE Model. These inter-relationships between climatic factors, and between climatic factors and volumetric water contents within subgrades are incorporated into the QE Model developed as part of this study.

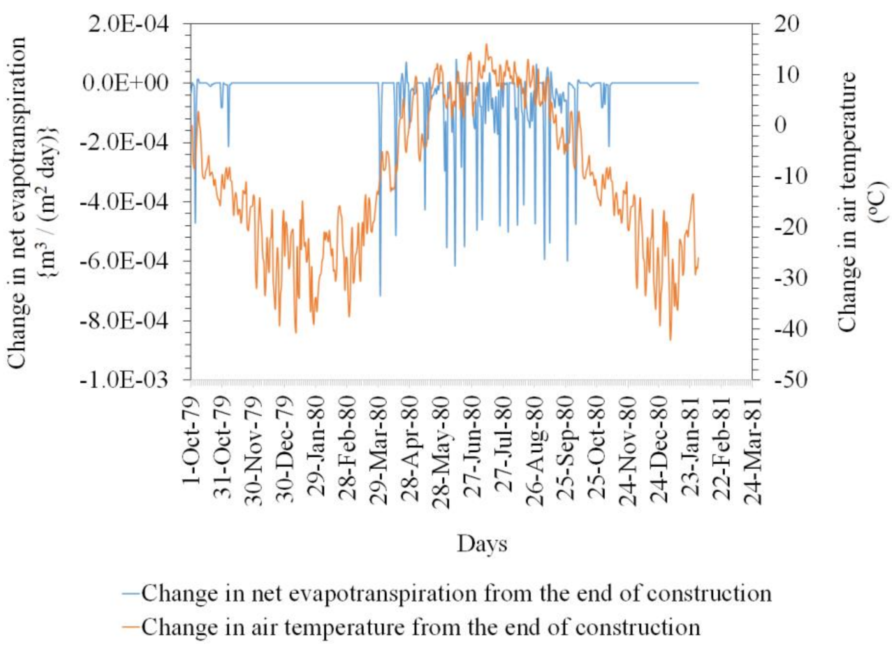

Figure 4.38: Change in air temperature vs change in net evapotranspiration

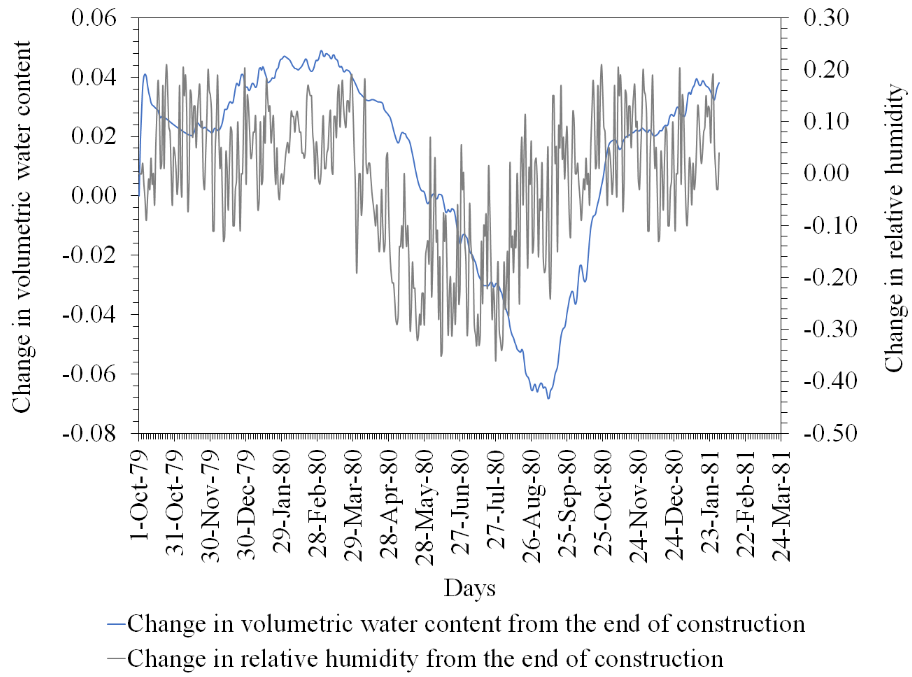

Figure 4.39: Change in relative humidity vs change in volumetric water content

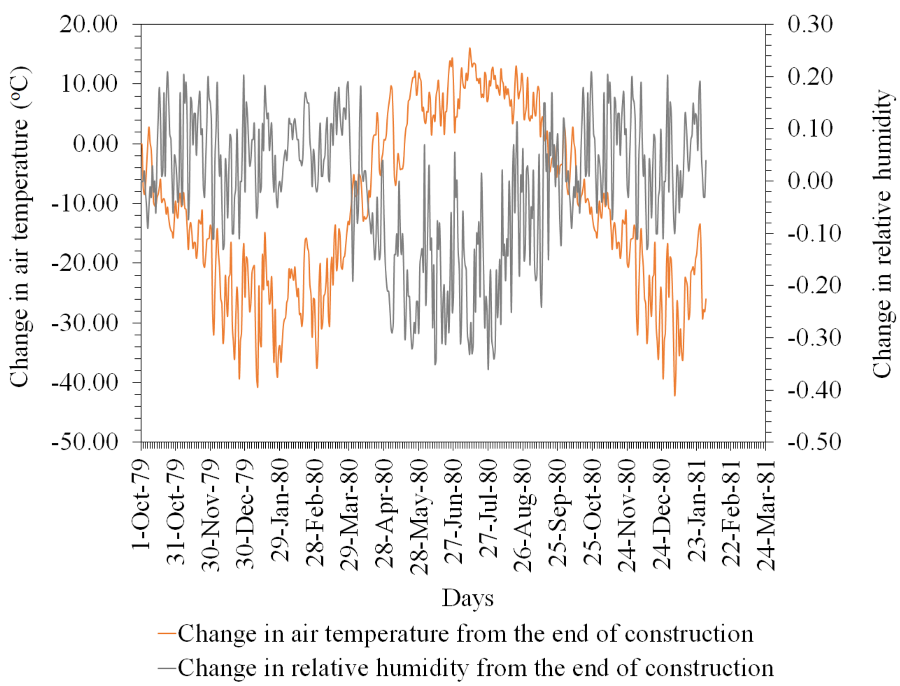

Figure 4.40: Change in air temperature vs change in relative humidity

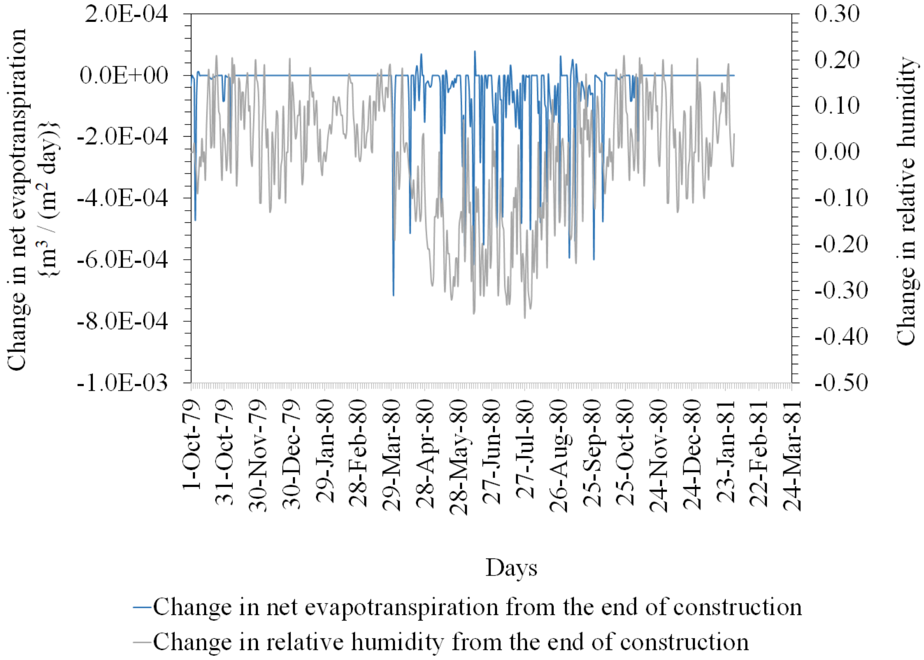

Figure 4.41: Change in relative humidity vs change in net evapotranspiration

The FEA models and the QE Model incorporate both liquid water and water vapour transfer within pavement structures. The water vapour represents a phase change from liquid water to a gas and incorporates evapotranspiration. The relationship between changes in volumetric water contents and net evapotranspiration for Research Site No.1 is presented in Figure 4.42. The analyses of data presented in Figure 4.42 indicated that changes in volumetric water contents are influenced by changes in the net evapotranspiration. Negative changes in the net evapotranspiration (the evapotranspiration) contribute to decreased volumetric water contents within subgrades. Positive changes in the net evapotranspiration (the condensation) contribute to increased volumetric water contents within subgrades. The evapotranspiration has a higher impact on the drying path, while condensation has a higher impact on the wetting path. The data presented in Figure 4.42b also show lag-times in the response of changes in volumetric water contents to changes in net evapotranspiration.

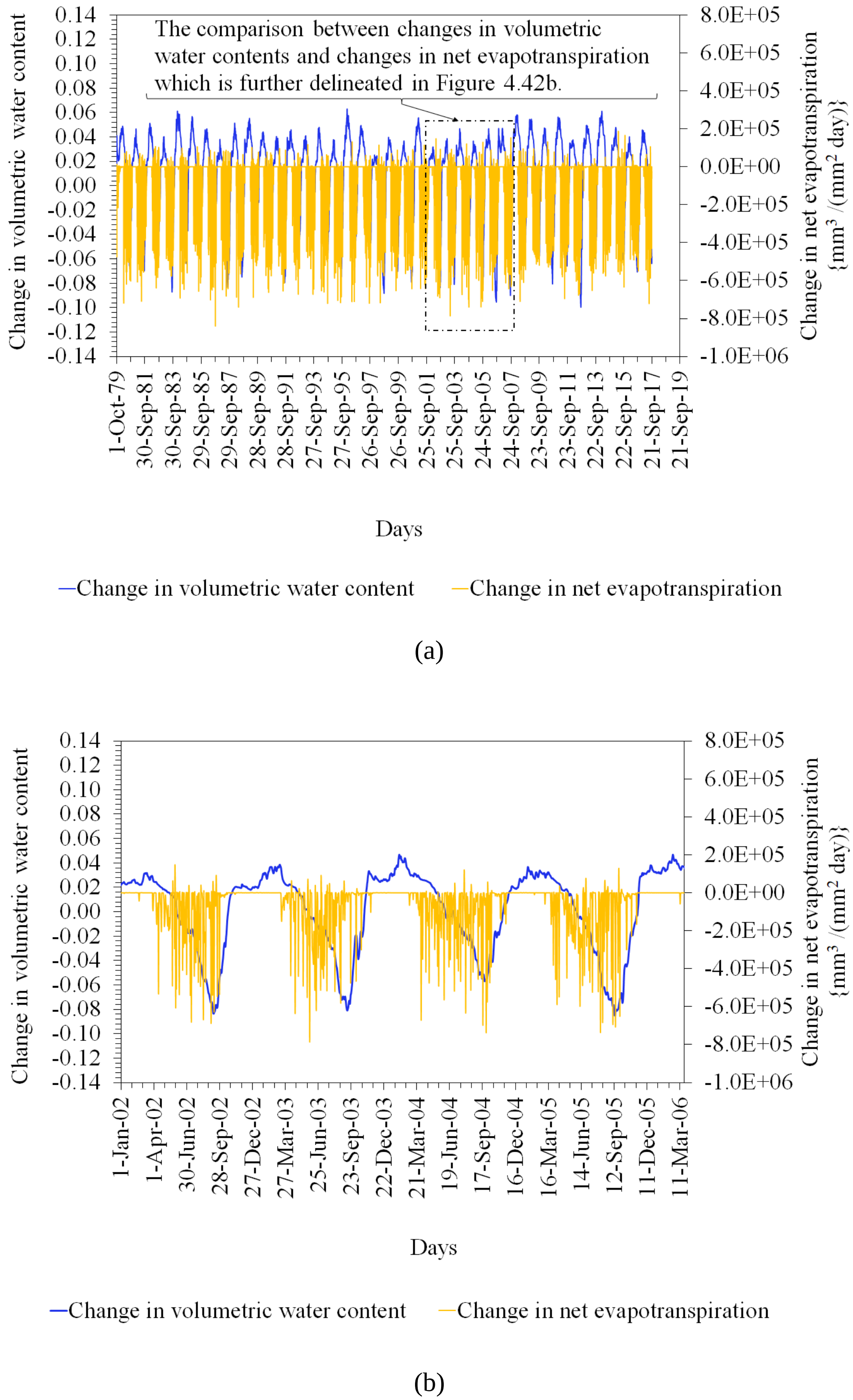

Figure 4.42: Change in net evapotranspiration vs change in volumetric water content

4.5.4 Evaluating the Accuracy of In-situ Volumetric Water Contents Measured Using TDR

In-situ volumetric water contents which are calculated using gravimetric water contents measured using time-domain reflectometer (TDR) probes (the measured in-situ volumetric water contents) may have inherent errors due to limitations in the TDR measurements. The six tasks which were conducted to verify the accuracy of the measured in-situ volumetric water contents used for verifying the 2-D FEA models, Quantitative Empirical Model (the QE Model) and EICM are listed below:

- Task No.1: Reviewed the calculated in-situ volumetric water contents and the measured in-situ gravimetric water contents which are provided in the LTPP and SMP database. The in-situ gravimetric water contents were measured using in-situ testing which were conducted in accordance with AASHTO T239-86 / T310 (gravimetric water contents obtained using the nuclear method). The LTPP and SMP database also consists of gravimetric water contents obtained from laboratory testing of undisturbed samples which were taken in the vicinity of the installed TDR probes. The field testing and laboratory testing of the undisturbed soil samples were completed on the same day, time, and location as the TDR data;
- Task No.2: In-situ gravimetric water contents which were measured using TDR probes were compared with gravimetric water contents obtained using the nuclear method and with gravimetric water contents obtained from laboratory testing;
- Task No.3: Reviewed in-situ volumetric water contents which were calculated using in-situ gravimetric water contents which were measured using TDR probes (the measured in-situ volumetric water contents);
- Task No.4: In-situ volumetric water contents were also calculated using gravimetric water contents, bulk density, dry density, and specific gravity (which are provided in the LTPP and SMP database), and using calculated void ratio values (the calculated in-situ volumetric water contents);
- Task No.5: The accuracy of the measured in-situ volumetric water contents were evaluated by plotting the calculated in-situ volumetric water contents against the measured in-situ volumetric water contents. The two datasets were also compared to determine the accuracy of the measured in-situ volumetric water contents; and
- Task No.6: The accuracy of the 2-D FEA models in predicting in-situ water contents were evaluated using only the measured in-situ volumetric water contents which correlated closely with the calculated in-situ volumetric water contents. The plots of the calculated vs measured in-situ volumetric water contents are presented in Figure 4.43 and Figure 4.44. The analysis of data presented in Figure 4.43 and Figure 4.44 indicated that the measured unfrozen in-situ volumetric water contents correlate closely with the calculated unfrozen in-situ volumetric water contents.

The in-situ volumetric water contents calculated using gravimetric water contents which were measured during freezing conditions were not used for calibrating the 2-D FEA models. The volumetric water contents calculated for the freezing conditions were not used because TDR probes have limitations in measuring in-situ gravimetric water contents during freezing. During freezing conditions, the water within subgrades consists of liquid water and freezing of the pore water. Hence, during freezing conditions the actual water contents within subgrades consist of the unfrozen and frozen water contents. The TDR probes measure only the unfrozen water contents within subgrades. The measurement of gravimetric water contents using the TDR probes is dependent on the dielectric constant of the soil water. The dielectric constant of the soil water is influenced by the soil bulk density, void ratio, texture, and temperature. Hence, the TDR probes measure gravimetric water contents poorly during freezing conditions due to the impact of reduced liquid water permeability and the reduction of the dielectric constant of water during freezing (Evett 2003b; Gong, et al 2003; Robinson, et al 2003; Tardif 2002; Evett 2000).

The Research Site No.1 and Research Site No.2 used Tektronix TR-100 TDR probes manufactured by the Federal Highway Administration (FHWA). The typical method used for the LTPP for calibrating the TDR probes is similar to the method used for Site B (in Fort Smith, Arkansas) in the study conducted by Hall, et al. (2013). The Hall, et al. (2013) study used CS615 moisture probes which use TDR technology and consist of a square wave with an amplitude of ±2.5 volts, direct current (VDC) and a period of 0.7 to 1.6 milliseconds. The impact of temperature on gravimetric water contents outputs of the TDR probes are calibrated under laboratory conditions to temperatures and water contents respectively of the site-specific subgrades. The site-specific densities and temperatures of the subgrade are the primary subgrade properties affecting the relationship between the dielectric constants and water contents (Hall, et al. 2013).

Comparison of Calculated and Measured In-situ Volumetric Water Contents: The Minnesota site

The analysis conducted for evaluating the accuracy of the measured in-situ volumetric water contents which were used for calibrating the 2-D FEA model for the site in Minnesota, United States is presented in Figure 4.43.

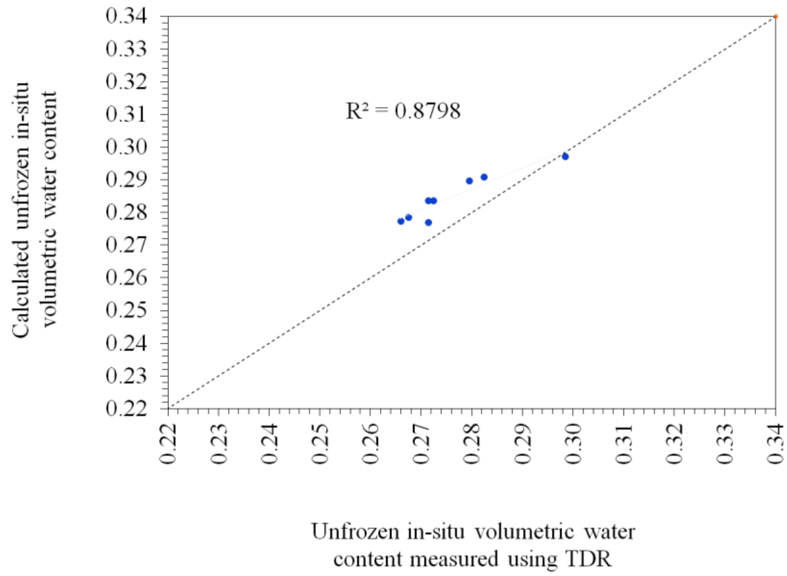

Figure 4.43: Calculated vs measured In-situ volumetric water contents

Comparison of Calculated and Measured In-situ Volumetric Water Contents: The Indiana Site

The analysis conducted for evaluating the accuracy of the measured in-situ volumetric water contents which were used for calibrating the 2-D FEA model for the site in Indiana, United States is shown in Figure 4.44.

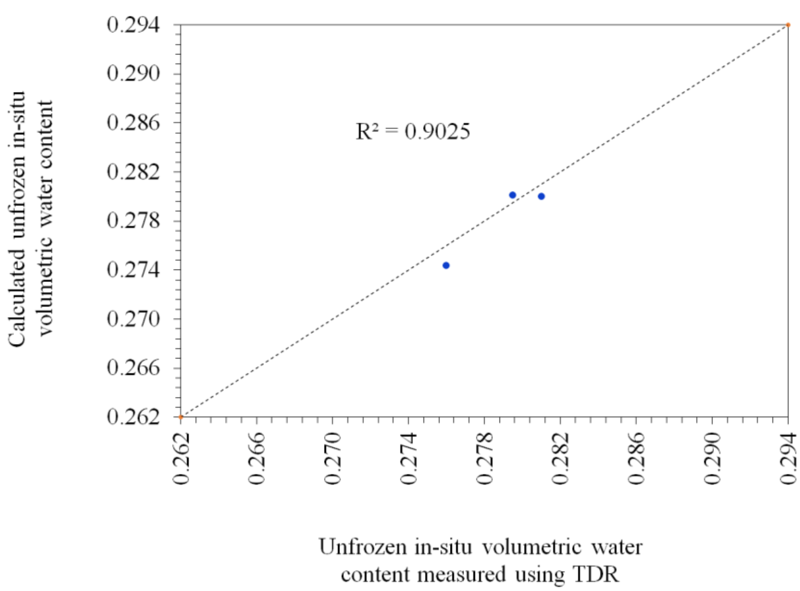

Figure 4.44: Calculated vs measured In-situ volumetric water contents

4.5.5 Comparison of Absolute Values of 2-D FEA Models Output to Absolute Values of Measured In-situ Volumetric Water Contents

The 2-D FEA models output were first compared to the measured in-situ volumetric water contents using a graphical approach. The comparison of the 2-D FEA models output to measured in-situ water contents was conducted by superimposing the 2-D FEA volumetric water content output values onto the measured in-situ volumetric water content values for the corresponding days and depth for each site. The measured in-situ volumetric water contents used for evaluating the accuracy of the 2-D FEA water and heat transfer models for Research Site No.1 and Research Site No.2 are shown in Figure 4.7 (is provided in Section 4.3). The graphical comparison is conducted to visualize the accuracy of the 2-D FEA models in simulating in-situ volumetric water contents.

The 2-D FEA output and measured in-situ volumetric water contents used for the comparison of water contents for Research Site No.1 (shown in Figure 4.45) were measured at a depth of 375.0 mm and for a water table located at 1.65 m below the subgrade surface. The 2-D FEA output and measured in-situ volumetric water contents used for the comparison of water contents for Research Site No.2 (shown in Figure 4.46 and Figure 4.47) were measured at a depth of 230.0 mm and for a water table located at 1.65 m and 2.65 m respectively below the subgrade surface. The 2-D FEA volumetric water contents output from a depth of 375.0 mm and 230.0 mm for Research Site No.1 and Research Site No.2 respectively were compared to the measured in-situ volumetric water contents for the respective research site at the corresponding depth and time. The 2-D FEA volumetric water contents output for a water table elevation at 1.65 m and 2.65 m below the subgrade surface were compared to the measured in-situ volumetric water contents associated with an in-situ dynamic water table located at approximately corresponding depths. The in-situ water table fluctuated from 0.32 m to 1.16 m and 1.00 m to 1.86 m below the subgrade surface at Research Site No.1 and Research Site No.2 respectively.

The analysis of data presented in Figure 4.45 to 4.47 indicated that the 2-D FEA volumetric water contents output correlated closely with the in-situ volumetric water contents which were measured during unfrozen conditions.

The statistical analyses used to evaluate the accuracy of the 2-D FEA volumetric water contents output against the measured in-situ volumetric water content values are shown in Section 5.3.

Comparison of Absolute In-situ and 2-D FEA Output Volumetric Water Contents: Research Site No.1: At a Depth of 375.0 mm and for a Water Table at 1.65 m Below the Subgrade Surface

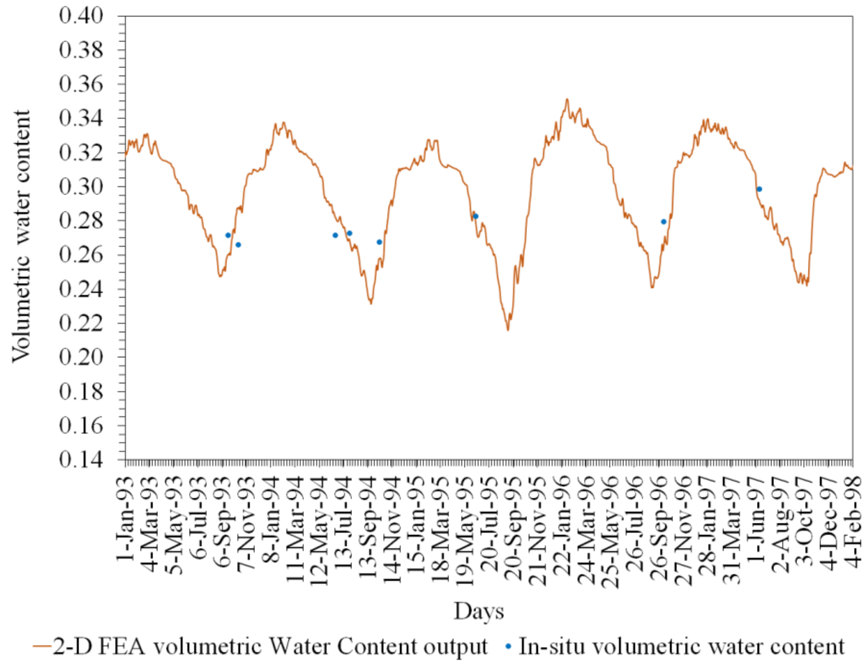

Figure 4.45: Comparison of the measured in-situ and 2-D FEA volumetric water contents output

Comparison of Absolute In-situ and 2-D FEA Output Volumetric Water Contents: Research Site No.2: At a Depth of 230.0 mm, and for a Water Table at 1.65 m (Figure 4.46) and 2.65 m (Figure 4.47) Below the Subgrade Surface

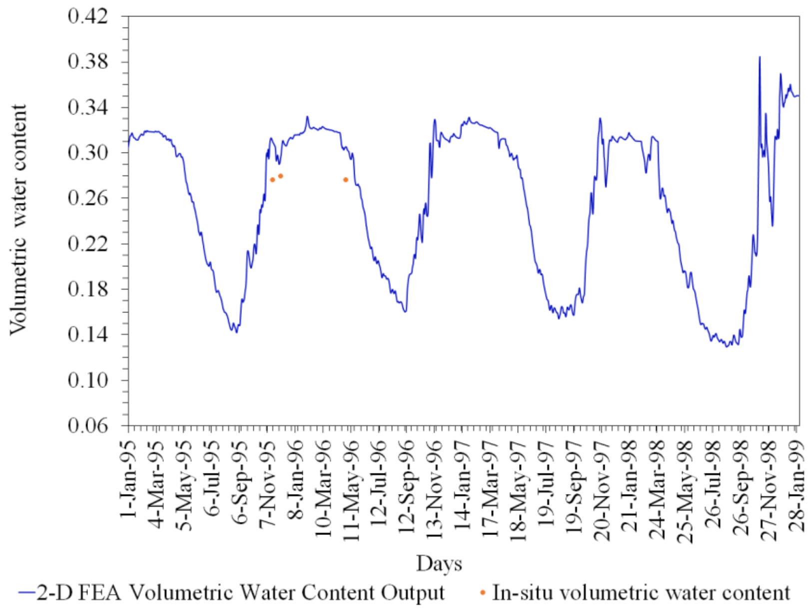

Figure 4.46: Comparison of the measured in-situ and 2-D FEA volumetric water contents output

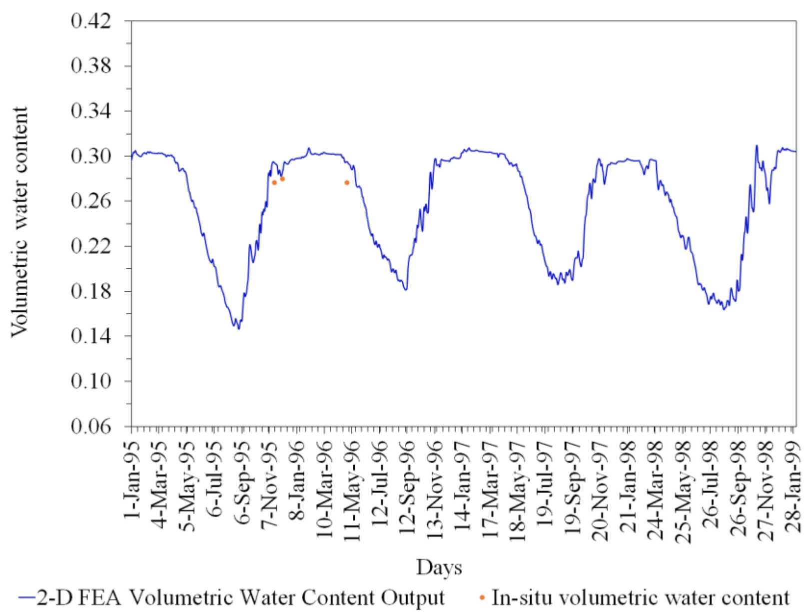

Figure 4.47: Comparison of the measured in-situ and 2-D FEA volumetric water contents output

4.5.6 *Comparison of Changes in 2-D FEA Models Output to Changes in In-situ Water Contents*

The changes in 2-D FEA volumetric water contents output were also compared to changes in the measured in-situ volumetric water contents. The changes in measured in-situ and 2-D FEA volumetric water contents output were determined relative to the measured in-situ volumetric water content within the subgrade at the completion of the pavement construction. The results of analyses for Research Site No. 1 are presented in Figure 4.48 and Figure 4.49 for volumetric water contents measured at a depth of 1.65 m below the subgrade surface. The analyses of results for Research Site No.2 are presented in Figure 4.50 and Figure 4.51, and Figure 4.52 and Figure 4.53 for volumetric water contents measured at a depth of 1.65 m and 2.65 m below the subgrade surface respectively. The volumetric water content values used for the comparison of the water contents for Research Site No.1 and Research Site No.2 were measured at a depth of 375.0 mm and 230.0 mm respectively below the subgrade surface.

The analyses of data presented in Figure 4.48 to Figure 4.53 indicated that changes in the measured in-situ and 2-D FEA volumetric water contents are comparable which indicates that the 2-D FEA models are adequately calibrated. The analyses also indicated that changes in the measured in-situ and 2-D FEA volumetric water contents fluctuated continually throughout the 38-year analysis period. The statistical analyses conducted to evaluate the accuracy of changes in 2-D FEA volumetric water contents output against changes in measured in-situ volumetric water contents are presented n Section 5.3.

Comparison of Changes in In-situ and 2-D FEA Output Volumetric Water Contents: Research Site No.1: At a Depth of 375.0 mm and for a Water Table at 1.65 m Below the Subgrade Surface

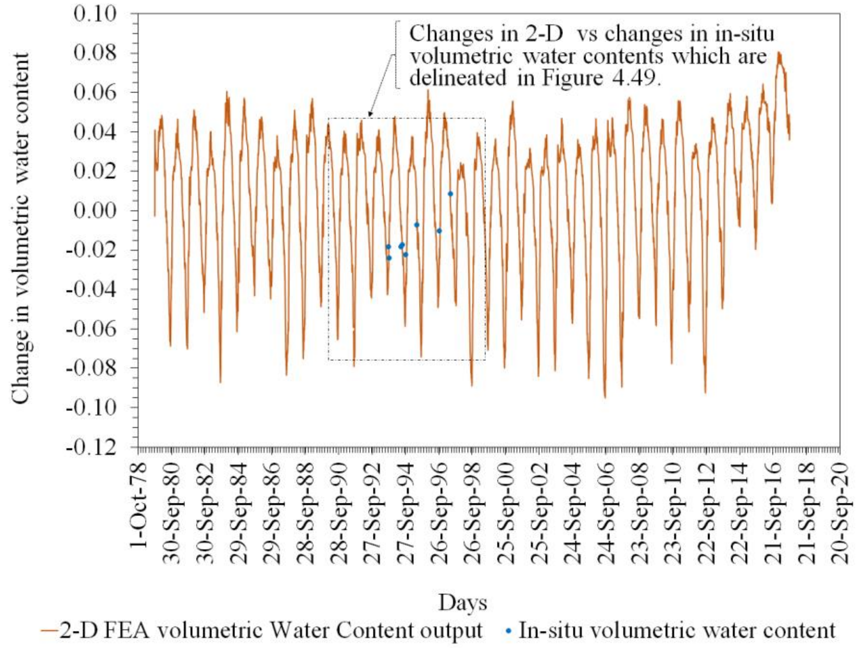

Figure 4.48: Comparison of changes in in-situ and 2-D FEA volumetric water contents output

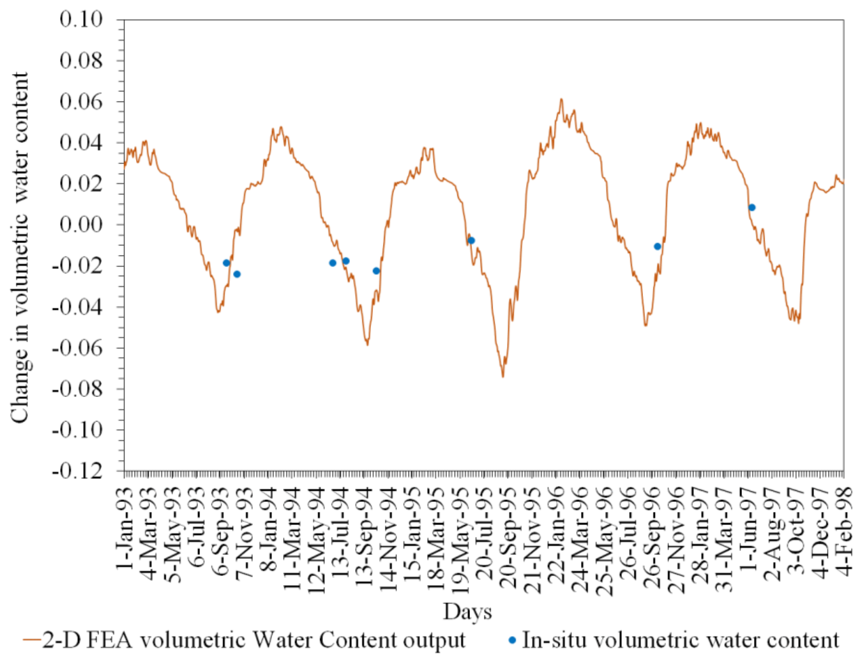

Figure 4.49: Comparison of changes in in-situ and 2-D FEA volumetric water contents output

Comparison of Changes in In-situ and 2-D FEA Output Volumetric Water Contents: Research Site No.2: At a Depth of 230.0 mm, and for a Water Table at 1.65 m (Figure 4.50) and at 2.65 m (Figure 4.52) Below the Subgrade Surface

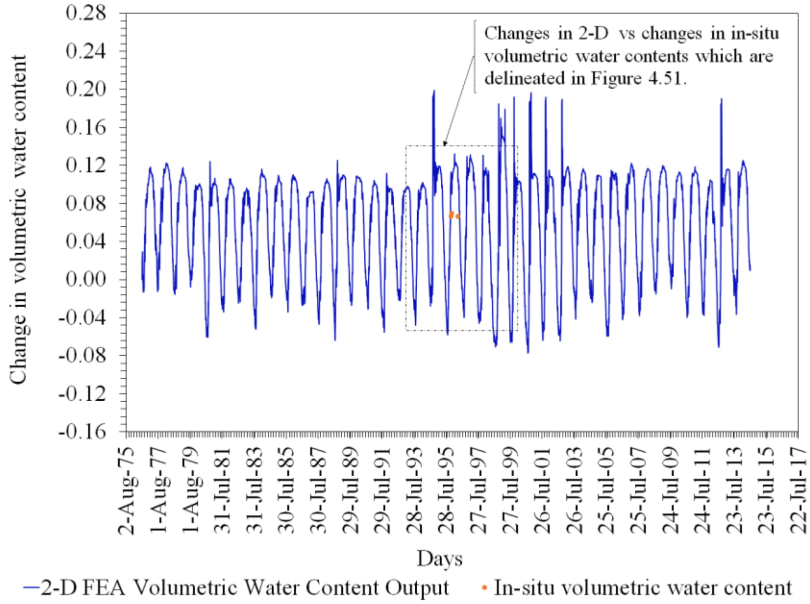

Figure 4.50: Comparison of changes in in-situ and 2-D FEA volumetric water contents output

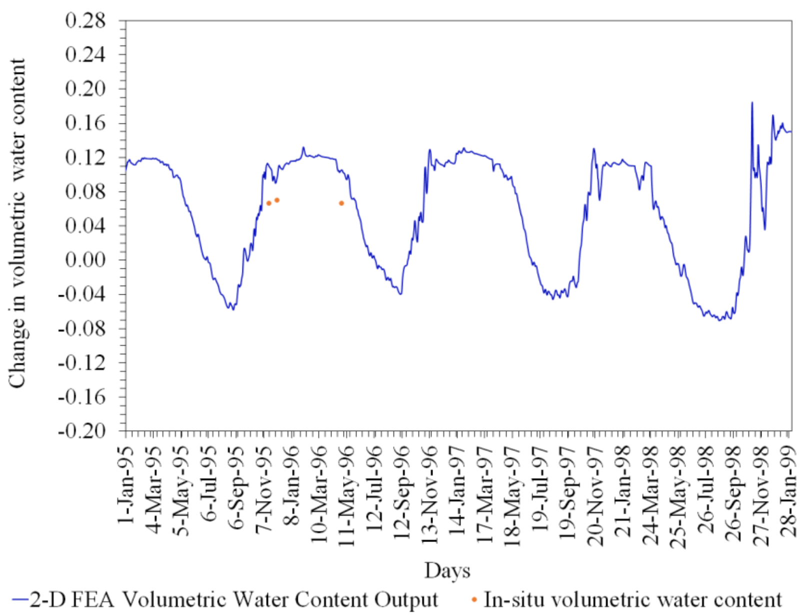

Figure 4.51: Comparison of changes in in-situ and 2-D FEA volumetric water contents output

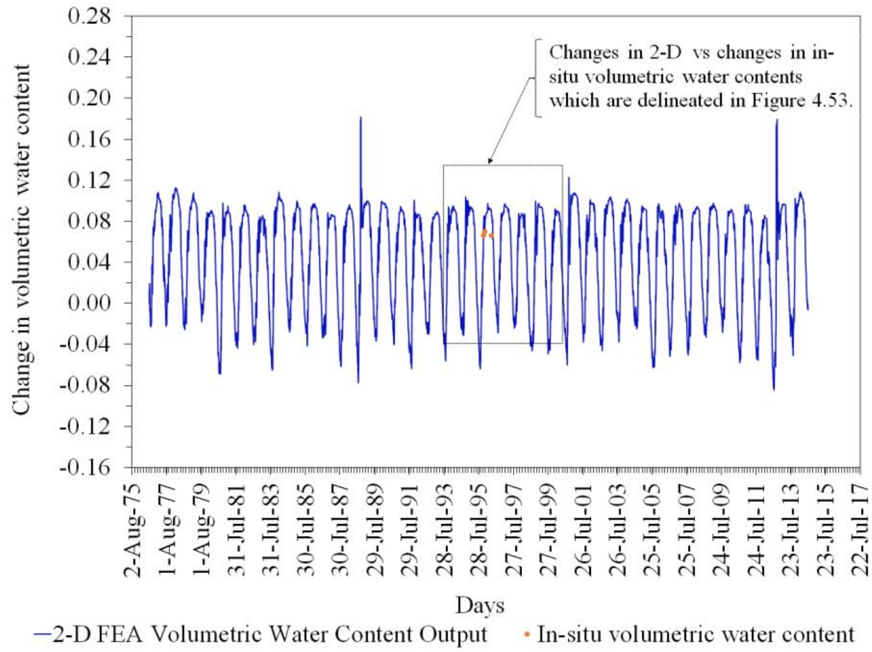

Figure 4.52: Comparison of changes in in-situ and 2-D FEA volumetric water contents output

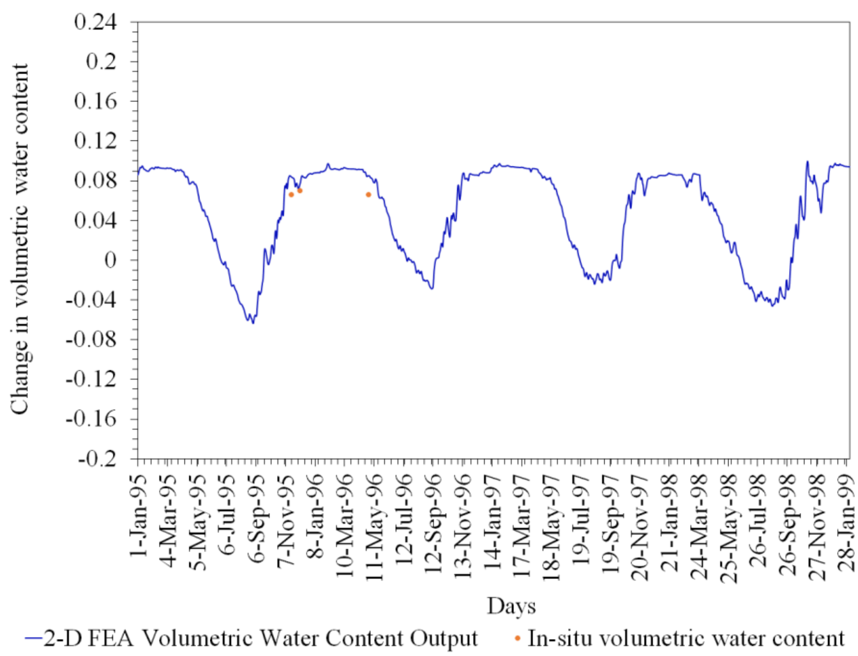

Figure 4.53: Comparison of changes in in-situ and 2-D FEA volumetric water contents output

4.5.7 Analyses of Net Infiltration Output from 1-D FEA Modeling

The 2-D water and heat transfer FEA modeling (the 2-D FEA) accounted for land climate interaction (LCI) by using the soil atmosphere boundary condition which was represented by the net infiltration flux obtained from the surface node of the 1-D water and heat transfer FEA modeling (the 1-D FEA). Net infiltration represents the component of rainfall and snowmelt transferred below the evapotranspiration zone. Net infiltration flux was used as the LCI surface boundary condition on vegetated and bare ground areas in the 2-D FEA (Net Infiltration Surface Boundary Condition). The Net Infiltration Surface Boundary Condition consists of positive net infiltration flux which facilitates water transfer from the surface boundary to subsurface soils below the evapotranspiration zone. The Net Infiltration Surface Boundary Condition also consists of negative net infiltration flux which represents water vapour transfer or evaporation from the surface boundary to the atmosphere. Net infiltration flux values for Research Site No.1 and Research Site No.2 were exported to Excel and analyzed as shown in Figure 4.54 and Figure 4.55 respectively.

Net Infiltration through Vegetated and Bare Ground Areas vs. Time for Research Site No.1

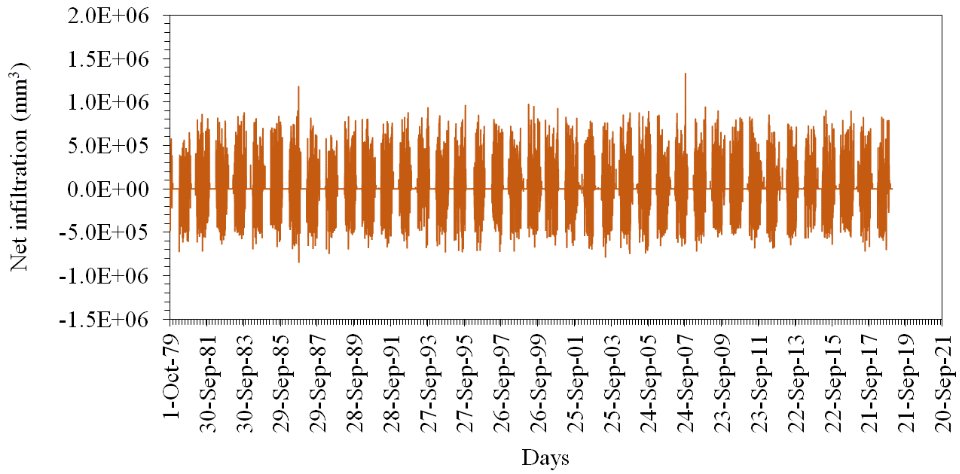

Figure 4.54: Net infiltration through vegetated and bare ground areas vs. time

Net Infiltration through Vegetated and Bare Ground Areas vs. Time for Research Site No.2

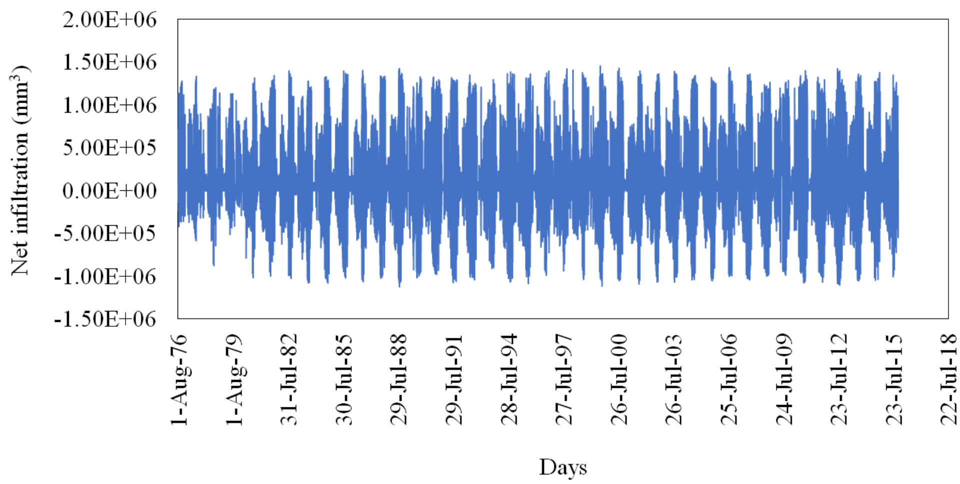

Figure 4.55: Net infiltration through vegetated and bare ground areas vs. time

Analyses of Cumulative Precipitation and Cumulative Net Infiltration for the Two Sites

The analyses of data presented in Figure 4.56 show that Research Site No.2 has higher cumulative precipitation than Research Site No.1. The analyses of data presented in Figure 4.57 show that Research Site No.2 also has higher cumulative net infiltration than Research Site No.1 primarily due to Research Site No.2 having higher cumulative precipitation. This observation shows that precipitation impact the net infiltration. Hence, precipitation should be incorporated into models used for simulating water transfer.

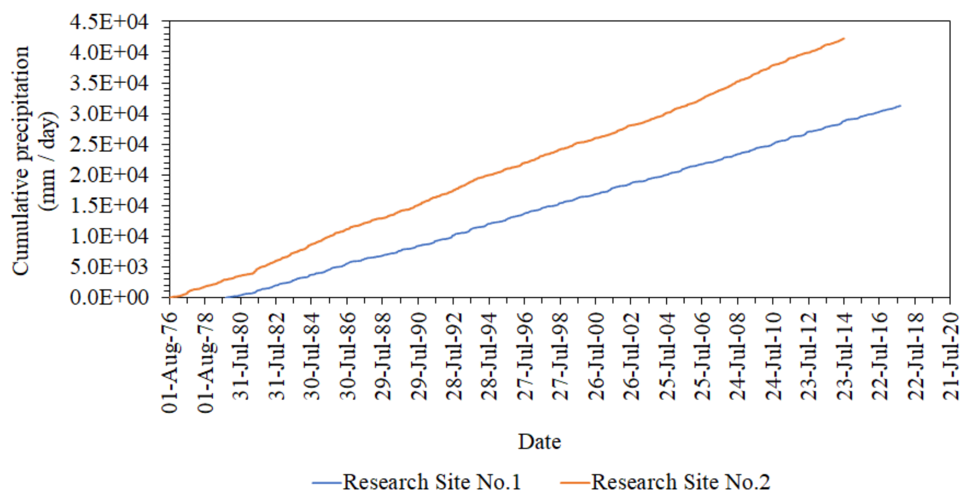

Figure 4.56: Cumulative precipitation vs. time

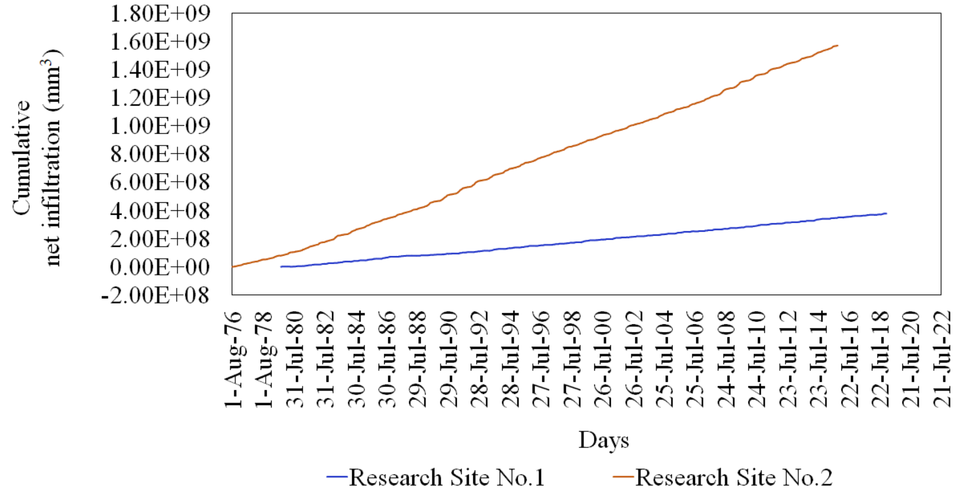

Figure 4.57: Cumulative net infiltration through vegetated and bare ground areas vs. time

4.5.8 Summary

The 2-D FEA water and heat transfer modeling (the 2-D FEA) was conducted primarily to delineate volumetric water contents from the 2-D FEA output to facilitate the development of the Quantitative Empirical Model (the QE Model). The analyses presented in Chapter 4 show relationships between changes in climatic factors and changes in volumetric water contents within subgrades. These relationships form the basis for incorporating the influence of changes in climatic factors on changes in water and heat transfer in the development of the QE Model.

The analyses of data presented in Chapter 4 show that the LCI boundary condition used for 2-D FEA models should be represented by the net infiltration flux. The LCI boundary condition should also incorporate the influence of changes in precipitation, net solar radiation and air temperature. Changes in air temperature should also be incorporated to facilitate the phase changes of water within subgrades. The LCI boundary condition should also account for changes in wind speed. Changes in wind speed should be accounted for to facilitate changes in air circulation and convective cooling. The LCI boundary condition should also incorporate changes in relative humidity to account for the influence of relative humidity on evapotranspiration.

4.5.9 Analyses of Volumetric Water Contents from 2-D FEA Modeling Output

The 2-D FEA volumetric water contents output for varying depths to the water table were analyzed. The analyses of the 2-FEA volumetric water contents were conducted for constant total head values of 4.0 m, 3.0 m, -5.0 m, -10.0 m, and -20.0 m (FEA Case No.1 to FEA Case No.5). FEA Case No.1 to FEA Case No.5 represent static water table elevations of 1.65 m, 2.65 m, 10.65 m, 15.65 m, and 25.65 m below the subgrade surface respectively. The analyses of data presented in Figure 4.58 to Figure 4.67 show the continual seasonal fluctuations in volumetric water contents over time within subgrades with distinctive hysteretic characteristics. The hysteresis in volumetric water contents indicate that volumetric water contents within subgrades over time are dependent on the preceding transient water and heat transfer, and volumetric water contents within subgrades. The hysteresis in volumetric water contents also indicate that volumetric water contents within subgrades over time are influenced by varying volumetric water content-matric suction relationships due to drying and wetting. The drying and wetting cycles are induced by changes in climatic factors.

An analytical summary for FEA Case No.1 to FEA Case No.5 for Research Site No.1 and for Research Site No.2 is presented in Figure 4.58 to Figure 4.62, and Figures 4.63 to Figure 4.67 respectively. Seasonal fluctuations in volumetric water contents observed in Figure 4.68 to Figure 4.73 indicate that water and heat transfer within subgrades is influenced by seasonal changes in climatic factors and LCI. The analyses of data presented in Figure 4.58 to 4.73 indicate that transient and thermal processes impact fluctuations in water and heat transfer within subgrades. Water transfer within subgrades is influenced by physical processes including heat conduction, forced convection with water transfer, evapotranspiration, and convective-thermal processes. The influence of forced convection with water transfer within subgrades was confirmed through analyses of data presented in Figure 4.58 to 4.73. These analyses indicate that seasonal changes in volumetric water contents correlate directly with corresponding seasonal changes in air temperature, precipitation, and heat transfer with water transfer within subgrades. The impact of evapotranspiration is reflected in fluctuations in volumetric water contents in response to changes in temperature induced evapotranspiration. The trends in the data indicate that subgrades are subjected to a wetting path from late fall to late spring and are subjected to a drying path from late spring to late fall.

The analyses of data presented in Figure 4.58 to Figure 4.67 also indicate that volumetric water contents within subgrades are time and location dependent. However, the 2-D FEA volumetric water contents output were taken at approximately positive 0.76 m from the interface of the outside lane and shoulder and at a depth of 375.0 mm and 230.0 mm below the subgrade surface for Research Site No. 1 and Research Site No. 2 respectively. The chosen locations of the 2-D FEA volumetric water contents output correspond to the in-situ installation layout of the time domain reflectometer (TDR) probes used for measuring water contents in the LTPP and SMP.

Volumetric Water Contents from 2-D FEA Modeling Output for Research Site No. 1

The 2-D FEA volumetric water contents output for varying static water table elevations for Research Site No. 1 are shown in Figure 4.58 to Figure 4.62. The 2-D FEA volumetric water contents output were obtained at a depth of 375.0 mm below the subgrade surface.

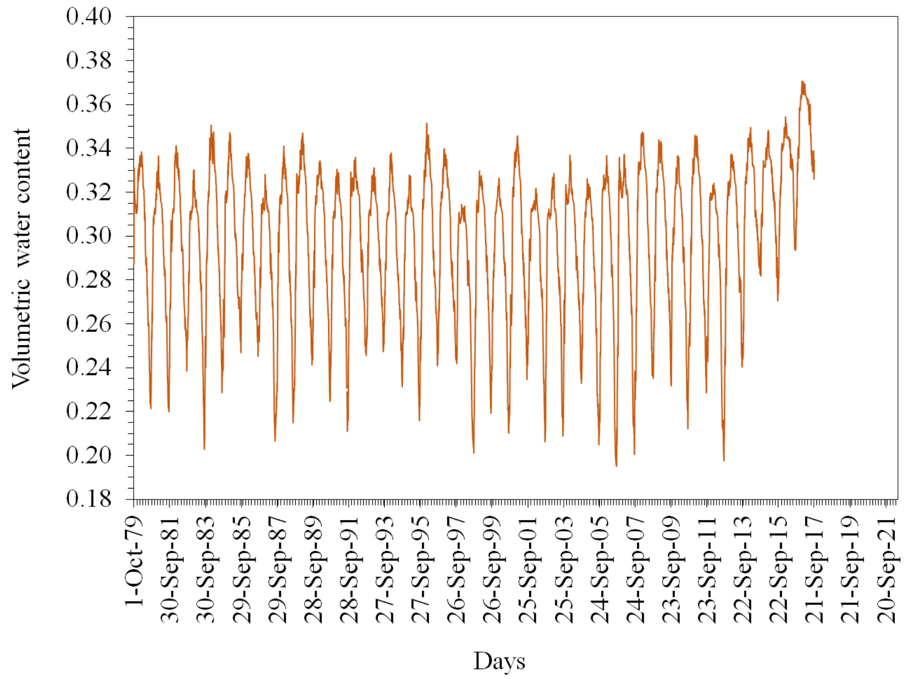

Figure 4.58: Volumetric water content vs. time with water table at 1.65 m below subgrade surface

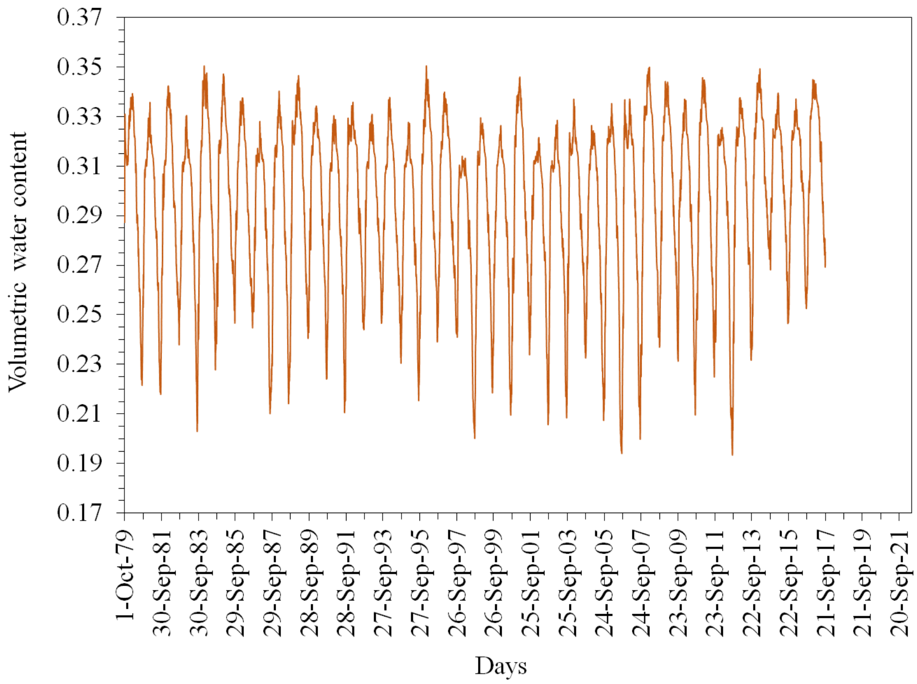

Figure 4.59: Volumetric water content vs. time with water table at 2.65 m below subgrade surface

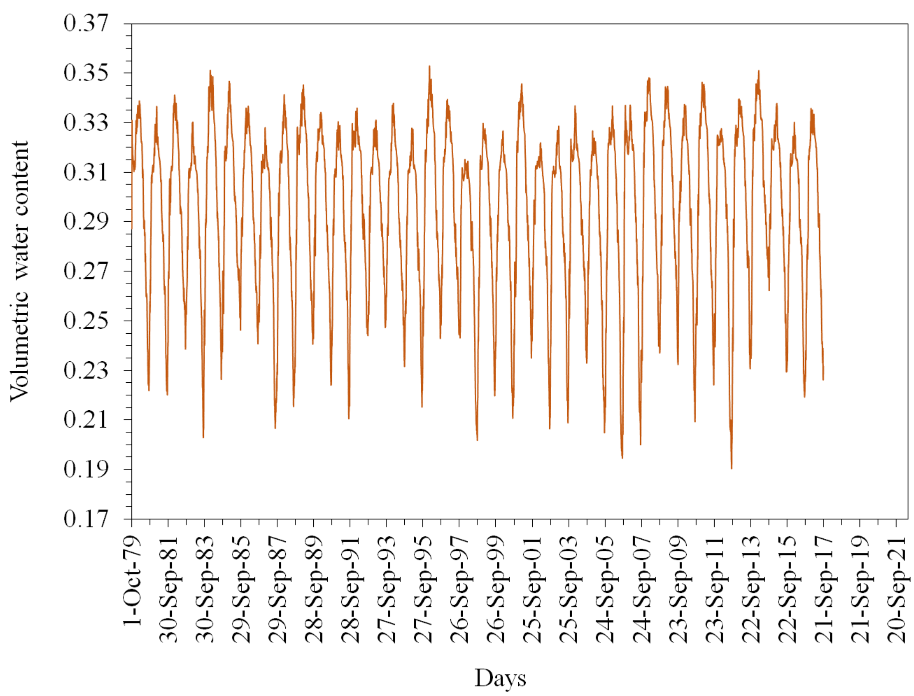

Figure 4.60: Volumetric water content vs. time with water table at 10.65 m below subgrade surface

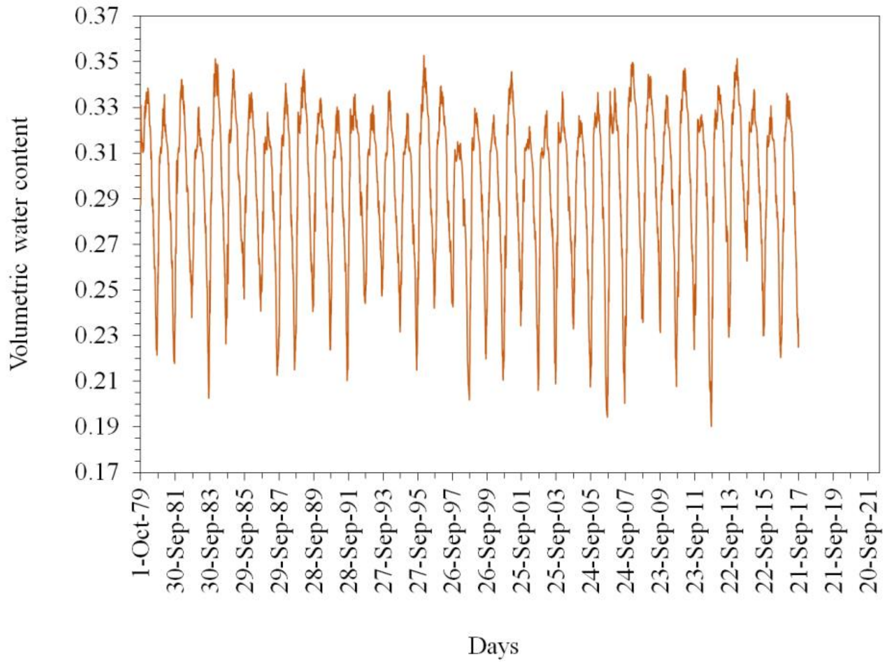

Figure 4.61: Volumetric water content vs. time with water table at 15.65 m below subgrade surface

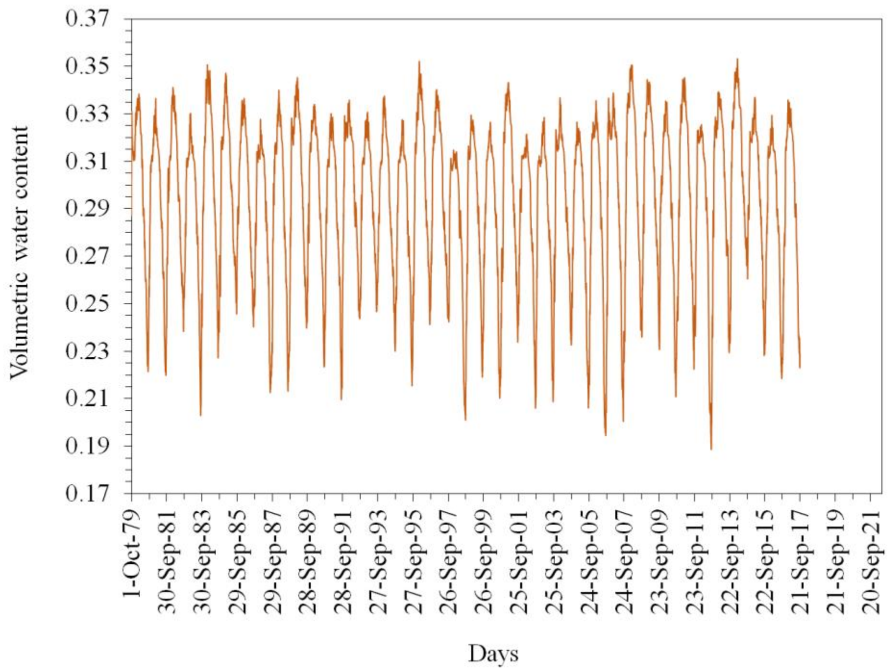

Figure 4.62: Volumetric water content vs. time with water table at 25.65 m below subgrade surface

Volumetric Water Contents from 2-D FEA Modeling Output for Research Site No. 2

The 2-D FEA volumetric water contents output for varying static water table elevations for Research Site No. 2 are shown in Figure 4.63 to Figure 4.67. The 2-D FEA volumetric water contents output were obtained at a depth of 230.0 mm below the subgrade surface.

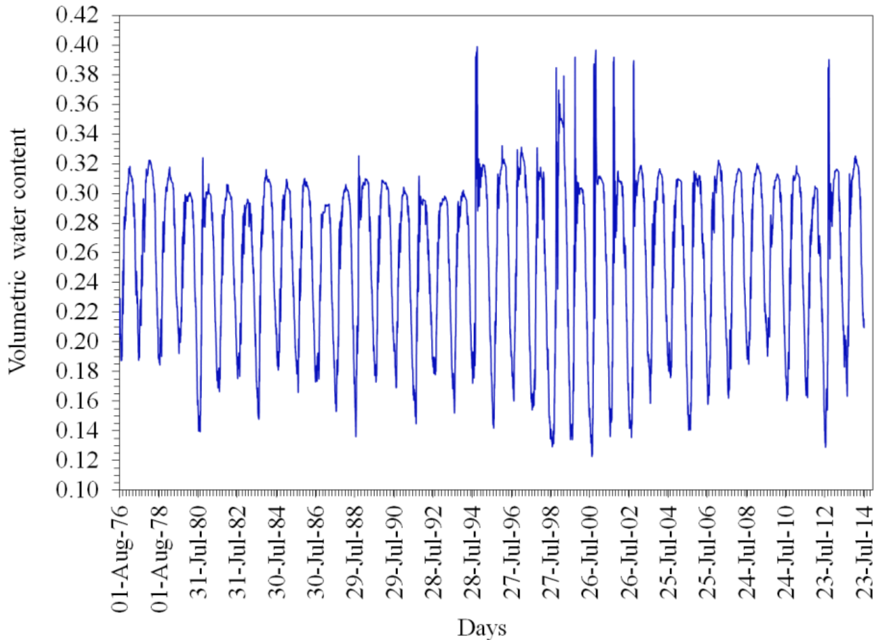

Figure 4.63: Volumetric water content vs. time with water table at 1.65 m below subgrade surface

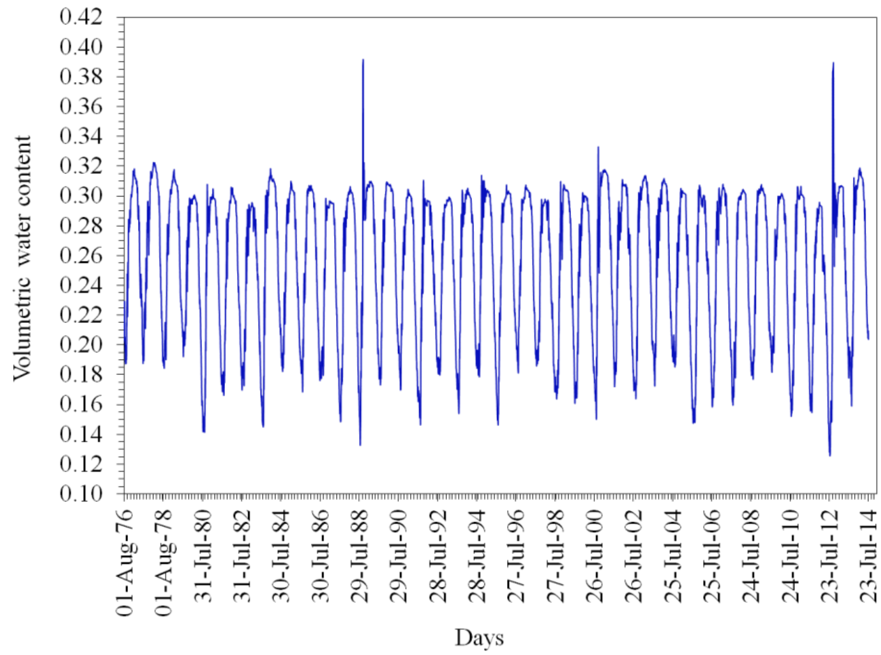

Figure 4.64: Volumetric water content vs. time with water table at 2.65 m below subgrade surface

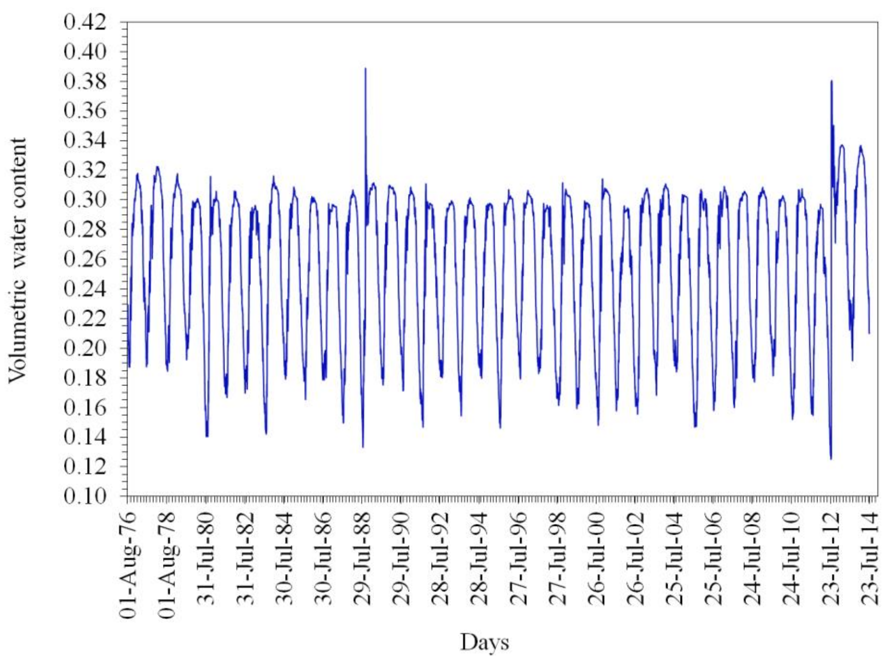

Figure 4.65: Volumetric water content vs. time with water table at 10.65 m below subgrade surface

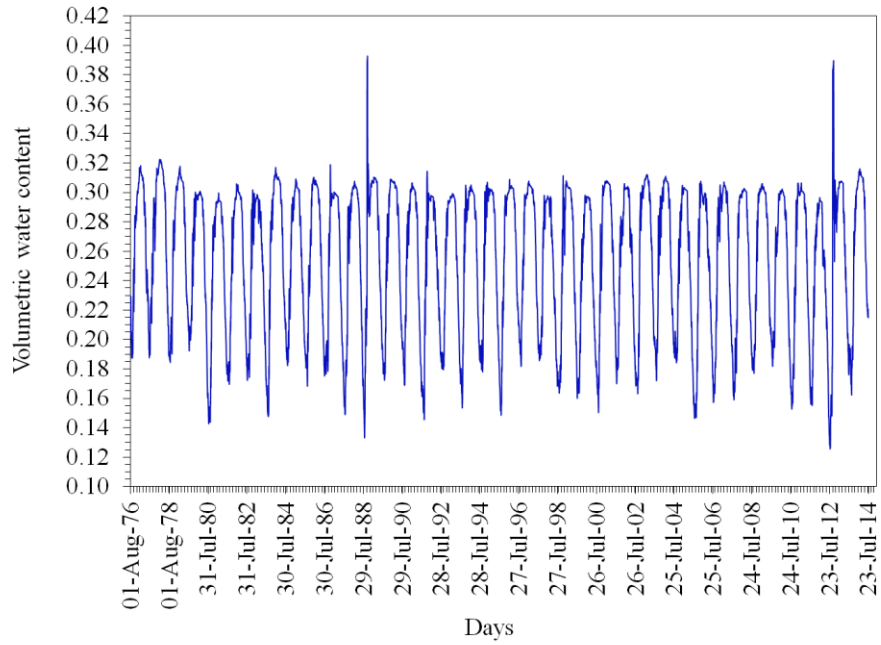

Figure 4.66: Volumetric water content vs. time with water table at 15.65 m below subgrade surface

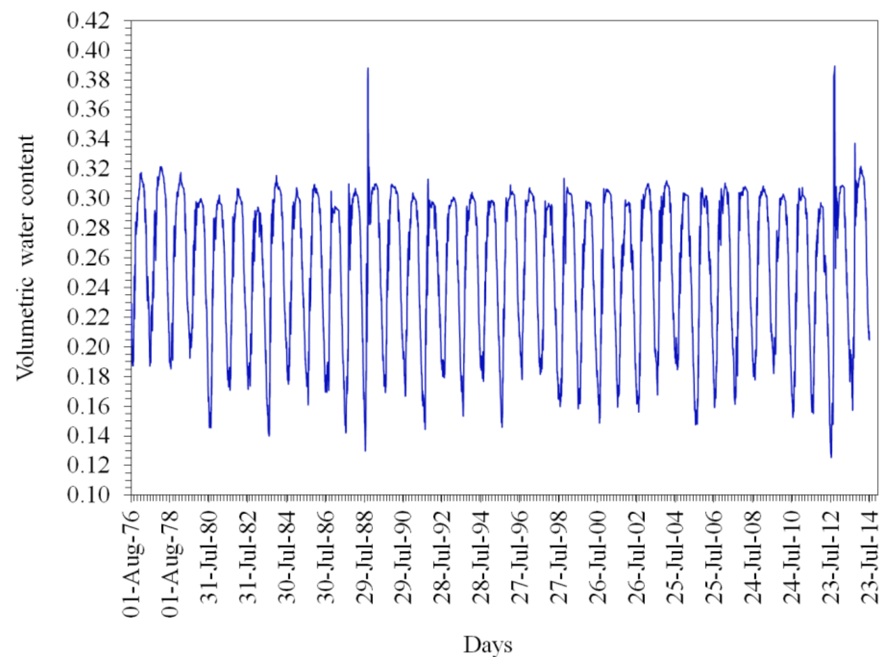

Figure 4.67: Volumetric water content vs. time with water table at 25.65 m below subgrade surface

Analyses of Minimum, Maximum and Average 2-D FEA Volumetric Water Contents Output

Figure 4.68 to Figure 4.73 were developed by analysing the daily 2-D FEA volumetric water contents output for the FEA Case No. 1 to FEA Case No. 5 for each site. The datasets were exported to Excel for further analyses. The minimum, maximum, and average 2-D FEA volumetric water contents output for each year (2-D FEA volumetric water contents) were determined for each respective site. The analyses of the 2-D FEA volumetric water contents presented in Figure 4.68 to 4.73 were conducted for each FEA Case. The analytical summaries of the 2-D FEA volumetric water contents for FEA Case No.4 for Research Site No.1 and for Research Site No.2 are presented in Figure 4.68 and Figure 4.69 respectively. The analytical summaries of the 2-D FEA volumetric water contents for Research Site No.1 for FEA Case No.1 to FEA Case No.3, and for FEA Case No.3 to FEA Case No.5 are presented in Figure 4.70 and Figure 4.71 respectively. The analytical summaries of the 2-D FEA volumetric water contents for Research site No.2 for FEA Case No.1 to FEA Case No.3, and for FEA Case No.3 to FEA Case No.5 are presented in Figure 4.72 and Figure 4.73 respectively. The analyses of data presented in Figure 4.68 to 4.73 highlight distinct variations in maximum, minimum, and average seasonal volumetric water contents within subgrades (water range). This finding indicates that the entire water range within subgrades should be considered in the performance evaluation of subgrades and associated resilient moduli. This evaluation would facilitate investigating the impact of seasonal maximum and seasonal average fluctuations in volumetric water contents on seasonal changes in resilient moduli of subgrades, pavement performance and service life.

The analyses of data presented in Figure 4.68 and Figure 4.69 imply that during periods with seasonal maximum volumetric water contents (such as during the spring thaw), the actual in-situ resilient moduli of subgrades are lower than the designed resilient moduli of subgrades. This is because the designed resilient modulus is associated with seasonal average volumetric water contents, rather than seasonal maximum volumetric water contents. Pavement structures designed using seasonal average volumetric water contents and associated seasonal average resilient moduli of subgrades are subjected to higher distress under traffic loading than the predicted design distress during the spring thaw.

Volumetric Water Content vs Time: Water Table at 15.65 m Below Subgrade Surface: Research Site No. 1.

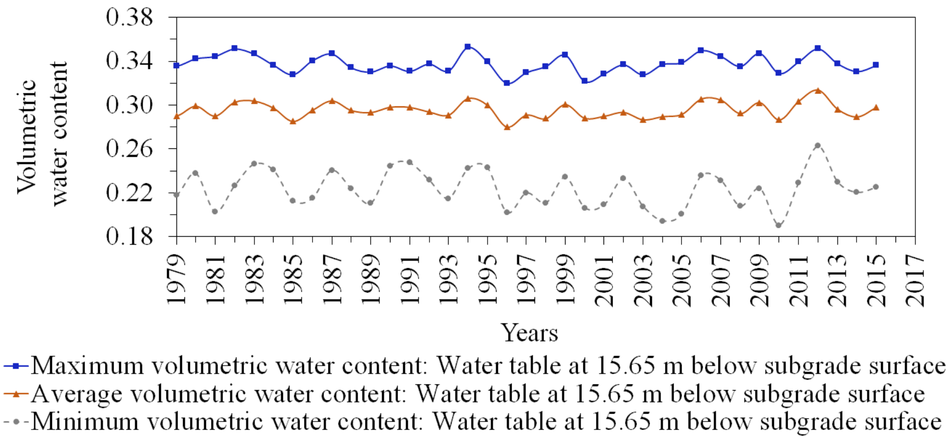

Figure 4.68: Comparison of maximum, average and minimum volumetric water contents vs time

Volumetric Water Content vs Time: Water Table at 15.65 m Below Subgrade Surface: Research Site No. 2.

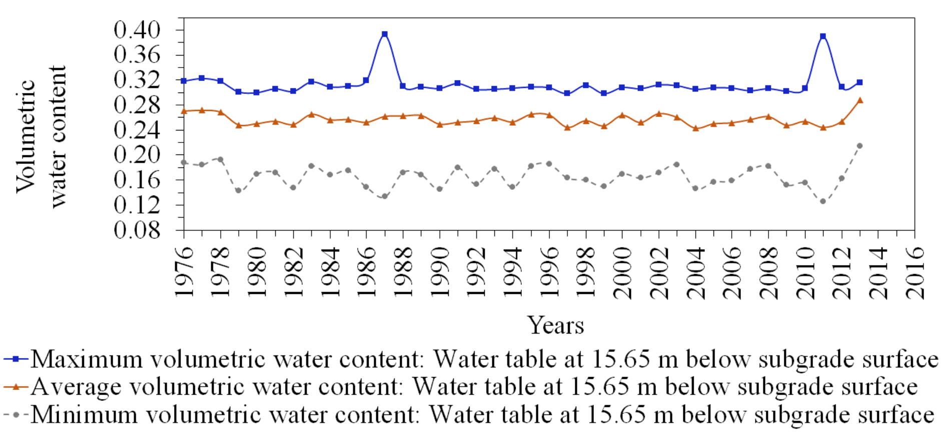

Figure 4.69: Comparison of maximum, average and minimum volumetric water contents vs time

Higher static water table elevations result in increased seasonal volumetric water contents within subgrades as shown in Figure 4.70 and Figure 4.72. These figures provide an analytical summary for FEA Case No.1 to FEA Case No.3 for Research Site No.1 and for Research Site No.2 respectively. These analyses indicate that the influence of the static water table on volumetric water contents within subgrades is impacted by the saturated volumetric water content and saturated hydraulic conductivity of subgrades. This observation indicates that the influence of the static water table on water transfer is a system dependent condition which is dependent on volumetric water contents, the subgrade type and the dry density.

The analyses of data presented in Figure 4.70 and Figure 4.72 also indicated that shallow static water tables influence the LCI processes and water transfer within subgrades. These analyses also show that LCI is a system dependent boundary condition which is dependent on the transient material water contents and shallow static water tables. These analyses also show that the actual infiltration within subgrades is influenced by the transient water contents within subgrades and is dependent on the infiltration capacity of subgrades. The analyses presented in Figure 4.71 and Figure 4.73 indicate that a static water table located at more than approximately 10.0 m below the subgrade surface has minimal impact on volumetric water contents within subgrades due to minimal capillary rise to subgrades. For such cases, liquid water and water vapour transfer within subgrades are influenced primarily by changes in climatic factors with minimal impact from the static water table. The seasonal fluctuating trends in water contents due to seasonal changes in climatic factors are similar for all five FEA Cases.

Volumetric Water Contents vs Time: Water Table at 1.65 m to 10.65 m Below Subgrade Surface: Research Site No. 1.

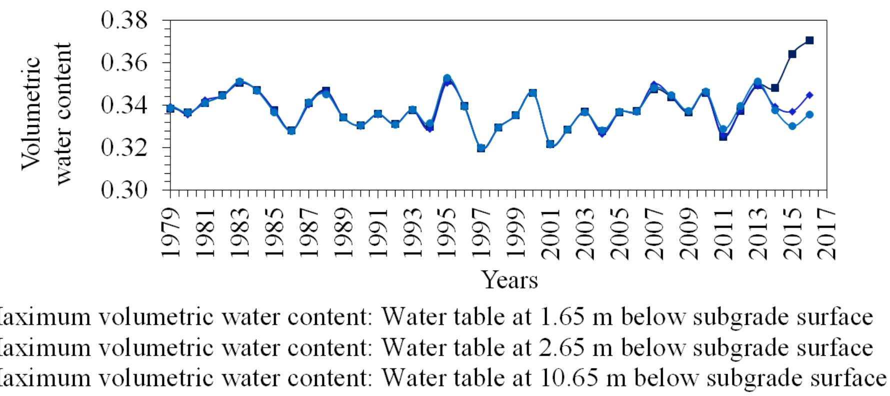

(a)

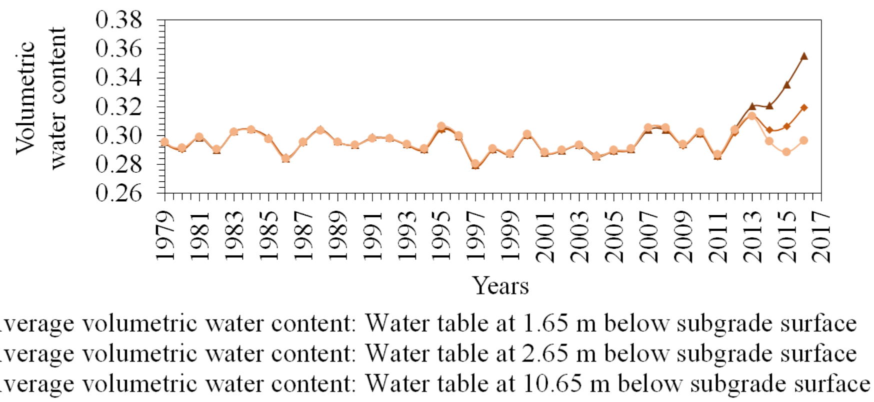

(b)

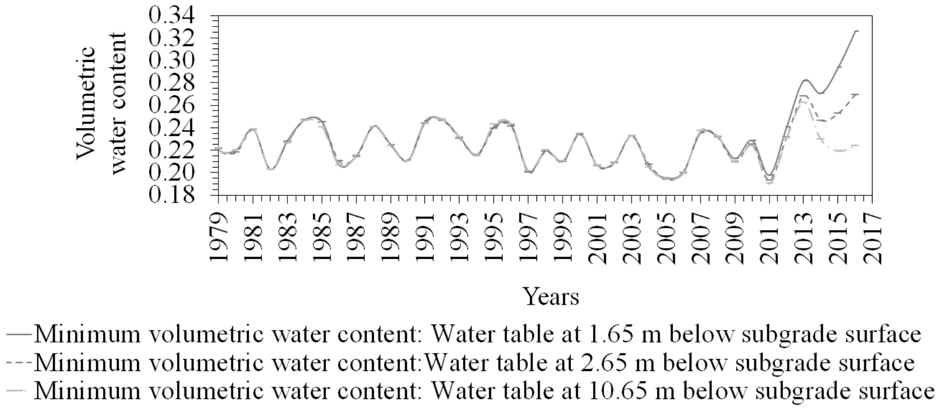

(c)

Figure 4.70: Comparison of maximum, average and minimum volumetric water contents vs time

Volumetric Water Contents vs Time: Water Table at 10.65 m to 25.65 m Below Subgrade Surface: Research Site No. 1.

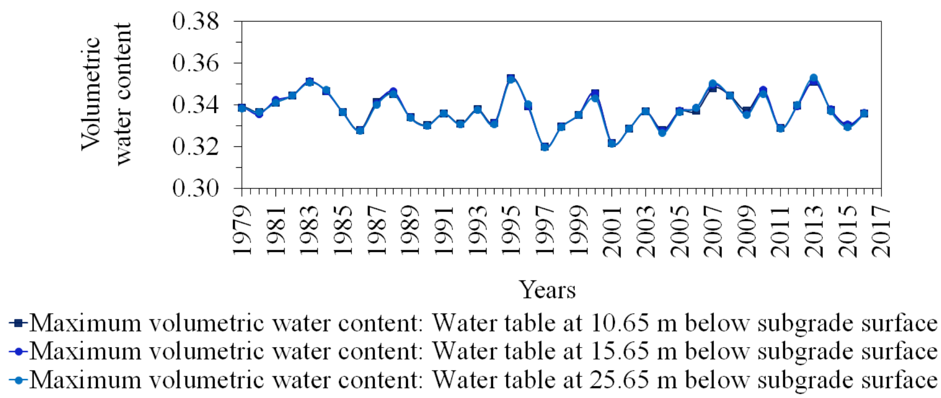

(a)

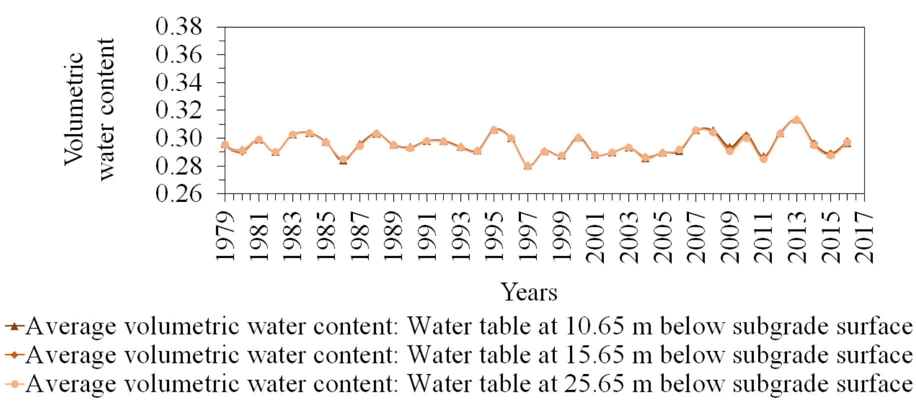

(b)

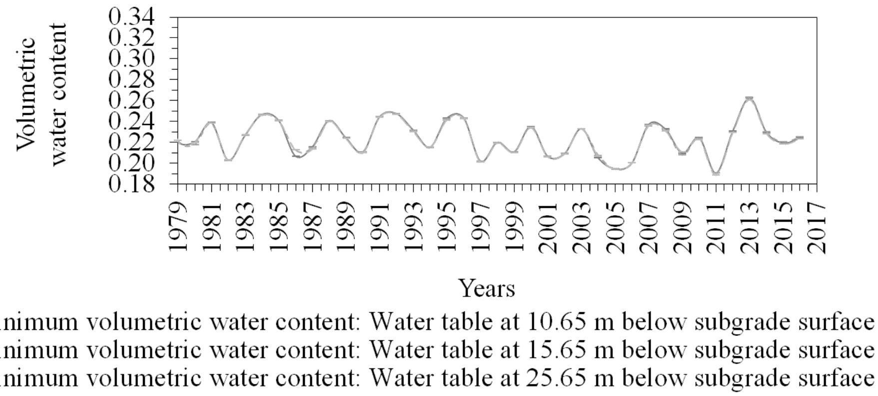

(c)

Figure 4.71: Comparison of maximum, average and minimum volumetric water contents vs time

Volumetric Water Contents vs Time: Water Table at 1.65 m to 10.65 m Below Subgrade Surface: Research Site No. 2.

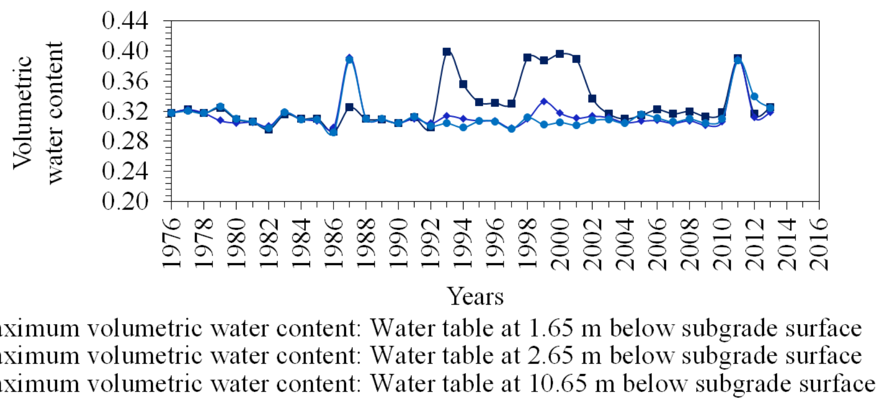

(a)

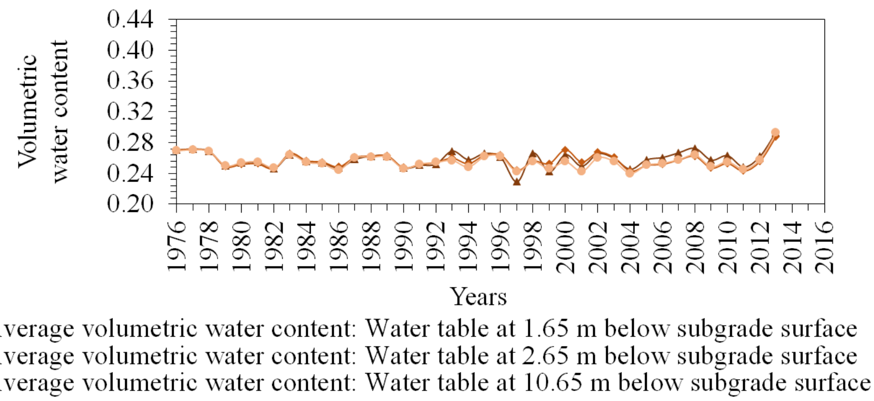

(b)

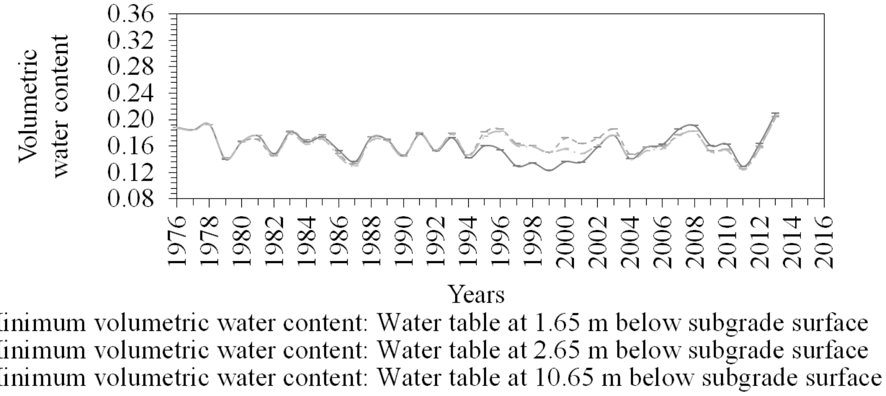

(c)

Figure 4.72: Comparison of maximum, average and minimum volumetric water contents vs time

__Volumetric Water Contents vs Time: Water Table at 10.65 m to 25.65 m Below Subgrade Surface: Research Site No. 2.__

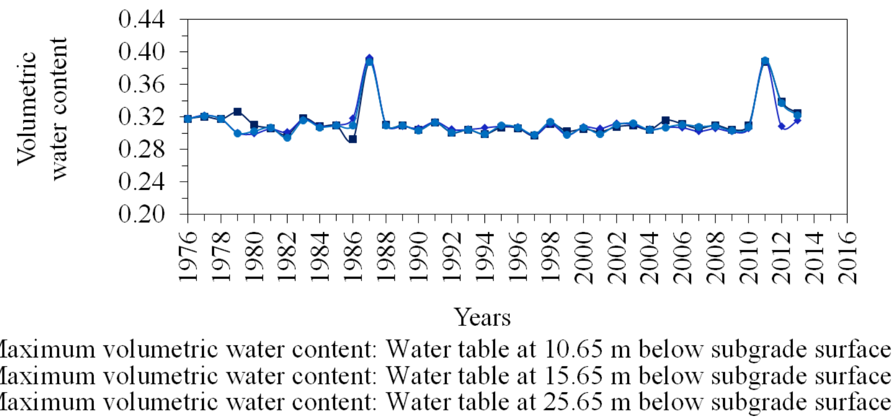

(a)

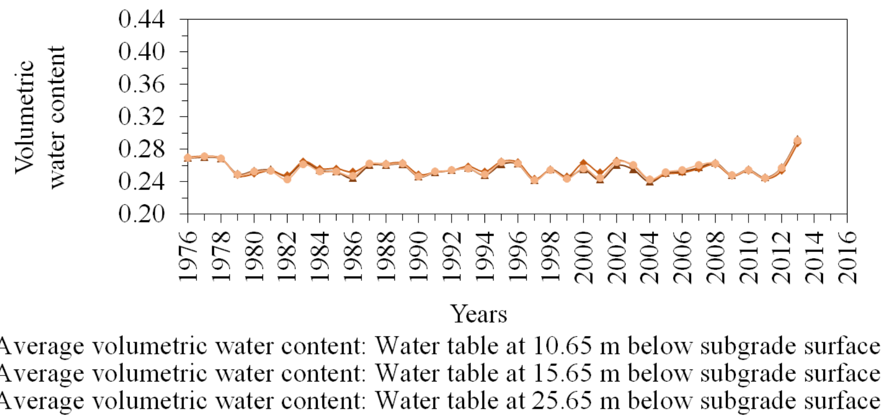

(b)

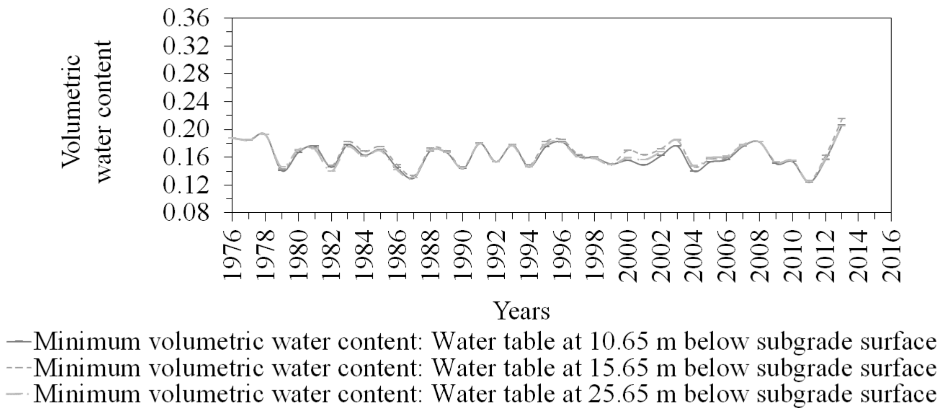

(c)

Figure 4.73: Comparison of maximum, average and minimum volumetric water contents vs time

4.5.10 Analyses of Spatial Variation in 2-D FEA Volumetric Water Contents Output

Spatial contour plots were developed using the 2-D FEA volumetric water contents output at 5-year intervals for a depth to the water table of 1.65 m below the subgrade surface for Research Site No.1. The plots are presented in Figure 4.74 to Figure 4.81. The analyses of the spatial contour plots indicated that volumetric water contents within the subgrade increased with depth. This observation implies that these spatial contour plots are associated with in-situ volumetric water contents measured during the dry season.

During the dry season, volumetric water contents at the ground surface are typically lower than volumetric water contents at lower elevations within the active zone. Hence, during the dry season the water contents profile is characterized by increased volumetric water contents with depth. During the wet season (characterized by increased precipitation), volumetric water contents at the ground surface are higher than volumetric water contents at lower elevations within the active zone. This produces a water contents profile which is characterized by decreased volumetric water contents with depth within the active zone (Heitor, et al. 2021).

The analyses of the spatial contour plots also indicated a net increase in volumetric water contents within subgrades at the end of the 38-year analysis period. The net increase in volumetric water contents is highlighted in differences between volumetric water contents at the end of construction (presented in Figure 4.74) and higher volumetric water contents at the end of the 35-year analysis period (presented in Figure 4.81). The analyses of data presented in Figure 4.74 to Figure 4.81 confirmed that volumetric water contents within subgrades are time and depth dependent. The analyses also indicated that volumetric water contents fluctuate continually and are influenced by continual changes in climatic factors. The analyses also indicated that water and heat transfer within subgrades are influenced by the location and the elevation of the inverts of the median and side ditches.

Volumetric Water Contents Spatial Contour Plots at 5-Year Intervals for a Water Table Located at 1.65 m Below the Subgrade Surface: Research Site No.1

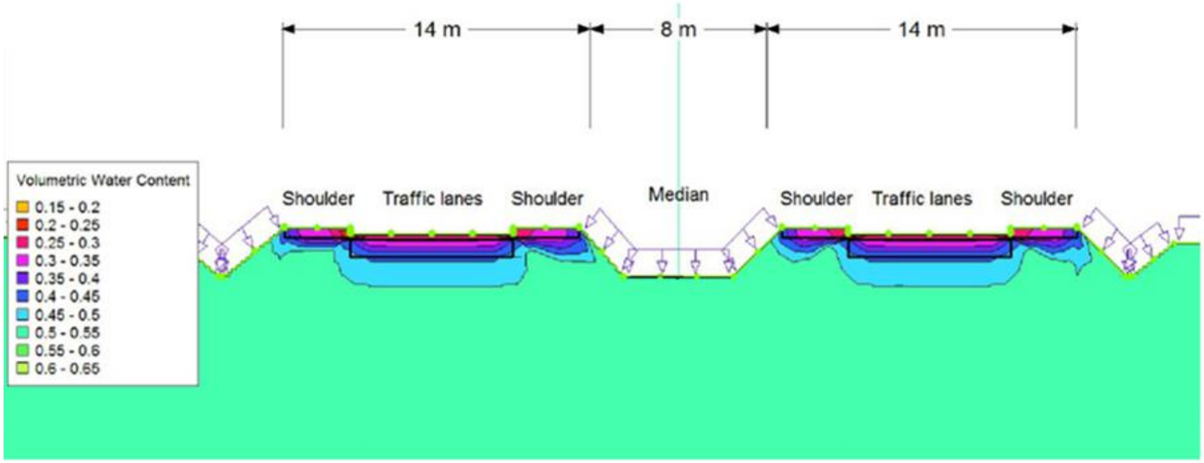

Figure 4.74: Volumetric water contents spatial contour plots for a water table located at 1.65 m below the subgrade surface at the end of construction (October 1st, 1979)

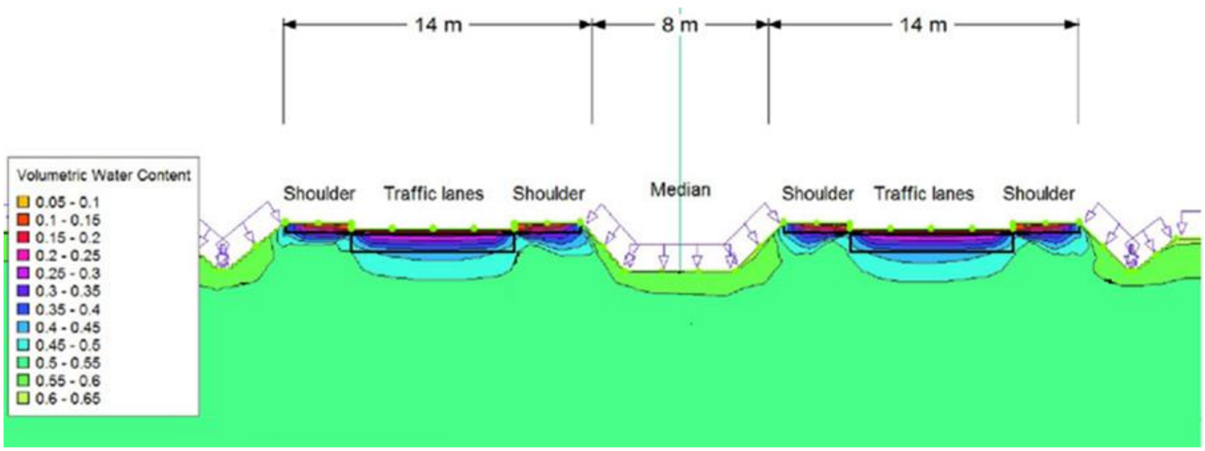

Figure 4.75: Volumetric water contents spatial contour plots for a water table located at 1.65 m below the subgrade surface after 5 years (28th September 1984)

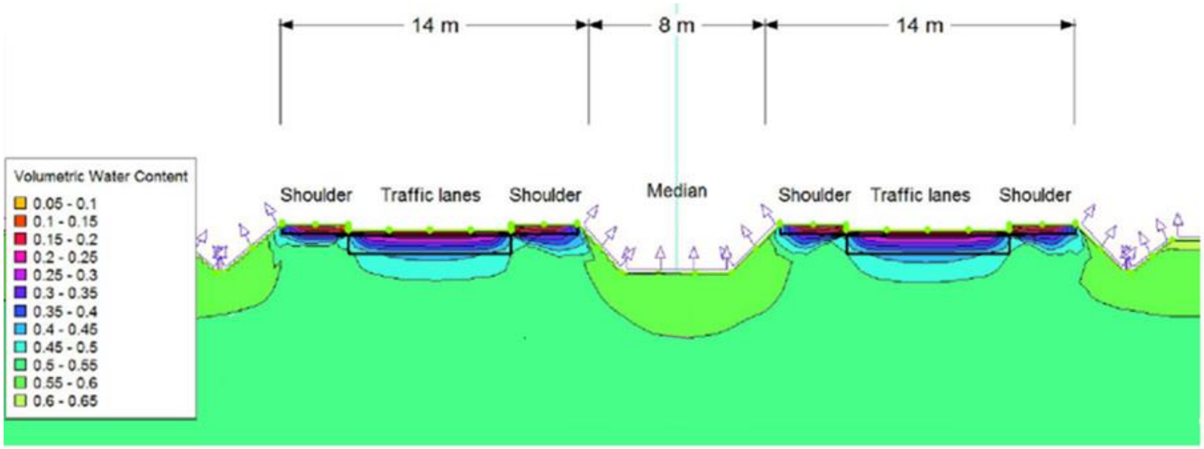

Figure 4.76: Volumetric water contents spatial contour plots for a water table located at 1.65 m below the subgrade surface after 10 years (27th September 1989)

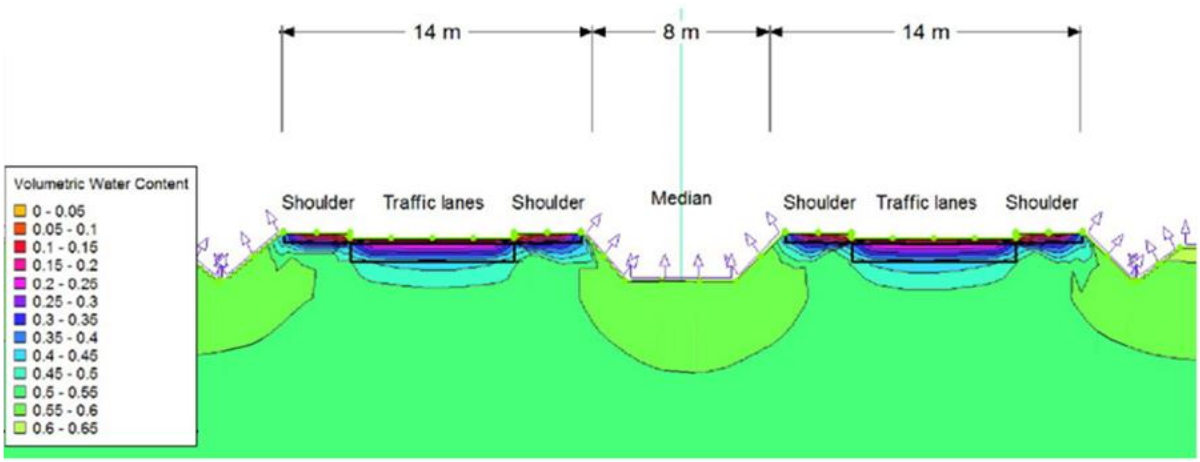

Figure 4.77: Volumetric water contents spatial contour plots for a water table located at 1.65 m below the subgrade surface after 15 years (26th September 1994)

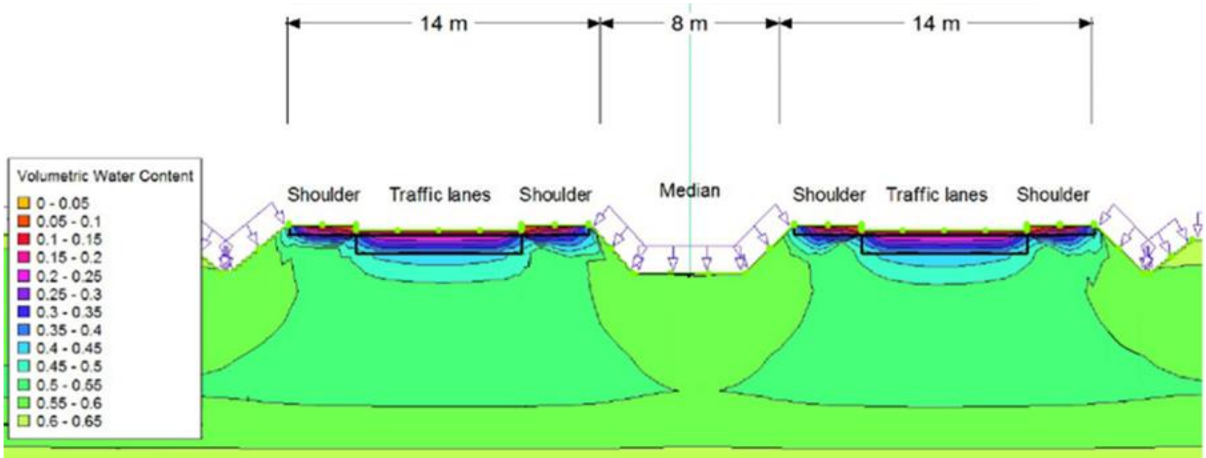

Figure 4.78: Volumetric water contents spatial contour plots for a water table located at 1.65 m below the subgrade surface after 20 years (25th September 1999)

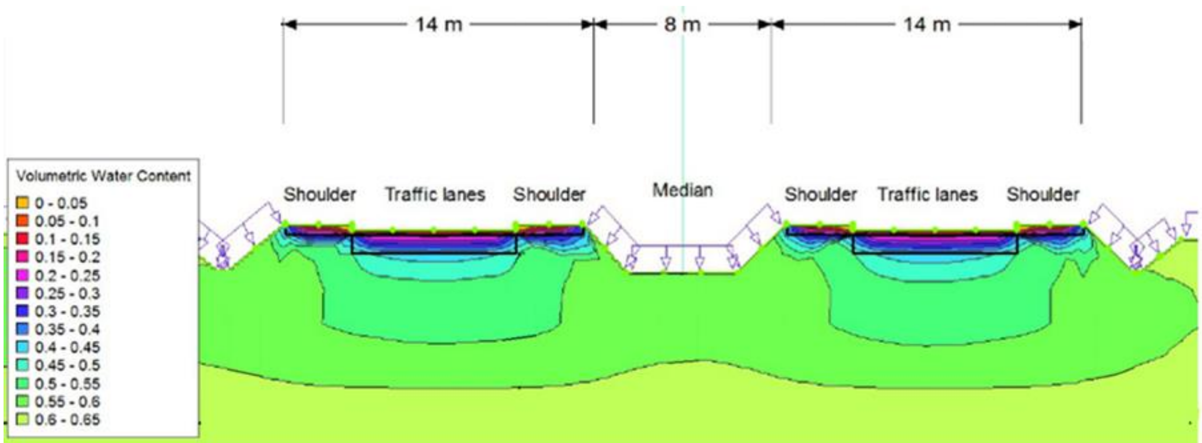

Figure 4.79: Volumetric water contents spatial contour plots for a water table located at 1.65 m below the subgrade surface after 25 years (23rd September 2004)

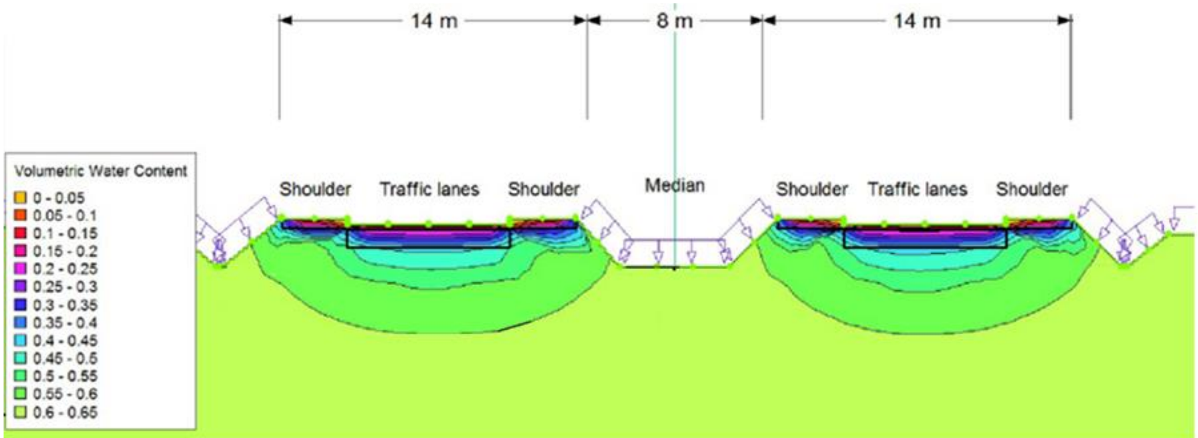

Figure 4.80: Volumetric water contents spatial contour plots for a water table located at 1.65 m below the subgrade surface after 30 years (22nd September 2009)

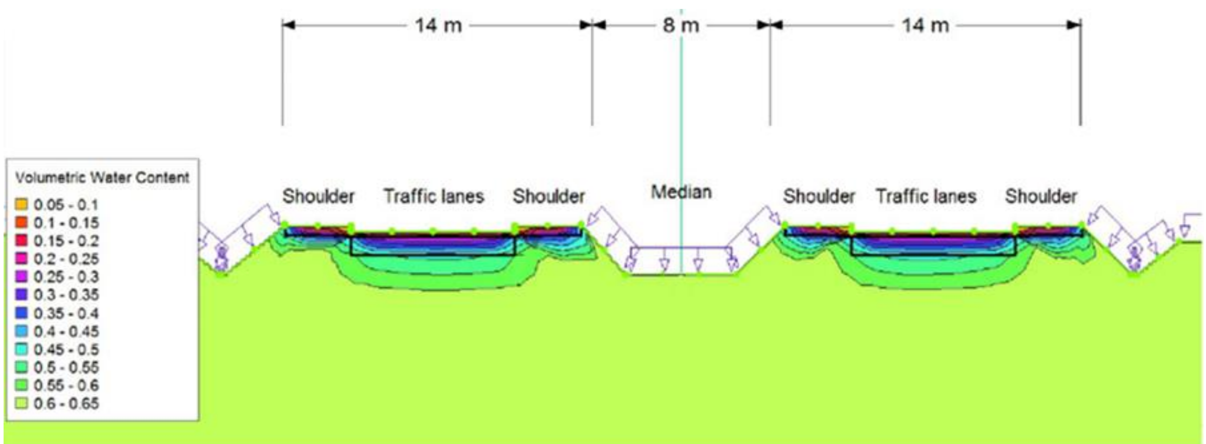

Figure 4.81: Volumetric water contents spatial contour plots for a water table located at 1.65 m below the subgrade surface after 35 years (21st September 2014)

4.5.11 Analyses of Evapotranspiration from 2-D FEA Modeling Output

The analyses of data presented in Section 4.5.3, Figure 4.82 and Figure 4.83 show that net evapotranspiration forms part of the physical processes which govern water and heat transfer within subgrades. The net evapotranspiration primarily consists of negative net evapotranspiration (the evaporation of surface and subsurface water and the transpiration from plants into the atmosphere), and positive net evapotranspiration (the condensation). The data imply that volumetric water contents within subgrades are reduced when the net evapotranspiration is negative. The data also imply that volumetric water contents within subgrades increase when the net evapotranspiration is positive. The analyses of net evapotranspiration for Research Site No.1 and for Research Site No.2 are shown in Figure 4.82 and Figure 4.83 respectively.

Net Evapotranspiration vs. time for Research Site No. 1

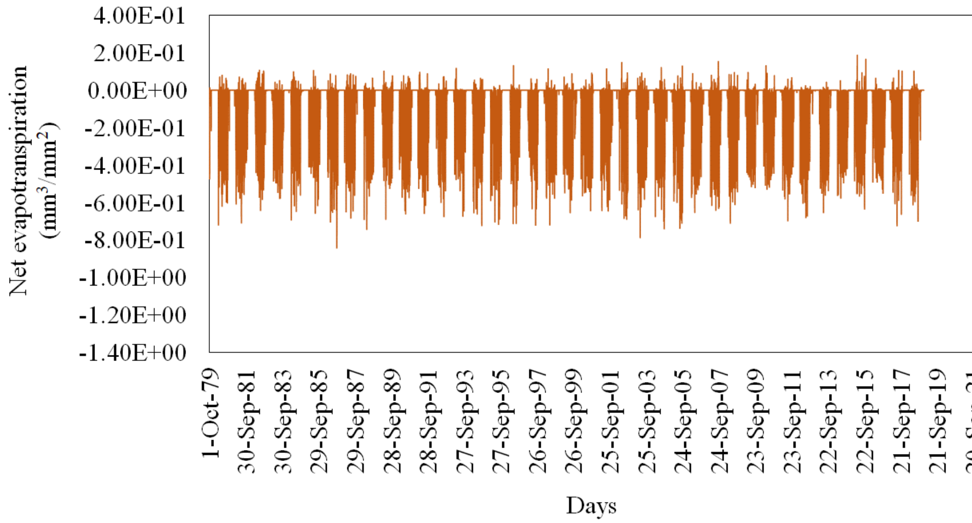

Figure 4.82: Net evapotranspiration vs. time

Net Evapotranspiration vs. time for Research Site No. 2

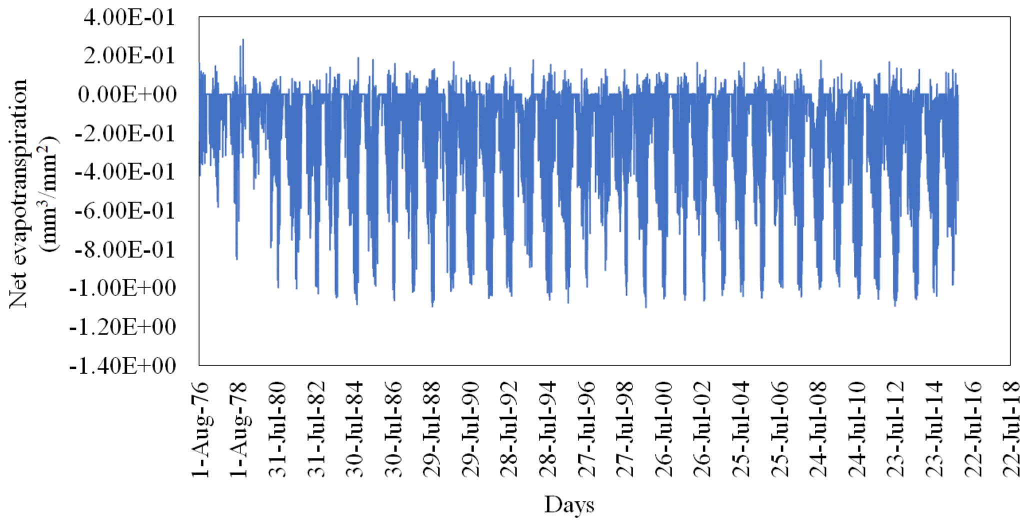

Figure 4.83: Net evapotranspiration vs. time

4.5.12 Analyses of Net and Cumulative Changes in Volumetric Water Contents: Research Site No.1

Analyses of net daily changes and cumulative changes in volumetric water contents within the subgrade were conducted for Research Site No.1 with the water table located at 1.65 m below the subgrade surface. The analyses were conducted to determine the distribution of net daily changes and cumulative changes in volumetric water contents primarily at the end of the 38-year analysis period as shown in Figure 4.84 and Figure 4.85, and Figure 4.86 respectively.

The analyses of data presented in Figure 4.84 and Figure 4.86 indicated continual seasonal fluctuations in net daily changes and cumulative changes in volumetric water contents respectively. Fluctuations in volumetric water contents shown in Figure 4.84 and Figure 4.86 are in response to changes in climatic factors based on long-term analyses. Further delineation of the net daily changes in volumetric water contents show continual daily fluctuations in volumetric water contents based on short-term analyses as shown in Figure 4.85. The analyses of data presented in Figure 4.84 also show a positive net daily change in volumetric water contents on the last day of the analysis period. The cumulative change in volumetric water contents at the end of the 38-year analysis period is also positive as shown in Figure 4.86. These observations indicate a net increase in volumetric water contents within the subgrade at the end of the 38-year analysis period relative to the initial volumetric water content within the subgrade at the end of construction. These observations also show that the equilibrium water condition assumed in EICM and MEPDG misrepresents in-situ water contents within subgrades. Hence, long-tern analyses of water and heat transfer within subgrades should incorporate continual fluctuations in volumetric water contents and resilient moduli due to climatic factors.

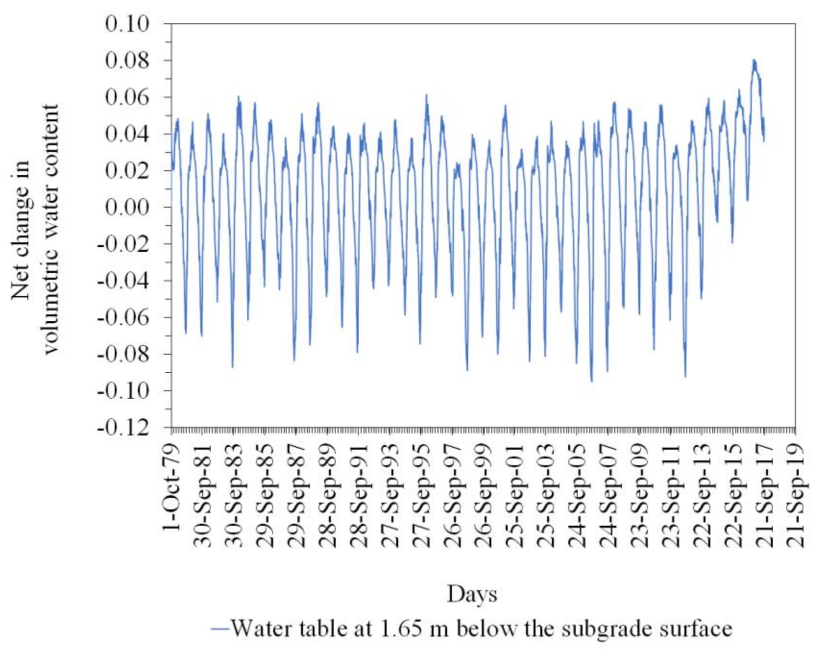

Figure 4.84: Net daily change in volumetric water content within the subgrade vs time: Long-term analysis

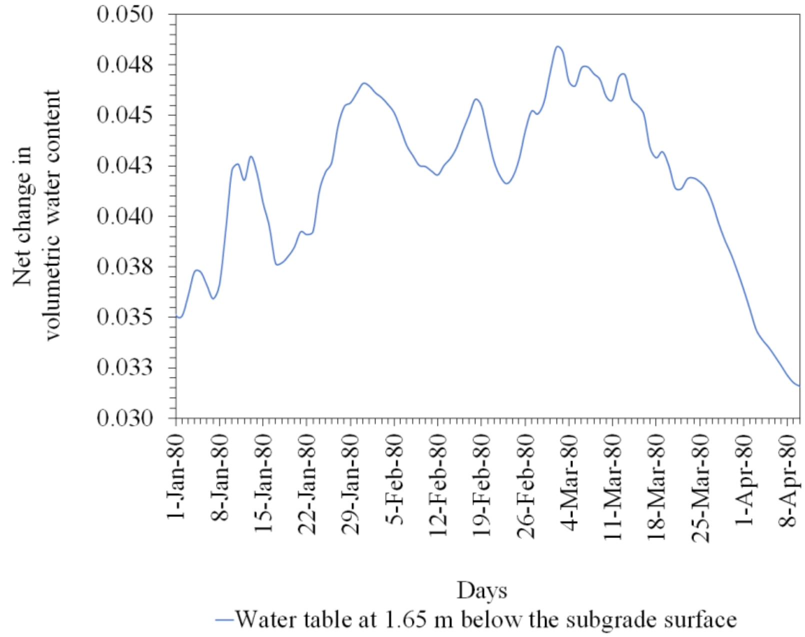

Figure 4.85: Net daily change in volumetric water content within the subgrade vs time: Short-term analysis

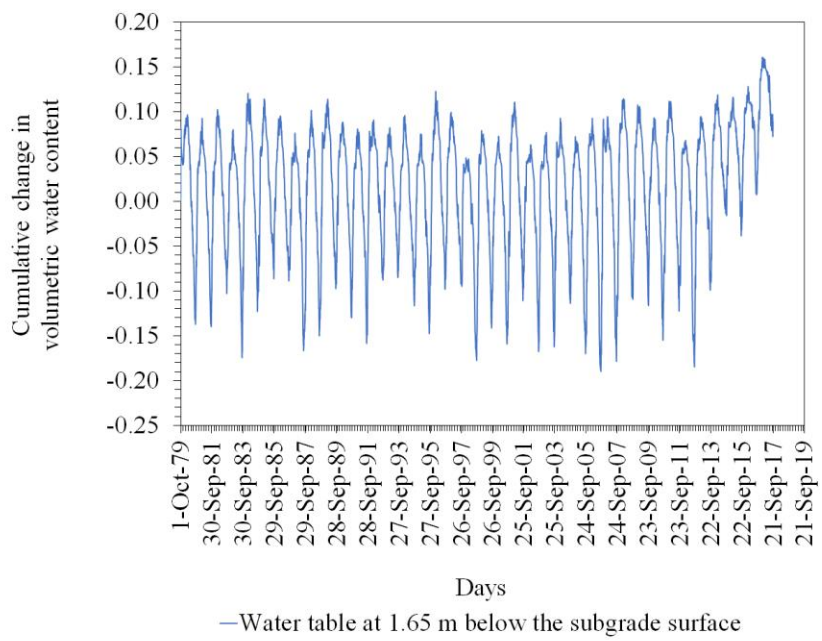

Figure 4.86: Cumulative change in volumetric water content within the subgrade vs time: Long-term analysis

4.6 Limitations of the 1-D and 2-D FEA Models

One of the primary goals of the study is to develop a Quantitative Empirical Model (the QE Model) using statistical analyses between changes in climatic factors and changes in water contents. The measured in-situ water contents are discontinuous and limited which do not facilitate accurate statistical analyses of the data. Hence, the 2-D FEA modeling was conducted to obtain more representative water contents datasets for developing the QE Model.

One of the limitations of the FEA models is that the properties of the vegetation and crops used as input in the FEA models were obtained from previous studies. The primary limitation of the FEA models is that the models were calibrated using the discontinuous and limited measured in-situ water contents datasets. The limitation associated with the vegetation and crops may result in inaccuracies in predicting the net evapotranspiration.

A no-flow boundary condition was used on the surface of traffic lanes and shoulders (wearing courses). An LCI boundary condition was used on the vegetated and bare ground areas in the 2-D FEA models. The use of a no-flow boundary condition on the wearing courses assumes that the wearing courses have no cracks, are impervious and that no water infiltrates the wearing courses. Although the use of a no-flow surface boundary condition may be seen as a limitation, typically there is minimal infiltration through the wearing courses and surface cracks.

The use of a no-flow boundary condition (on the wearing courses) and the use of the LCI boundary condition (on the vegetated and bare ground areas) show that the contribution of climatic factors to the water and heat transfer within pavement structures is the primary source of water infiltrating pavement structures. This observation indicates that climatic factors also induce continual fluctuations in volumetric water contents and resilient moduli of subgrades.

4.7 Summary

The analyses presented in Chapter 4 show interrelationships between climatic factors, and between climatic factors and volumetric water contents within subgrades. The Chapter also shows that LCI on vegetated and bare ground areas adjacent to pavement structures directly impact the water and heat transfer within subgrades. Chapter 4 also shows that changes in volumetric water contents are impacted by liquid water and water vapour transfer.

These findings highlight limitations in EICM in predicting water and heat transfer within subgrades because EICM neglects LCI and accounts only for infiltration through cracks on the pavement surface. In addition, EICM only accounts for liquid water transfer and neglects water vapour transfer. The analyses presented in Chapter 4 also show continual fluctuations in water and heat transfer, and volumetric water contents within subgrades. These findings also highlight limitations in EICM because EICM assumes an equilibrium water content and assumes a constant subgrade temperature. EICM neglects fluctuations in volumetric water contents because EICM neglects the impact of climatic factors. The FEA modeling conducted in Chapter 4 mitigate limitations in the current version of EICM by incorporating the impact of climatic factors on both liquid water and water vapour transfer within pavement structures.

The analyses of interrelationships between climatic factors, and between climatic factors and volumetric water contents presented in Chapter 4 are supported by statistical analyses shown in Chapter 5.

The development of the Quantitative Empirical Model (the QE Model) presented in Chapter 6 mitigates the limitations in EICM by incorporating the findings presented in Chapter 4 including the impact of climatic factors, LCI, liquid water and water vapour transfer, and the system dependency of water and heat transfer within subgrades.

Chapter 5 Statistical Analyses For Verifying 2-D FEA Models And For Formulating And Verifying Quantitative Empirical Model

5.1 Introduction

Chapter 5 consists of details of statistical analyses conducted to verify the FEA models, evaluate the relationship between in-situ climatic factors and volumetric water contents, formulate the general form equation for the Quantitative Empirical Model (the QE Model), verify and validate the QE Model. The statistical analyses were conducted using XLSTAT statistical software. The software was published by ADDINSOFT which is located in Paris, France.

The Chapter presents statistical analyses including correlation testing used to evaluate the inter-relationships between climatic factors and to determine the extent to which changes in climatic factors influence changes in in-situ volumetric water contents within subgrades. The statistical correlation testing was conducted using the correlation coefficient (r-value). The r-values were used for evaluating the relationship between changes in climatic factors and changes in in-situ volumetric water contents to determine the influence of changes in climatic factors on water and heat transfer within subgrades.

Chapter 5 also presents the correlation of determination (R^2) analysis conducted to determine the correlation between the measured in-situ volumetric water contents and volumetric water contents obtained from the 1-D and 2-D water and heat transfer FEA modeling output. The "R^2" analysis was used for calibrating and verifying the 1-D and 2-D FEA models.

The Chapter also presents the R^2 analysis conducted to evaluate the accuracy of the QE Model and EICM in predicting in-situ volumetric water contents, and their suitability for use in calculating the composite environmental adjustment factor (F_{env}). This analysis was conducted by comparing the F_{env} values calculated using volumetric water contents obtained from the QE Model and EICM with F_{env} values calculated using the measured in-situ volumetric water contents.

The Chapter also provides details of the Two-tailed F-test and Two-tailed Partial F-test statistics used to determine which climatic factors produced the best fitting climatic factors dataset for developing the QE Model.

Chapter 5 also provides the Two-tailed F-test statistics used for conducting a comparison between the exponential, sine and power functions to determine the best fitting function for use as the general form equation for the QE Model.

The Chapter also provides the Two-tailed F-test statistics used for evaluating whether there are statistical correlations, and statistical significance between P_1 and X_1, P_2 and X_2, and P_3 and X_3.

5.2 Pearson Correlation Coefficient (r-value) Analysis

The Pearson correlation coefficient (r-value) is a test statistic output which represents the strength of the linear statistical relationship between two continuous variables. The r-value of two random variables is determined from the ratio of the covariance of the two variables, and the product of the standard deviations of the two variables. The covariance of the two variables is determined from the mean of the product of the first variable minus the mean of the first variable, and the second variable minus the mean of the second variable. The r-value is a normalized representation of the covariance and has a range of -1.0 to 1.0. An r-value of more than zero represents a positive linear relationship, an r-value lower than zero represents a negative linear relationship, and an r-value of zero indicates that there is no linear relationship between the two variables. A positive r-value represents a linear relationship where an increase in one variable is associated with an increase in the other variable. A negative r-value represents a linear relationship where an increase in one variable is associated with a decrease in the other variable. The Pearson correlation assumes that the data in all the datasets are random, variables are continuous, each data point is paired, variables are normally distributed, there is a linear relationship between the two variables, and there are no outliers in the datasets (Ott, and Longnecker 2016). The r-value is calculated using Eq. 5.1.

$$r = \frac{[\{n*\sum(X*Y)\}-\{\sum X*\sum Y\}]}{\sqrt{[n*\{(\sum X^2)-(\sum X)^2\}]*[n*\{(\sum Y^2)-(\sum Y)^2\}]}} \quad (5.1)$$

r = Correlation coefficient; n = Number of observations; X = First variable dataset; Y = Second variable dataset.

The correlation coefficient was used for the following task:

- Task A.1: Evaluated inter-relationships between climatic factors, and between climatic factors and in-situ volumetric water contents.

5.2.1 Task A.1: Evaluating Climatic Factors-In-situ Volumetric Water Contents Relationships

The statistical correlation testing was conducted using the r-value for evaluating relationships between the climatic factors, and between climatic factors and in-situ volumetric water contents. The statistical analyses were conducted using Pearson's method and were based on a statistical significance of 5.0 % (p-value $\leq$ 0.05). A p-value $\leq$ 0.05 represents a probability of 0.05 that the r-values representing the statistical correlation between the two variables were obtained by chance. The statistical analyses were conducted to evaluate inter-relationships between changes in climatic factors, and to evaluate the influence of changes in climatic factors on changes in in-situ volumetric water contents. The statistical analyses were also conducted to evaluate relationships between changes in climatic factors and changes in depths to water table. The statistical analyses were conducted using changes in each climatic factor, changes in in-situ volumetric water contents within the subgrade and changes in the depth to water table on corresponding days. The results of the in-situ climatic factors-volumetric water contents relationships are shown in Table 4.9 presented in Section 4.5.2.

5.3 The Pearson Coefficient of Determination (R^2) Analysis

The coefficient of determination (R^2) is a value obtained from a linear regression analysis which is used to evaluate the accuracy of a statistical model in predicting the dependent variable. The "R^2" analysis is conducted by evaluating the influence of changes in the independent variable on changes in the dependent variable. The "R^2" range from a value of 0 to 1.0. An "R^2" value of 0 represents an analysis in which a model poorly predicts the dependent variable. An "R^2" value of 1.0 represents an analysis in which the model predicts the dependent variable perfectly (Ott, and Longnecker 2016). The "R^2" value is calculated using Eq. 5.2.

$$R^2 = \left[\frac{[\{n*\sum(X*Y)\}-\{\sum X*\sum Y\}]}{\sqrt{[n*\{(\sum X^2)-(\sum X)^2\}]*[n*\{(\sum Y^2)-(\sum Y)^2\}]}}\right]^2 \qquad (5.2)$$

R^2 = Coefficient of determination; n = Number of observations; X = First variable dataset; Y = Second variable dataset.

The coefficient of determination was used for the following tasks:

- Task B.1: Calibrated and verified the 2-D FEA models using the R^2-value; and
- Task B.2: Verified the QE Model in predicting in-situ volumetric water contents for Site A, Site B, Site C, and Site D using the R^2-value.

5.3.1 Task B.1: Calibration and Verification of the 2-D FEA Models using the R^2-values.

The 2-D FEA models for Research Site No.1 and Research site No.2 were calibrated and verified using the coefficient of determination (R^2) analysis between changes in measured in-situ volumetric water contents (independent variable) and changes in volumetric water contents obtained from the 2-D water and heat transfer FEA modeling output (dependent variable). The "R^2" analysis was conducted using data from the independent and dependent variables on the corresponding day and depth below the subgrade surface.

The "R^2" analysis which was conducted for calibrating and verifying the 2-D FEA model for Research Site No.1 was conducted using volumetric water contents obtained at a depth of 375.0 mm below the subgrade surface, and for a static water table located at a depth of 1.65 m below the subgrade surface. The "R^2" analysis conducted for calibrating and verifying the 2-D FEA model for Research Site No. 2 was conducted using volumetric water contents at a depth of 230.0 mm below the subgrade surface, and for a static water table located at a depth of 1.65 m and 2.65 m below the subgrade surface. The water contents used in the analyses were selected at shallow depths because climatic factors have higher impact on water contents at shallow depths.

The "R^2" analyses presented in Table 5.1 to Table 5.3 show a strong statistical correlation between the measured in-situ volumetric water contents and the 2-D FEA volumetric water contents output for the two research sites. These "R^2" analyses also indicate that the 2-D FEA models for the two research sites were adequately calibrated in simulating in-situ volumetric water contents within subgrades. The analyses presented in Table 5.1 to Table 5.3 also show that for Research Site No. 2, the 2-D FEA model was calibrated with a higher accuracy against the measured in-situ volumetric water contents obtained at a depth of 2.65 m below the subgrade surface, relative to the accuracy of the 2-D FEA model calibrated against the measured in-situ volumetric water contents obtained at a depth of 1.65 m below the subgrade surface. The "R^2" analyses for Research Site No.1 and Research Site No.2 are summarized in Table 5.1, and Table 5.2 and Table 5.3 respectively.

The "R^2" Analysis conducted between the measured and 2-D FEA volumetric water contents output for calibrating and verifying the 2-D FEA model: Research Site No.1.

Table 5.1: Summary of the "R^2" analysis conducted using volumetric water contents obtained at a depth of 375.0 mm, and for a water table located at 1.65 m below the subgrade surface

Statistical Data	Nonlinear regression output	
	1993 and 1994	1995 to 1997
Observations	5	3
r	0.946	0.952
R^2	0.895	0.906

The R^2 Analysis conducted between the measured and 2-D FEA volumetric water contents output for calibrating and verifying the 2-D FEA model: Research Site No.2.

Table 5.2: Summary of the "R^2" analysis conducted using volumetric water contents obtained at a depth of 230.0 mm, and for a water table located at 1.65 m below the subgrade surface

Statistical Data	Nonlinear regression output
	1995 and 1996
Observations	3
r	0.840
R^2	0.706

Table 5.3: Summary of the "R^2" analysis conducted using volumetric water contents obtained at a depth of 230.0 mm, and for a water table located at 2.65 m below the subgrade surface

Statistical Data	Nonlinear regression output
	1995 and 1996
Observations	3
r	0.973
R^2	0.947

5.3.2 *Task B.2: Verification of the Quantitative Empirical Model in Predicting in-situ volumetric water contents for Site A, Site B, Site C, and Site D using the R^2-values.*

The Quantitative Empirical Model (the QE Model) was verified using the "R^2" analysis between changes in measured in-situ volumetric water contents (the independent variable) and changes in volumetric water contents predicted using the QE Model (the dependent variable). The "R^2" analysis was conducted using data from the independent and dependent variables on the corresponding day and at a depth of 150.0 mm below the subgrade surface.

The "R^2" analysis presented in Table 5.4 shows a strong statistical correlation between the measured in-situ volumetric water contents and the in-situ volumetric water contents predicted using the QE Model. This analysis indicates that the QE Model accurately predicts the impact of changes in climatic factors on changes in in-situ volumetric water contents within subgrades.

Table 5.4: Summary of the "R^2" analysis conducted to evaluate the accuracy of the Quantitative Empirical Model in predicting in-situ volumetric water contents within subgrades

Statistical Data	Values			
	Site A	Site B	Site C	Site D
Observations	8	5	4	5
r	0.889	0.960	0.916	0.884
R^2	0.791	0.922	0.839	0.781

5.4 The Two-tailed F-test conducted for Developing, Evaluating and Verifying the Model

The Fisher's F-test (F-test) is a statistical analysis which is used for testing a hypothesis which evaluates whether variances of two datasets are equal, and to determine whether the two datasets have statistical significance. The F-test statistics consists of the statistical analysis of datasets using an F-distribution (each random variable is divided by their respective degree of freedom). The F-test may be conducted using a One-tailed or Two-tailed F-test. The One-tailed F-test only evaluates the variance in one direction and determines whether the variance for the dataset No.1 is either greater than or less than the variance for dataset No.2. The Two-tailed F-test evaluates both the null and alternative hypotheses and evaluates the variance in both direction (determines whether the variance for the dataset No.1 is greater than and less than the variance for dataset No.2).

The Two-tailed F-test statistics consists of a null hypothesis as shown in Eq. 5.3 and an alternative hypothesis as shown in Eq. 5.4. The null hypothesis assumes that the two datasets have an equal statistical significance due to the datasets having the same variance (assumes F-Statistic = 1.0). The alternative hypothesis which assumes that one dataset has a higher statistical significance than the other due to unequal variances (assumes F-Statistic ≠ 1.0). The analyses of the Two-tailed F-test statistics are conducted using the F-value obtained from the F-statistics output (F-statistic) presented in Eq. 5.5 to Eq 5.7. The Two-tailed F-test statistics is based on the assumption that the datasets are independent of each other and that the values in both datasets are normally distributed (symmetric about the mean of the dataset).

$$H_0: \quad \sigma_x^2 = \sigma_y^2 \tag{5.3}$$

$$H_a: \quad \sigma_x^2 \neq \sigma_y^2 \tag{5.4}$$

$$F\text{–}Statistic = \frac{\sigma_x^2}{\sigma_y^2} \tag{5.5}$$

$$\sigma_x^2 = \left(\frac{1}{n_x - 1}\right) * \sum_{i=1}^{n_x} (x_i - \bar{x})^2 \tag{5.6}$$

$$\sigma_y^2 = \left(\frac{1}{n_y - 1}\right) * \sum_{i=1}^{n_y} (y_i - \bar{y})^2 \tag{5.7}$$

H_0 = Null hypothesis; H_a = Alternative hypothesis; *F Statistic* = A value on the F-distribution; σ_x^2 = Larger sample variance; σ_y^2 = Smaller sample variance; x_i = Independent values from the dataset with the larger variance; $\bar{x}$ = Sample mean for the dataset with the larger variance; y_i = Independent values from the dataset with the smaller variance; $\bar{y}$ = Sample mean for the dataset with the smaller variance; n_x = Number of observed values in the dataset with the larger variance; n_y = Number of observed values in the dataset with the smaller variance.

The analysis of the Two-tailed F-test statistics also consists of calculating the degrees of freedom as shown in Eq. 5.8 and Eq. 5.9.

$$Degree\ of\ freedom\ No.1 = n_1 - 1 \quad (5.8)$$

$$Degree\ of\ freedom\ No.2 = n_2 - 1 \quad (5.9)$$

Degree of freedom No. 1 = Degree of freedom in the numerator; *Degree of freedom No. 2* = Degree of freedom in the denominator; n_1 = Number of observed values in dataset No.1; n_2 = Number of observed values in dataset No.2.

The Critical F-value is determined from the F-table for a probability of 0.025 (50.0 % of the threshold p-value of 0.05 which is assigned to each of the two tails) using the "n_1" and "n_2". The threshold p-value is used in the statistical analysis and represents a probability of up to 0.05 of mistakenly rejecting the null hypothesis at a critical data point which is equal to the Critical-F value. The analyses of the Two-tailed F-test statistics includes comparing the F-statistic with the Critical-F value. The null hypothesis is rejected if the F-Statistic is not equal to 1.0 at the threshold p-value. This is verified by conducting a statistically significant analysis to determine whether the null hypothesis should be rejected. The verification testing is done by comparing the threshold p-value to the calculated p-value to evaluate the probability that the decision to reject the null hypothesis is unacceptable. The decision to reject the null hypothesis is deemed acceptable if the calculated p-value is lower than the threshold p-value (NIST-SEMATECH 2022; Snedecor, and Cochran 1989). The framework which is used for conducting the Two-tailed F-test is presented in Figure 5.1.

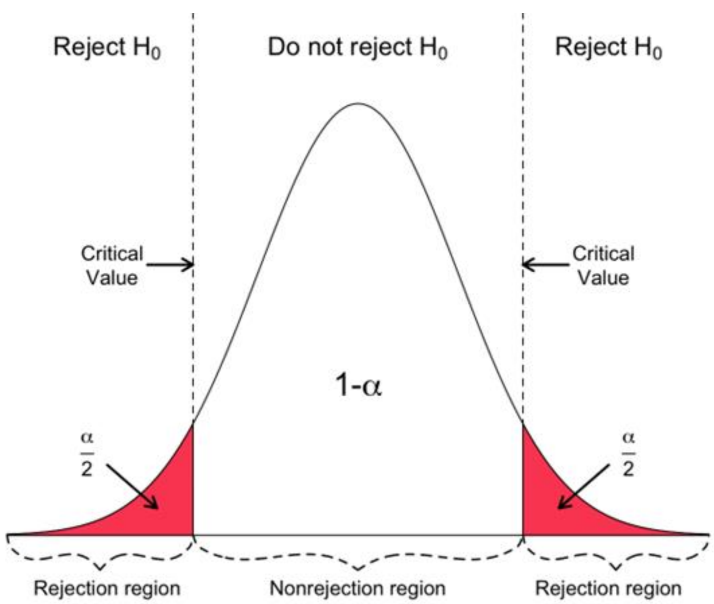

Figure 5.1: The framework used for conducting the Two-tailed F-test (Hartmann et al. 2018)

The Two-tailed F-test statistics was conducted for evaluating the following tasks:

- Task C.1: Determined the best fitting reference point for calculating changes in climatic factors and changes in volumetric water content;
- Task C.2: Determined the climatic factors that produce the best fitting climatic factors dataset for developing the Quantitative Empirical Model (QE Model);
- Task C.3: Conducted a comparison between the exponential, sine and power functions to determine the best fitting function for use as the general form equation for the QE Model;
- Task C.4: Evaluated the extent of the statistical correlations, and statistical significance between P_1 and X_1, P_2 and X_2, and P_3 and X_3; and
- Task C.5: Determine the accuracy of the QE Model and EICM in predicting in-situ volumetric water contents for use in calculating the composite environmental adjustment factor (F_{env}).

5.4.1 Task C.1: Two-tailed F-test Statistics Conducted to Determine the Best Fitting Reference Point for Calculating Changes in Climatic Factors and changes in Volumetric Water Contents

A sensitivity analysis was conducted using the exponential function presented in Eq 6.5 to predict in-situ volumetric water contents. The exponential function was developed using nonlinear regression between changes in climatic factors (the independent variable) and changes in volumetric water contents obtained from the 2-D FEA modeling (the dependent variable). The value of the dependent and independent variables which were measured at the end of the construction of the pavement structure was used as the respective reference value (the reference value A and B respectively). The dependent and independent variables were calculated relative to the reference value A and B respectively. For the purpose of this sensitivity analysis, the exponential function was developed using the dependent and independent variables which were calculated using the reference values A and B (the exponential function No.1). Similarly, the dependent and independent variables were also calculated using values from each previous day as reference values. The exponential function was also developed using the dependent and independent variables which were calculated using values from each previous day as reference values (the exponential function No.2).

The Two-tailed F-test statistics was conducted using in-situ volumetric water contents predicted using the exponential function No.2 as the dataset No.1, and in-situ volumetric water contents predicted using the exponential function No.1 as the dataset No.2. The null hypothesis assumes that the exponential function No.2 is more accurate than the exponential function No.1 in predicting in-situ volumetric water contents. Hence, the null hypothesis assumes that it is better to use the previous day as the reference point for calculating the dependent and independent variables. The alternative hypothesis assumes that it is better to use the values of the dependent and independent variables which were measured on the construction completion date as the reference values for calculating the dependent and independent variables. A summary of the Two-tailed F-test statistics is presented in Table 5.5.

The analysis of the data presented in Table 5.5 indicates that the null hypothesis should be rejected because the F-Statistic is more than the F-Critical. In addition, the calculated p-value is less than the Threshold p-value which indicates that the decision to reject the null hypothesis is acceptable. Based on the analysis of the data presented in Table 5.5, values for the dependent and independent variables which were measured on the construction completion date are used as reference values for calculating the dependent and independent variables.

Table 5.5: The summary of the Two-tailed F-test statistics conducted to determine the best fitting reference values for calculating the dependent and independent variables

Statistical Data	Values
F-statistic	2.941
F-Critical	1.00
Calculated p-value	<0.0001
Threshold p-value	0.05

5.4.2 Task C.2: Two-tailed Partial F-test Statistics Conducted to Determine Climatic Factors that Produce the Best Fitting Model

The Two-tailed Partial F-test statistics is a form of the Two-tailed F-test statistics which is used in multivariate linear regression analysis (the dependent variable is a function of two or more independent variables). The Two-tailed Partial F-test statistics is used to determine whether there is a statistically significant difference between a regression model and a reduced form of the model (the reduced model). The reduced model consists of a subset of the independent variables incorporated into the model and excludes one or more of the independent variables. The Two-tailed Partial F-test statistics is used to evaluate the independent variable(s) which should be included to produce the best fitting model (Chaurasia, and Harel 2014; Jamshidian, et al. 2007).

The Quantitative Empirical Model (the QE Model) was developed to predict changes in in-situ volumetric water contents as a nonlinear function of changes in climatic factors. The climatic factors include precipitation, air temperature, net solar radiation, wind speed, relative humidity, evapotranspiration, and water vapour transfer through the wearing course to the atmosphere (the climatic factors).

Sensitivity analyses were conducted to evaluate whether the QE Model should be developed to predict changes in volumetric water contents as a nonlinear function of changes in the climatic factors, climatic factors which excludes precipitation (the reduced climatic factors No.1), climatic factors which excludes relative humidity (the reduced climatic factors No.2), climatic factors which excludes net solar radiation (reduced climatic factors No.3), and using only air temperature (the reduced climatic factors No.4). Sensitivity analyses were conducted using the Two-tailed Partial F-test statistics, and were conducted using the following options:

- Partial F-test Option No.1: Changes in volumetric water contents as a nonlinear function of the reduced climatic factors No.1 was used for dataset No.1, and changes in volumetric water contents as a nonlinear function of changes in climatic factors was used for dataset No.2;
- Partial F-test Option No.2: Changes in volumetric water contents as a nonlinear function of the reduced climatic factors No.2 was used for dataset No.1, and changes in volumetric water contents as a nonlinear function of changes in climatic factors was used for dataset No.2;
- Partial F-test Option No.3: Changes in volumetric water contents as a nonlinear function of the reduced climatic factors No.3 was used for dataset No.1, and changes in volumetric water contents as a nonlinear function of changes in climatic factors was used for dataset No.2; and
- Partial F-test Option No.4: Changes in volumetric water contents as a nonlinear function of the reduced climatic factors No.4 was used for dataset No.1, and changes in volumetric water contents as a nonlinear function of changes in climatic factors was used for dataset No.2.

The null hypothesis assumes that quantitative empirical models incorporating the reduced climatic factors No.1 to No.4 are more accurate than the quantitative empirical model which incorporates the complete set of climatic factors. The alternative hypothesis assumes that the quantitative empirical model which incorporates the complete set of climatic factors is more accurate than the models incorporating the reduced climatic factors.

The analysis of the data presented in Table 5.6 shows that the F-statistic is more than the F-Critical, and that the calculated p-value is less than the threshold p-value for all the analysis options. This indicates that the null hypothesis should be rejected and the decision to reject the null hypothesis is acceptable for all the analysis options. The analysis of the data presented in Table 5.6 also shows that the alternative hypothesis should be accepted. This means that the QE Model predicts changes in volumetric water contents more accurately by incorporating changes in the complete set of climatic factors, rather than incorporating the reduced climatic factors. This indicates that excluding precipitation (the primary source of water) misrepresents the impact of climatic factors on the in-situ water and heat transfer within subgrades. The analysis of the data presented in Table 5.6 also shows that excluding the relative humidity neglects the impact of changes in the relative humidity on changes in the evapotranspiration. The analysis of the data presented in Table 5.6 also shows that excluding the impact of the net solar radiation which is associated with the albedo (the ability of a surface to reflect sunlight) neglects the impact of the net solar radiation on the ground surface temperatures.

The analysis of the data presented in Table 5.6 indicates that the exclusion of precipitation, relative humidity, and net solar radiation results in inaccurate prediction of changes in in-situ volumetric water content, F_{env} and resilient moduli of subgrades. Hence, the QE Model was developed by incorporating the complete set of climatic factors.

Table 5.6: The summary of the Two-tailed Partial F-test statistics conducted to determine the best fitting climatic factors for use in the Quantitative Empirical Model

Statistical Data	Values			
	Partial F-test Option N0.1	Partial F-test Option N0.2	Partial F-test Option N0.3	Partial F-test Option N0.4
F-statistic	275.01	340.67	452.44	1.616
F-Critical	1.00	1.00	1.00	1.00
Calculated p-value	<0.0001	<0.0001	<0.0001	<0.0001
Threshold p-value	0.05	0.05	0.05	0.05

5.4.3 Task C.3: Two-tailed F-test Statistics Conducted to Determine the Best Fitting General Form Equation for use in the Quantitative Empirical Model

The Quantitative Empirical Model (the QE Model) was developed by incorporating a general form equation which represents changes in volumetric water contents as a nonlinear function of changes in climatic factors. The general form equations considered in the analysis include an exponential and sine functions. The sensitivity analyses were conducted to evaluate the better fitting function for use in the development of the model. The sensitivity analyses were conducted using Two-tailed F-test statistics, and were conducted using the following option:

- Two-tailed F-test Option A: Changes in volumetric water contents as a nonlinear function of changes in climatic factors predicted using a sine function was used for dataset No.1, and changes in volumetric water contents as a nonlinear function of changes in climatic factors predicted using an exponential function was used for dataset No.2.

The null hypothesis assumes that the sine function produces a better fitting model than the model developed using the exponential function. The alternative hypothesis assumes that the exponential function produces the better fitting QE Model. The analysis of the data presented in Table 5.7 shows that the F-Statistic is more than the F-Critical, and the calculated p-value is less than the threshold p-value. The data show that the null hypothesis should be rejected, and that the alternative hypothesis should be accepted. It is concluded that the exponential function produces the better fitting model and is incorporated into the QE Model.

Table 5.7: The summary of the Two-tailed F-test statistics conducted to determine the better fitting function for use in the Quantitative Empirical Model

Statistical Data	Values
	Two-tailed F-test Option A
F-Statistic	6.159
F-Critical	1.00
Calculated p-value	<0.0001
Threshold p-value	0.05

5.4.4 *Task C.4: Two-tailed F-test Statistics Conducted to Evaluate the Statistical Correlation and Statistical Significance between P_1 and X_1, P_2 and X_2, and P_3 and X_3.*

The Two-tailed F-test statistics was conducted to evaluate the statistical correlation and statistical significance between P_1 and X_1, P_2 and X_2, and P_3 and X_3. The relationships between P_1 and X_1, P_2 and X_2, and P_3 and X_3 are incorporated into the Quantitative Empirical Model (the QE Model) to account for the impact of the system dependent properties of subgrades on the water and heat transfer.

The Two-tailed F-test statistics was conducted using X_1 values as the dataset No.1 and P_1 values as the dataset No.2 for Test No.1, X_2 values as the dataset No.1 and P_2 values as the dataset No.2 for Test No.2, and X_3 values as the dataset No.1 and P_3 values as the dataset No.2 for Test No.3. The null hypothesis assumes that there is no statistical correlation, and no statistical significance between P_1 and X_1, P_2 and X_2, and P_3 and X_3. The alternative hypothesis assumes that there is statistical correlation, and statistical significance between P_1 and X_1, P_2 and X_2, and P_3 and X_3. A summary of the Two-tailed F-test statistics is presented in Table 5.8.

The analysis of the data presented in Table 5.8 indicates that the null hypothesis should be rejected for each of the three tests because the F-Statistic is more than the F-Critical in all of the three tests. Hence, for each of the three tests, the alternative hypothesis should be accepted because the calculated p-value is less than the Threshold p-value in all of the three tests. It is concluded that the relationships between P_1 and X_1, P_2 and X_2, and P_3 and X_3 have statistical correlations, and statistical significance.

X_1, X_2, and X_3 are incorporated into the QE Model to account for the impact of the site specific system dependent properties of subgrades and properties of liquid water and water vapour on the water and heat transfer within subgrades. The system dependent properties of subgrades which are accounted for in

X_1, X_2, and X_3 include the initial degree of saturation, and the residual and saturated hydraulic conductivity. The properties of liquid water and water vapour which are accounted for in X_1, X_2, and X_3 include the heat of vaporization, vapour pressure, specific heat capacity, thermal diffusivity and the density. X_1, X_2, and X_3 also account for the gravitational acceleration of the materials.

Table 5.8: The summary of the Two-tailed F-test statistics conducted to evaluate the statistical correlation and significance between P_1 and X_1, P_2 and X_2, and P_3 and X_3

Statistical Data	Values		
	Test No.1: P_1 and X_1	Test No.2: P_2 and X_2	Test No.3: P_3 and X_3
F-statistic	Positive Infinity	5.285E+06	Positive Infinity
F-Critical	4.026	4.026	4.026
Calculated p-value	<0.0001	<0.0001	<0.0001
Threshold p-value	0.05	0.05	0.05

5.4.5 Task C.5: Two-tailed F-test Conducted to Determine Accuracy of the Quantitative Empirical Model and EICM in Predicting In-situ Volumetric Water Contents for Calculating F_{env}

Two-tailed F-test statistics were conducted to evaluate the accuracy of the Quantitative Empirical Model (the QE Model) and EICM in predicting in-situ volumetric water contents. The volumetric water contents are predicted for use in calculating the composite environmental adjustment factor (F_{env}) and resilient moduli of subgrades for Site C and Site D.

Two-tailed F-test statistics were conducted using F_{env} values which were calculated using in-situ volumetric water contents predicted using EICM as the dataset No.1, and F_{env} values which were calculated using in-situ volumetric water contents predicted using the QE Model as the dataset No.2 for both sites. The null hypothesis assumes that EICM is more accurate than the QE Model in predicting in-situ volumetric water contents for use in calculating the F_{env} and resilient moduli of subgrades. The alternative hypothesis assumes that the QE Model is more accurate than EICM in predicting in-situ volumetric water contents for use in calculating the F_{env} and resilient moduli of subgrades. A summary of Two-tailed F-tests statistics is presented in Table 5.9.

The analysis of the data presented in Table 5.9 shows that the null hypothesis should be rejected for both tests because the F-Statistic is more than the F-Critical. The alternative hypothesis should be accepted for both tests because the calculated p-value is less than the Threshold p-value. It is concluded that the QE Model is more accurate than EICM in predicting the in-situ volumetric water contents for use in calculating the F_{env} and resilient moduli of subgrades.

Table 5.9: The summary of Two-tailed F-test statistics conducted to evaluate use of the Quantitative Empirical Model and EICM in predicting in-situ volumetric water contents for calculating F_{env}

Statistical Data	Values	
	Site C	Site D
F-statistic	252.36	1136.38
F-Critical	39.50	8.26
Calculated p-value	0.008	<0.0001
Threshold p-value	0.05	0.05

5.5 Development of P_1, P_2 and P_3 Values Incorporated into the General Form of the Equation for the Quantitative Empirical Model

The general form of the equation for the Quantitative Empirical Model (the QE Model) was developed using nonlinear regression between changes in volumetric water contents within the subgrades (the dependent variable) and changes in climatic factors (the independent variable). The data was fitted using nonlinear regression based on an exponential function, a sine function and a power function. The nonlinear regression analyses resulted in a QE Model which incorporates changes in volumetric water contents within subgrades as a nonlinear function of changes in climatic factors.

XLSTAT uses the Levenberg-Marquardt method (the damp least-squares method) for calculating nonlinear regression parameters of nonlinear functions. The function parameters form part of the nonlinear regression analysis and is based on the chi-square error criteria presented in Eq. 5.10. The damp least-squares method is a curve-fitting approach which integrates the gradient decent and the Gauss-Newton method. In the gradient decent method, the sum of the square errors is reduced while the function parameters decrease in the direction with the highest rate of change and are subsequently updated. In the Gauss-Newton method, it is assumed that the sum of the square errors is based on a quadratic equation and subsequently determining the minimum output of the quadratic equation.

Nonlinear relationships between the dependent and independent variables were represented using an exponential function. Functions representing changes in the dependent variable was fitted based on the relationships between data points of the independent variable and model parameters (*P*) which is represented by $\Delta\theta(\Delta A, P)$. The methodology includes determining the differences between changes in the dependent variable as a function of changes in the independent variable $\{\Delta\theta(\Delta A)\}$, and changes in the dependent variable as a function of changes in the independent variable and *P* which is represented by $\{\Delta\theta(\Delta A, P)\}$. The function represented by $\Delta\theta(\Delta A, P)$ represents the fitting function for the dependent variable. The sum of the squares of the errors between $\{\Delta\theta(\Delta A)\}$ and $\{\Delta\theta(\Delta A, P)\}$ were minimized using Eq. 5.10. Because the function $\Delta\theta(\Delta A, P)$ and *P* values are nonlinear, the minimization of the sum of the square errors with respect to P values were conducted through an iterative process aimed at producing a reduction in the sum of the square errors. The iteration process was conducted until the sum of the square errors was at the optimal value on the basis that optimal P values were achieved. The damp least squares method calculates varying values of the damping parameter which is updated after each iteration. The solution of the function parameters are improved as the damping parameter is reduced (Gavin 2022, Lourakis 2005; Marquardt 1965).

$$x(P)^2 = \sum_{i=1}^{n} \left(\frac{\Delta\theta\,(\Delta A) - \Delta\theta\,(\Delta A,\ P)}{\omega_{\Delta\theta i}} \right)^2 \qquad (5.10)$$

$\Delta\theta(\Delta A)$ = Changes in the dependent variable as a function of changes in the independent variable, $\Delta\theta(\Delta A, P)$ = Changes in the dependent variable as a function of changes in the independent variable and P values, P values = Nonlinear regression parameters, and $\omega_{\Delta\theta I}$ = The error determined at each data point for the function $\Delta\theta\,(\Delta A)$.

5.6 Summary

The statistical analyses presented in Chapter 5 are used for calibrating and verifying the 2-D finite element analysis (2-D FEA) water and heat transfer models which are presented in Chapter 4. The statistical analyses are also used for verifying the suitability of climatic factors and the exponential function used for the development of the Quantitative Empirical Model (QE Model) presented in Chapter 6. The statistical analyses are also used for verifying the QE Model and EICM.

The statistical analyses presented in Chapter 5 confirm that the 2-D FEA water and heat transfer models, and the QE Model are verified within acceptable limits. The statistical analyses also show that the volumetric water contents predicted using the QE Model are more suitable for calculating the unfrozen composite environmental adjustment factor (F_{env}) and resilient moduli of subgrades than the volumetric water contents predicted using EICM.

The data used for conducting the statistical analyses were also used for conducting the graphical verification and evaluation of the accuracy of the QE Model and EICM which are presented in Chapter 7.

Chapter 6 Development of the Quantitative Empirical Model

6.1 Introduction

Chapter 6 provides an overview of inter-relationships between climatic factors, and between climatic factors and in-situ volumetric water contents within subgrades. Chapter 6 also presents the methodology for developing the Quantitative Empirical Model (the QE Model) for predicting the influence of changes in climatic factors on changes in in-situ water and heat transfer within subgrades. The Chapter includes background on the hydrological cycle and the most pertinent climatic processes that influence changes in in-situ water and heat transfer within subgrades. The Chapter also provides background on climatic factors and land climate interaction. The Chapter also provides background on nonlinear regression and its application in the development of models used for predicting the influence of climatic factors on in-situ water and heat transfer within subgrades.

Chapter 6 provides a detailed methodology for developing the QE Model including the method used to formulate the most pertinent climatic factors incorporated into the model. The Chapter also includes details of the nonlinear regression analysis used to evaluate the statistical relationship between volumetric water contents within subgrades and climatic factors. The Chapter also provides details of the method used for developing and selecting the general form of the equation used in the formulation of the QE Model. Chapter 6 also provides details of the mathematical formulations including the integration used in the development of the QE Model. The Chapter also provides details of the method used to incorporate the system dependent properties of subgrades into *f-functions* which are incorporated into the QE Model. Chapter 6 also provides a summary of the QE Model and the model's input parameters.

Chapter 6 also provides details of the application of the QE Model in the engineering practice. The Chapter also provides details of the modified composite environmental adjustment factor (the F_{envCF} model) which was developed for incorporating the impact of climatic factors into resilient moduli and performance evaluation of subgrades. The Chapter also provides details of the modified resilient modulus of the subgrade (M_{RCF}) which was developed to account for the impact of climatic factors on the pavement performance.

6.2 Interrelationships between Climatic Factors and Land-Pavement-Climate Interaction

Climatic processes consist of many components which are integrated through physical, chemical and biological interactions in the atmosphere and aquatic environments. The atmospheric and aquatic environment interactions influence heat and water vapour transfer through evaporation which forms part of the hydrological cycle (the atmosphere-land interaction). The atmosphere-land interaction influences evaporation, condensation, cloud formation, precipitation, and runoff. Air temperature and precipitation are fundamental components of climatic processes (IPCC 2001).

Changes in air temperature directly influence the extent of precipitation. These changes in precipitation are associated with the influence of changes in air temperature on changes in evaporation (IPCC 2013). This indicates that precipitation is associated with air temperature. Changes in air temperature are influenced by changes in solar radiation, while solar radiation is associated with the daily air temperature range (Wang, and Dickinson 2013). An increase in solar radiation and associated increase in air temperature induce a reduction in the relative humidity. The reduction in relative humidity is associated with a decrease in water contents within subgrades (Shrestha, et al. 2019). Changes in wind speed influence the circulation of heat in the atmosphere and at the surface of aquatic environments, and impact land climate interaction (LCI). Changes in air temperature and wind speed influence evaporation at the surface of aquatic environments, evapotranspiration and water vapour transfer at ground surfaces. These inter-relationships show that evapotranspiration is associated with air temperature and wind speed. Studies show that each climatic factor may not exist independently and that climatic factors influence water and heat transfer (Liuzzo, et al. 2016; Kousari, and Ahani 2012; Dinpashoh, et al. 2011). The characteristics of plant species also impact the water and heat transfer within subgrades through evapotranspiration. The water and heat transfer within subgrades is influenced by the leaf area index (LAI). The LAI impacts evaporation and transpiration which are influenced by the extent of ground coverage provided by leaves and the canopy (Dong, et al. 2021; Ramirez-Garcia, et al. 2012; Mullan and Reynolds 2010; Anapalli, et al. 2005). The water and heat transfer is also influenced by the root characteristics (which impact water uptake and transpiration) (Thorup-Kristensen, et al. 2009; Evans, et al. 1996). These observations form the basis for climatic factors and their interaction which are incorporated into the development of the QE Model.

LCI consists of continuous transfer of heat, liquid water and water vapour between the land surface and atmosphere which impacts the hydrological cycle and environmental conditions. LCI occurs through conduction, convection, evapotranspiration and through longwave radiation from the ground surface. During daytime hours, heat transfer occurs from the warmer ground surface to the lower atmosphere. During nighttime hours, heat transfer occurs from the warmer atmosphere to the ground surface (Schmidli, and Rotunno 2010; Memon, et al. 2008).

Infiltration is primarily influenced by precipitation and is impacted by the rainfall intensity. Infiltration typically decreases with an increase in the rainfall intensity (Xue, and Gavin 2007). In addition, the rate of infiltration increases with an increase in air temperature and the associated increase in the temperature profile within subgrades (Liu, et al. 2021; Braga, et al. 2007; Lin, et al. 2003; Viessman, and Lewis 2003; Dempsey 1970). This also implies that the hydraulic conductivity and infiltration within subgrades decrease during freezing (Liu, et al. 2021; Williams, and Smith 1989). During ponding, the rate of infiltration is system dependent and is dependent on the soil texture and hydraulic properties (Bulut, and Javid 2019; Lazarovitch, et al. 2005; Franke, et al. 1987). An increase in the rate of evapotranspiration is caused by an increase in air temperature and facilitate water vapour transfer from the ground surface to the atmosphere. The evapotranspiration is assessed as a negative flux which impacts the net infiltration (Viessman, and Lewis 2003).

The influence of pavement-climate interaction on water and heat transfer within pavement structures is shown in Figure 6.1a. Pavement structures are typically constructed on soil-embankments which are impacted by climatic factors due to their exposure to the environment. Changes in climatic factors cause changes in the net infiltration and heat transfer within the pavement structure embankment. Changes in the net infiltration and heat transfer induce changes in volumetric water contents and temperature profile within the pavement structure (Herb, et al 2006; McCartney, et al. 2010). The water and heat transfer within the pavement structure is influenced by the seasonal variations in precipitation and the temperature profile within pavement structure (McCartney, et al. 2010). The analysis of data shown in Figure 6.1b indicates that during the dry season, water contents within the pavement structure are at their lowest at the surface and increase with depth to a depth corresponding to the depth of water change or the bottom of the active zone (H_s). This observation indicates that during the dry season, water contents within pavement structures are primarily influenced by the elevation of the water table. During the wet season, water contents within pavement structures are at their highest at the surface and decrease with depth to a depth corresponding to H_s. This observation indicates that during the wet season, water contents within pavement structures which are located in the active zone are influenced primarily by climatic factors. For both the dry and wet seasons, water contents increase from the depth corresponding to H_s to the top of the capillary fringe zone. The water content generally remains constant from the top of the capillary fringe zone to the water table (Heitor, et al 2021). These climatic processes result in changes in the strength and stability of the soil-embankment and subgrade supporting the pavement structure (Heitor, et al 2021; Herb, et al 2006; McCartney, et al. 2010).

The impact of climatic factors on water and heat transfer within pavement structures may be simulated by incorporating changes in site-specific precipitation, air temperature, relative humidity, net solar radiation and wind speed (the climatic factors) (Pk, et al. 2021; Heitor, et al. 2021; Tang, et al. 2017; Schmidli, and Rotunno 2010; Memon, et al. 2008; Braga, et al. 2007; Herb, et al. 2006; Lin, et al. 2003; Viessman, and Lewis 2003). Studies have shown that climatic factors and their interactions influence fluctuations in in-situ volumetric water contents of subgrades. Volumetric water contents of subgrades increase in response to an increase in precipitation, while an increase in air temperature results in a corresponding decrease in volumetric water contents of subgrades due to evapotranspiration (Farhat 2018;

Stéfanon, et al. 2014; Wohl, et al. 2012; Suseela, et al. 2012; Lofgren, et al., 2011; Holsten, et al. 2009; Wang, et al., 2008; Allen, et al. 1998). The rate of evapotranspiration is also impacted by net solar radiation, air temperature and relative humidity. The rate of evapotranspiration decreases in response to an increase in the relative humidity (Farhat 2018).

An increase in wind speeds results in an increase in air circulation and convective cooling resulting in a corresponding increase in evapotranspiration (Bryce, et al. 2021). These observations indicate that precipitation, air temperature, net solar radiation, relative humidity, and wind speed should be incorporated in the formulation of models used for simulating interrelationships between and the impact of climatic factors on water and heat transfer within subgrades (Farhat 2018; Stéfanon, et al. 2014; Wohl, et al. 2012; Suseela, et al. 2012; Lofgren, et al., 2011; Holsten, et al. 2009; Wang, et al., 2008; Allen, et al. 1998). The inter-relationships between climatic factors and their influence on the LCI form the basis for formulating and incorporating climatic factors into the QE Model.

The evaluation of the physical processes which govern the impact of climatic factors on water and heat transfer within subgrades requires an understanding of the influence of the principles of geotechnical and transportation engineering, physics, and climatology on pavement performance. The transient water and heat transfer processes within pavement structures are presented in Figure 6.1c (McCartney, et al. 2010). The analysis of data presented in Figure 6.1c shows that the water and heat transfer within pavement structures is influenced by liquid water transfer due to precipitation induced infiltration (through surface cracks, vegetation and bare ground) and capillary rise. The data also show that the water and heat transfer is influenced by liquid water diffusion, net solar radiation, water vapour transfer, heat transfer through diffusion, and convective cooling due to increased wind speed.

The water transfer processes which are accounted for in EICM include liquid water transfer due to capillary rise (the primary water transfer process accounted for in EICM) and minimal precipitation induced infiltration through surface cracks. EICM neglects water vapour transfer, liquid water diffusion and precipitation induced infiltration through vegetation and bare ground (McCartney, et al. 2010; Zapata, and Houston 2008; Zapata, et al. 2007; Drumm, and Meier 2003).

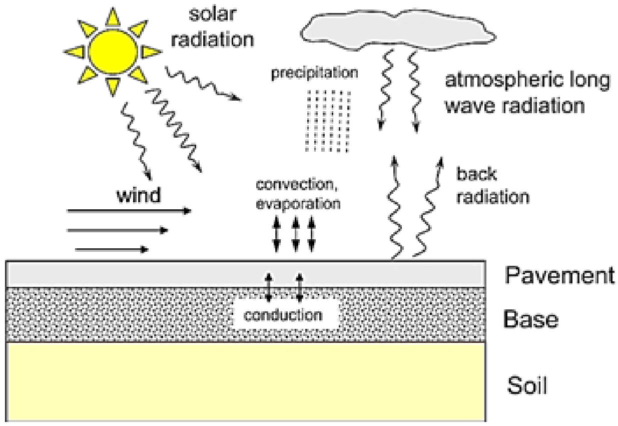

(a) Pavement-climate interaction

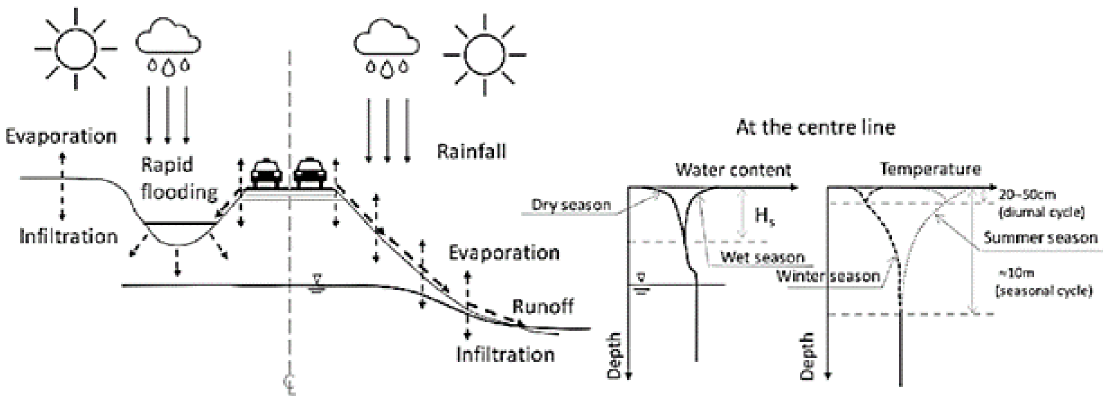

(b) Land-climate interaction

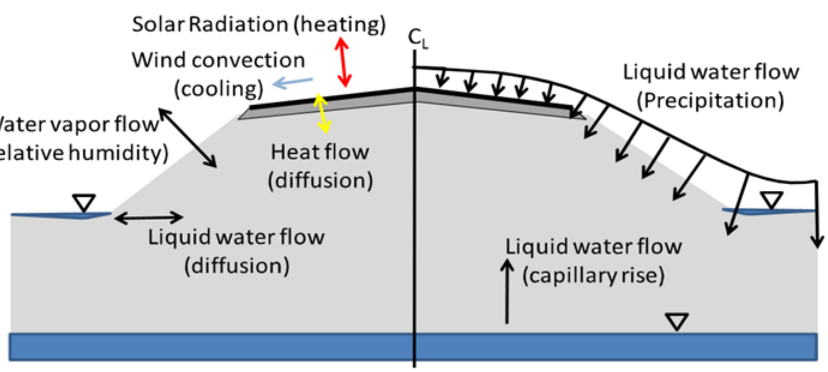

(c) Transient water and heat transfer processes within pavement structures

Figure 6.1: Influence of land-pavement-climate interaction on water and heat transfer within pavement structures (a) (Herb, et al 2006); (b) (Heitor, et al 2021); (c) (McCartney, et al. 2010)

6.3 Development of the Quantitative Empirical Model: General Form Exponential Function

The development of the Quantitative Empirical Model (the QE Model) consisted of eight primary tasks. These tasks were conducted for 1) formulating the mathematical framework for the QE Model, 2) developing and evaluating climatic factors which are incorporated into the QE Model, 3) developing the general form equation for the QE Model, 4) conducting nonlinear regression between changes in climatic factors and changes in volumetric water contents within subgrades and analyzing regression parameters from the general form exponential equation, 5) incorporating the system dependent properties into function parameters, 6) formulating *f-functions* which are incorporated into the QE Model, 7) incorporating the integral functions into the QE Model, and 8) verifying the accuracy of the computation of the integral functions. The development of the QE Model consists of mathematical computations including integration of the general form equation, and analyses of regression parameters. Mathematical computations are also conducted to incorporate the thermal properties and density of liquid water and water vapour, and hydraulic properties of subgrades and wearing courses into the resulting functions and formulating *f-functions*.

Nonlinear regression analyses were used to develop empirical correlations between changes in volumetric water contents and changes in climatic factors to account for the influence of changes in climatic factors on water and heat transfer. The use of nonlinear regression between changes in volumetric water contents and changes in climatic factors mitigates inaccuracies in the analytical methods used for predicting in-situ water and heat transfer in the current EICM. These inaccuracies are due to the current EICM inaccurately accounting for the impact of climatic factors, the surface mass balance and LCI boundary conditions (Drumm, and Meier 2003). The use of nonlinear regression between changes in volumetric water contents and changes in climatic factors forms the basis of the development of the QE Model.

6.3.1 Task 1: Formulating the Mathematical Framework for the Quantitative Empirical Model

The mathematical computations conducted for the development of the Quantitative Empirical Model (the QE Model) are based on the mathematical framework presented in Figure 6.2. Figure 6.2 represents fluctuations in changes in in-situ volumetric water contents within subgrades over time due to changes in climatic factors. Eq. 6.1 represents the total in-situ volumetric water content at the end of time "*n*". The total in-situ volumetric water content at the end of time "*n*" comprises of the initial in-situ volumetric water content at the end of construction and the accumulation of all changes in in-situ volumetric water contents at the end of time "*n*". The accumulation of all changes in in-situ volumetric water contents at the end of time "*n*" is represented by the function shown in Eq. 6.2.

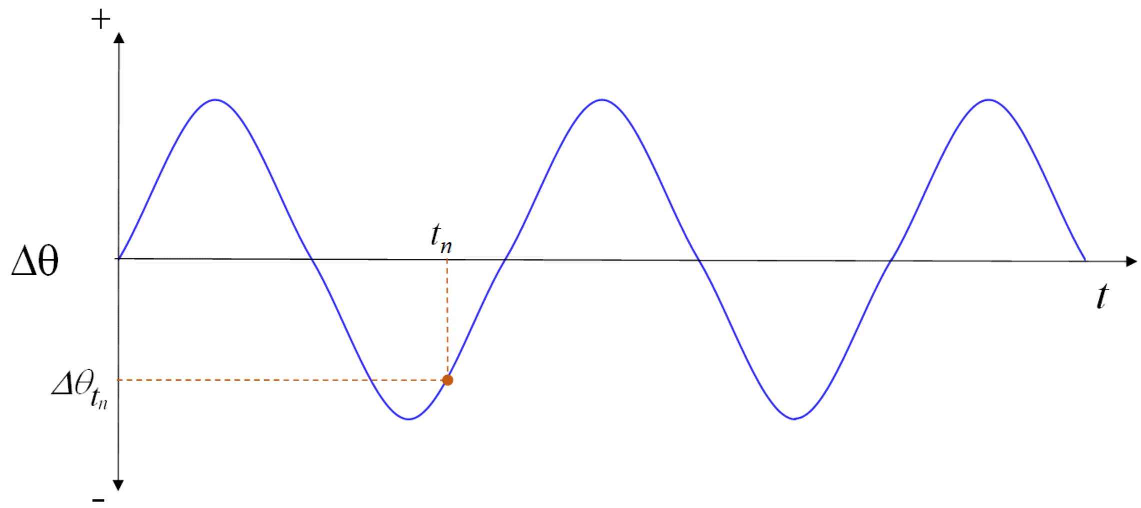

Figure 6.2: Representation of the governing equation for the Quantitative Empirical Model.

$$\theta_{tn} = \theta_{t0} + \Delta\theta_{tn} \qquad (6.1)$$

$$\Delta\theta_{tn} = \int_0^{tn} \Delta\theta\,(\Delta A)\; dt \qquad (6.2)$$

θ_{tn} = The total in-situ volumetric water content at the end of time "*n*"; θ_{to} = The initial in-situ volumetric water content at the end of construction (at time = 0); $\Delta\theta_{tn}$ = The accumulation of all changes in in-situ volumetric water contents at the end of time "*n*"; ΔA = Change in climatic factors which is presented in Eq. 6.3.

6.3.2 Task 2: The Analyses Conducted for Developing and Evaluating Climatic Factors

The development of climatic factors is based on the analysis of inter-relationships between changes in climatic factors conducted in Section 4.5.2, Section 4.5.3, Section 5.4.2, and the analysis of findings of previous studies. These relationships indicate that both the strong and weak interrelationships between climatic factors should be incorporated into models developed to simulate the impact of climatic factors on the water and heat transfer within subgrades (Pk, et al. 2021; Heitor, et al. 2021; Shrestha, et al. 2019; Farhat 2018; Liuzzo, et al. 2016; IPCC 2013; Wang, and Dickinson 2013; Kousari, and Ahani 2012; Dinpashoh, et al. 2011; Herb, et al 2006; IPCC 2001).

The Quantitative Empirical Model (the QE Model) is developed by incorporating the influence of changes in climatic factors on changes in volumetric water contents within fine-grained subgrades in wet freeze climates. Changes in climatic factors which are incorporated into the QE Model include changes in precipitation, air temperature, net solar radiation, wind speed, relative humidity, evapotranspiration, and water vapour transfer through the wearing course to the atmosphere. The influence of changes in climatic factors on changes in in-situ volumetric water contents within subgrades is incorporated into the QE Model by conducting nonlinear regression between changes in climatic factors and changes in volumetric water contents within subgrades.

A nonlinear regression analysis was conducted between changes in in-situ volumetric water contents (the dependent variable) and changes in climatic factors (the independent variable) using an exponential function. This nonlinear regression analysis was conducted to develop a function which represents changes in in-situ volumetric water contents as a nonlinear function of changes in climatic factors to support the statistical analyses presented in Section 5.4.2. The statistical analyses presented in Section 5.4.2 were conducted to determine the climatic factors that produce the best fitting model. The initial nonlinear regression was conducted between changes in climatic factors and changes in in-situ volumetric water contents within subgrades recorded from 1993 to 1997. The 1993 to 1997 in-situ volumetric water contents datasets were limited and discontinuous and did not facilitate accurate nonlinear regression. A more representative nonlinear regression analysis was conducted between changes in climatic factors and changes in volumetric water contents within subgrades obtained from the 2-D FEA modeling output. The 2-D FEA modeling was conducted for a 38-year analysis period for depths to the static water table of 1.65 m, 2.65 m, 10.65 m, 15.65 m and 25.65 m below the subgrade surface (the analysis Case No.1 to Case No.5). The climatic data used in the formulation of climatic factors (which were used to conduct the nonlinear regression) were obtained from field measurements with the exception of the evapotranspiration and evaporation through the wearing course to the atmosphere which were obtained from 1-D FEA modeling output.

Changes in climatic factors and in volumetric water contents are referenced from climatic factors and the volumetric water content measured on the construction completion date. The volumetric water content and climatic factors measured on the construction completion date are used as reference points because the QE Model is formulated by incorporating the absolute in-situ volumetric water content measured at the end of construction. The absolute volumetric water content within the subgrade for each day is calculated by adding the change in the in-situ volumetric water content on that day to the absolute in-situ volumetric water content that was measured on the day that the construction of the pavement structure was completed. The statistical analyses presented in Section 5.4.1 indicate that using values for the dependent and independent variables which were measured on the construction completion date as reference points for calculating changes in the dependent and independent variables produced the better fitting model.

The analysis of Eq. 6.3 shows a poor statistical relationship between changes in climatic factors and changes in volumetric water contents when the change in any climatic factor or the change in volumetric water content is zero. This limitation is mitigated by applying a factor to each component of the climatic factors. These factors are also applied to facilitate the best solution for the formulated climatic factors when the change in any climatic factor is zero. These factors were adjusted until the nonlinear regression between changes in climatic factors and changes in volumetric water contents produced the best fitting statistical relationship between changes in climatic factors and changes in volumetric water contents. The analyses of data presented in Chapter 4 and Eq. 6.3 indicated that the formulated climatic factors should account for cases when the change in wind speed is zero. The limitations observed when the change in wind speed is zero is mitigated by incorporating a factor of 0.05 to the change in wind speed. Similarly, limitations observed when the change in net solar radiation and the change in air temperature are both zero, are mitigated by applying a factor of 0.05 to both the change in net solar radiation and the change in air temperature. A factor of 1.2 is also applied to the change in relative humidity to mitigate limitations observed when the change in relative humidity is zero. A factor of 3.5 is applied to the difference between the change in precipitation and the change in evapotranspiration to mitigate limitations observed when the change in either variable is zero. The factor of 3.5 is also applied to the difference between the change in precipitation and the change in water vapour transfer through the wearing courses to the atmosphere.

The analysis of data presented in Section 5.4.2 shows that incorporating the complete dataset of climatic factors into the model produces a better fitting model relative to the fit of the model obtained by incorporating reduced climatic factors. The reduced climatic factors are obtained by conducting sensitivity analyses which include excluding only precipitation, excluding only net solar radiation, excluding only relative humidity, and including only air temperature in developing the climatic factors. The formulated equation for the complete dataset of climatic factors is presented in Eq. 6.3. Eq. 6.3 is incorporated into the development of the QE Model. Incorporating Eq. 6.3 into the QE Model results in the model accounting for the following relationships:

- The positive relationship between air temperature and evapotranspiration;
- The positive relationship between wind speed and evapotranspiration;
- The negative relationship between air temperature and relative humidity;
- The negative relationship between relative humidity and evapotranspiration; and
- The negative relationship between wind speed and relative humidity.

$$\Delta A = \left\{ \left(\frac{(0.05+\Delta R_s) * (0.05+\Delta T_{Air}) * (0.05+\Delta V_w)}{(1.2 + \Delta RH)} \right) * \left(3.5^{(\Delta Precp - \Delta ET - \Delta E_{Wa})} \right) \right\} \qquad (6.3)$$

ΔA = Change in climatic factors (MJ °C / (s^2 day)); ΔT_{Air} = Change in air temperatures (°C); ΔR_s = Change in net solar radiation (MJ / (s m^2)); *ΔRH* = Change in relative humidity (decimal); ΔV_w,= Change in wind speed (m / s); *ΔPrecp* = Change in precipitation (m / day); *ΔET* = Change in evapotranspiration (m^3 / (day m^2)); ΔE_{wa} =Change in evaporation through wearing course to atmosphere (m^3 / (day $m^{2)}$)).

It is assumed that the best fitting equation for ΔA as a function of time {ΔA (time)} may be represented by the exponential function shown in Eq. 6.4. The graphical representation of ΔA vs time for Site A (in Nebraska) is presented in Figure 6.3. A sine function was not used to represent ΔA (time) because the sine function is periodic in predicting changes in in-situ volumetric water contents (the sine function produces the same minimum and maximum volumetric water contents in every seasonal cycle) which does not represent the actual fluctuations in the measured in-situ minimum and maximum seasonal volumetric water contents.

$$\Delta A\ (t) = \left[P_q * e^{\{-P_r * \{t\}\}}\right] + P_s \qquad (6.4)$$

ΔA = Change in climatic factors (MJ °C / (s^2 day)); t = Time in day; P_q, P_r, and P_s = The site-specific ΔA (time) function parameters.

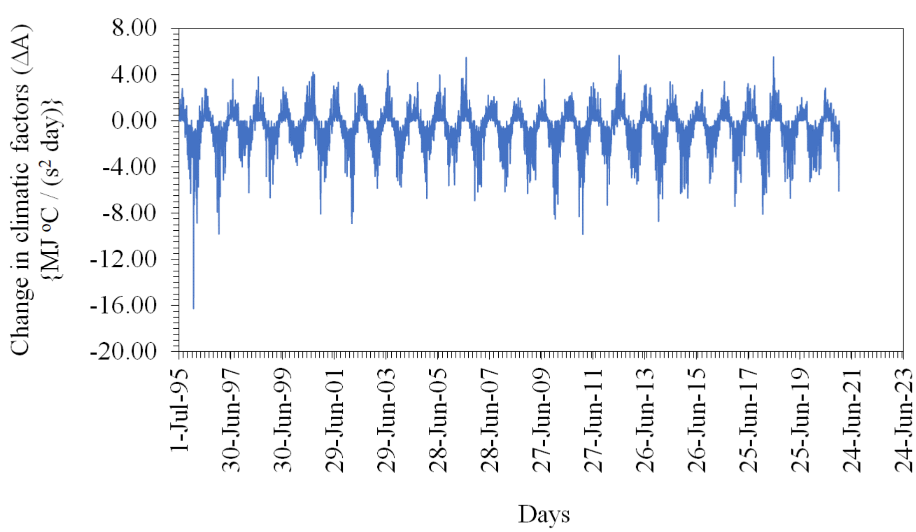

Figure 6.3: The graphicial representation of ΔA vs time

The analyses of data presented in Figure 6.4 (for Site A) represent the output of a model developed to account for changes in volumetric water contents as a nonlinear function of changes in a reduced climatic factor consisting of only changes in air temperature. The analyses of data presented in Figure 6.4 show that positive changes in air temperatures result in both negative and positive changes in in-situ volumetric water contents. Negative changes in air temperatures result in both positive and negative changes in in-situ volumetric water contents. These observations imply that during high summer temperatures, a positive change in the air temperature results in a negative change in the in-situ volumetric water content due to evaporation. During freezing conditions, a positive change in the air temperature results in an increase in the in-situ volumetric water content due to thawing. Figure 6.4 also shows that a change in air temperature of less than -35.0 ^{o}C from the initial condition has minimal impact on changes in in-situ volumetric water contents.

The analyses of data presented in Figure 6.5 (for Site A) represent the output of a model developed to account for changes in volumetric water contents as a nonlinear function of changes in a reduced climatic factor consisting of only changes in precipitation. The analyses of data presented in Figure 6.5 show that large positive changes in precipitation are associated with large negative changes in in-situ volumetric water contents. The data also show that minimal changes in precipitation are associated with large positive changes in in-situ volumetric water contents. These observations imply that high rainfall intensity events are associated with decreased net infiltration and lower in-situ volumetric water contents. The data also show that low rainfall intensity events over time are associated with increased net infiltration and higher in-situ volumetric water contents. The data presented in Figure 6.5 also show positive changes in in-situ volumetric water contents due to negative changes in precipitation. This observation implies that volumetric water contents within subgrades increase when the rainfall intensity decreases. The data in Figure 6.5 also show that the highest increase in changes in in-situ volumetric water contents are associated with periods with little to no change in precipitation. This observation implies that rainfall events with minimal to no change in intensity over time result in the highest increase in in-situ volumetric water contents.

The data presented in Figure 6.4 and Figure 6.5 show that the impact of changes in precipitation on water contents within subgrades is minimal compared to the impact of changes in air temperatures. Despite this observation, both air temperature and precipitation should be incorporated into models which are used for predicting water and heat transfer within subgrades. The precipitation should be included because it is the primary source of the water which infiltrates pavement structures. The precipitation is also the primary source of the water which facilitates phase changes from liquid water to water vapour (through evaporation) and from water vapour to liquid water (through condensation) due to temperature gradients.

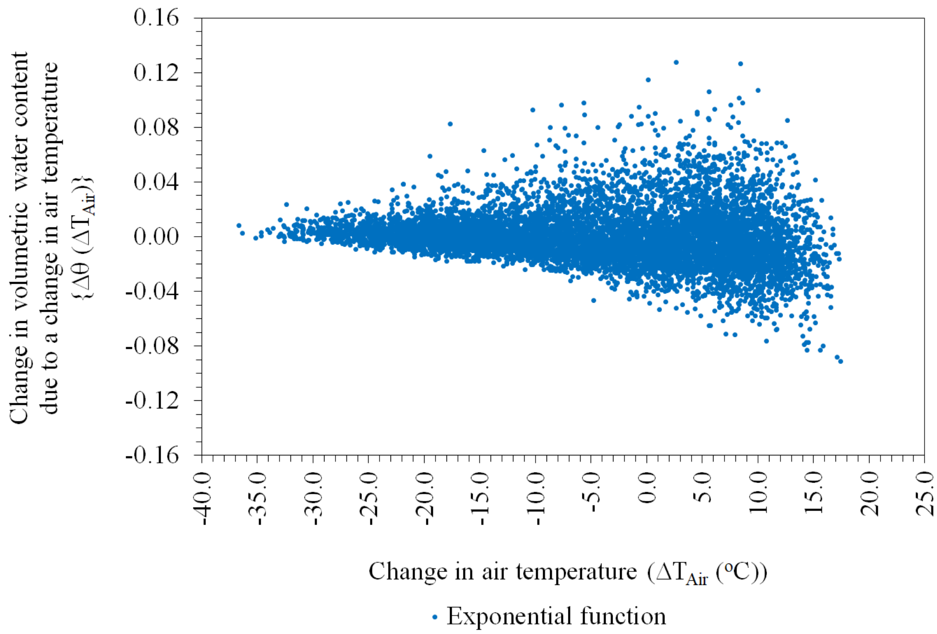

(a)

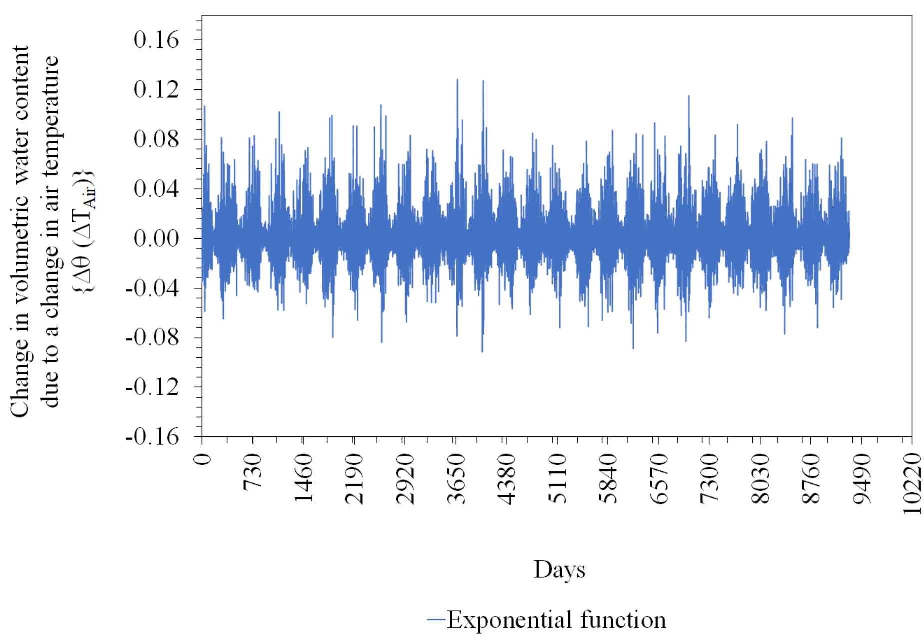

(b)

Figure 6.4: Changes in in-situ volumetric water contents as a function of changes in air temperatures

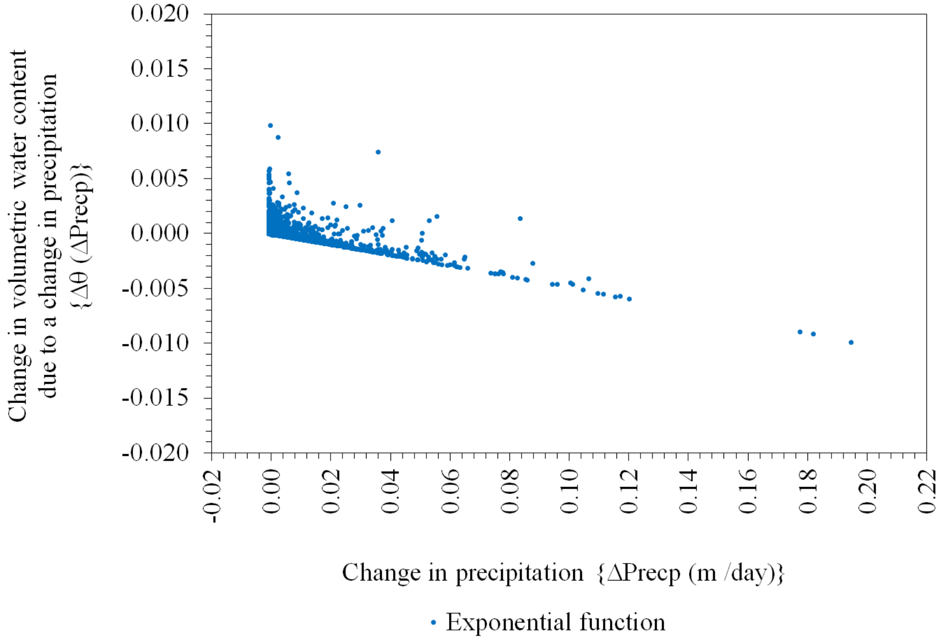

(a)

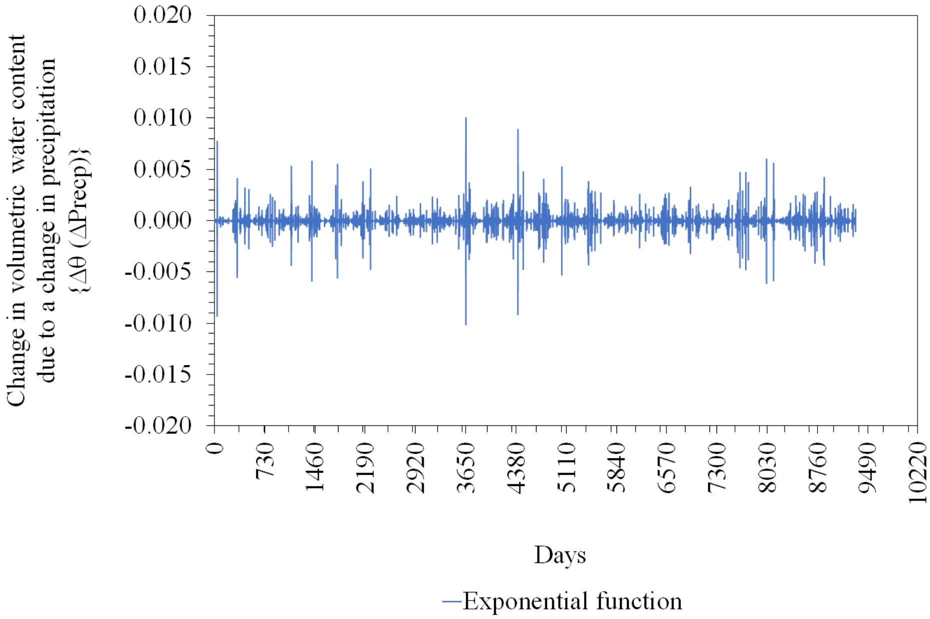

(b)

Figure 6.5: Changes in in-situ volumetric water contents as a function of changes in precipitation

The analyses of data presented in Figure 6.6 (for Site A) represent the output of a model developed to account for changes in volumetric water contents as a nonlinear function of changes in a reduced climatic factor consisting of only changes in net evapotranspiration. The analyses of data presented in Figure 6.6 show that the QE Model accounts for both condensation and evapotranspiration. The data also show that the net evapotranspiration causes minimal changes in volumetric water contents within fine-grained subgrades. This observation implies that the water transfer within fine-grained subgrades occurs primarily through internal circulation of the water vapour (induced by a phase change from liquid water to water vapour) and through condensation (due to a phase change from water vapour to liquid water). The net evapotranspiration has minimal impact on volumetric water contents within the fine-grained subgrade at Site A because the top of the subgrade is located at 775.0 mm below the surface of the wearing course. The subgrade is also located at a significant distance from vegetated areas with the exception of minimal vegetation in the adjacent median and ditches. Hence, the root water uptake of the vegetation and the associated transpiration have minimal impact on in-situ volumetric water contents within fine-grained subgrades.

The analyses of data presented in Figure 6.6b show that volumetric water contents within subgrades decrease with increased evapotranspiration. The data also show that volumetric water contents within subgrades increase with increased condensation. A change in the net evapotranspiration of less than -1.0 x 10^6 mm^3 /(mm^2 day) has no impact on changes in volumetric water contents within fine-grained subgrades. This implies that increased evapotranspiration beyond a value of -1.0 x 10^6 mm^3 /(mm^2 day) have no impact of the residual water content within subgrades.

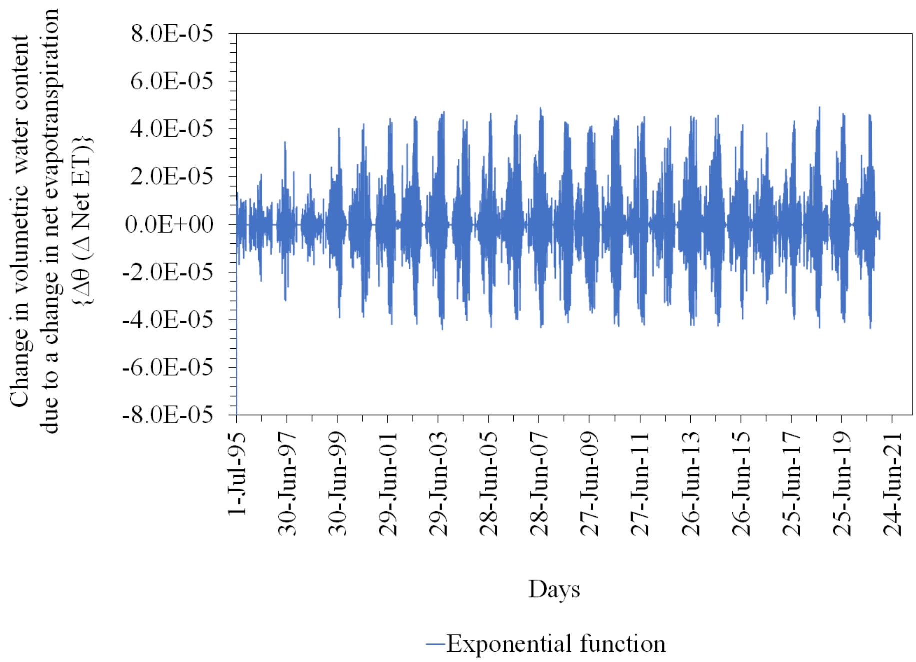

(a)

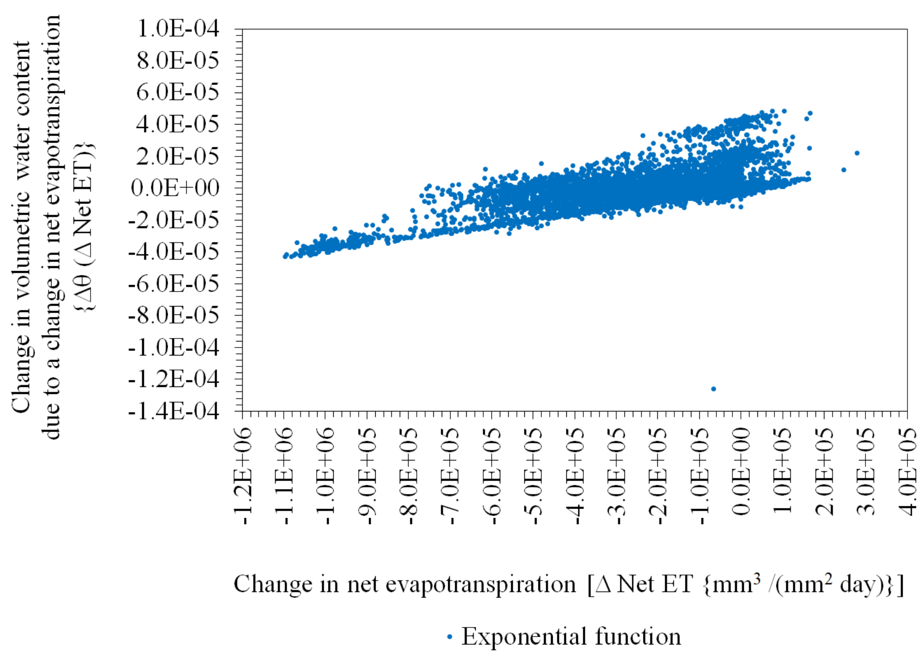

(b)

Figure 6.6: Changes in in-situ volumetric water contents as a function of changes in net evapotranspiration

The Significance of the Various Factors Incorporated into the Changes in Climatic Factors (ΔA) Function

Changes in climatic factors (ΔA) function incorporates various factors which include a factors of 0.05 which is added to ΔR_s, ΔT_{Air} and ΔV_w, 1.2 which is added to ΔRH and 3.5 which is applied to $\Delta Precp - \Delta ET$. These factors are incorporated in the ΔA function to facilitate a solution when either ΔR_s, ΔT_{Air}, ΔV_w, ΔRH and $\Delta Precp - \Delta ET$ is zero. The factors used were chosen based on those which produce the best fitting Quantitative Empirical Model (the QE Model).

Changes in each climatic factor which is incorporated into ΔA are referenced from the end of construction (time zero). Hence, if a pavement structure were constructed on the 1st of August 2022 when the subgrade temperature was 25.0 ^oC, this subgrade would be assigned an initial temperature of 25.0 ^oC at time zero (the initial subgrade temperature). Assuming that the lowest subgrade temperature during the first winter season (during freezing) after construction was -10.0 ^oC, the post construction change in temperature (ΔT_{Air}) at that time would be -35.0 ^oC. It is also assumed that changes in the subgrade temperature typically fluctuate during the winter season. It is also assumed that during the subsequent summer season the subgrade temperature may be 26.0 ^oC which equates to a ΔT_{Air} of +1.0 ^oC at that time. The subgrade temperature during the first summer after construction may also be the same as the initial subgrade temperature of 25.0 ^oC which equates to a ΔT_{Air} of 0.0 ^oC at tat time.

The change in temperature of -35.0 ^oC from the initial subgrade temperature during the first freezing period causes significant decrease in the subgrade water content. Further freezing temperatures cause further reduction in the unfrozen water contents within the subgrade. The freezing condition causes fissures/cracking which facilitates further paths for infiltration and the advancement of the wetting front. A subsequent subgrade temperature of 26 ^oC (ΔT_{Air} = +1.0 ^oC) or 25.0 ^oC (ΔT_{Air} = 0.0 ^oC) causes post winter thawing which significantly increase water contents of the subgrade. The increase in water contents within subgrades (due to thawing) cause decreased resilient moduli of subgrades. This implies that a change of zero in any climatic factor has significant impact on the solution of the ΔA function and on the solution of the QE Model. These observations show the significance of incorporating the various factors into the ΔA function to provide a solution of the ΔA function and a solution of the QE Model when either ΔR_s, ΔT_{Air}, ΔV_w, ΔRH and $\Delta Precp - \Delta ET$ is zero.

The continual seasonal fluctuations of ΔA, induce freeze and thaw cycles within subgrades which directly impact the water and heat transfer within subgrades. One freeze and thaw cycle causes a change of approximately 20.0 % to 60.0 % reduction in resilient moduli of subgrades. The resilient modulus of the subgrade decreases further as the number of the freeze and thaw cycles increase (Wang, et al. 2007; Simonsen, et al. 2002; Lee, et al. 1995; Fredlund, et al. 1975). Hence, fluctuations in ΔA (observed in the plot of ΔA vs time presented in Figure 6.3) have a significant impact of the freeze and thaw cycles, water contents and resilient moduli of subgrades. The values of ΔA impact the output of the QE Model (volumetric water contents as a function of climatic factors) regardless of how small the positive and negative changes in ΔΔ are from time zero. It is expected that in wet freeze climates, there will be more low negative changes than high positive changes in ΔA. But it is important to determine how these changes impact the freeze and thaw cycles, water contents and resilient moduli of subgrades.

Based on the examples provided above, a change in the subgrade temperature of zero from the initial subgrade temperature may appear insignificant. But it represents a subgrade temperature of 25 ^{o}C during the spring or summer which causes significant thawing, increased water contents and decreased resilient moduli. This is the primary reason for the poor performance of pavement structures during the spring thaw period in wet freeze climates.

6.3.3 Task 3: Developing the General Form Equation for the Quantitative Empirical Model

The general form equations that were evaluated for the development of the Quantitative Empirical Model (the QE Model) were developed by conducting nonlinear regression between changes in climatic factors presented in Eq. 6.3 and changes in volumetric water contents obtained from the 2-D FEA modeling output. The nonlinear regression was conducted using the exponential function, sine function, and power function that is presented in Eq. 6.5, Eq. 6.6, and Eq. 6.7 respectively. Eq. 6.5 to Eq. 6.7 represent changes in in-situ volumetric water contents as a nonlinear function of changes in climatic factors.

$$\Delta\theta(\Delta \mathrm{A}) = \left[\mathrm{P}_1 * \mathrm{e}^{\{-\mathrm{P}_2 * \{\Delta A\}\}}\right] + \mathrm{P}_3 \quad (6.5)$$

$$\Delta\theta(\Delta \mathrm{A}) = \mathrm{P}_a + [\mathrm{P}_b * Sin\,\{2 * \pi * \mathrm{P}_c * \Delta A\}] \quad (6.6)$$

$$\Delta\theta(\Delta \mathrm{A}) = \left[\mathrm{P}_{r1} * \Delta \mathrm{A}^{\mathrm{P}_{r2}}\right] + \mathrm{P}_{r3} \quad (6.7)$$

$\Delta\theta(\Delta A)$ = Changes in in-situ volumetric water contents within the subgrade as a function of changes in climatic factors; ΔA = Changes in climatic factors; e = 2.71828; π = 3.14159, P_1, P_2, P_3, P_a, P_b, P_c, P_{r1}, P_{r2}, P_{r3}, = Nonlinear regression parameters.

The analyses of data presented in Section 5.4.3, and Figure 6.7 show that the use of the exponential function produces the best fitting QE Model relative to the models which are developed using the sine and power functions. The analyses of data presented in Figure 6.7 also show that for the models developed using the exponential and sine functions, positive changes in climatic factors up to a change in climatic factors of zero result in both positive and negative changes in in-situ volumetric water contents. Positive changes in climatic factors from a change in climatic factors of zero result in both negative and positive changes in in-situ volumetric water contents. The data presented in Figure 6.7 also show that a change in climatic factors of zero (a change in the energy state of zero) causes no change in the in-situ volumetric water contents.

These observations indicate that changes in climatic factors impact the in-situ volumetric water contents differently during the frozen and unfrozen conditions. This also implies that freezing (due to negative changes in climatic factors during winter conditions) and thawing (due to positive changes in climatic factors during winter conditions) impact the water and heat transfer within subgrades differently. The analyses of data presented in Figure 6.7 show that during freezing conditions, negative changes in climatic factors (the negative changes in energy) result in negative changes in in-situ volumetric water contents (the decrease in unfrozen water contents). During unfrozen conditions, negative changes in climatic factors result in positive changes in in-situ volumetric water contents (the increase in water contents due to reduced evapotranspiration and increased condensation). The analyses of data presented in Figure 6.7 also show that during freezing conditions, positive changes in climatic factors induce thawing which result in positive changes in in-situ volumetric water contents. During unfrozen conditions, positive changes in climatic factors induce increased evapotranspiration which result in negative changes (the reduction) in in-situ volumetric water contents.

The data presented in Figure 6.7 also show that the model developed using the sine function has a higher variability in predicting changes in in-situ volumetric water contents (as a nonlinear function of changes in climatic factors) relative to the variability in changes in in-situ volumetric water contents (as a nonlinear function of changes in climatic factors) predicted using the exponential function. The data presented in Figure 6.7 also show that the model developed using the power function neglects the impact of changes in climatic factors on fluctuations in changes in in-situ volumetric water contents.

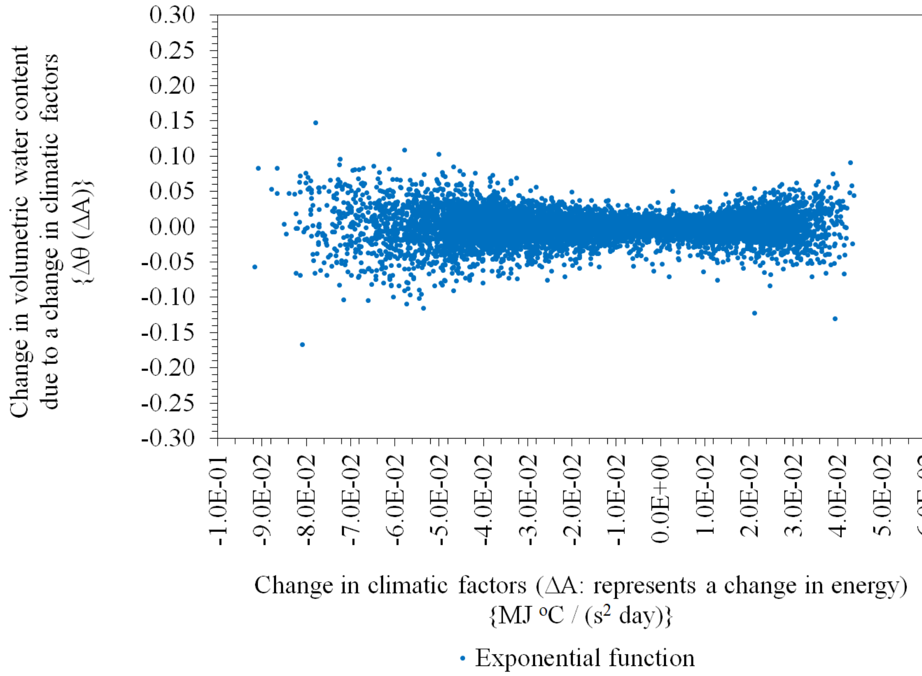
Change in volumetric water content due to a change in climatic factors {Δθ (ΔA)}
0.30
0.25
0.20
0.15
0.10
0.05
0.00
-0.05
-0.10
-0.15
-0.20
-0.25
-0.30
-1.0E-01
-9.0E-02
-8.0E-02
-7.0E-02
-6.0E-02
-5.0E-02
-4.0E-02
-3.0E-02
-2.0E-02
-1.0E-02
0.0E+00
1.0E-02
2.0E-02
3.0E-02
4.0E-02
5.0E-02
6.0E-02
Change in climatic factors (ΔA: represents a change in energy) {MJ °C / (s² day)}
Exponential function

(a)

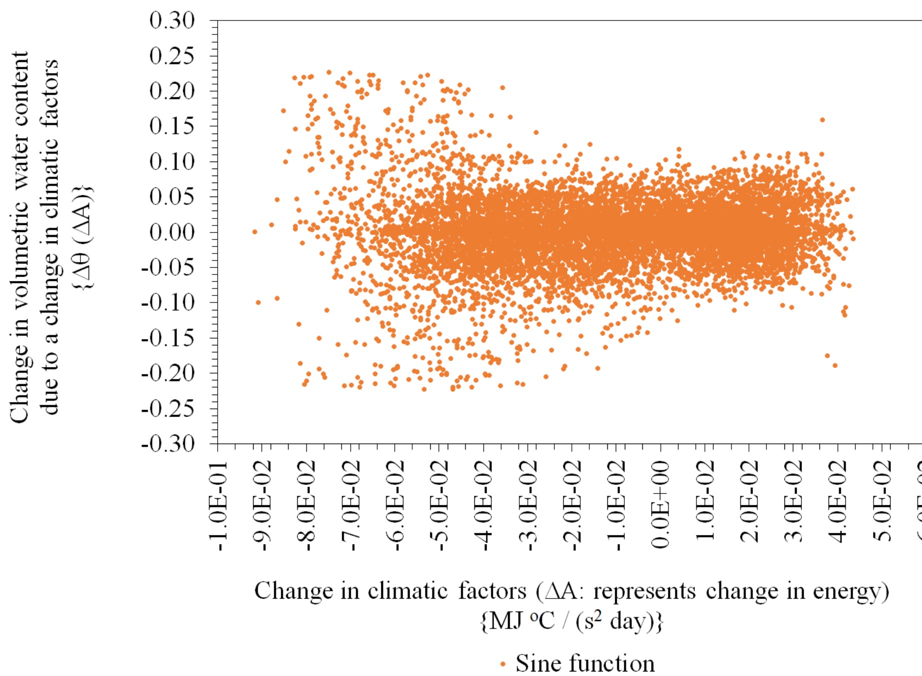
Change in volumetric water content due to a change in climatic factors {Δθ (ΔA)}
0.30
0.25
0.20
0.15
0.10
0.05
0.00
-0.05
-0.10
-0.15
-0.20
-0.25
-0.30
-1.0E-01
-9.0E-02
-8.0E-02
-7.0E-02
-6.0E-02
-5.0E-02
-4.0E-02
-3.0E-02
-2.0E-02
-1.0E-02
0.0E+00
1.0E-02
2.0E-02
3.0E-02
4.0E-02
5.0E-02
6.0E-02
Change in climatic factors (ΔA: represents change in energy) {MJ °C / (s² day)}
Sine function

(b)

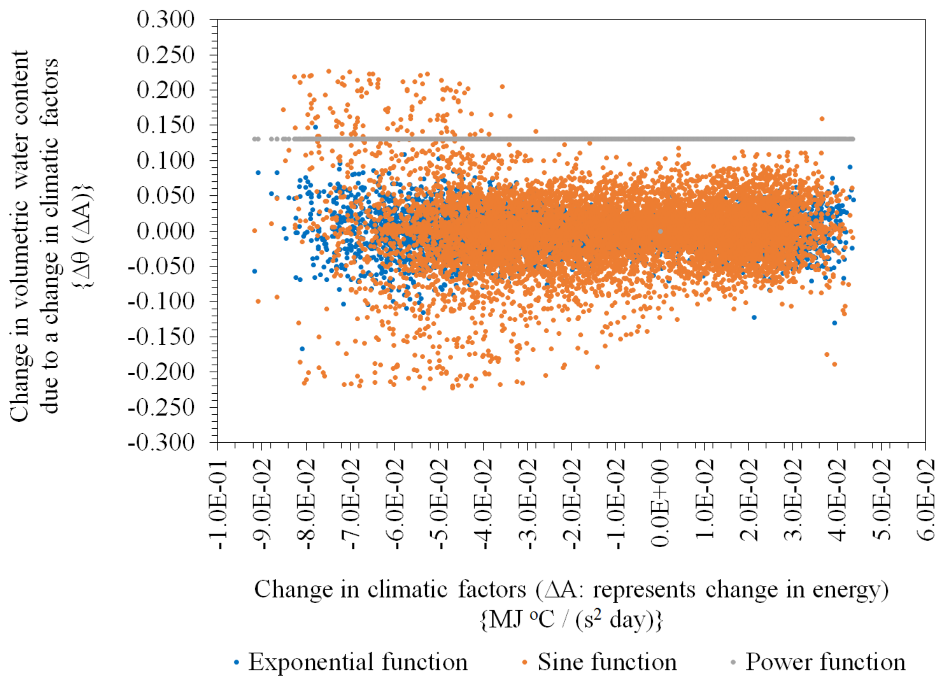

(c)

Figure 6.7: Changes in in-situ volumetric water contents vs changes in climatic factors predicted using the exponential, sine and power functions

The analyses of data presented in Figure 6.8 show changes in in-situ volumetric water contents as a nonlinear function of changes in climatic factors over time. The data show that the model developed using the sine function predicts higher maximum and lower minimum seasonal changes in in-situ volumetric water contents within subgrades. The output of the model developed using the sine function is periodic which causes the model to predict similar maximum and similar minimum seasonal in-situ water contents throughout the analysis period. This observation indicates that the model developed using the sine function misrepresents the seasonal fluctuations in in-situ water contents.

Unlike the model developed using the sine function, the model developed using the exponential function predicts continual fluctuations in the maximum and in the minimum seasonal in-situ volumetric water contents that better represent fluctuations in in-situ volumetric water contents due to changes in climatic factors. On the basis of observations highlighted above, the exponential function was selected as the preferred general form equation for developing the QE Model because it best represents the relationship between changes in in-situ volumetric water contents and changes in climatic factors. The exponential function also produces the best fitting model for simulating the water and heat transfer within subgrades.

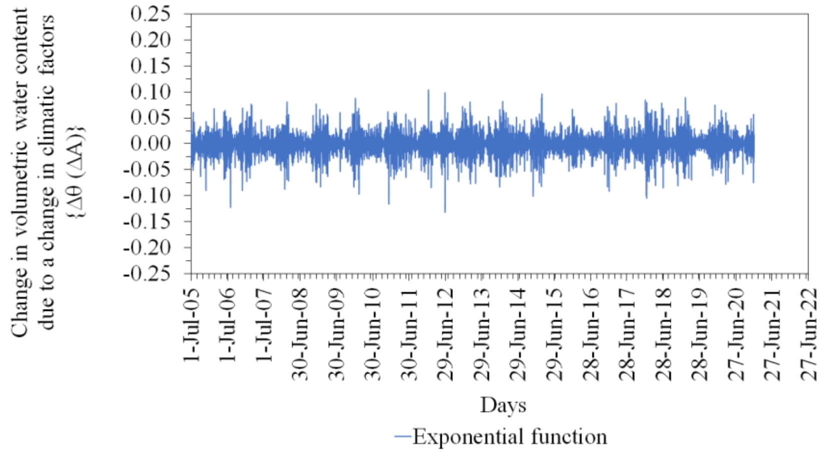

(a)

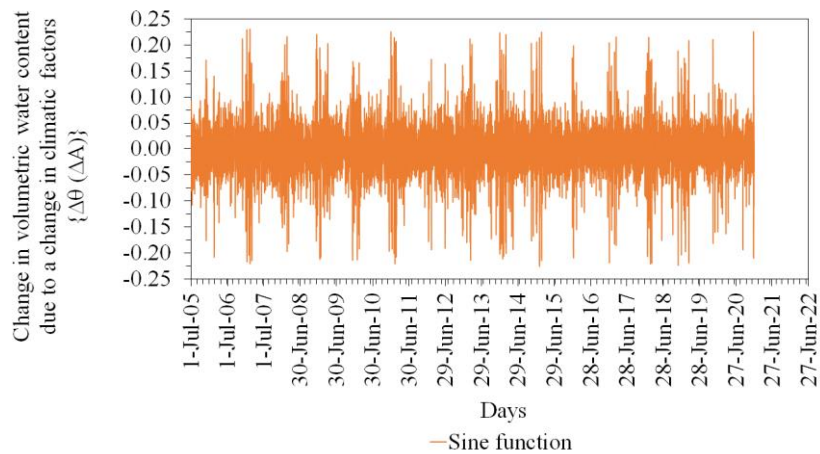

(b)

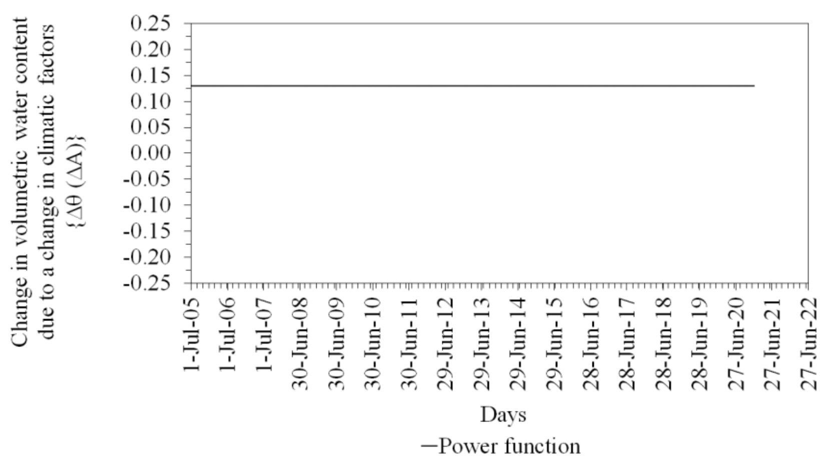

(c)

Figure 6.8: Δθ (ΔA) vs time (predicted using the exponential, sine and power functions)

6.3.4 *Task 4: Analyses of Regression Parameters from the General Form Exponential Equation*

The analyses of volumetric water contents obtained from the 2-D water and heat transfer FEA modeling are presented in Chapter 4. The analyses presented in Chapter 4 indicated that the water and heat transfer within subgrades is influenced by water contents within subgrades. The data also show that the water and heat transfer is influenced by the saturated volumetric water content and hydraulic properties of subgrades, the depth to water table, and thermal properties and density of liquid water and water vapour (system dependent properties). The analyses presented in Chapter 4 also indicated that the influence of climatic factors on water and heat transfer within subgrades is also a system dependent process.

The exponential function presented in Eq. 6.5 which is selected as the general form of the equation for the QE Model consists of nonlinear regression parameters (P_T, P_2, *and* P_3). Section 5.5 provides details of the statistical analyses used for developing P_T, P_2, *and* P_3. The nonlinear regression which was used for developing the general form of the equation was conducted using the 2-D FEA volumetric water contents output obtained from the 2-D FEA water and heat transfer sensitivity analyses. The sensitivity analyses were conducted using varying depths to the water table (1.65 m to 25.65 m below the subgrade surface). The nonlinear regression which was conducted between changes in climatic factors and changes in the 2-D FEA volumetric water contents output produced corresponding P_T, P_2, *and* P_3 values for each sensitivity analysis conducted using each depth to the water table. The values of P_T, P_2, *and* P_3 for varying depths to the water table for Research Site No.1 and Research Site No.2 are presented in Table 6.1. The analysis of data presented in Table 6.1 indicated that P_1, P_2, *and* P_3 are influenced by the depth to water table which is a system dependent property. The analysis of data presented in Table 6.1 also show that P_1, P_2, *and* P_3 are different for the two sites although the sites were analyzed at the same varying depths to the water table. However, the saturated volumetric water content of the subgrade is the primary system dependent property which is different for the two sites. The analysis of data presented in Table 6.1 indicated that, for a similar depth to the water table for the two sites, a change in the saturated volumetric water content produces changes in P_1, P_2, *and* P_3. This observation indicates that P_1, P_2, *and* P_3 are site specific and are influenced by the system dependent properties including the saturated volumetric water content of the subgrade. Therefore, site specific changes in the system dependent properties are expected to result in corresponding changes in P_1, P_2, *and* P_3. Hence, the system dependent properties are incorporated into P_1, P_2, *and* P_3.

The use of average values for P_1, P_2, and P_3 were considered. The use of average values for P_1, P_2, and P_3 would produce a QE Model which is applicable for simulating the water and heat transfer within subgrades only for sites used in this study. The model would require local calibration for use in every region with climatic factors, depths to the water table, and material properties that are different from those used for sites used in this study (a primary limitation of the current version of EICM and MEPDG).

X_1, X_2, and X_3 are developed to account for the site-specific depths to the water table and properties of subgrades (including the initial degree of saturation, and saturated and residual hydraulic conductivity) to avoid the need for local calibration of the QE Model.

Table 6.1: Function parameters for the general form of the exponential equation

Exponential function parameters	Depth from the subgrade surface to the static water table (m)				
	1.65	2.65	10.65	15.65	25.65
	Values of statistical correlation function parameters for Research Site No.1.				
P_1	1.26E-01	1.29E-01	1.36E-01	1.35E-01	1.33E-01
P_2	-1.003E-01	-1.004E-01	-1.012E-01	-1.024E-01	-1.137E-01
P_3	-1.199E-01	-1.256E-01	-1.338E-01	-1.322E-01	-1.315E-01
	Values of statistical correlation function parameters for Research Site No.2.				
P_1	5.59E-01	4.66E-01	4.09E-01	4.48E-01	4.45E-01
P_2	-1.026E-02	-1.275E-02	-1.945E-02	-1.798E-02	-2.198E-02
P_3	-5.245E-01	-4.300E-01	-3.729E-01	-4.128E-01	-4.112E-01

6.3.5 Task 5: Incorporating the System Dependent Properties into the Function Parameters

The initial degree of saturation within unsaturated subgrades (the ratio of the volume of water to total volume of voids) increases due to an increase in the infiltration capacity and volumetric water contents as shown in Figure 6.9 (Fredlund 1967). Previous studies show that at a specific volumetric water content and corresponding matric suction, the initial degree of saturation increases due to a decrease in the initial void ratio (due to an increase in the initial compacted density) of subgrades as shown in Figure 6.10. But the degree of saturation at the residual volumetric water content is independent of the initial compacted density (Zhou, et al. 2012; Romero-Morales 1999). Previous studies also show that at a specific hydraulic conductivity, the volumetric water content decreases as the saturated hydraulic conductivity of the subgrade increases as shown in Figure 6.11 (Robbins 1977). An increase in the depth to the water table results in a decrease in volumetric water contents within subgrades in the active zone as shown in Figure 6.12 (Malik, et al. 2021). Shallow depths to the water table cause higher contributions of liquid water transfer to in-situ water contents within subgrades (in the active zone) relative to the impact of deep water tables on contributions of liquid water transfer to in-situ water contents within subgrades (Malik, et al. 2021; Saadeldin, and Henni 2016; Zhou, et al. 2012; Chen, and Hu 2004; Romero-Morales 1999; Philip 1998; Robbins 1977; Fredlund 1967; Wesseling 1961). The analyses of data presented in Figure 6.9 to Figure 6.12 form the basis for the development of X_1, X_2 and X_3.

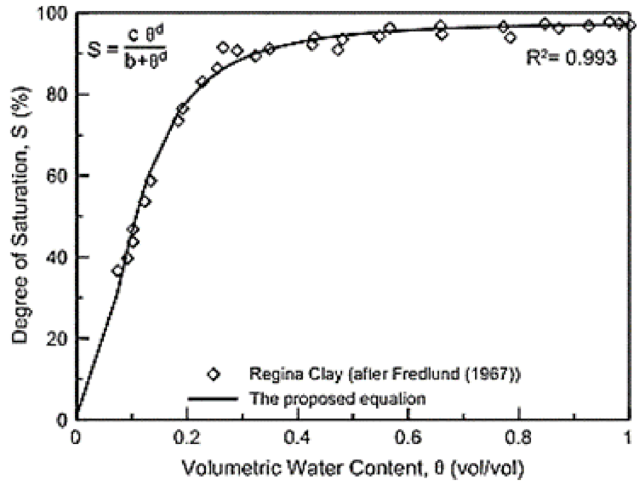

Figure 6.9: Degree of saturation vs volumetric water content (Fredlund 1967)

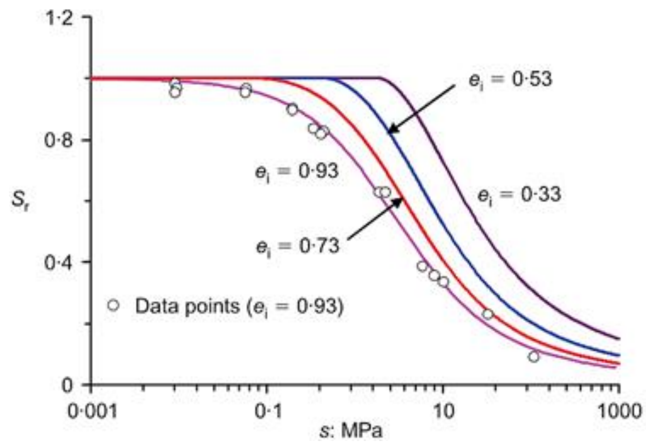

Figure 6.10: Relationship between SWCC and initial void ratio (Romero-Morales 1999)

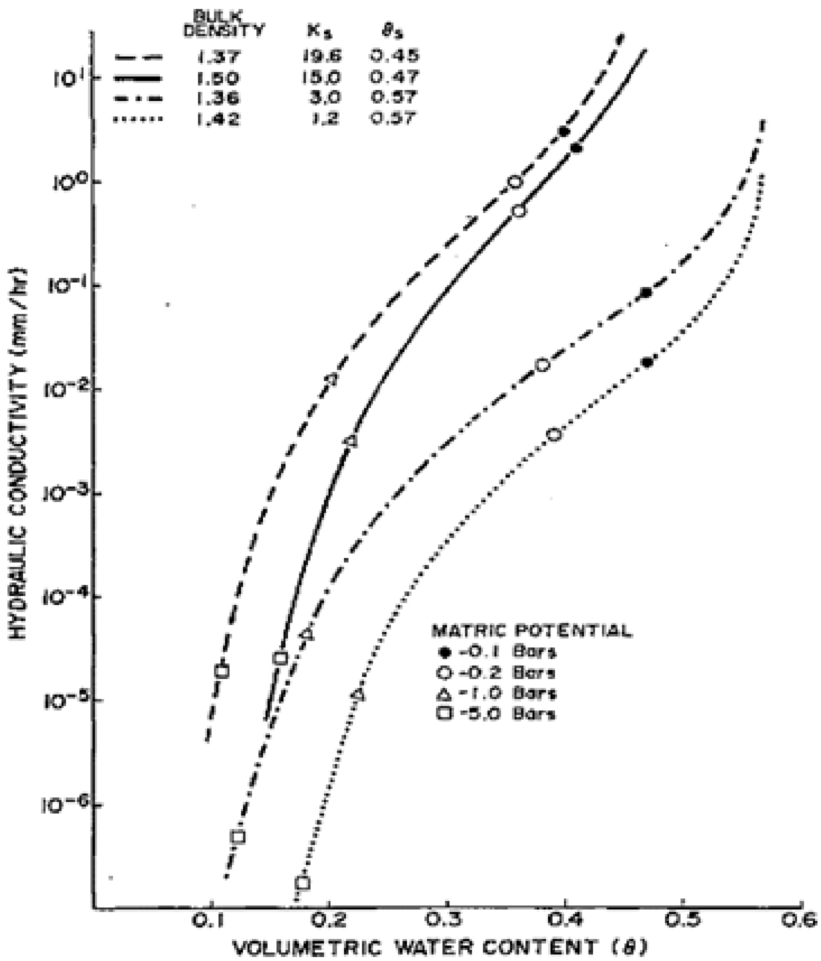

Figure 6.11: Saturated hydraulic conductivity vs volumetric water content (Robbins 1977)

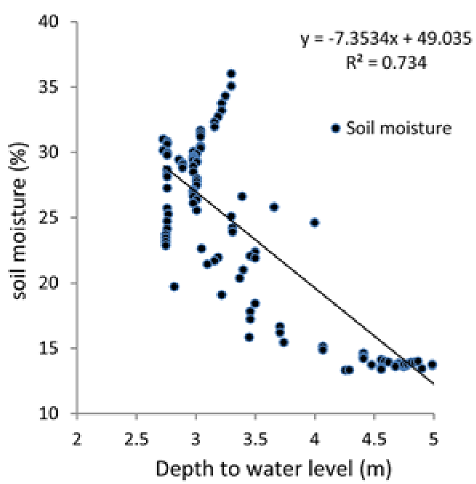

Figure 6.12: Water contents (at 1.5 m below surface) vs depths to the water table (Malik, et al. 2021)

Previous studies show a positive relationship between the vapour pressure and water contents within unsaturated subgrades as shown in Figure 6.13. The analysis of data presented in Figure 6.13 shows that the relationship between the water content and vapour pressure is influenced by the type and characteristics of the subgrade (Alexander, and Haring 1936; Puri, et al. 1925). The positive relationship between the vapour pressure and water content is incorporated into X_1, X_2 and X_3.

Water contents within subgrades have a negative relationship with the soil water density as shown in Figure 6.14 (De Wit, and Arens 1950). This observation indicates that the relationship between the soil water density and water content should be incorporated into models used for simulating the water and heat transfer within subgrades. This relationship accounts for the impact of temperature changes on the water density and on water contents within subgrades (Zhang, and Lu 2018; De Wit, and Arens 1950). This relationship is also incorporated into X_1, X_2 and X_3.

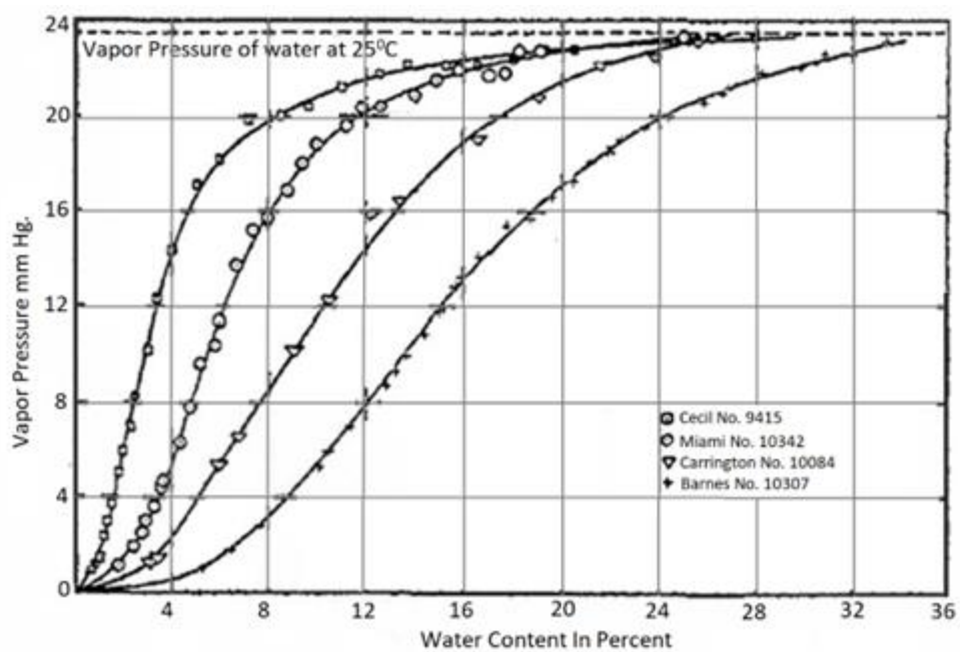

Figure 6.13: Vapour pressure vs water content (Alexander, and Haring 1936)

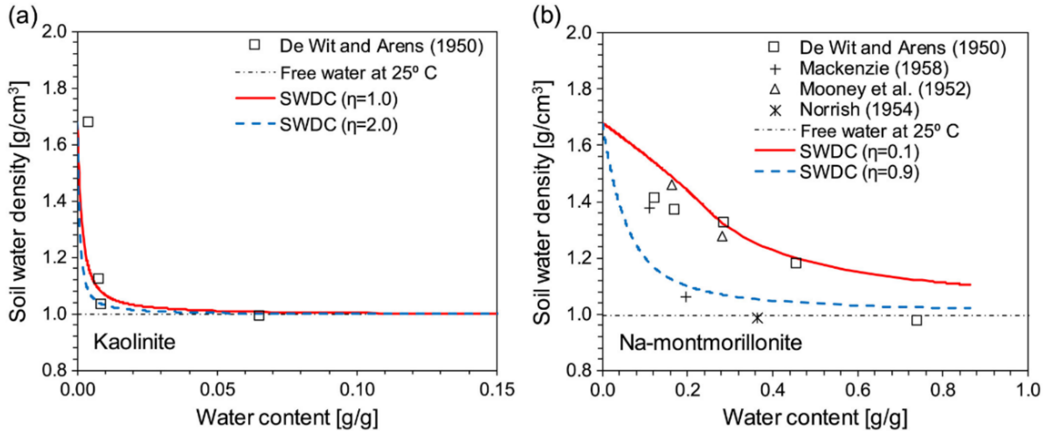

Figure 6.14: Soil water density vs water content (De Wit, and Arens 1950)

Previous studies show that the specific heat capacity at constant pressure, and the thermal diffusivity of water increase due to an increase in temperature. The water contents within subgrades have a positive relationship with thermal properties of subgrades as shown in Figure 6.15 (Guan, et al. 2009). These studies show that the rate of water and heat transfer increases due to an increase in temperature. These observations show that thermal properties of water impact the water and heat transfer within subgrades (Guan, et al. 2009; Abu-Hamdeh 2003; Bowden, and Jones 1947). These relationships are incorporated into X_1, X_2 and X_3.

The data presented in Figure 6.16 show that the heat of vaporization of water decreases due to an increase in air temperature (Pellicer, et al. 2002). This observation implies that an increase in the evapotranspiration is associated with a decrease in the heat of vaporization of water. The negative relationship between the heat of vaporization of water and evapotranspiration is incorporated into X_1, X_2 and X_3.

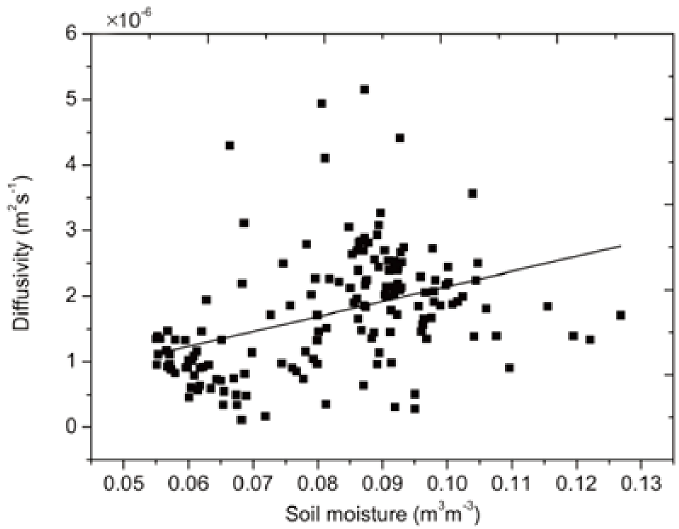

(a)

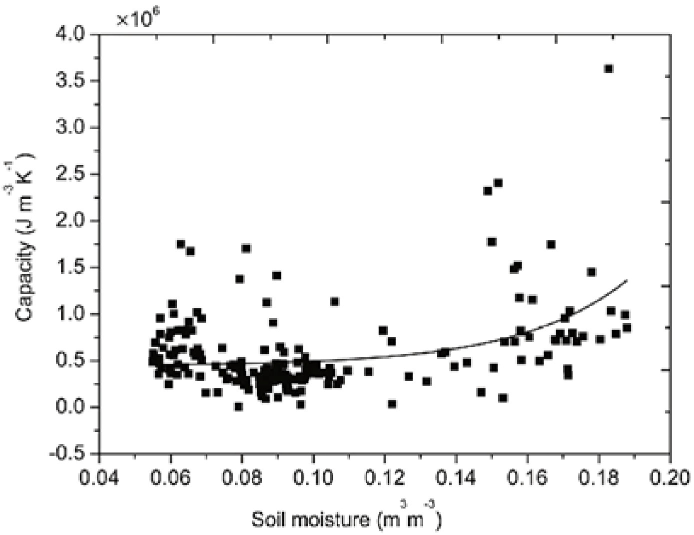

(b)

Figure 6.15: Soil thermal properties vs water content (Guan, et al. 2009)

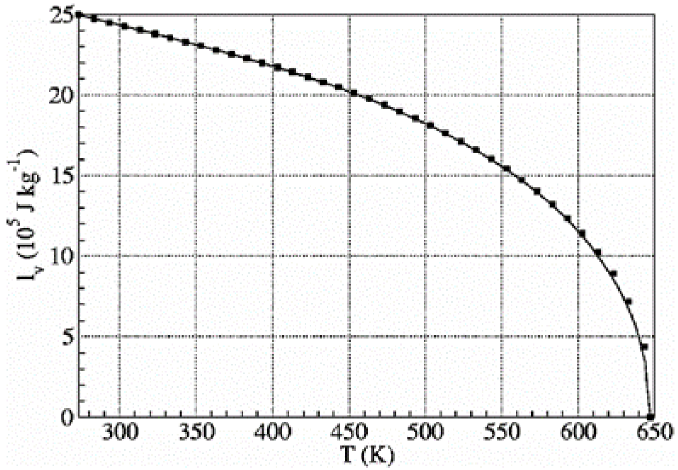

Figure 6.16: Heat of vaporization of water vs temperature (Pellicer, et al. 2002)

The relationships which are presented in Figure 6.9 to Figure 6.16 were assessed as system dependent properties and are incorporated into P_1, P_2, *and* P_3. The system dependent properties are incorporated on the basis that P_1, P_2, *and* P_3 are system dependent and are nonlinear parameters of the exponential function (which represents changes in volumetric water contents as a nonlinear function of changes in climatic factors). The system dependent properties are represented by the site-specific parameters X_1, X_2 *and* X_3 as shown in Eq. 6.8 to Eq. 6.10.

X_1 was developed to account for liquid water and water vapour transfer through diffusion by incorporating the thermal diffusivity of liquid water and water vapour. It also incorporates the equilibrium vapour pressure. X_1 also accounts for the saturated condition by incorporating the saturated hydraulic conductivity of the subgrade. The function parameter P_1 is presented as a function of X_1 {P_1 (X_1)} in the development of the function f_1 (X_1) as shown in Eq. 6.11.

X_2 was developed to account for liquid water and water vapour transfer due to gravity by incorporating the gravitational acceleration. X_2 also accounts for the saturated condition by incorporating the saturated hydraulic conductivity of the subgrade. X_2 also incorporates the specific heat capacity of liquid water which accounts for the heat energy required to change the temperature of a unit mass of liquid water by one degree. The heat of vaporization is incorporated to accounts for the heat energy required to changes a unit mass of liquid water to water vapour without any change in temperature. The equilibrium vapour pressure is incorporated to account for the vapour pressure at which the vapour pressure is in equilibrium with the liquid water pressure and influences the rate of evaporation. The function parameter P_2 is presented as a function of X_2 {P_2 (X_2)} in the development of the function f_2 (X_2) as shown in Eq. 6.12.

X_3 was also developed to account for liquid water and water vapour transfer through diffusion by incorporating the thermal diffusivity of liquid water and water vapour. It also incorporates the equilibrium vapour pressure. X_3 accounts for the residual condition by incorporating the residual hydraulic conductivity of the subgrade. The function parameter P_3 is presented as a function of X_3 {P_3 (X_3) in the development of the function f_3 (X_3) as shown in Eq. 6.13.

X_1, X_2 *and* X_3 also incorporate the density of liquid water and the density of water vapour. X_1, X_2 *and* X_3 also incorporate the site-specific initial degree of saturation of the subgrade and of the wearing course, and the depth to water table.

In Eq. 6.14, f_2 (X_2) is multiplied by ΔA. Hence, the unit for X_2 was developed so that it is the reciprocal of and in unity with the unit for ΔA (MJ ^{o}C / (s^2 day)). This results in the product of f_2 (X_2) and ΔA being unitless. The unit for X_1 was developed so that it is the same as the unit for X_3 and is unitless. X_1, X_2 *and* X_3 account for the following processes which govern the water and heat transfer within subgrades:

- The influence of the initial degree of saturation of the subgrade (S_i) on water and heat transfer using the positive relationship between volumetric water contents and S_i;
- The influence of the initial degree of saturation of wearing courses (S_c) on water and heat transfer within subgrades using the positive relationship between volumetric water contents and S_c;
- The impact of the specific heat capacity of water (C_p) on water and heat transfer within subgrades using the positive relationship between volumetric water contents and C_p;
- The impact of the vapour pressure (P_v) on the water and heat transfer within subgrades using the positive relationship between volumetric water contents and P_v;
- Liquid water transfer which is influenced by gravity using the acceleration due to gravity (g), and by diffusion using the positive relationship between volumetric water contents and the thermal diffusivity of liquid water (α_w);
- Water vapour transfer which is influenced by diffusion using the positive relationship between volumetric water contents and the thermal diffusivity of water vapour (α_v),
- The influence of the saturated and residual hydraulic conductivity of subgrades (k_{sat} and k_{res} respectively) on water and heat transfer using the negative relationship between volumetric water contents. and k_{sat} and k_{res};
- The impact of the heat of vaporization on water ($\Delta Hvap$) on water and heat transfer using the negative relationship between evapotranspiration and $\Delta Hvap$;
- The impact of the density of liquid water (ρ_w) and water vapour (ρ_v) on the water and heat transfer within subgrades using the negative relationship between water contents, and ρ_w and ρ_v; and

- The influence of the depth to the water table (D_{swt}) on the water and heat transfer within subgrades using the negative relationship between the D_{swt} and the contribution of capillary rise to volumetric water contents.

$$X_1 = \left(\frac{a_w a_v (P_v)^2 S_i\ S_c}{\rho_w \rho_v (k_{sat})^2 (D_{swt})^4}\right) \qquad (6.8)$$

$$X_2 = \left(\frac{C_P P_v S_i\ S_c}{(\Delta H_{vap})^2 \rho_w \rho_v g (D_{swt})^2 k_{sat}}\right) \qquad (6.9)$$

$$X_3 = \left(\frac{a_w a_v (P_v)^2 S_i\ S_c}{\rho_w \rho_v (k_{res})^2 (D_{swt})^4}\right) \qquad (6.10)$$

X_1 to X_3 = System dependent properties which form part of the *f-function* parameters; *Cp* =Specific heat capacity of liquid water at 25.0 ºC (0.0042 MJ / (kg ºC); S_i = Initial degree of saturation of subgrades (*decimal*); S_c = Initial degree of saturation of wearing courses (*decimal*); *ΔHvap* = Heat of vaporization of liquid water (2.27 MJ / kg); ρ_w = Density of liquid water at 25.0 ºC (1000.0 kg / m^3); *g* = Gravitational acceleration (9.81 m / s^2); P_v = Vapour pressure of water (equilibrium vapour pressure) (244.7 kg / m^2); α_w = Thermal diffusivity of liquid water at 25.0 ºC (0.0126 m^2 / day); ρ_v = Density of water vapour at 20.0 ºC (0.013 kg / m^3); α_v = Thermal diffusivity of water vapour at 1.0 atm and 100.0 ºC (2.2118 m^2 / day); D_{swt} = Depth from subgrade surface to static water table (m); k_{sat} = Saturated hydraulic conductivity of subgrade (m / day); k_{res} = Residual hydraulic conductivity of subgrade (m / day); and *t* = time (days).

The site-specific solutions for *X_1, X_2 and X_3* for the two sites are summarized in Table 6.2.

Table 6.2: Summary of the solutions for the site-specific X_1, X_2 and X_3 values

Parameters	Depth from top of subgrade to the static water table (m)				
	1.65	2.65	10.65	15.65	25.65
	Values of statistical correlation function parameters for Research Site No.1.				
X_1	1.01E+06	1.51E+05	5.80E+02	1.24E+02	1.72E+01
X_2	2.59E+02	1.01E+02	6.22E+00	2.88E+00	1.07E+00
X_3	9.06E+12	1.36E+12	5.22E+09	1.12E+09	1.55E+08
	Values of statistical correlation function parameters for Research Site No.2.				
X_1	9.60E+05	1.44E+05	5.53E+02	1.19E+02	1.64E+01
X_2	2.47E+02	9.59E+01	5.94E+00	2.75E+00	1.02E+00
X_3	8.64E+12	1.30E+12	4.98E+09	1.07E+09	1.48E+08

6.3.6 *Task 6: Formulating f-functions which are Incorporated into the Quantitative Empirical Model*

The system dependent nonlinear regression parameters P_1, P_2 and P_3 were formulated as a function of the system dependent parameters X_1, X_2 and X_3 respectively. The system dependent nonlinear regression parameters are represented by $P_1(X_1)$, $P_2(X_2)$ and $P_3(X_3)$ respectively. To differentiate between the various parameters in the Quantitative Empirical Model (the QE Model), $P_1(X_1)$, $P_2(X_2)$ and $P_3(X_3)$ are represented by $f_1(X_1)$, $f_2(X_2)$ and $f_3(X_3)$ respectively and are referred to as the *f-function* parameters f_1, f_2 and f_3, respectively. These *f-functions* which are incorporated into the QE Model were formulated by plotting the respective P_1, P_2, and P_3 values summarized in Table 6.1 vs the respective X_1, X_2, *and* X_3 values (representing solutions to the site-specific system dependent properties) summarized in Table 6.2. These relationships are presented in Figure 6.17 to Figure 6.19. The resulting function for each of the trend lines shown in Figure 6.17 to Figure 6.19 represents the respective *f-function*. The *f-function*s were formulated such that f_2 accounts for liquid water and water vapour transfer due to gravity and the pressure at which the phase change occurs respectively. The *f-functions* f_1 and f_3 account for liquid water and water vapour transfer due to diffusion.

The analyses of data presented in Figure 6.17 to Figure 6.19 show that deeper depths to the water table result in smaller values of f_1 and f_2. This observation indicates that deeper depths to the water table cause lower contribution of the liquid water transfer due to lower capillary rise to the subgrade. The analyses of data presented in Figure 6.17 and Figure 6.18 also show that a water table depth of at least 10.65 m below the subgrade surface has minimal impact on liquid water transfer within subgrades relative to the impact of shallower depths to the water table on liquid water transfer. This trend is reflected in the plots shown in Figure 6.17 and Figure 6.18 in the vicinity of the first three points which represent the depth to water table of 25.65 m, 15.65 m and 10.65 m below the subgrade surface (first three points) respectively. The analysis of data presented in Figure 6.19 show that deeper depths to the water table result in larger values of f_3. This observation indicates that during the residual water content condition, deeper depths to the water table cause higher contribution of the water vapour transfer within subgrades, relative to the contribution of the water vapour transfer caused by shallower depths to the water table. This trend is reflected in the plot shown in Figure 6.19 in the vicinity of the first three points.

The statistical analyses presented in Section 5.4.4 show that there are high statistical correlations and statistical significance between values of P_1 and X_1, P_2 and X_2, and P_3 *and* X_3.

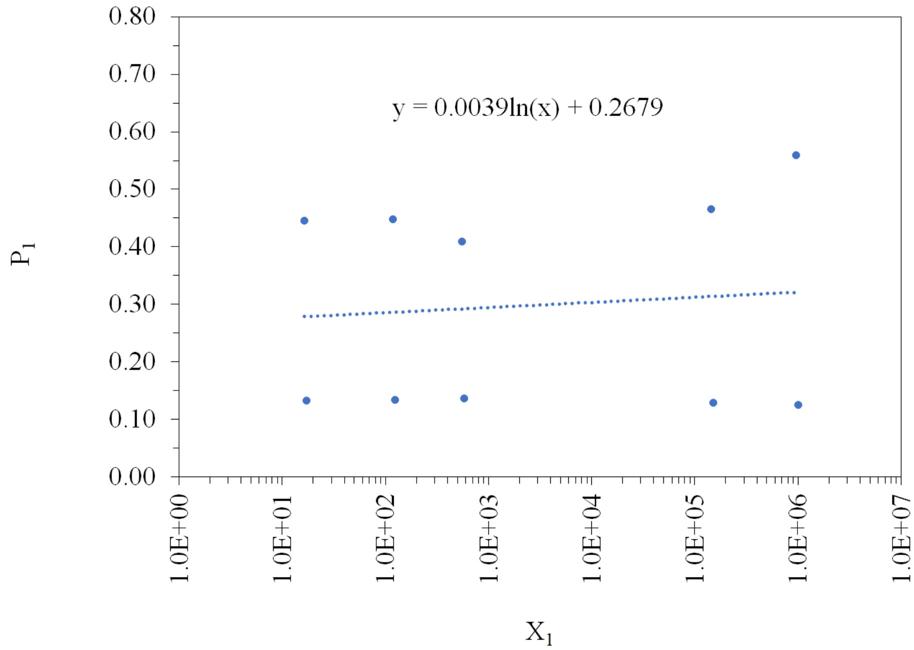

Figure 6.17: Plot showing f_1 function parameter

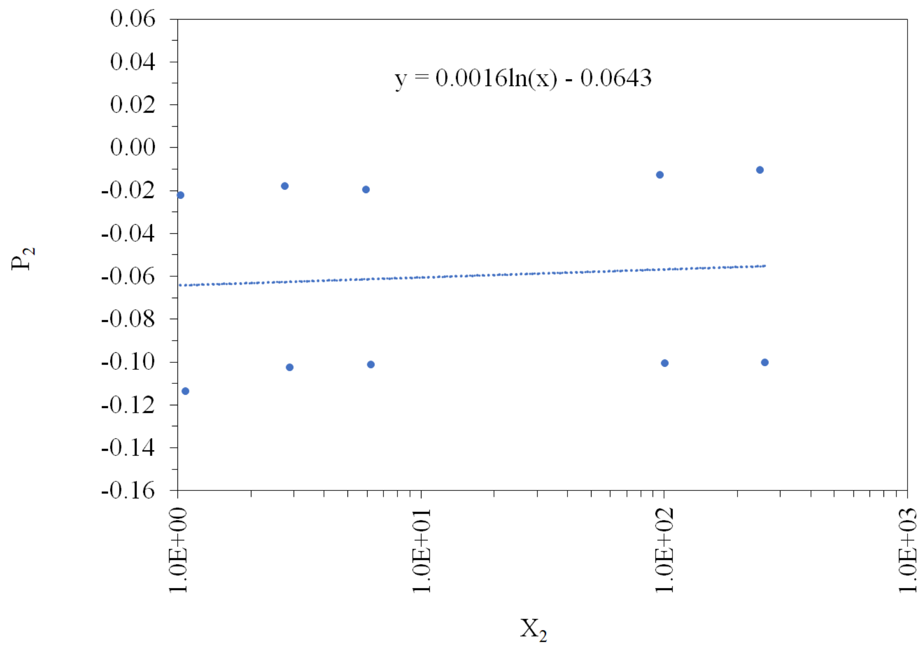

Figure 6.18: Plot showing f_2 function parameter

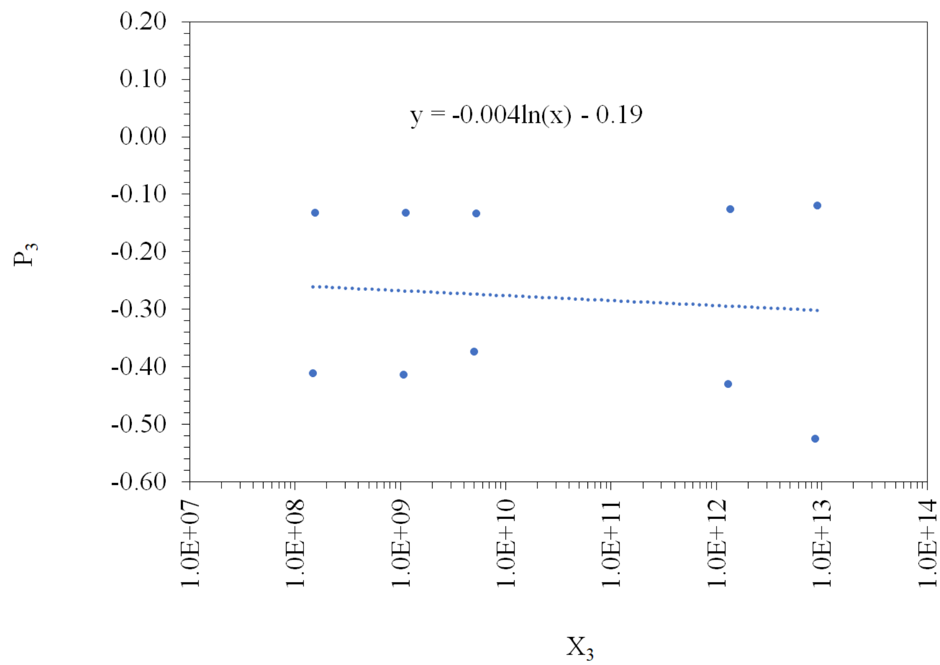

Figure 6.19: Plot showing f_3 function parameter

6.3.7 Summary of f-Function Parameters and the Resulting General Form Exponential Equation

The *f-functions* (f_1, f_2, and f_3) presented in Eq. 6.11, Eq. 6.12 and Eq. 6.13 respectively represent the system dependency of the influence of climatic factors on the water and heat transfer within subgrades. P_1, P_2, and P_3 were replaced by f_1, f_2, and f_3 respectively in the general form exponential equation. The resulting general form of the exponential equation used for the Quantitative Empirical Model (the QE Model) shown in Eq. 6.14 accounts for the site-specific system dependent properties associated with the subgrade.

$$f_1 = P_1(x_1) = \left[\{3.9 * 10^{-3}\} * \left\{ln\left(\frac{a_w a_v (P_v)^2 S_i S_c}{\rho_w \rho_v (k_{sat})^2 (D_{swt})^4}\right)\right\}\right] + (0.2679) \quad (6.11)$$

$$f_2 = P_2(x_2) = \left[\{1.6 * 10^{-3}\} * \left\{ln\left(\frac{C_P P_v S_i S_c}{(\Delta H_{vap})^2 \rho_w \rho_v g (D_{swt})^2 k_{sat}}\right)\right\}\right] - (0.0643) \quad (6.12)$$

$$f_3 = P_3(x_3) = \left[\{-4.0 * 10^{-3}\} * \left\{ln\left(\frac{a_w a_v (P_v)^2 S_i S_c}{\rho_w \rho_v (k_{res})^2 (D_{swt})^4}\right)\right\}\right] - (0.19) \quad (6.13)$$

$$\Delta\theta(\Delta A) = \left[f_1 * e^{\{-f_2 * \{\Delta A\}\}}\right] + f_3 \quad (6.14)$$

6.3.8 Task 7: Development of the Integral Function for the Quantitative Empirical Model

The mathematical computation include substituting Eq. 6.14 into Eq. 6.2 resulting in the integral function presented in Eq. 6.15. The integral function representing the accumulation of changes in volumetric water contents as a function of changes in climatic factors from time "*0*" to time "*n*" is presented in Eq. 6.16. Eq. 6.16 is further factorized as shown in Eq. 6.17. The solution of the integral function presented in Eq. 6.17 is shown in Eq. 6.18 to Eq. 6.21.

$$\Delta\theta_{tn} = \int_0^{tn} \Delta\theta(\Delta A)\ dt\ = \int_0^{tn} \left[f_1 * e^{\{-\ f_2 * \{\Delta A\}\}} \right] + f_3\ \ dt \qquad (6.15)$$

$$\int_0^{tn} \Delta\theta(\Delta A)\ dt\ = \int_0^{tn} \left[f_1 * e^{\{-\ f_2 * \{\Delta A\}\}} \right] + f_3\ \ dt \qquad (6.16)$$

$$\int_0^{tn} \Delta\theta(\Delta A)\ dt\ = \int_0^{tn} \left[f_1 * e^{\{U\}} \right] + f_3\ \ dt \qquad (6.17)$$

$$\int_0^{tn} \left[f_1 * e^{\{U\}} \right] dt = \left[\frac{\{f_1 * e^{\{U\}}\}}{\left\{\frac{du}{dt}\right\}} \right] + C \qquad (6.18)$$

$$\int_0^{tn} f_3\ \ dt = \int_0^{tn} f_3 * t^0\ dt\ = \{f_3 * t\}\ +\ C \qquad (6.19)$$

$$\int_0^{tn} \left[f_1 * e^{\{U\}} \right] + \{f_3\}\ \ dt\ = \left[\frac{\{f_1 * e^{\{U\}}\}}{\left\{\frac{du}{dt}\right\}} \right] + \{f_3 * t\} + C \qquad (6.20)$$

$$\int_0^{tn} \Delta\theta(\Delta A)\ dt\ = \left[\frac{\left\{f_1 * e^{\{-\ f_2 * \{\Delta A\}\}}\right\}}{\left\{\frac{du}{dt}\right\}} \right] +\ \{f_3 * t\} +\ C \qquad (6.21)$$

6.3.9 Task 8: Verifying the Accuracy of the Integral Function Computation

The accuracy of the integral computation was verified by conducting the first order partial derivatives of the anti-derivative function which is presented in Eq. 6.21. The verification of the integral computation is shown in Eq. 6.22 to Eq. 6.26. This computation produced the original function shown in Eq. 6.14 which confirms the accuracy of the integral computation.

$$\Delta\theta\ (\Delta A)\ \ =\ \frac{d}{dt} \left[\frac{\{f_1 * e^{\{U\}}\}}{\left\{\frac{du}{dt}\right\}} \right] + \frac{d}{dt}\ \{f_3 * t\} \qquad (6.22)$$

$$\frac{d}{dt}\left[\frac{\{f_1 * \mathrm{e}^{\{U\}}\}}{\{\frac{du}{dt}\}}\right] = \left[\frac{\{f_1 * \mathrm{e}^{\{U\}}\}}{\{\frac{du}{dt}\}}\right] * \left\{\frac{du}{dt}\right\} = \{f_1 * \mathrm{e}^{\{U\}}\} \tag{6.23}$$

$$\frac{d}{dt}\{f_3 * t\} = f_3 * t^0 = f_3 \tag{6.24}$$

$$\Delta\theta\ (\Delta A) = [f_1 * e^{\{u\}}] + f_3 \tag{6.25}$$

$$\Delta\theta\ (\Delta A) = [f_1 * e^{\{-\ f_2 * \{\Delta A\}\}}] + f_3 \tag{6.26}$$

6.3.10 Summary of the Quantitative Empirical Model

The Quantitative Empirical Model (the QE Model) was developed through nonlinear regression between changes in climatic factors and changes in volumetric water contents within subgrades (the statistical correlation function), integral computations of the statistical correlation function, and mathematical computations (to incorporate the thermal and physical properties of liquid water and water vapour transfer). The development of the QE Model also included incorporating the initial degree of saturation of subgrades and wearing courses, hydraulic properties of subgrades, and the depth to water table.

The QE Model is a land climate interaction (LCI) boundary condition model which accounts for the influence of changes in climatic factors and LCI (on the adjacent vegetated and bare ground areas) on changes in the water and heat transfer within subgrades. The QE Model accounts for the influence of changes in site-specific precipitation, air temperature, net solar radiation, wind speed, relative humidity, evapotranspiration, and evaporation through the wearing courses to the atmosphere on changes in volumetric water contents within subgrades. The QE Model is summarized in Eq. 6.27 to Eq. 6.30.

$$\theta_{tn} = \theta_{t0} + \Delta\theta_{tn} \tag{6.27}$$

$$\theta_{tn} = \theta_{t0} + \int_0^{tn} \Delta\theta\,(\Delta A)\ dt \tag{6.28}$$

$$\int_0^{tn} \Delta\theta\,(\Delta A)\ dt = \left[\frac{\{f_1 * \mathrm{e}^{\{-\ f_2 * \{\Delta A\}\}}\}}{\{\frac{du}{dt}\}}\right] + \{f_3 * t\} + C \tag{6.29}$$

$$\theta_{tn} = \theta_{t0} + \left[\left[\frac{\{f_1 * \mathrm{e}^{\{-\ f_2 * \{\Delta A\}\}}\}}{\{\frac{du}{dt}\}}\right] + \{f_3 * t\} + C\right] \tag{6.30}$$

Summary of f-functions which are Incorporated into the Quantitative Empirical Model

Eq. 6.31 to Eq. 6.33 provide a summary of *f-functions* which form part of the QE Model.

$$f_1 = P_1\,(x_1) = \left[\left\{3.9 * 10^{-3}\right\} * \left\{ln\left(\frac{a_w\, a_v\, (P_v)^2\, S_i\; S_c}{\rho_w\, \rho_v\, (k_{sat})^2 (D_{swt})^4}\right)\right\}\right] + (0.2679) \qquad (6.31)$$

$$f_2 = P_2\,(x_2) = \left[\left\{1.6 * 10^{-3}\right\} * \left\{ln\left(\frac{C_P\, P_v\, S_i\; S_c}{(\Delta H_{vap})^2\, \rho_w\, \rho_v\, g\, (D_{swt})^2 k_{sat}}\right)\right\}\right] - (0.0643) \qquad (6.32)$$

$$f_3 = P_3\,(x_3) = \left[\left\{-4.0 * 10^{-3}\right\} * \left\{ln\left(\frac{a_w\, a_v\, (P_v)^2\, S_i\; S_c}{\rho_w\, \rho_v\, (k_{res})^2 (D_{swt})^4}\right)\right\}\right] - (0.19) \qquad (6.33)$$

θ_{tn} =Total volumetric water content at the end of time "n" (*Unitless*), θ_{to} = Initial volumetric water content at the end of construction (*Unitless*), ΔA = Changes in climatic factors (MJ ºC / (s^2 day)), S_i = Initial degree of saturation of the subgrade (*decimal*); S_c = Initial degree of saturation of the wearing course (*decimal*); t = Total time (days) ⇒ t_i + t_{lag}; t_i = Any time t; t_{lag} = Lag time; f_1, f_1 and f_3 = Function properties which form part of the QE Model; f_1 ⇒ Unitless, f_2 ⇒ day s^2 / (MJ ºC); f_3 ⇒ Unitless; Cp =Specific heat capacity of liquid water at 25.0 ºC (0.0042 MJ / (kg ºC); $\Delta Hvap$ = Heat of vaporization of liquid water (2.27 MJ / kg); ρ_w = Density of liquid water at 25.0 ºC (1000.0 kg / m^3); g = Gravitational acceleration (9,81 m / s^2); P_v = Vapour pressure of water (equilibrium vapour pressure) (244.7 kg / m^2); α_w = Thermal diffusivity of liquid water at 25.0 ºC (0.0126 m^2 / day); ρ_v = Density of water vapour at 20.0 ºC (0.013 kg / m^3); α_v = Thermal diffusivity of water vapour at 1.0 atm and 100.0 ºC (2.2118 m^2 / day); D_{swt} = Depth from subgrade surface to static water table (m); k_{sat} = Saturated hydraulic conductivity of the subgrade (m / s); and k_{res} = Residual hydraulic conductivity of the subgrade (m / s).

Summary of Processes and Mechanisms which are Incorporated into the Quantitative Empirical Model

The Quantitative Empirical Model (the QE Model) accounts for the site-specific climatic factors, the thermal properties and density of liquid water and water vapor, the site-specific properties of the subgrade and wearing courses. The processes and mechanisms that are accounted for in the QE Model are listed below.

- The QE Model is applicable for fine-grained subgrades in wet freeze climates;
- The model accounts for the site-specific subgrade and wearing course properties including the initial degree of saturation of subgrades and wearing courses, and the saturated and residual hydraulic conductivity of subgrades;
- The model accounts for site-specific changes precipitation, air temperature, net solar radiation, relative humidity, wind speed, and evapotranspiration (changes in climatic factors);

- The model accounts for LCI boundary conditions on vegetated and bare ground areas adjacent to pavement structures;
- The model accounts for liquid water transfer due to gravity flow and diffusion, and water vapour transfer due to diffusion, latent heat and gravity;
- The model incorporates the thermal diffusivity of liquid water and water vapour, specific heat capacity of liquid water, heat of vaporization of liquid water, density of liquid water and water vapour, and the vapour pressure of water at equilibrium;
- The model accounts for infiltration through vegetated and bare ground areas beyond the traffic lanes and shoulders including the median, ditches, and green spaces adjacent to pavement structures;
- The model assumes impervious wearing courses on traffic lanes and shoulders which are associated with new and rehabilitated pavements;
- The model accounts for heat transfer through the pavement structure and through vegetated and bare ground areas;
- The model accounts for a static water table at any depth; and
- The model accounts for fluctuations in water and heat transfer due to changes in climatic factors.

The input parameters for the QE Model for liquid water and water vapour, subgrade, wearing courses, and water table are summarized in Table 6.3, Table 6.4, and Table 6.5, respectively.

Table 6.3: Quantitative Empirical Model input parameters for liquid water and water vapour

Properties of Liquid Water and Water Vapour	
Properties	Value
Specific heat capacity of liquid water at 25 ºC (MJ / (kg ºC))	0.0042
Heat of vaporization of liquid water (MJ / kg)	2.27
Density of liquid water at 25 ºC (kg / m^3)	1000.0
Vapour pressure of water at equilibrium (kg / m^2)	244.7
Thermal diffusivity of water vapour at 1 atm, 100 ºC (m^2 / day)	2.2118
Thermal diffusivity of liquid water at 25 ºC (m^2 / day)	0.0126
Density of water vapour at 20 ºC (kg m^{-3})	0.013
Gravitational Acceleration	
Gravitational acceleration (m sec^{-2})	9.81

Table 6.4: Quantitative Empirical Model input parameters for the subgrade

Subgrade Properties	Values
Initial degree of saturation (S_i) Saturated hydraulic conductivity (k_{sat}), (m / sec) Residual hydraulic conductivity (k_{res}), (m / sec) Volumetric water content at end of construction (θ_{t0})	Site specific

Table 6.5: Quantitative Empirical Model input parameters for the wearing course and water table

Pavement Properties	Value
Initial degree of saturation of the wearing course (S_c)	Site specific
Depth to water table below subgrade surface (m)	Site specific

Limitations of the Quantitative Empirical Model

The two primary limitations of the Quantitative Empirical Model (the QE Model) are listed below:

- The QE Model accounts for the density of liquid water and water vapour at 25.0 ^{o}C and at 20.0 ^{o}C respectively. However, the QE Model neglects the impact of temperature changes on changes in density of liquid water and water vapour; and
- The QE Model accounts for the thermal diffusivity of liquid water and water vapour at 25.0 ^{o}C, and at at 1.0 atm and 100.0 ^{o}C respectively. However, the QE Model neglects the impact of temperature gradients on changes in the thermal diffusivity of liquid water and water vapour.

6.3.11 The Application of the Quantitative Empirical Model

The Quantitative Empirical Model (the QE Model) has many applications in the engineering practice. The QE Model may be used for predicting the impact of climatic factors on the water and heat transfer within highway and runway pavement structures, railway structures and landfill covers. The QE Model represents the impact of climatic factors on the in-situ soil water characteristic curve (the in-situ SWCC) for fine-grained subgrades. The QE Model may also be incorporated into EICM and MEPDG to account for the influence of climatic factors on water and heat transfer, resilient moduli of subgrades and for implementing economical pavement structures.

The QE Model Represents the Influence of Climatic Factors on the In-situ SWCC

The QE Model is applicable for predicting the influence of climatic factors on the water and heat transfer within fine-grained and coarse-grained subgrades in wet freeze and wet no-freeze climatic zones. The analyses of data presented in Figure 6.20 indicate that the QE Model represents the influence of changes in climatic factors on changes in volumetric water contents within subgrades. Changes in climatic factors represent the energy state within subgrades. Further analyses of data presented in Figure 6.7a (which is provided in more details in Figure 6.20) also show that the QE Model represents the influence of climatic factors on the in-situ soil water characteristic curve (the in-situ SWCC) for fine-grained subgrades. The QE Model accounts for the impact of climatic factors on the drying and wetting paths (hysteresis). The QE Model also accounts for the impact of freeze and thaw cycles on the in-situ water and heat transfer, the in-situ water storage and the in-situ SWCC for fine-grained subgrades.

The data presented in Figure 6.20 show that the subgrade starts to desaturate at a change in climatic factors value of approximately -5.0 x 10^{-2} {MJ ^{o}C / (s^2 day)} which represents the air entry value (AEV) of the subgrade. The data presented in Figure 6.20 also show that the AEV represents the energy state at which the subgrade starts to desaturate. On the drying path, a change in climatic factors (a change in the energy state) of less than the AEV causes minimal changes in volumetric water contents within subgrades. The residual water content phase starts at an energy state of approximately 3.0 x 10^{-2} {MJ ^{o}C / (s^2 day)}. Also on the drying path, an increase in the energy state beyond 3.0 x 10^{-2} {MJ ^{o}C / (s^2 day)} causes minimal changes in volumetric water contents. On the wetting path, negative changes in the energy state cause decreased volumetric water contents within subgrades. This indicates that on the wetting path, further negative changes in the energy state cause further reduction in the unfrozen volumetric water contents within subgrades. Also on the wetting path, an increase in the energy state beyond 3.0 x 10^{-2} {MJ ^{o}C / (s^2 day)} causes minimal changes in volumetric water contents within subgrades. The data also show that the maximum volumetric water content within the subgrade subsequent to the wetting process, is less than the initial maximum volumetric water content on the drying path. This is due to the presence of water vapour in the macro pores at the end of the wetting path. This observation indicates that the QE Model accounts for both liquid water and water vapour transfer within subgrades.

The QE Model is applicable for new and rehabilitated pavement structures because the model accounts for a no-flow surface boundary condition on traffic lanes and shoulders which is applicable for impervious wearing courses with no cracks. The QE Model is also applicable for unpaved roads because the model accounts for land climate interaction (LCI) boundary conditions on vegetated and bare ground areas adjacent to pavement structures which are applicable for surfaces of unpaved roads.

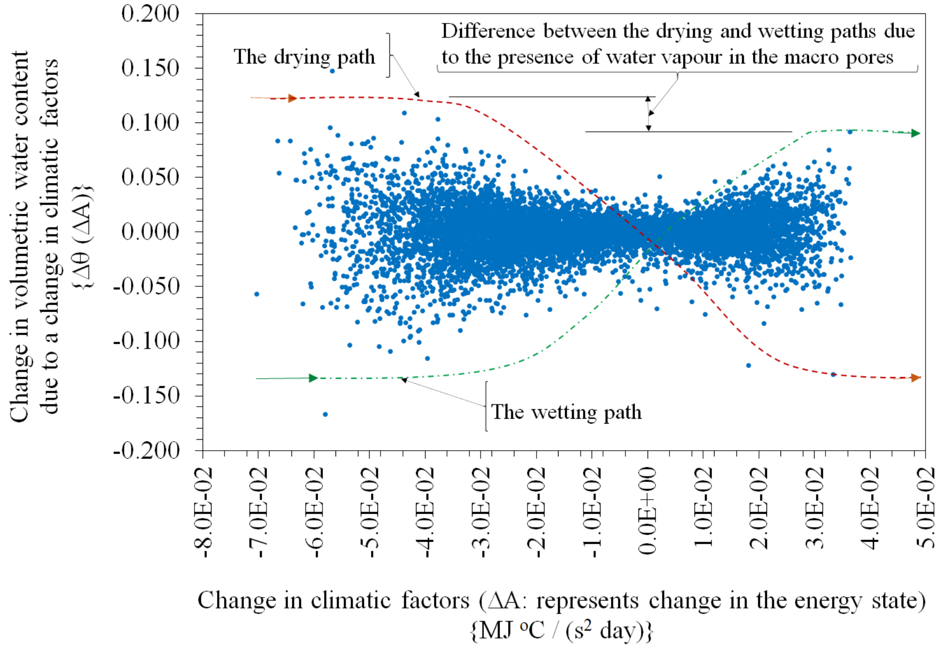

Figure 6.20: The Quantitative Empirical Model output {Δθ (ΔA)} vs the energy state (ΔA): represents the in-situ SWCC for fine-grained subgrades

Incorporating the QE Model into EICM and MEPDG

This Section provides details of the modified version of the composite environmental adjustment factor (F_{envCF}) developed as part of this study. The F_{envCF} was developed for incorporating the impact of climatic factors into resilient moduli and performance evaluation of subgrades.

The Quantitative Empirical Model (the QE Model) accounts for the influence of climatic factors on water and heat transfer within subgrades. The model predicts changes in volumetric water contents within subgrades due to changes in climatic factors. Hence, volumetric water contents predicted using the QE Model may be used as input in EICM for calculating the degree of saturation. This results in the degree of saturation values which account for the impact of changes in climatic factors on changes in the degree of saturation (S_{CF}) as shown in Eq. 6.34. The S_{CF} values may be used as input into EICM for calculating the unfrozen environmental adjustment factor (F_U) used in EICM to account for the impact of changes in climatic factors on changes in resilient moduli of subgrades over time (which is represented by the modified F_U values (F_{UCF})) which is presented in Eq. 6.35. The $F_{U\text{-}CF}$ values may be used as input into the composite environmental adjustment factor (F_{env}) used in EICM to predict the F_{envCF} values as shown in Eq. 6.36.

The use of volumetric water contents predicted using the QE Model as input to calculate the $F_{env\text{-}CF}$ will facilitate EICM and MEPDG incorporating the impact of changes in climatic factors on changes in resilient moduli of subgrades over time (M_{RCF}) as shown in Eq. 6.37. Incorporating the QE Model into the $F_{env\text{-}CF}$ also facilitates EICM and MEPDG to incorporate the impact of changes in climatic factors on the pavement structure performance, the pavement structure life cycle cost analysis, and the pavement structure service life. Incorporating climatic factors into EICM and MEPDG will also facilitate the design and construction of more economical pavement structures.

$$S_{CF} = \frac{\theta_{CF}}{n_e} = \frac{\theta_{CF}}{\theta_{sat}} \tag{6.34}$$

$$log\{F_{UCF}\} = log\left\{\frac{M_{RCF}}{M_{ROpt}}\right\} = a + \frac{\{b-a\}}{1+EXP\left\{ln\left(\frac{-b}{a}\right)+k_m\left(S_{CF}-S_{Opt}\right)\right\}} \tag{6.35}$$

S_{CF} = Modified degree of saturation at a specific volumetric water content predicted using the QE Model which accounts for climatic factors (in decimals); $\theta_{CF} = \theta_{tn}$ = Volumetric water content at time "n" predicted using the QE Model which accounts for climatic factors; θ_{sat} = Saturated volumetric water content; n = Porosity of the subgrade; F_{UCF} = Modified unfrozen environmental adjustment factor which accounts for climatic factors by incorporating the QE Model; M_{RCF} = Modified resilient modulus at a specific volumetric water content or a specific degree of saturation and incorporates the QE Model; M_{Ropt} = Resilient modulus at optimum water content and maximum dry density (MPa); S_{opt} = Degree of saturation at optimum water content (decimals); a = Minimum of log $\{M_R/M_{R\text{-}opt}\}$. For fine-grained subgrades a = -0.5934, and a = -0.3123 for coarse-grained subgrades; b = Maximum of log $\{M_R/M_{R\text{-}opt}\}$. For fine-grained subgrades b = 0.4, and b = 0.3 for coarse-grained subgrades; k_m = Regression parameter. For fine-grained subgrades k_m = 6.1324, and k_m = 6.8157 for coarse-grained subgrades.

$$F_{envCF} = \frac{\{h_{total} * t_{total}\}}{\sum_{t=1}^{total}\left\{\sum_{node=1}^{n}\left(\frac{h_{node}}{F_{nodeCF,t}}\right)\right\}} \tag{6.36}$$

F_{envCF} = Modified unfrozen composite environmental adjustment factor for the material layer under consideration which accounts for climatic factors by incorporating the QE Model; $F_{nodeCF,t}$ = Modified unfrozen environmental adjustment factor at a specific node and time which accounts for climatic factors by incorporating the QE Model and is represented by F_{UCF}; t = Time; t_{total} = Total number of time increments for which the resilient modulus is being calculated; h_{node} = Length of the spring assigned to the node; and h_{total} = Total height of the material layer.

$$M_{RCF} = F_{envCF} * M_{ROpt} \quad (6.37)$$

M_{RCF} = Modified resilient modulus at a specific depth and time which accounts for climatic factors by incorporating the QE Model; F_{envCF} = Modified composite environmental adjustment factor for the material layer under consideration which accounts for climatic factors by incorporating the QE Model; and M_{ROpt} = Resilient modulus at optimum conditions (optimum water content and maximum dry density).

Chapter 7 Verification of the Quantitative Empirical Model

7.1 Introduction

Chapter 7 provides background details of the methodology used for the development of the Quantitative Empirical Model, primary features and application of the model. Chapter 7 also provides the strategy implemented for verifying the QE Model. The Chapter provides details of data sources, locations of the sites, and details of the pavement sections used for verifying the model.

Chapter 7 also provides a summary of the ten tasks conducted for verifying and for evaluating the accuracy of the QE Model. The tasks include 1) determined input data including subgrade properties, 2) obtained climatic data used as input, 3) compared the measured in-situ water contents to the calculated water contents to evaluate the accuracy of the measured in-situ water contents, 4) used the data obtained in Tasks 1 to Task 3 as input in the QE Model, 5) calculated and review the accuracy of predicted volumetric water contents output, 6) evaluated the accuracy of the QE Model against EICM using predicted water contents, 7) evaluated the accuracy of the QE Model against EICM using the calculated F_{env} values, 8) evaluated the accuracy of the QE Model against EICM using the calculated M_R values, 9) evaluated the general trends in the predicted cumulative water contents obtained using the QE Model, and 10) evaluated the accuracy of the QE Model against EICM using coefficient of determination (R^2) values.

The QE Model was verified by comparing the predicted volumetric water contents calculated using the model to the measured in-situ volumetric water contents. The QE Model was also verified against EICM by comparing F_{env} values calculated using the predicted volumetric water contents which were calculated using the QE Model and EICM, to F_{env} values calculated using the measured in-situ volumetric water contents. The QE Model was also verified against EICM by comparing resilient moduli values of subgrades calculated using the unfrozen F_{env} values calculated using water contents predicted using the QE Model (M_{RCF}), to resilient moduli values of subgrades calculated using F_{env} values calculated using water contents predicted using EICM (M_R). The M_{RCF} and M_R values were compared to the calculated and measured in-situ resilient moduli values.

The Chapter also provides a summary of the evaluation and verification process, limitations in EICM which are mitigated by the QE Model, and details of primary features of the QE Model. The summary presented in the Chapter also provides details of the contribution of the QE Model to improving EICM and MEPDG to account for the impact of climatic factors on water and heat transfer, resilient modulus of subgrades, pavement performance and service life.

7.2 Background

The Quantitative Empirical Model (the QE Model) was developed using nonlinear regression between changes in volumetric water contents within subgrades and changes in precipitation, air temperature, net solar radiation, wind speed, relative humidity, evapotranspiration and water vapor transfer through the wearing course to the atmosphere (climatic factors). The nonlinear regression was conducted using an exponential function. The analyses presented in this Chapter were conducted to verify and to evaluate the accuracy of the QE Model in predicting the influence of climatic factors on water and heat transfer within subgrades.

The QE Model accounts for changes in volumetric water contents within subgrades as a nonlinear function of changes in climatic factors (changes in volumetric water contents). Changes in volumetric water contents also account for the site-specific system dependent properties of subgrades including the initial degree of saturation, and the saturated and residual hydraulic conductivity. Changes in volumetric water contents also account for the site-specific depth to the water table. Changes in volumetric water contents are added to the initial volumetric water content within the subgrade which was measured at the end of construction to obtain the total volumetric water content within the subgrade over time. The QE Model accounts for liquid water and water vapour transfer. The model also accounts for the land climate interaction (LCI) on vegetated and bare ground areas adjacent to pavement structures.

7.3 An Overview of the Strategy Implemented for Verifying the Quantitative Empirical Model

The Quantitative Empirical Model (the QE Model) was developed to predict changes in in-situ volumetric water contents within subgrades due to changes in climatic factors for pavement structures in wet freeze climates (predicted in-situ volumetric water contents). The predicted in-situ volumetric water contents within the subgrade may be used as an input in EICM incorporated into MEPDG to determine the degree of saturation over time. This accounts for the impact of changes in climatic factors on changes in in-situ resilient modulus of the subgrade during the unfrozen conditions. This mechanism of water and heat transfer within subgrades is accounted for in the unfrozen environmental adjustment factor (F_U). The predicted changes in the in-situ resilient modulus due to changes in climatic factors may be used to evaluate the impact of changes in climatic factors on the pavement performance and service life.

The accuracy of the QE Model was evaluated by comparing in-situ volumetric water contents predicted using the QE Model, to the measured in-situ volumetric water contents at similar times and locations within subgrades. The QE Model was also verified by comparing F_{env} values calculated using in-situ volumetric water contents predicted using the QE Model, to F_{env} values calculated using the measured in-situ volumetric water contents. The verification of the QE Model was conducted using rigid and flexible pavement sections in wet freeze and wet no-freeze climates. The sites and pavement sections which were used for verifying the QE Model are different from those used in the development of the QE Model. The verification strategy was implemented to evaluate the accuracy of the QE Model in predicting the impact of climatic factors on the in-situ volumetric water contents within subgrades and associated resilient moduli.

7.4 The In-situ Pavement Sections used for Verifying the Quantitative Empirical Model

The Quantitative Empirical Model (the QE Model) was verified using climatic data, in-situ volumetric water contents, and pavement material properties (the model input parameters) from pavement sections from the four sites listed below:

- A site in Nebraska, United States on US Highway 81 which forms part of the long-term pavement performance (LTPP) and the seasonal monitoring program (SMP) with State Code 31 and SHRP ID 0114 (Site A);
- A site in Fort Smith, Arkansas, United States on Highway 253, near the intersection of Highway 540 and highway 253 (Site B);
- A site in Ohio, United States on US Highway 23 which forms part of LTPP and SMP with State Code 39 and SHRP ID 0108 (Site C); and
- A site in Ohio, United States on US Highway 23 which forms part of LTPP and SMP with State Code 39 and SHRP ID 0203 (Site D).

The construction of Site A and Site B was completed on 1st July 1995, and 1st June 2002 respectively. The construction of Site C and Site D was completed on 1st November 1995 and 1st September 1996 respectively. Site A, Site C and Site D are in a wet freeze climatic zone, and Site B is in a wet no-freeze climatic zone (the model verification sites). The model verification sites are independent of the Minnesota and Indiana LTPP and SMP sites used for the development of the QE Model.

7.4.1 Pavement Cross-section Details

The pavement cross-section details and the subgrade classification for each pavement section used for verifying the QE Model are presented in Table 7.1 and Table 7.2 respectively.

Table 7.1: Pavement cross-section details for the model verification sites: Site A, Site C and Site D (LTPP and SMP database 2020); Site B (Hall, et al 2013)

Pavement component	Description	Layer Thickness (mm)			
		Site A	Site B	Site C	Site D
Wearing course	AC	165	230	168	-
	PCC	-	-	-	285
Base course	Unbound granular	610	100	205	155
	Treated granular	-	-	100	
Subbase	Unbound granular	-	-	-	-
Subgrade	Engineered fill	305	-	-	-

Table 7.2: Classification of subgrades for the model verification sites: Site A, Site C and Site D (LTPP and SMP database 2020); Site B (Hall, et al 2013)

Property	Site A	Site B	Site C	Site D
Subgrade classification	A-7-6	A-6	A-6	A-6
	silty Clay	clayey Gravel with sand	silty Clay	silty Clay

7.5 Tasks Conducted for the Verification of the Quantitative Empirical Model

The verification of the Quantitative Empirical Model (the QE Model) consisted of ten tasks listed below:

- Task A: Determined input data for the QE Model, and the resilient modulus of each subgrade at the optimum volumetric water content and at the maximum dry density (M_{Ropt}). The input data include the subgrade properties, wearing course properties, water table elevation, and properties of liquid water and water vapour;
- Task B: Obtained climatic data for each climatic factor used as input for the QE Model;
- Task C: Compared the measured in-situ water contents to the calculated water contents. The comparison was conducted to evaluate the suitability of the measured in-situ water contents for evaluating the accuracy of the 2-D FEA models and the QE Model in predicting in-situ water contents within subgrades;
- Task D: Used the data obtained in Task A to Task C as input in the QE Model summarized in Eq. 6.27 to Eq. 6.33, and calculated volumetric water contents output;
- Task E: Reviewed and analyzed the accuracy of the in-situ volumetric water contents predicted using the QE Model. The accuracy of the QE Model was evaluated by comparing the in-situ volumetric water content values predicted using the QE Model to the measured in-situ volumetric water content values at similar times and locations within subgrades;

- Task F: Compared the in-situ volumetric water contents predicted using the QE Model to the in-situ volumetric water contents predicted using EICM. This comparison was conducted to evaluate the accuracy of the QE Model relative to the accuracy of EICM in predicting the impact of climatic factors on the measured in-situ volumetric water contents;
- Task G: Calculated the unfrozen composite environmental adjustment factor (the unfrozen F_{env}) values using the in-situ volumetric water contents predicted using the QE Model, and using Eq. 6.35 and Eq. 6.36 (the F_{envCF} values). The unfrozen F_{env} values were also calculated using the in-situ volumetric water contents predicted using the EICM, and using Eq. 3.1 and Eq. 3.2 (the F_{env} values). The unfrozen F_{env} values were also calculated using the measured in-situ volumetric water contents, and using Eq. 3.1 and Eq. 3.2 (the measured in-situ F_{env} values). The F_{envCF} values and the F_{env} values were compared to the measured in-situ F_{env} values. This analysis was conducted to verify the suitability of volumetric water contents predicted using the QE Model and EICM for use in calculating the impact of climatic factors on the measured in-situ F_{env} of subgrades;
- Task H: Calculated resilient moduli values using the F_{envCF} values as input in Eq. 6.37 (M_{RCF} values). The resilient moduli values were also calculated using the F_{env} values as input in Eq. 3.4 (M_R values). The resilient moduli values were also calculated using the measured in-situ F_{env} values as input in Eq. 3.4 (the measured in-situ M_R values). The M_{RCF} values and the M_R values were compared to the measured in-situ M_R values. This analysis was conducted to verify the suitability of volumetric water contents predicted using the QE Model and EICM for use in calculating the impact of climatic factors on the measured in-situ resilient moduli of subgrades;
- Task I: Evaluated the general trends in the predicted cumulative in-situ volumetric water contents; and
- Task J: Coefficient of determination (R^2) analysis was conducted to determine the accuracy of the QE Model in predicting in-situ volumetric water contents. The summary of the R^2 analysis is presented in Section 5.3.2. Two-tailed F-test was also conducted to determine the accuracy of the QE Model vs EICM in predicting in-situ volumetric water contents for calculating the in-situ F_{env}. The summary of the Two-tailed F-test is presented in Section 5.4.5.

7.5.1 Task A: Determined Input Data for Materials and Water for the Quantitative Empirical Model

The hydraulic properties of subgrades, and initial degree of saturation used as input for verifying the QE Model are presented in Table 7.3 and Table 7.4. The hydraulic properties for the Portland cement concrete wearing course, asphalt concrete wearing course, and the depth to water table are presented in Table 7.5.

The liquid water and water vapour thermal properties, and density used as input in the QE Model are presented in Table 7.6.

Table 7.3: Input parameters for subgrades: Site A (LTPP and SMP database 2020; Wösten et al. 1999); Site B (Hall, et al 2013; Wösten et al. 1999)

Subgrade Properties	Site A	Site B
Initial degree of saturation (S_i)	0.74	0.75
Saturated hydraulic conductivity (k_{sat}), (m / s)	3.0 x 10^{-8}	9.0 x 10^{-6}
Residual hydraulic conductivity (k_{res}), (m / s)	3.0 x 10^{-11}	9.0 x 10^{-9}
Volumetric water content at end of pavement construction (θ_{t0})	0.35	0.30

Table 7.4: Input parameters for subgrades: Site C and Site D (LTPP and SMP database 2020; Wösten et al. 1999)

Subgrade Properties	Site C	Site D
Initial degree of saturation (S_i)	0.74	0.74
Saturated hydraulic conductivity (k_{sat}), (m / s)	3.0 x 10^{-9}	3.0 x 10^{-9}
Residual hydraulic conductivity (k_{res}), (m / s)	3.0 x 10^{-11}	3.0 x 10^{-11}
Volumetric water content at end of pavement construction (θ_{t0})	0.37	0.38
Resilient modulus at optimum conditions (M_{Ropt}), (MPa)	87	102

Table 7.5: Input parameters for wearing courses and water table: Site A, Site C and Site D (LTPP and SMP database 2020; Wösten et al. 1999); Site B (Hall, et al 2013; Wösten et al. 1999))

Pavement Properties	site A	Site B	Site C	Site D
Initial degree of saturation	0.75	0.75	0.75	0.75
Depth to water table below subgrade surface (m)	4.2	2.1	1.3	1.3

Table 7.6: Input parameters for the liquid water and water vapour (Online 2023)

Properties	Value
Specific heat capacity of liquid water at 25 ºC (MJ / (kg ºC))	0.0042
Heat of vaporization of liquid water (MJ / kg)	2.27
Density of water at 25 ºC (kg / m^3)	1000.0
Vapour pressure of water at equilibrium (kg / m^2)	244.7
Thermal diffusivity of water vapour at 1 atm, 100 ºC (m^2 / day)	2.2118
Thermal diffusivity of liquid water at 25 ºC (m^2 / day)	0.0126
Density of water vapour at 20 ºC (kg / m^3)	0.013
Gravitational acceleration (m / s^2)	9.81

7.5.2 *Task B: Obtained Input Climatic Factors for use in the Quantitative Empirical Model*

The climatic factors used as input in the QE Model were obtained from the LTPP and SMP database (2020). The climatic factors consist of site-specific historical daily climatic data obtained using the Modern Era Retrospective-Analysis for Research and Applications (MERRA). MERRA was developed by the National Aeronautics and Space Administration (NASA). Climatic factors used for verifying the QE Model consist of 15 to 25 years of data. The time period used for collecting climatic factors was based primarily on capturing specific days in the climatic factors dataset. This method was used so that the impact of the climatic factors on the predicted and measured in-situ volumetric water contents can be compared on the corresponding days that the measured in-situ volumetric water contents were collected.

The analysis of the climatic data indicated that it is useful to use many years of climatic factors to capture trends in climatic factors over time. The analysis of long-tern climatic factors is conducted by incorporating the average of climate factors over a 10-year to 30-year period (Climate Normals) to capture the long-term climatic trends due to natural and man-made factors (NCEI 2022; NOAA 2022). However, Climate Normals were not used in verifying the QE Model.

Climatic Data for Site A

The climatic factors for Site A used as input for verifying the Quantitative Empirical Model are presented in Figure 7.1 to Figure 7.5.

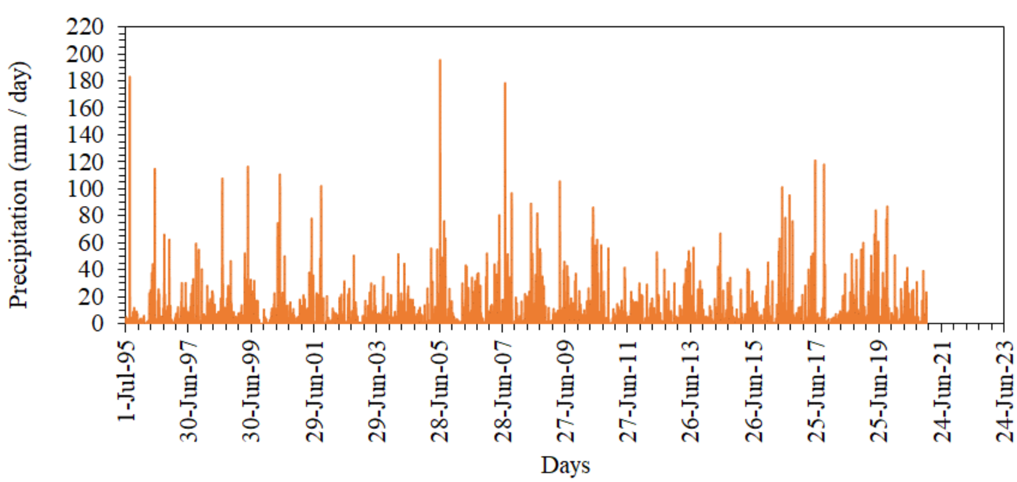

Figure 7.1: Precipitation data used as input for verifying the Quantitative Empirical Model

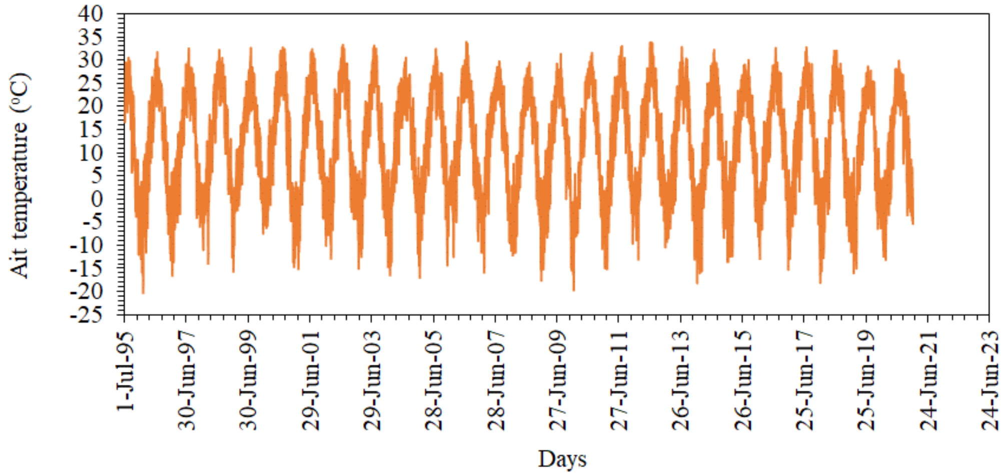

Figure 7.2: Air temperature data used as input for verifying the Quantitative Empirical Model

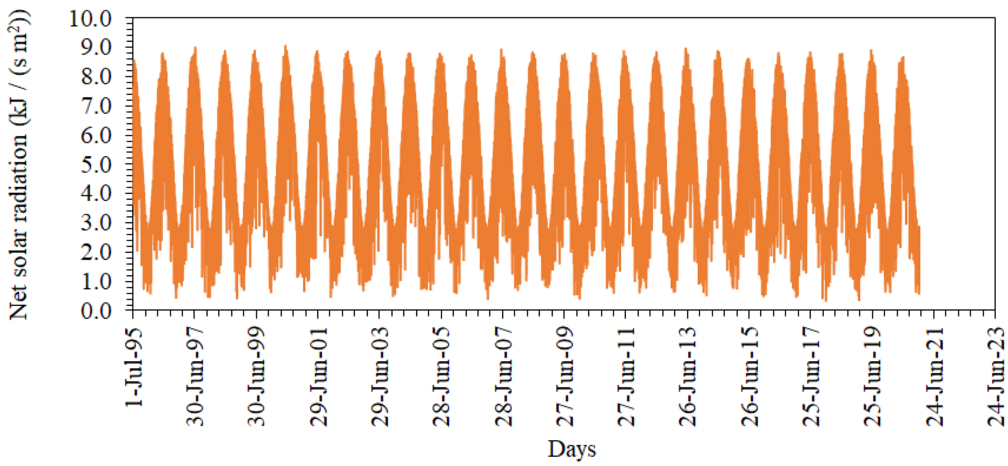

Figure 7.3: Net solar radiation data used as input for verifying the Quantitative Empirical Model

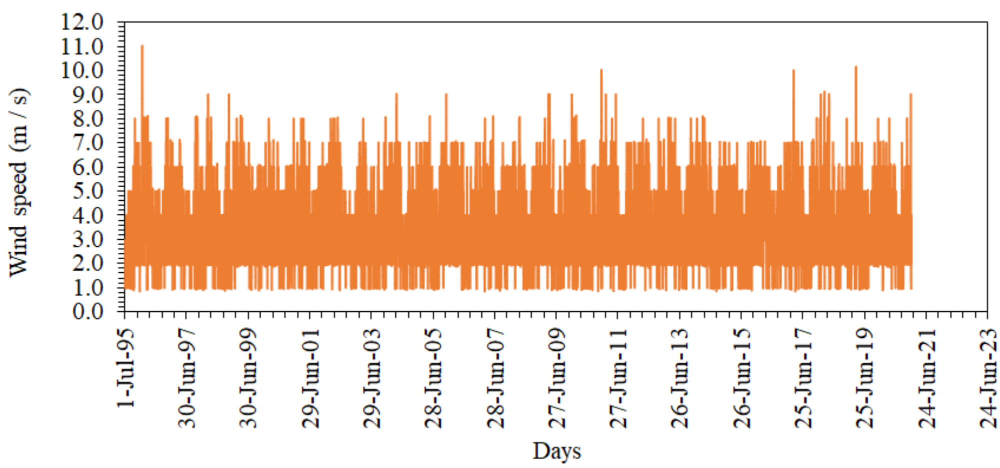

Figure 7.4: Wind speed data used as input for verifying the Quantitative Empirical Model

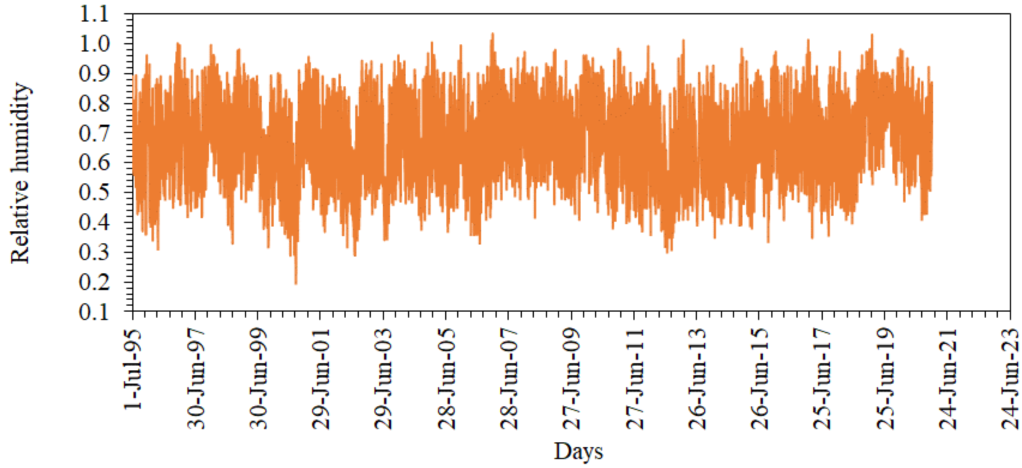

Figure 7.5: Relative humidity data used as input for verifying the Quantitative Empirical Model

Climatic Data for Site B

The climatic factors for Site B used as input for verifying the Quantitative Empirical Model are presented in Figure 7.6 to Figure 7.10.

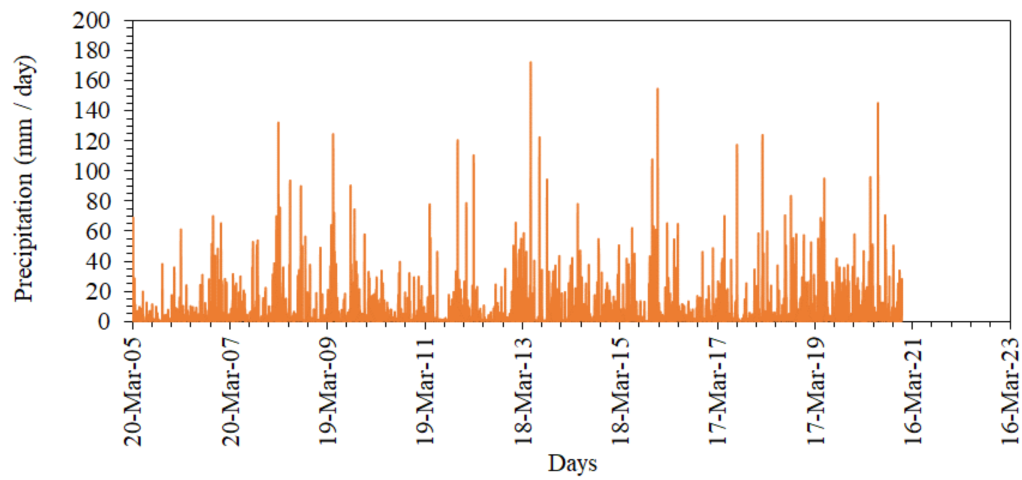

Figure 7.6: Precipitation data used as input for verifying the Quantitative Empirical Model

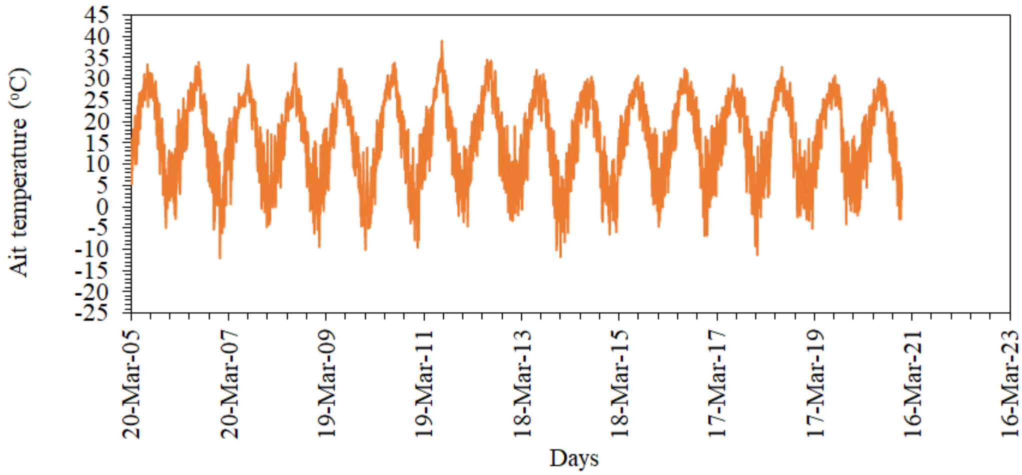

Figure 7.7: Air temperature data used as input for verifying the Quantitative Empirical Model

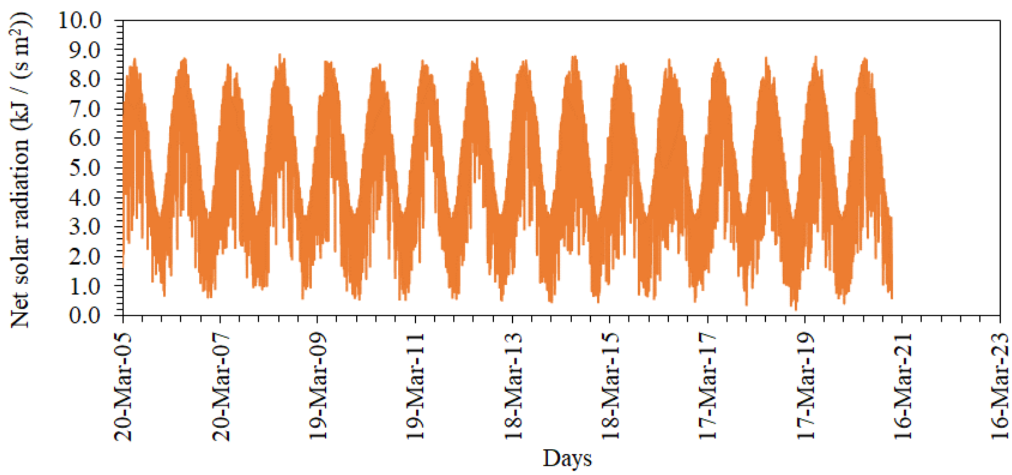

Figure 7.8: Net solar radiation data used as input for verifying the Quantitative Empirical Model

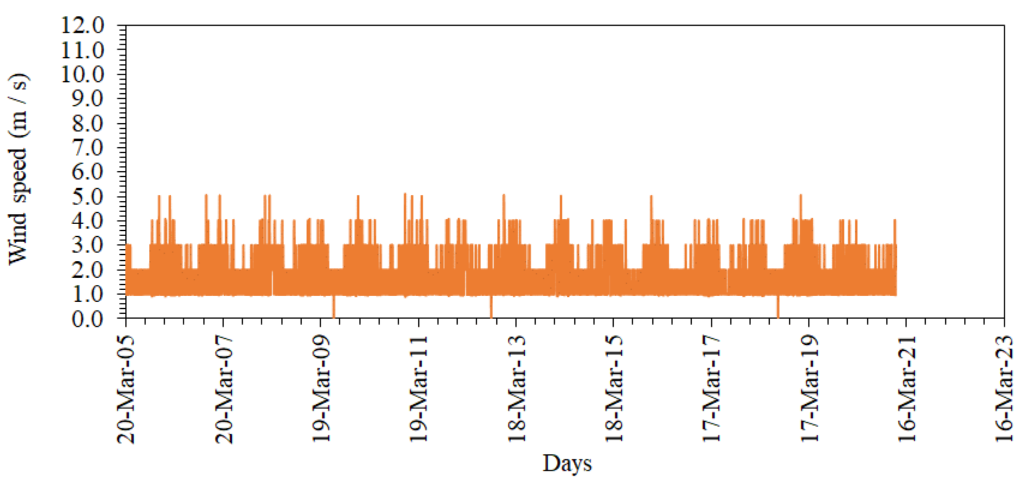

Figure 7.9: Wind speed data used as input for verifying the Quantitative Empirical Model

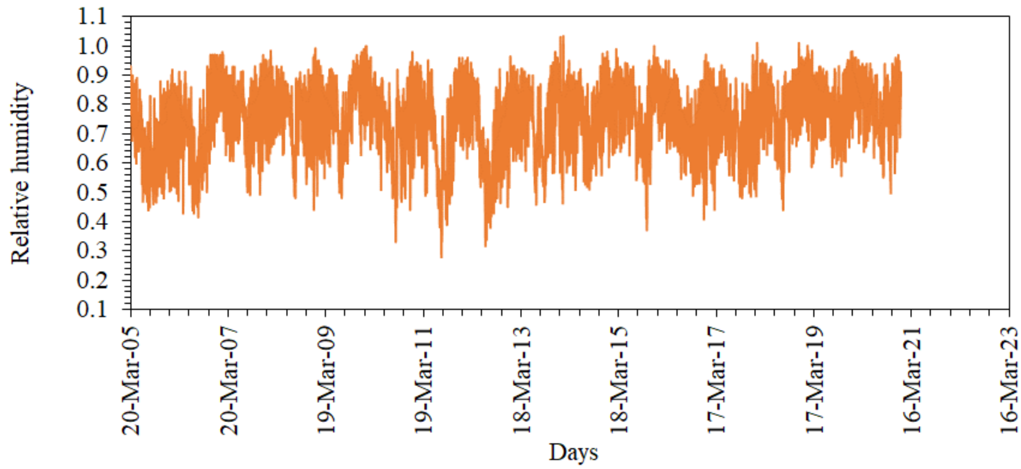

Figure 7.10: Relative humidity data used as input for verifying the Quantitative Empirical Model

<u>*Climatic Data for Site C and Site D*</u>

The climatic factors for Site C and Site D used as input for verifying the Quantitative Empirical Model (the QE Model) are presented in Figure 7.11 to Figure 7.15. Site C and Site D are approximately 450.0 m apart on adjacent traffic lanes. Hence, the same climatic factors are used as input in the QE Model for both sites.

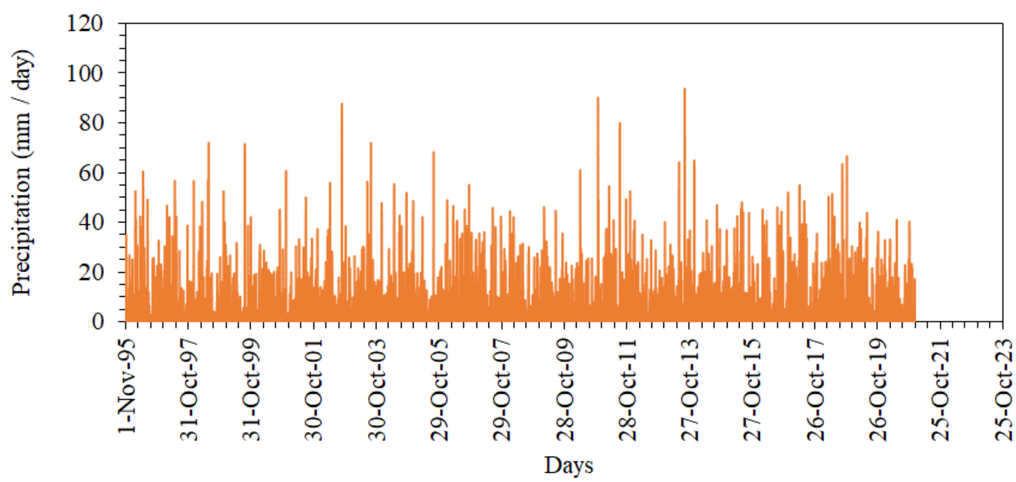

Figure 7.11: Precipitation data used as input for verifying the Quantitative Empirical Model

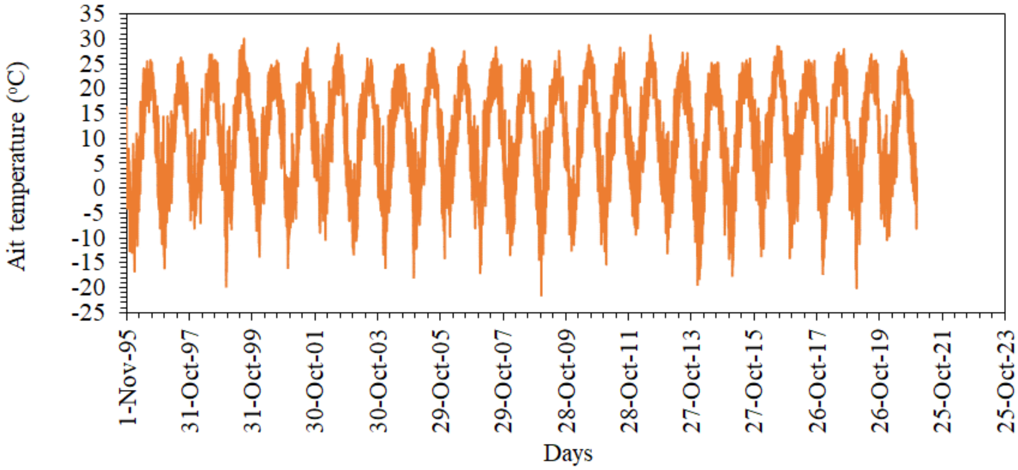

Figure 7.12: Air temperature data used as input for verifying the Quantitative Empirical Model

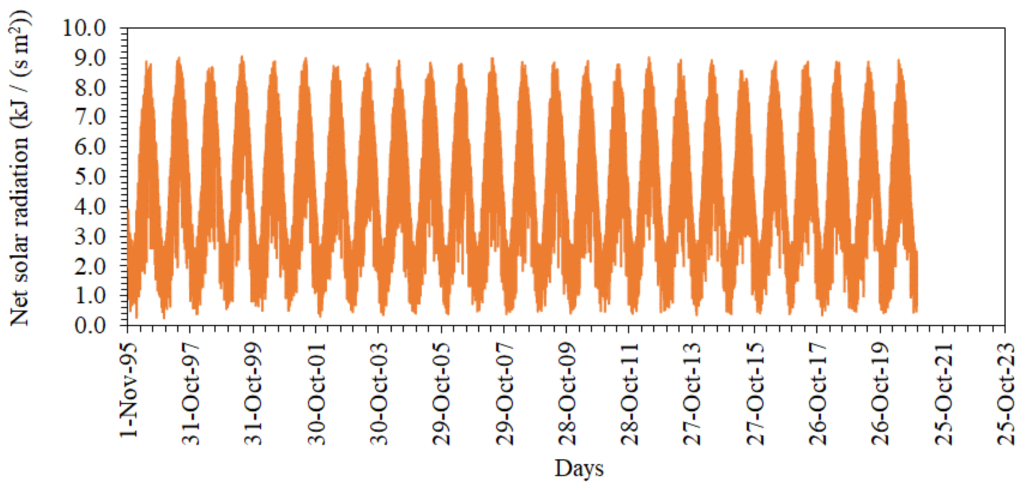

Figure 7.13: Net solar radiation data used as input for verifying the Quantitative Empirical Model

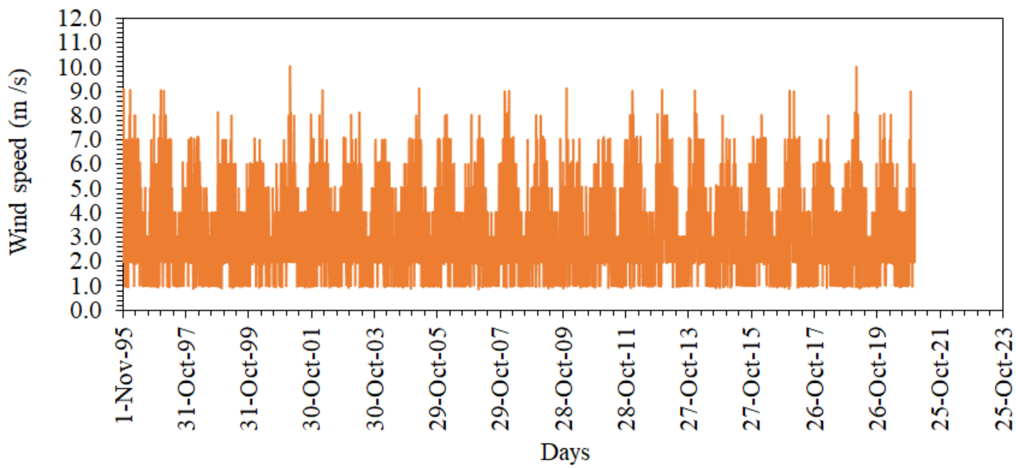

Figure 7.14: Wind speed data used as input for verifying the Quantitative Empirical Model

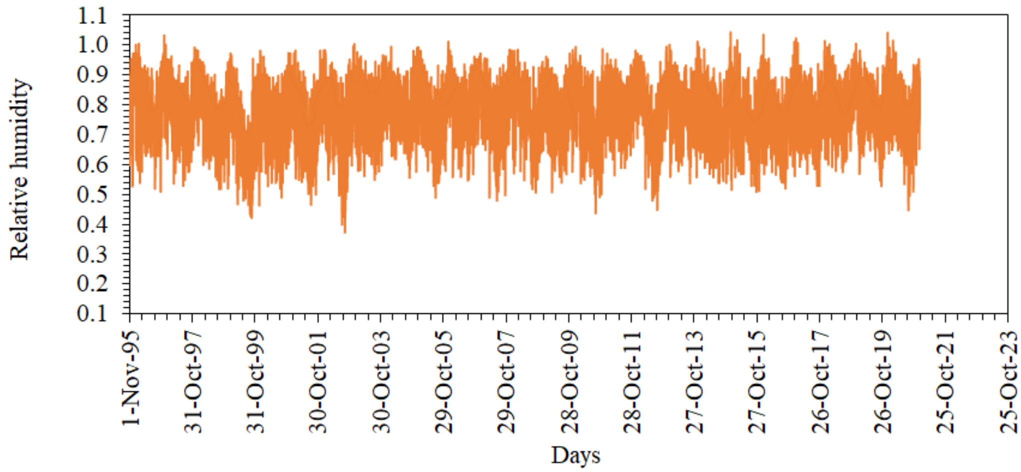

Figure 7.15: Relative humidity data used as input for verifying the Quantitative Empirical Model

7.5.3 Task C: Comparison of Calculated and Measured In-situ Water Contents: Sites A, B, C and D

The four sites used for verifying the Quantitative Empirical Model (the QE Model) and EICM include a site in Nebraska, United States (Site A), a site in Fort Smith, Arkansas, United States (Site B), and two sites in Ohio, United States (Site C and Site D). The accuracy of measured in-situ volumetric water contents for the four sites which were used for verifying the QE Model and EICM are presented in Figure 7.16.

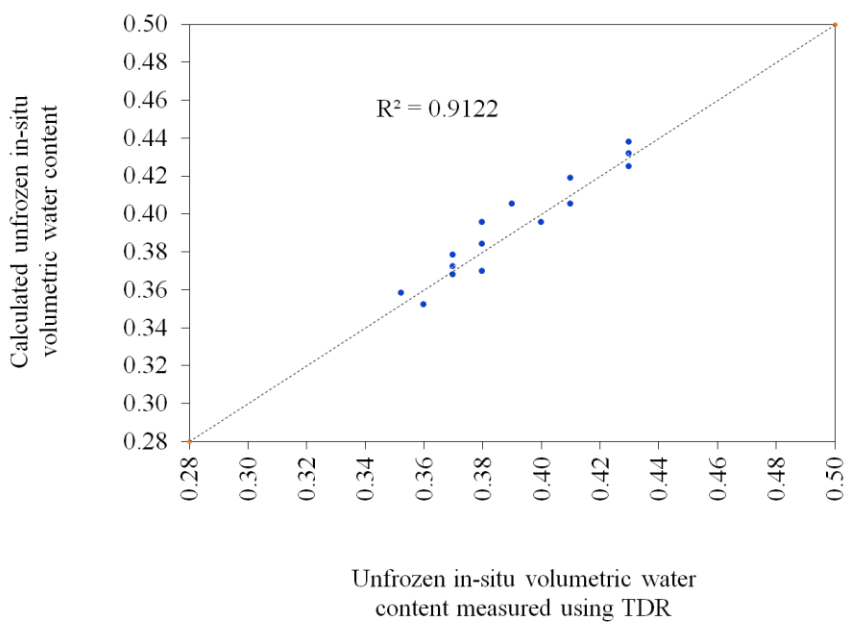

Figure 7.16: Calculated vs measured In-situ volumetric water contents

7.5.4 Task D: Calculated In-situ Volumetric Water Contents using the Quantitative Empirical Model

The Quantitative Empirical Model (the QE Model) presented in Eq. 6.27 to Eq. 6.30 and *f-functions* presented in Eq. 6.31 to Eq. 6.33 were inserted into an Excel spreadsheet. The input data for the materials, water table, liquid water and water vapour properties (water properties), and climatic factors were inserted into a separate Excel spreadsheet. Each input data point was linked to its respective material, water table and water property input parameter in *f-functions*. Each input climatic factor data point was then linked to its respective input parameter in Eq. 6.30.

Daily changes in the predicted in-situ volumetric water contents within subgrades were calculated from time "*0*" (the construction completion date for the wearing courses) to the end of the analysis period (ranged from 7,300 days to 13,870 days) for the four verification sites. The analysis of the in-situ volumetric water contents predicted using the QE Model indicated daily changes in the predicted in-situ volumetric water contents within subgrades. The daily changes in the in-situ volumetric water contents are associated with daily fluctuations above and below the initial volumetric water content within subgrades (measured at the end of the construction of the wearing courses). The daily fluctuations in in-situ volumetric water contents are due to daily changes in climatic factors. Hence, the total predicted in-situ volumetric water content for each day is calculated by adding the change in the predicted in-situ volumetric water content for each day to the initial volumetric water content.

7.5.5 Task E: Compared the Quantitative Empirical Model Output to Measured Volumetric Water Contents

The analyses conducted to evaluate the accuracy of the Quantitative Empirical Model (the QE Model) in predicting in-situ volumetric water contents were conducted using four independent pavement sections (the verification of the QE Model). Site A, Site B and Site C are flexible pavement sections and Site D is a rigid pavement section. Site A, Site C and Site D are in a wet freeze climate and Site B is in a wet no-freeze climate.

The verification of the QE Model was conducted by comparing the in-situ volumetric water contents predicted using the QE Model (predicted in-situ volumetric water contents) to the measured in-situ volumetric water contents. The predicted and measured in-situ volumetric water contents were obtained at a depth of 150.0 mm below the subgrade surface for each pavement section. The analysis conducted for verifying the QE Model also included comparing the accuracy of the QE Model against the accuracy of EICM in predicting in-situ volumetric water contents. This was done by comparing the in-situ volumetric water contents predicted using the QE Model and using EICM, to the measured in-situ volumetric water contents. The predicted and measured in-situ volumetric water contents were also compared on corresponding days.

The QE Model was also verified against EICM using the unfrozen composite environmental adjustment factor (F_{env}). The F_{env} values were calculated using the respective unfrozen environmental adjustment factor (F_U) as an input. The F_U values were calculated using the in-situ volumetric water contents predicted using the QE Model and EICM (the predicted in-situ F_U). The F_U values were also calculated using the measured in-situ volumetric water contents (the measured in-situ F_U). The predicted in-situ F_{env} values were calculated using the predicted in-situ F_U values, and the measured in-situ F_{env} values were calculated using the measured in-situ F_U values for both sites. The predicted in-situ F_{env} values were compared to the measured in-situ F_{env} values. The QE Model was also verified by comparing the predicted in-situ M_R values to the measured in-situ M_R values. The comparison was conducted for each site at the corresponding time and at a depth of 150.0 mm below the subgrade surface. This analysis was conducted to evaluate the suitability of the predicted in-situ volumetric water contents for use in calculating the degree of saturation used as input to calculate the F_U values. This analysis was also conducted to evaluate whether the predicted in-situ volumetric water contents account for the impact of climatic factors on the F_{env} and associated resilient moduli of subgrades.

Compared Quantitative Empirical Model Output to Measured In-situ Volumetric Water Content: Site A

The verification of the Quantitative Empirical Model (the QE Model) for Site A was conducted using volumetric water contents which were measured and predicted from August to December 1995, and from February to August 1996 as shown in Figure 7.17 and Figure 7.18 respectively. The analyses of data presented in Figure 7.17 and Figure 7.18 show that the QE Model predicts in-situ volumetric water contents at Site A within $\pm$ 0.02 from the measured in-situ volumetric water contents. The analyses of data presented in Figure 7.17 and Figure 7.18 also show that the QE Model accurately predicts changes in, and total volumetric water contents within subgrades due to changes in climatic factors over time. These analyses also show a good correlation between the predicted and measured in-situ volumetric water contents within subgrades.

<u>*Comparing the Quantitative Empirical Model Output to In-situ Volumetric Water Contents: Site A in 1995*</u>

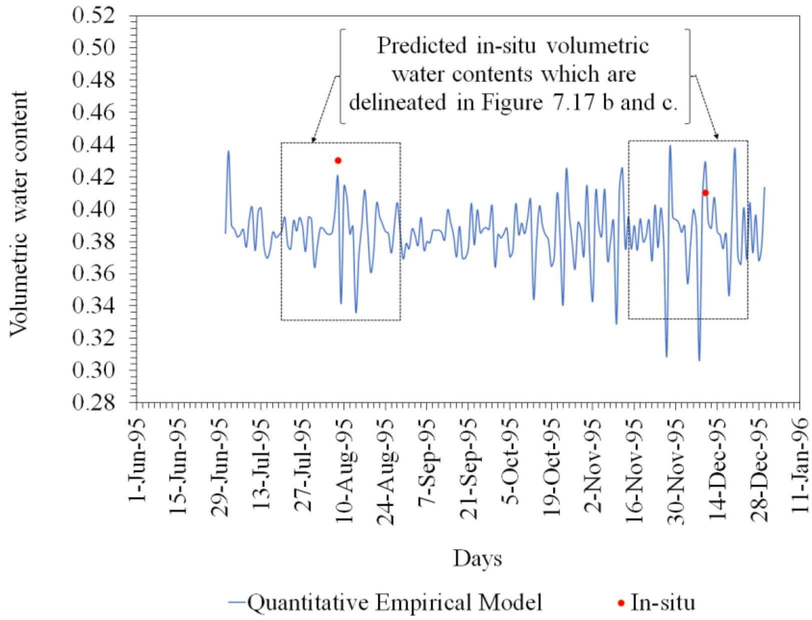

(a)

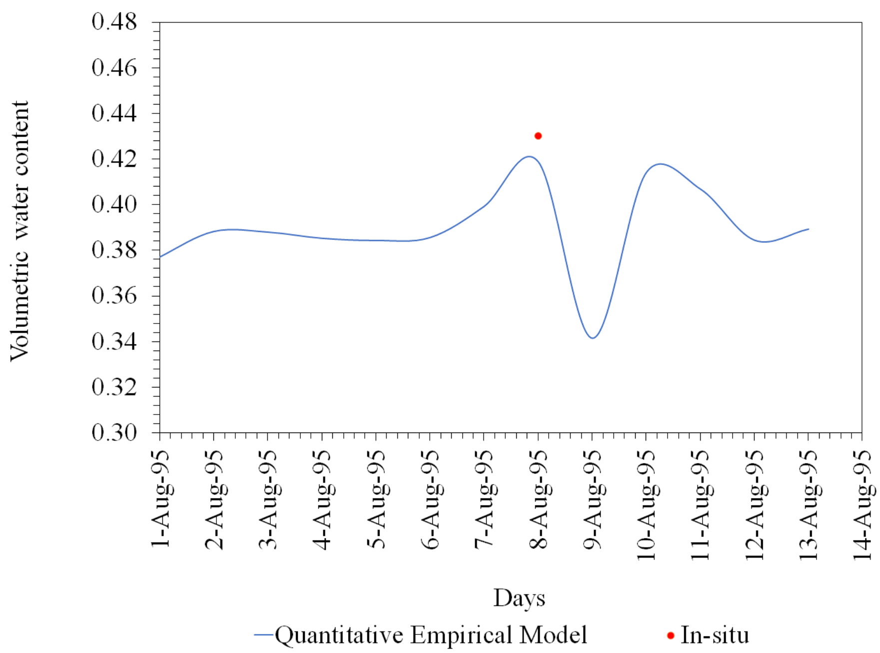

(b)

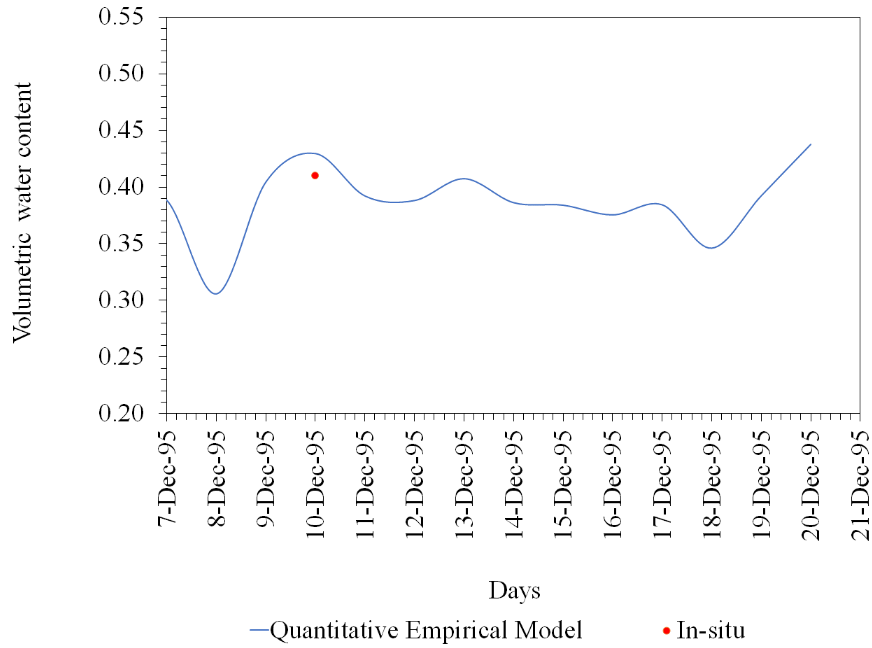

(c)

Figure 7.17: Measured vs predicted in-situ volumetric water contents obtained using the QE Model

<u>Comparing the Quantitative Empirical Model Output to In-situ Volumetric Water Contents: Site A in 1996</u>

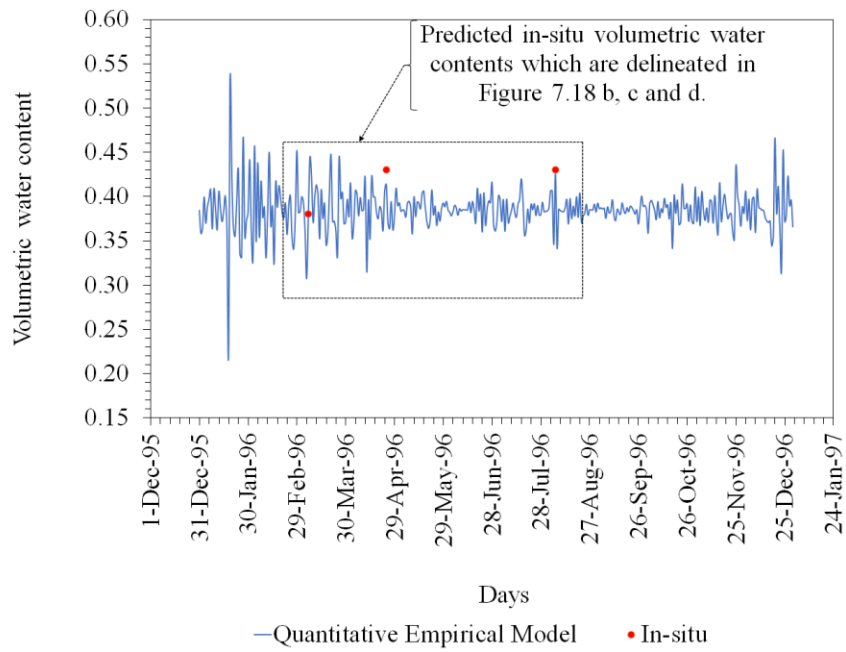

(a)

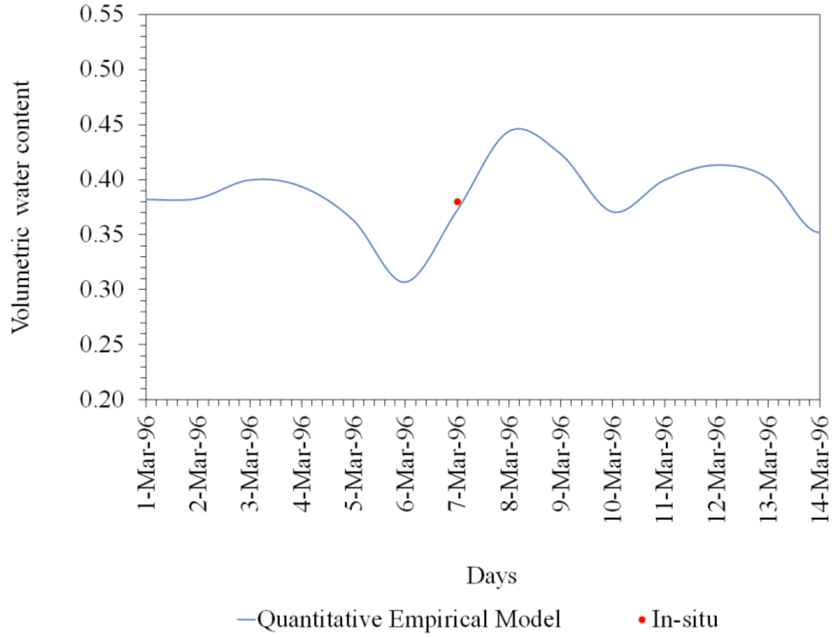

0.55
0.50
0.45
0.40
0.35
0.30
0.25
0.20
Volumetric water content
1-Mar-96
2-Mar-96
3-Mar-96
4-Mar-96
5-Mar-96
6-Mar-96
7-Mar-96
8-Mar-96
9-Mar-96
10-Mar-96
11-Mar-96
12-Mar-96
13-Mar-96
14-Mar-96
Days
Quantitative Empirical Model
In-situ

(b)

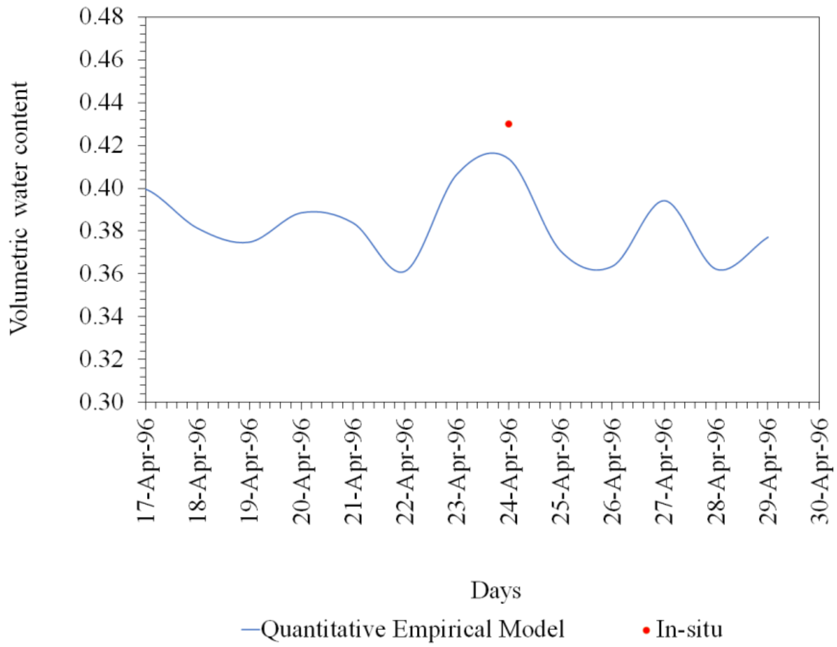

0.48
0.46
0.44
0.42
0.40
0.38
0.36
0.34
0.32
0.30
Volumetric water content
17-Apr-96
18-Apr-96
19-Apr-96
20-Apr-96
21-Apr-96
22-Apr-96
23-Apr-96
24-Apr-96
25-Apr-96
26-Apr-96
27-Apr-96
28-Apr-96
29-Apr-96
30-Apr-96
Days
Quantitative Empirical Model
In-situ

(c)

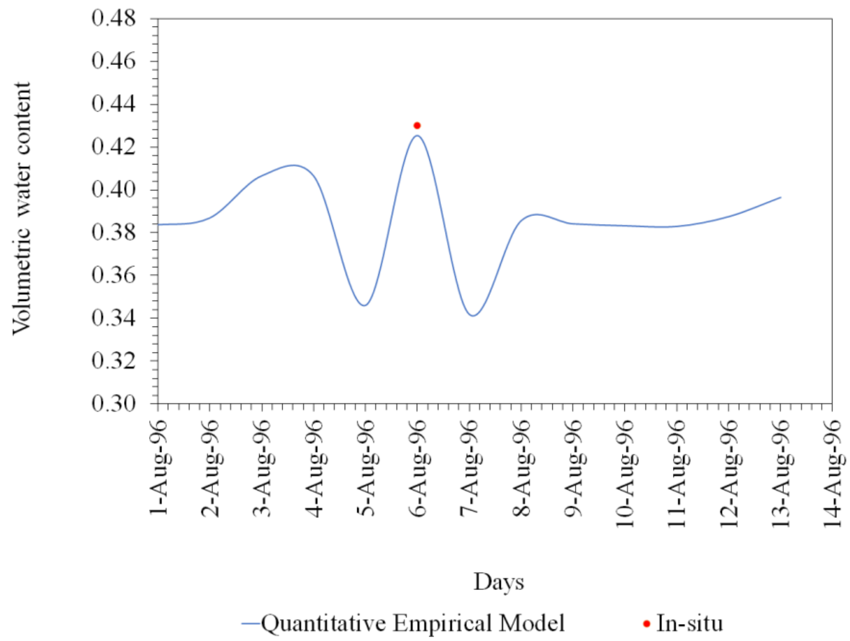

(d)

Figure 7.18: Measured vs predicted in-situ volumetric water contents obtained using the QE Model

Comparing Quantitative Empirical Model Output to Measured In-situ Volumetric Water Content: Site B

The verification of the Quantitative Empirical Model (the QE Model) for Site B was conducted using volumetric water contents which were measured and predicted from August to December 1995 as shown in Figure 7.19. The analysis of data presented in Figure 7.19 shows that the QE Model predicts in-situ volumetric water contents at Site B within ± 0.02 of the measured in-situ volumetric water contents which was deemed to be acceptable. The analysis of data presented in Figure 7.19 also shows that the QE Model accounts for the influence of freeze and thaw cycles. This observation is highlighted in the minimal predicted volumetric water contents within the subgrade during freezing conditions and the increase in the predicted volumetric water contents within the subgrade immediately after the spring thaw as shown in Figure 7.19a.

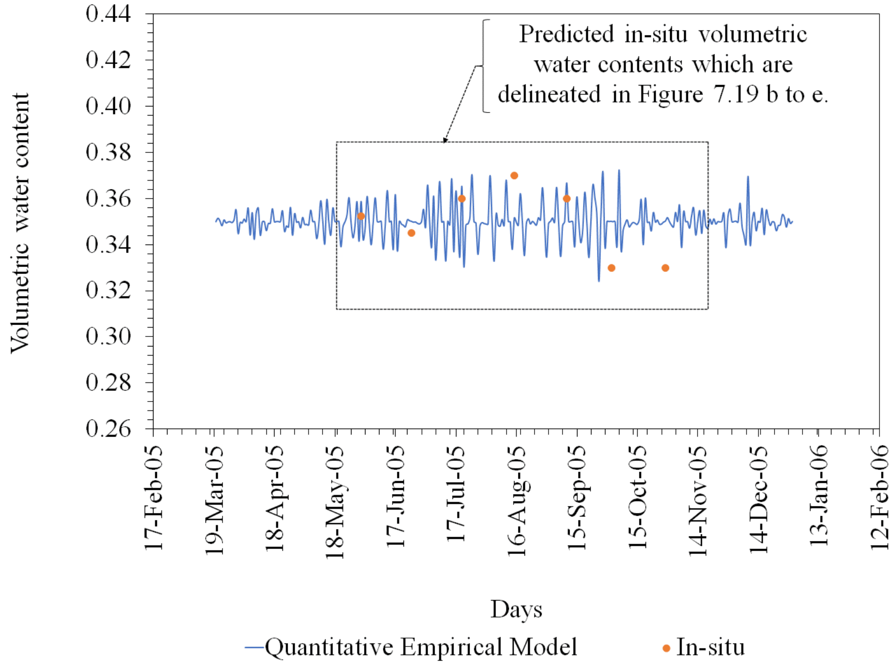
Predicted in-situ volumetric water contents which are delineated in Figure 7.19 b to e.
Volumetric water content
0.44
0.42
0.40
0.38
0.36
0.34
0.32
0.30
0.28
0.26
17-Feb-05
19-Mar-05
18-Apr-05
18-May-05
17-Jun-05
17-Jul-05
16-Aug-05
15-Sep-05
15-Oct-05
14-Nov-05
14-Dec-05
13-Jan-06
12-Feb-06
Days
Quantitative Empirical Model
In-situ

(a)

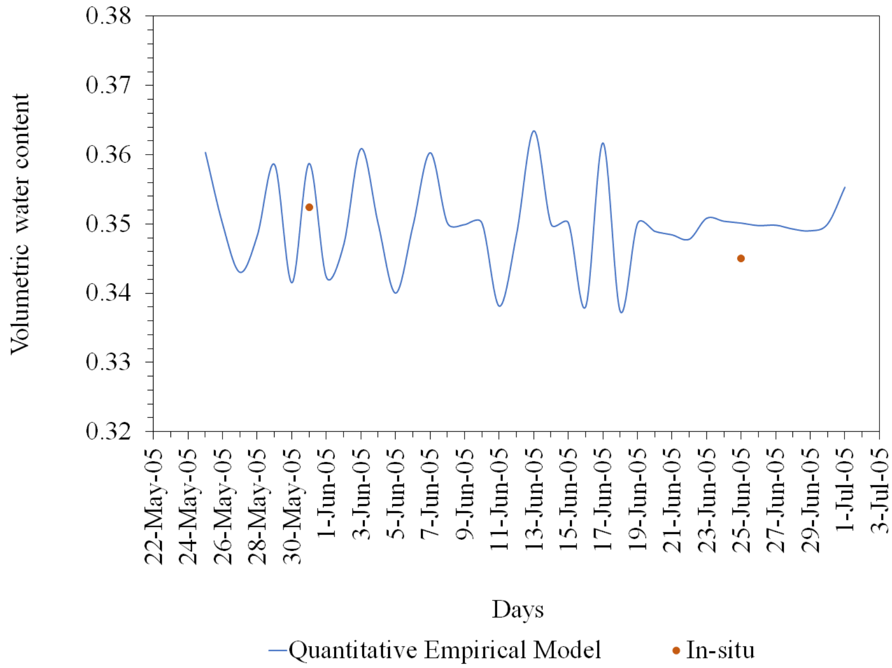
Volumetric water content
0.38
0.37
0.36
0.35
0.34
0.33
0.32
22-May-05
24-May-05
26-May-05
28-May-05
30-May-05
1-Jun-05
3-Jun-05
5-Jun-05
7-Jun-05
9-Jun-05
11-Jun-05
13-Jun-05
15-Jun-05
17-Jun-05
19-Jun-05
21-Jun-05
23-Jun-05
25-Jun-05
27-Jun-05
29-Jun-05
1-Jul-05
3-Jul-05
Days
Quantitative Empirical Model
In-situ

(b)

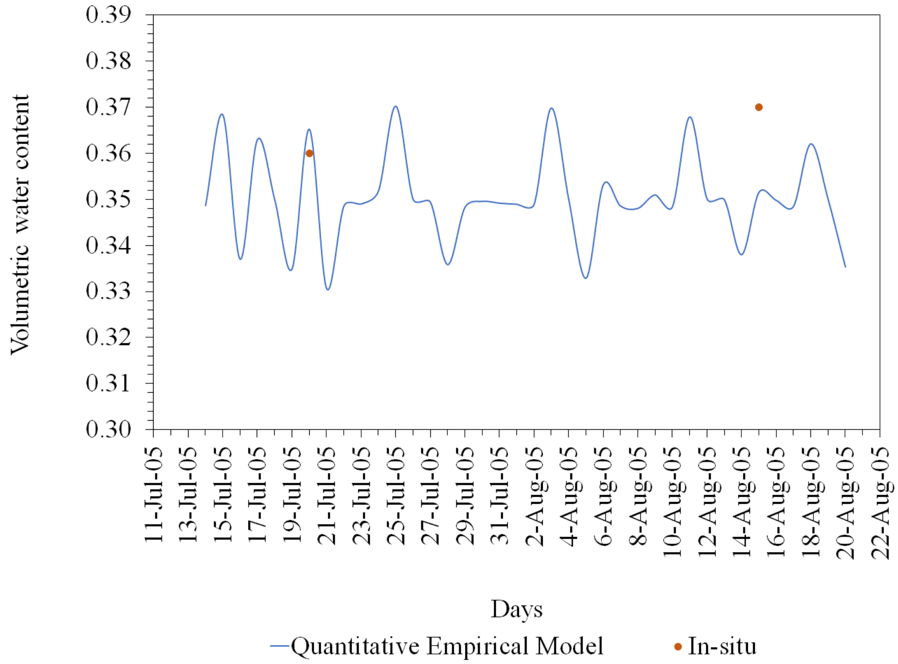
0.39
0.38
0.37
0.36
0.35
0.34
0.33
0.32
0.31
0.30
Volumetric water content
11-Jul-05
13-Jul-05
15-Jul-05
17-Jul-05
19-Jul-05
21-Jul-05
23-Jul-05
25-Jul-05
27-Jul-05
29-Jul-05
31-Jul-05
2-Aug-05
4-Aug-05
6-Aug-05
8-Aug-05
10-Aug-05
12-Aug-05
14-Aug-05
16-Aug-05
18-Aug-05
20-Aug-05
22-Aug-05
Days
Quantitative Empirical Model
In-situ

(c)

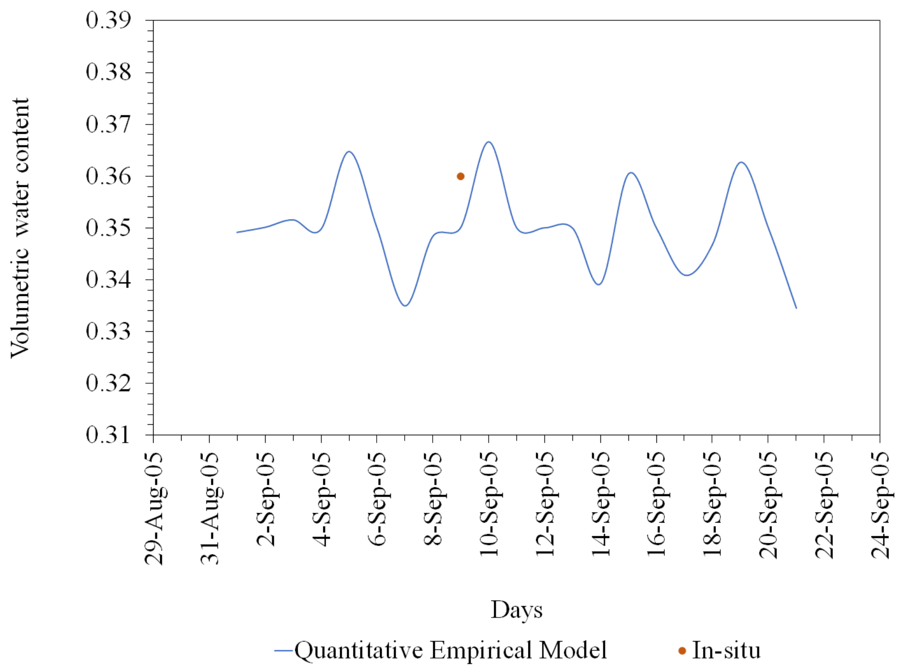
0.39
0.38
0.37
0.36
0.35
0.34
0.33
0.32
0.31
Volumetric water content
29-Aug-05
31-Aug-05
2-Sep-05
4-Sep-05
6-Sep-05
8-Sep-05
10-Sep-05
12-Sep-05
14-Sep-05
16-Sep-05
18-Sep-05
20-Sep-05
22-Sep-05
24-Sep-05
Days
Quantitative Empirical Model
In-situ

(d)

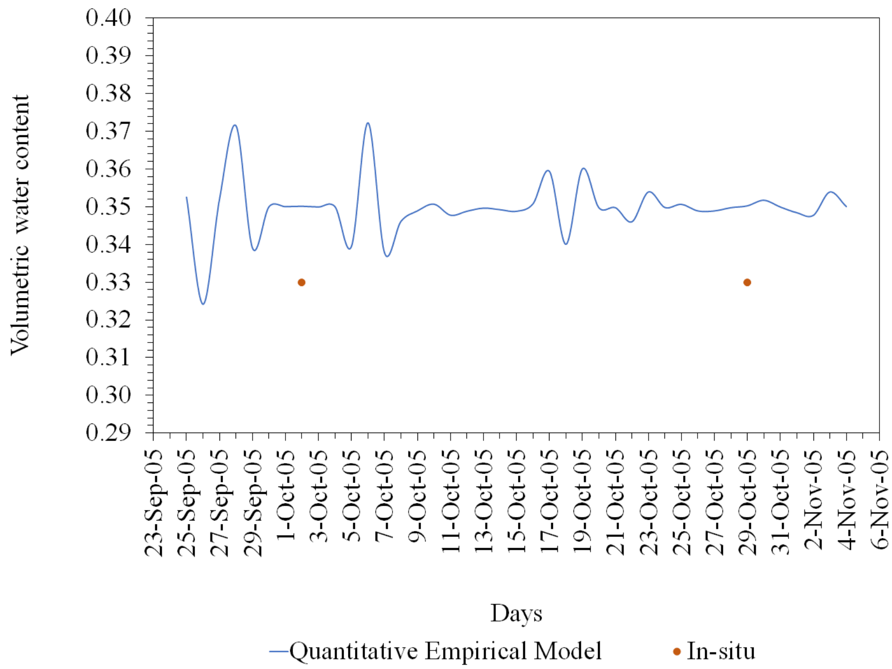

(e)

Figure 7.19: Measured vs predicted in-situ volumetric water contents obtained using the QE Model

7.5.6 Task F: Accuracy of Quantitative Empirical Model vs EICM: Using Volumetric Water Content

The accuracy of the Quantitative Empirical Model (the QE Model)and the accuracy of EICM in predicting in-situ volumetric water contents were also evaluated. This was done by comparing the in-situ volumetric water contents predicted using the QE Model and EICM to the measured in-situ volumetric water contents within the subgrade. These analyses were conducted using the pavement sections at Site C and Site D. The comparison of the accuracy of the QE Model and EICM in predicting in-situ volumetric water contents within the subgrade at Site C and Site D is presented in Figure 7.20 and Figure 7.21 respectively. The analyses of data presented in Figure 7.20 and Figure 7.21 show that the QE Model has a higher accuracy than EICM in predicting in-situ volumetric water contents within subgrades. The QE Model accurately predicts fluctuations in in-situ volumetric water contents due to changes in climatic factors. EICM predicts horizontal clusters in volumetric water contents which indicate that EICM predicts fluctuations in in-situ volumetric water contents poorly. This is due to EICM neglecting the impact of changes in climatic factors on fluctuations in water and heat transfer.

The analysis of data presented in Figure 7.20 and Figure 7.21 also show that the QE Model predicts in-situ volumetric water contents within $\pm$ 0.02 of the measured in-situ volumetric water contents. However, this analysis indicated that EICM generally underestimates in-situ volumetric water contents by 0.06 to 0.13

from the measured in-situ volumetric water contents. EICM underpredicting in-situ volumetric water contents results in EICM overpredicting the in-situ resilient modulus. This results in a pavement structure during the operation period having a lower in-situ resilient modulus relative to the resilient modulus predicted by EICM. This results in the pavement structure being subjected to higher distress including higher rutting under traffic loading. The higher rutting results in a pavement structure with a higher maintenance cost, lower performance and a shorter service life. These observations show that EICM and MEPDG produce uneconomical pavement structures.

Comparing the Quantitative Empirical Model to EICM Using Volumetric Water Contents: Site C: 1997 to 2002.

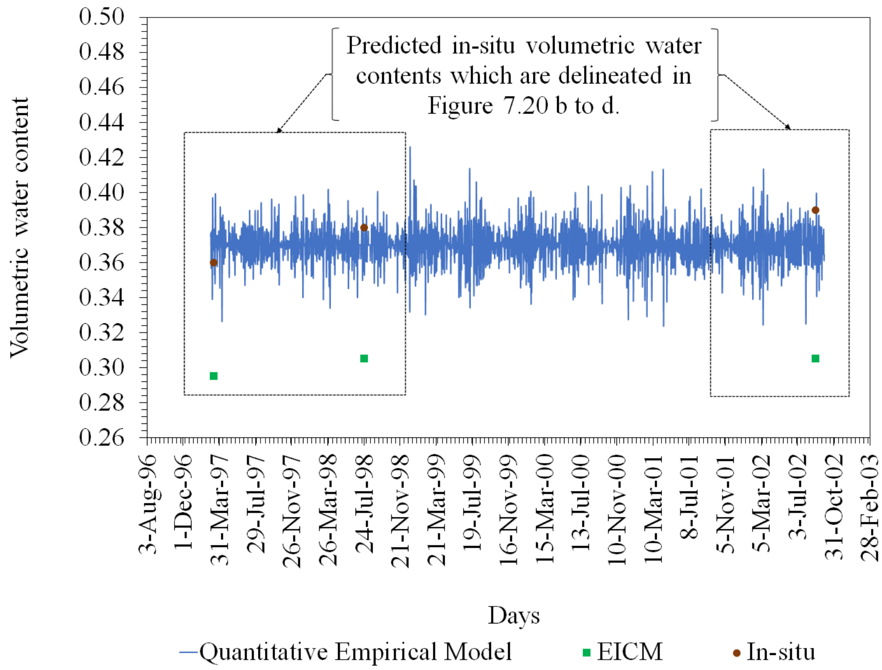

(a)

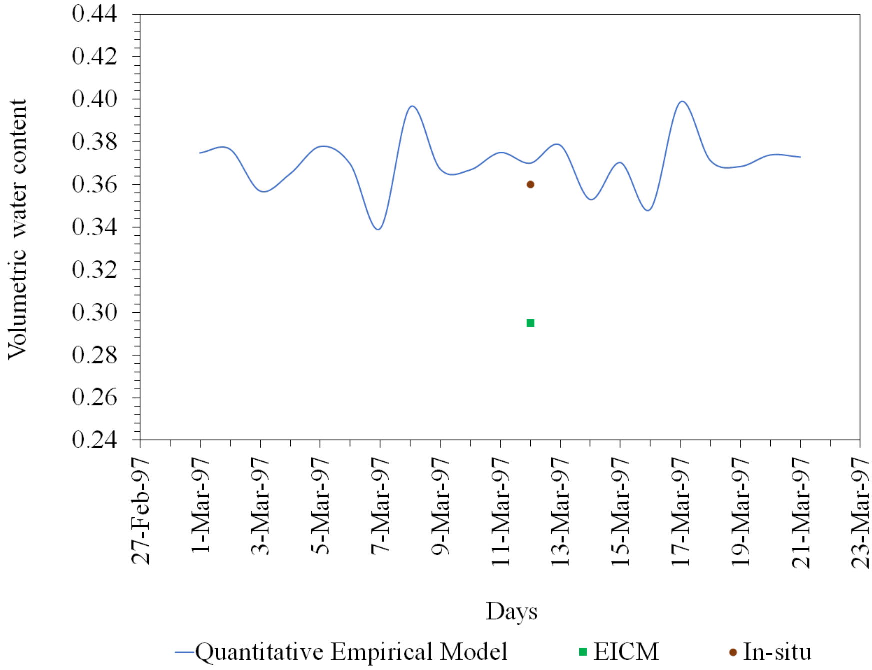
0.44
0.42
0.40
0.38
0.36
0.34
0.32
0.30
0.28
0.26
0.24
Volumetric water content
27-Feb-97
1-Mar-97
3-Mar-97
5-Mar-97
7-Mar-97
9-Mar-97
11-Mar-97
13-Mar-97
15-Mar-97
17-Mar-97
19-Mar-97
21-Mar-97
23-Mar-97
Days
Quantitative Empirical Model
EICM
In-situ

(b)

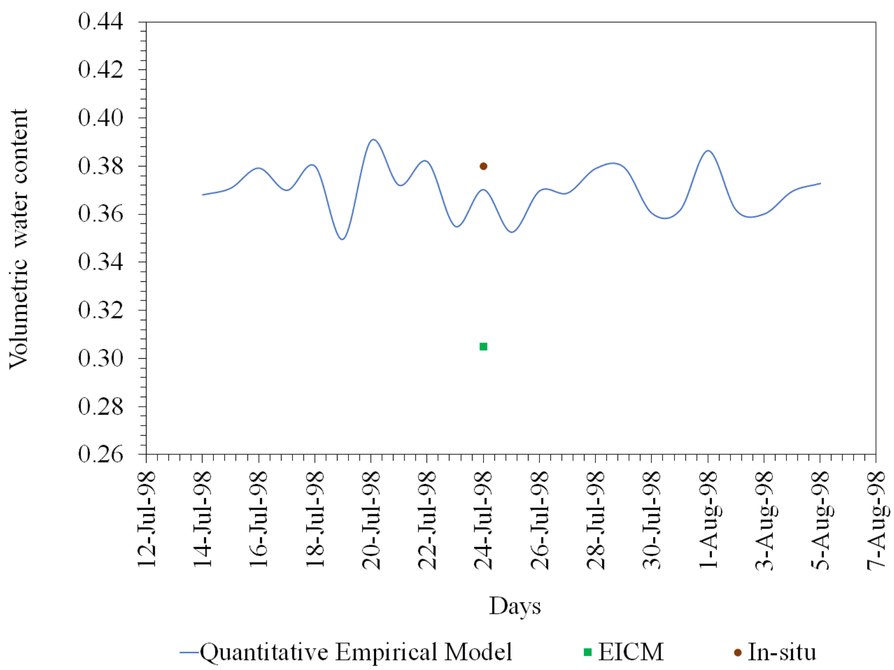
0.44
0.42
0.40
0.38
0.36
0.34
0.32
0.30
0.28
0.26
Volumetric water content
12-Jul-98
14-Jul-98
16-Jul-98
18-Jul-98
20-Jul-98
22-Jul-98
24-Jul-98
26-Jul-98
28-Jul-98
30-Jul-98
1-Aug-98
3-Aug-98
5-Aug-98
7-Aug-98
Days
Quantitative Empirical Model
EICM
In-situ

(c)

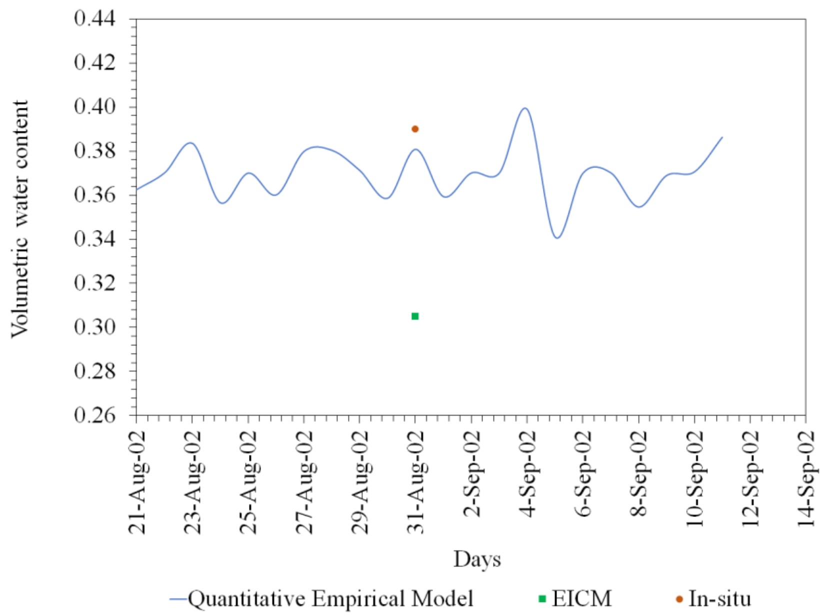

(d)

Figure 7.20: Measured vs predicted in-situ volumetric water contents obtained using the QE Model and EICM

Comparing the Quantitative Empirical Model to EICM Using Volumetric Water Contents from Site D: 1997 to 2001.

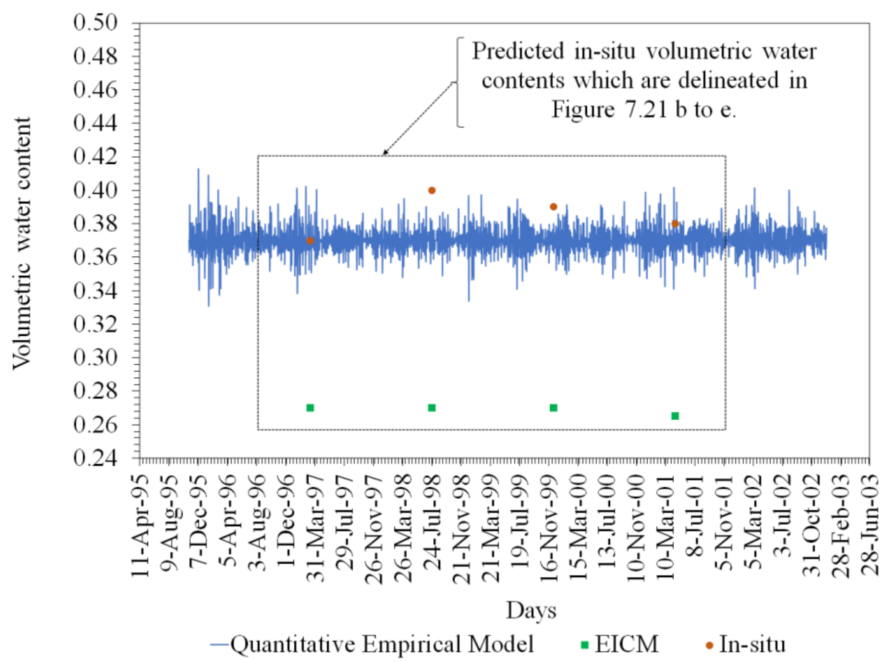

(a)

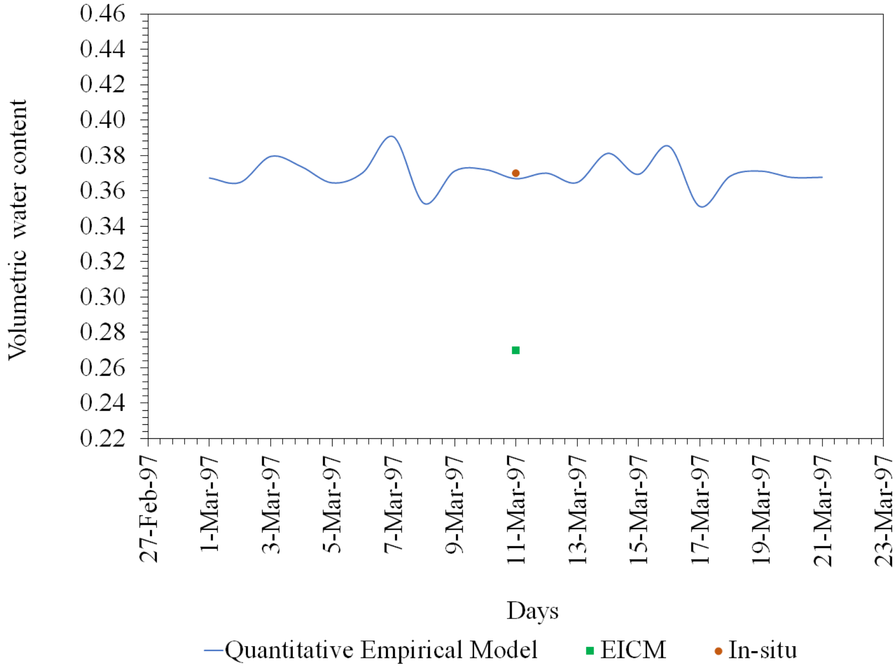

Volumetric water content
0.46
0.44
0.42
0.40
0.38
0.36
0.34
0.32
0.30
0.28
0.26
0.24
0.22
27-Feb-97
1-Mar-97
3-Mar-97
5-Mar-97
7-Mar-97
9-Mar-97
11-Mar-97
13-Mar-97
15-Mar-97
17-Mar-97
19-Mar-97
21-Mar-97
23-Mar-97
Days
Quantitative Empirical Model
EICM
In-situ

(b)

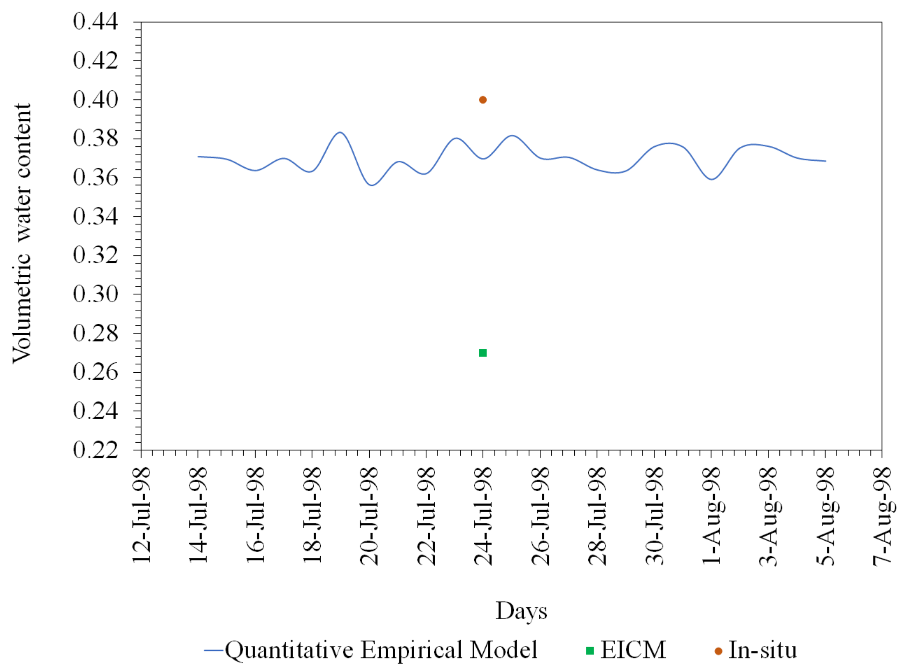

Volumetric water content
0.44
0.42
0.40
0.38
0.36
0.34
0.32
0.30
0.28
0.26
0.24
0.22
12-Jul-98
14-Jul-98
16-Jul-98
18-Jul-98
20-Jul-98
22-Jul-98
24-Jul-98
26-Jul-98
28-Jul-98
30-Jul-98
1-Aug-98
3-Aug-98
5-Aug-98
7-Aug-98
Days
Quantitative Empirical Model
EICM
In-situ

(c)

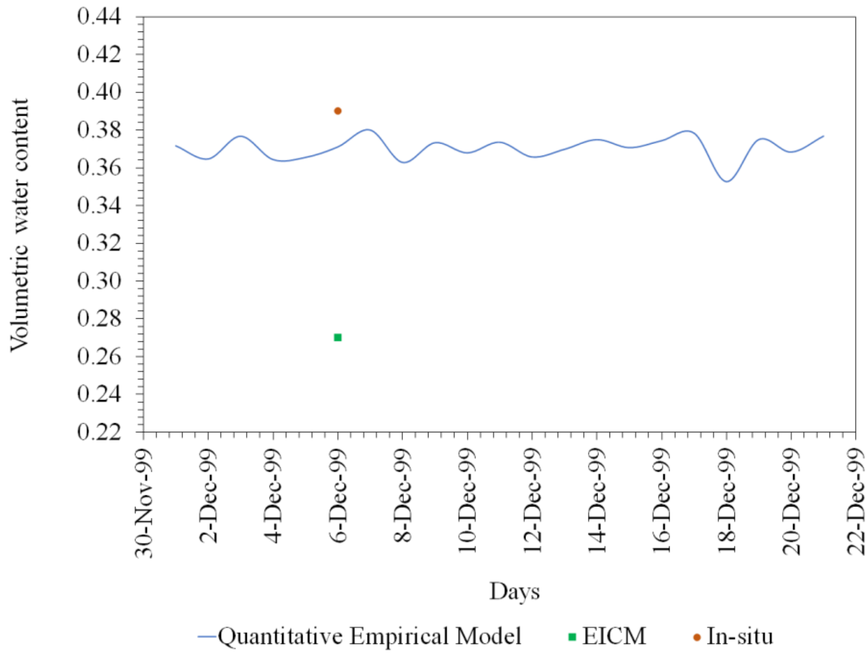

(d)

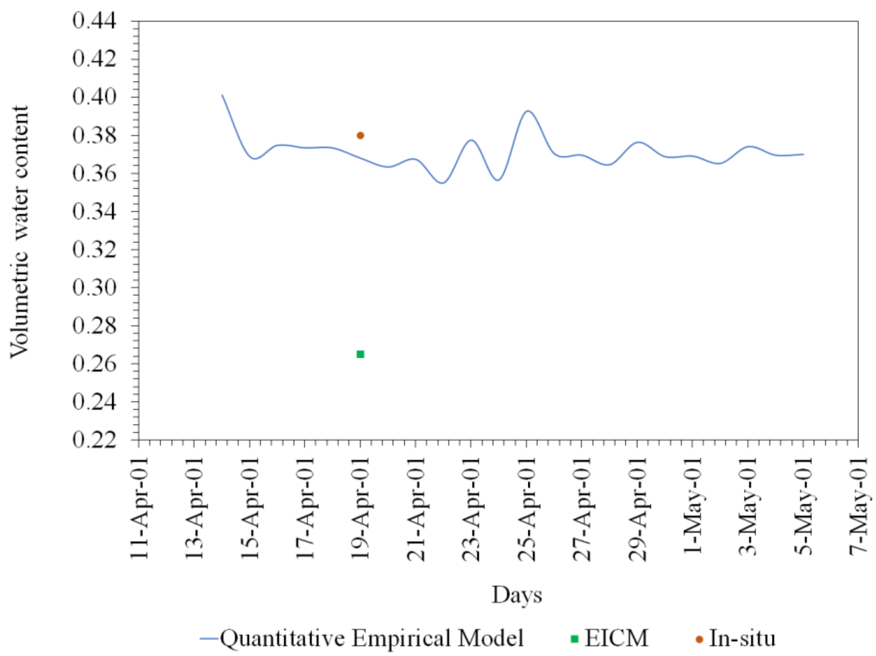

(e)

Figure 7.21: Measured vs predicted in-situ volumetric water contents obtained using the QE Model and EICM

7.5.7 *Task G: The Accuracy of the Quantitative Empirical Model vs EICM: Using Calculated F_{env} and M_R*

The Quantitative Empirical Model (QE Model) was also verified against EICM using the unfrozen composite environmental adjustment factor (the unfrozen F_{env}). The unfrozen F_{env} values were calculated using the in-situ volumetric water contents predicted using the QE Model, and using Eq. 6.35 and Eq. 6.36 (the F_{envCF} values). The unfrozen F_{env} values were also calculated using the in-situ volumetric water contents predicted using EICM, and using Eq. 3.1 and Eq. 3.2 (the F_{env} values). The unfrozen F_{env} values were also calculated using the measured in-situ volumetric water contents, and using Eq. 3.1 and Eq. 3.2 (the measured in-situ F_{env} values). The F_{envCF} values and the F_{env} values were compared to the measured in-situ F_{env} values. This analysis was conducted to verify the suitability of volumetric water contents predicted using the QE Model and EICM for use in calculating the impact of climatic factors on the measured in-situ F_{env} of subgrades.

The analyses of the data presented in Figure 7.22 and Figure 7.23 show that the QE Model predicts in-situ F_{env} values within ± 0.05 of the measured in-situ F_{env} values. The data show that EICM generally overpredicts in-situ F_{env} values by 0.5 to 0.9 from the measured in-situ F_{env} values. The analyses of the data presented in Figure 7.22 and Figure 7.23 also show that the QE Model is more accurate than EICM in predicting the in-situ F_{env} values and the associated in-situ resilient moduli of subgrades. EICM underpredicting in-situ volumetric water contents results in EICM overpredicting the in-situ F_{env} values. EICM overpredicting in-situ F_{env} values results in EICM overpredicting in-situ resilient moduli of subgrades. Hence, EICM overpredicting in-situ F_{env} values results in pavement structures with lower in-situ resilient moduli during the operation period relative to resilient moduli predicted by EICM. This results in pavement structures being subjected to higher rutting under traffic loading relative to the rutting predicted by EICM. This also results in uneconomical pavement structures with higher maintenance cost, lower performance and shorter service life.

Comparing the Quantitative Empirical Model to EICM Using the Calculated F_{env} for Site C: 1997 to 2002

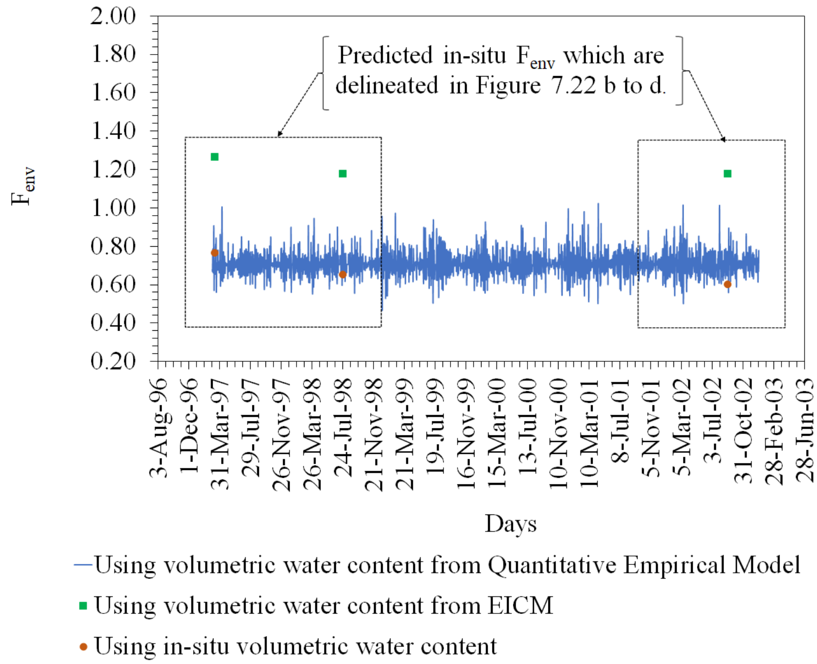

(a)

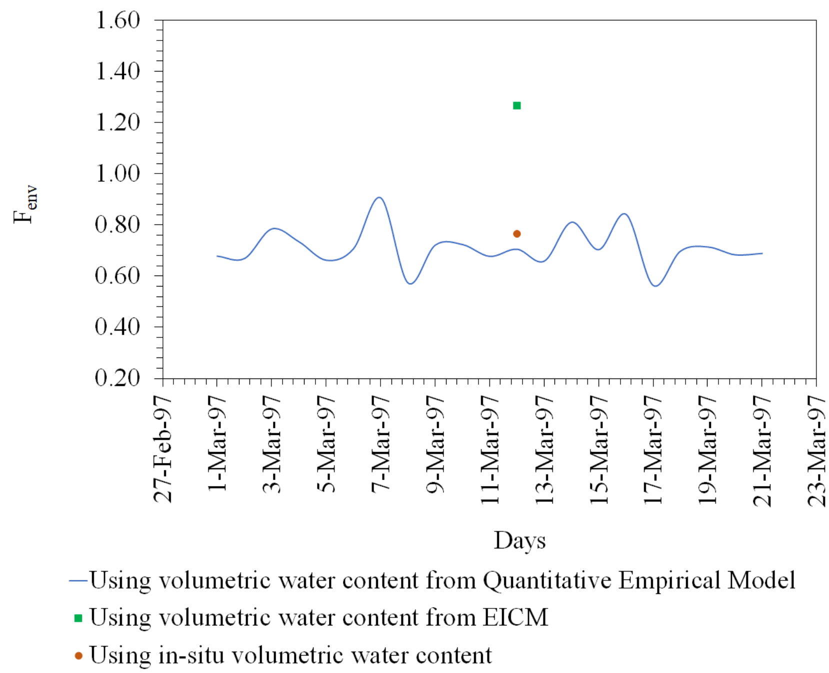

(b)

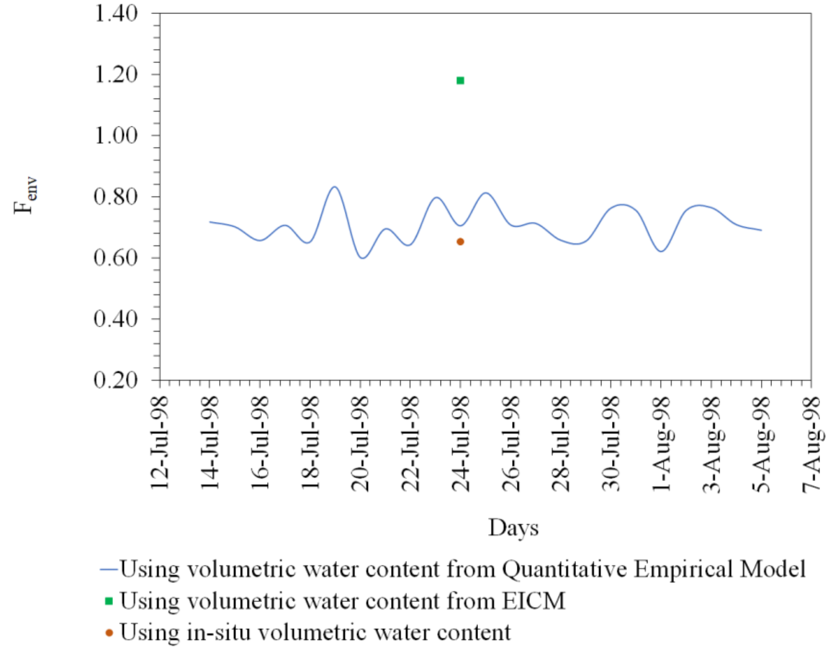

(c)

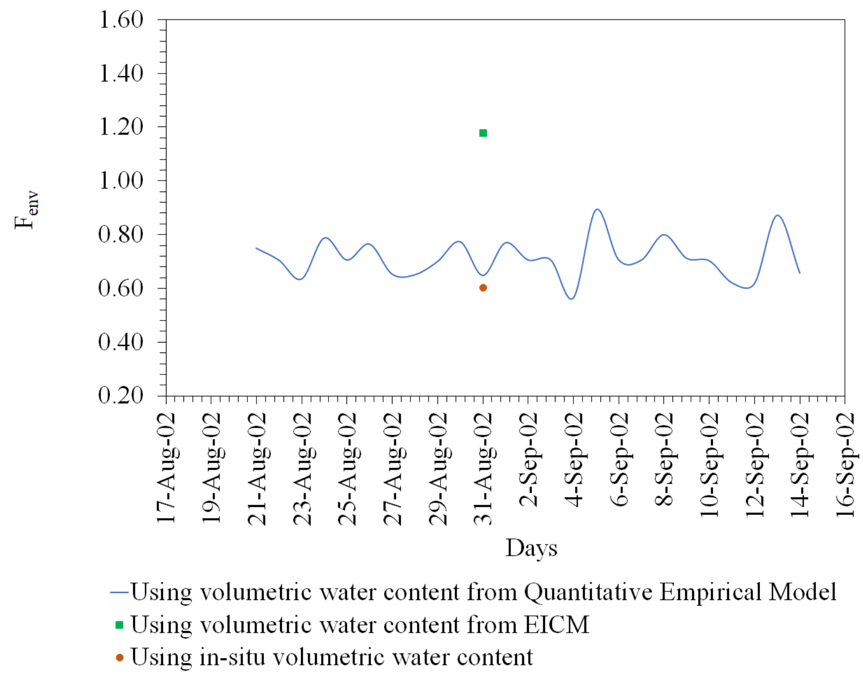

(d)

Figure 7.22: Calculated in-situ F_{env} vs F_{env} calculated using predicted in-situ volumetric water contents obtained using the QE Model and EICM.

Comparing the Quantitative Empirical Model to EICM Using the Calculated F_{env} for Site D: 1997 to 2001.

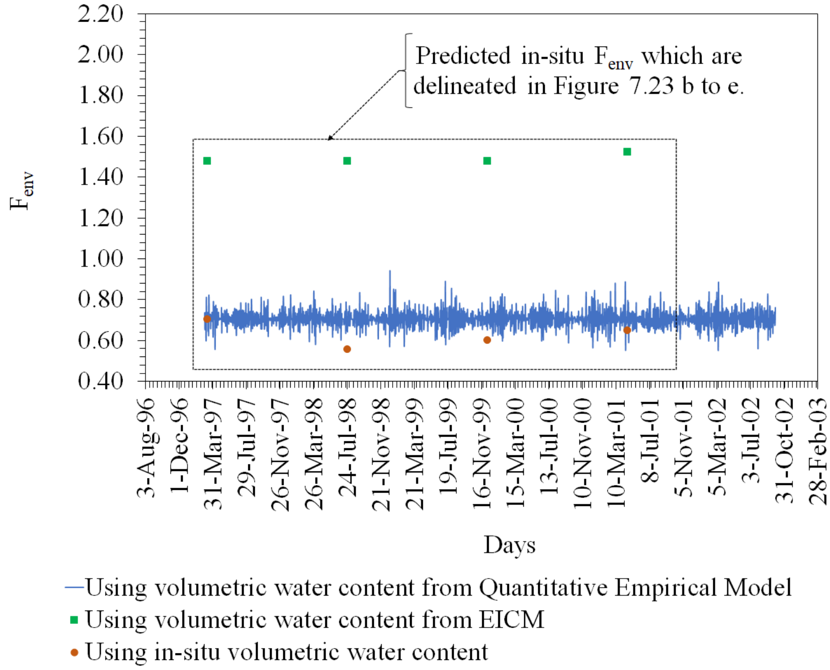

(a)

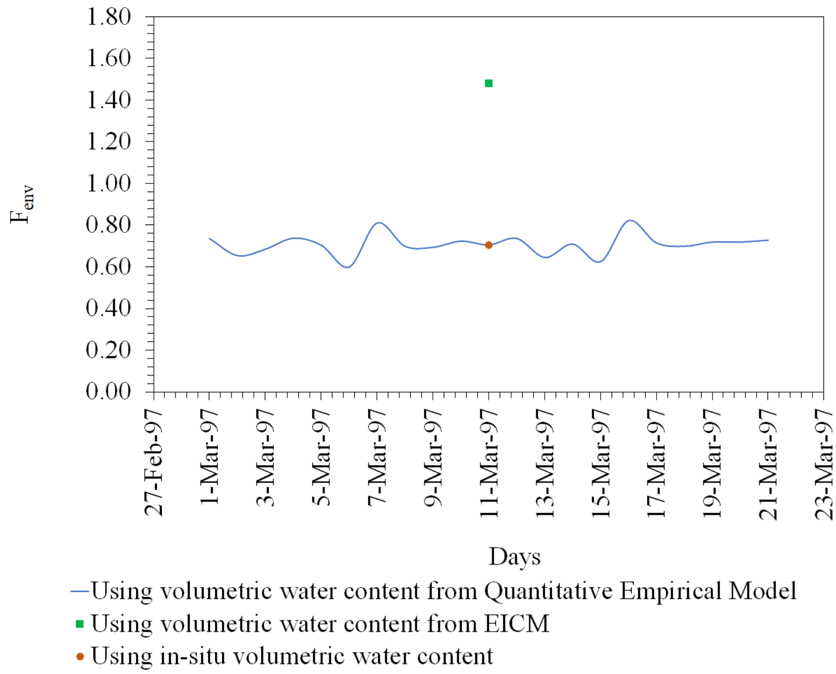

(b)

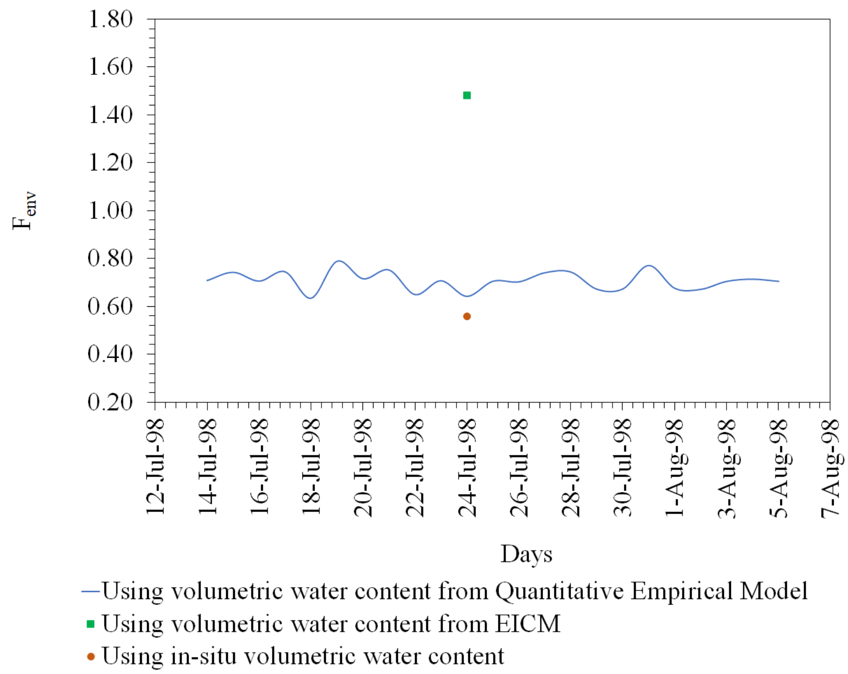
1.80
1.60
1.40
1.20
1.00
0.80
0.60
0.40
0.20
F_{env}
12-Jul-98
14-Jul-98
16-Jul-98
18-Jul-98
20-Jul-98
22-Jul-98
24-Jul-98
26-Jul-98
28-Jul-98
30-Jul-98
1-Aug-98
3-Aug-98
5-Aug-98
7-Aug-98
Days
Using volumetric water content from Quantitative Empirical Model
Using volumetric water content from EICM
Using in-situ volumetric water content

(c)

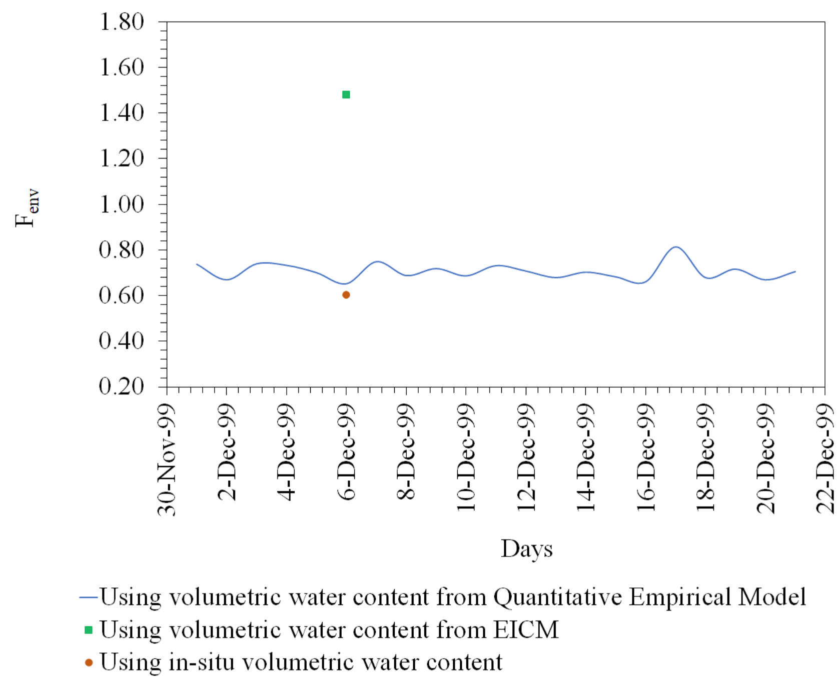
1.80
1.60
1.40
1.20
1.00
0.80
0.60
0.40
0.20
F_{env}
30-Nov-99
2-Dec-99
4-Dec-99
6-Dec-99
8-Dec-99
10-Dec-99
12-Dec-99
14-Dec-99
16-Dec-99
18-Dec-99
20-Dec-99
22-Dec-99
Days
Using volumetric water content from Quantitative Empirical Model
Using volumetric water content from EICM
Using in-situ volumetric water content

(d)

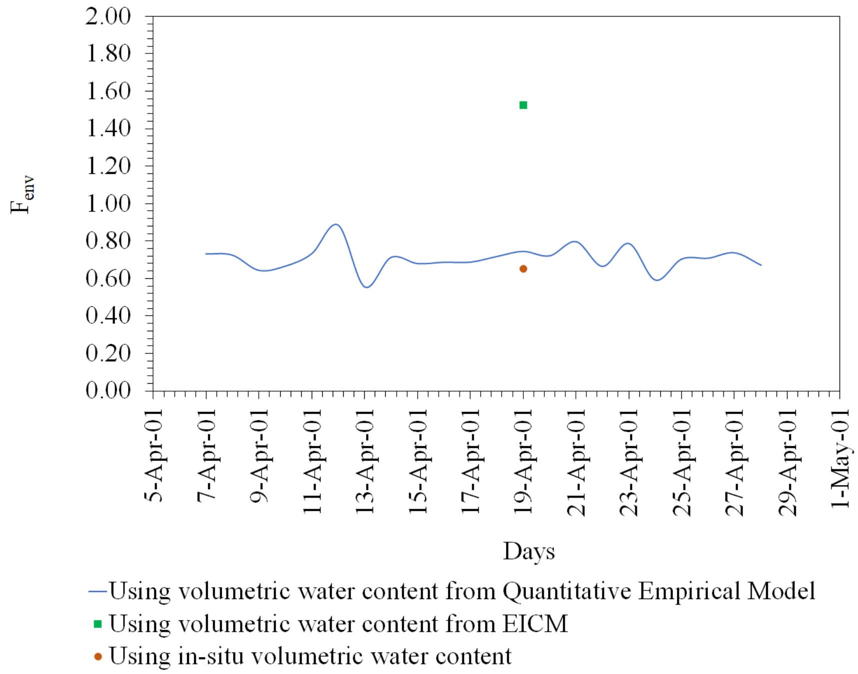

(e)

Figure 7.23: Calculated in-situ F_{env} vs F_{env} calculated using predicted in-situ volumetric water contents obtained using the QE Model and EICM.

7.5.8 Task H: Comparing the Quantitative Empirical Model to EICM Using the Calculated M_R Values: Site C and Site D

The Quantitative Empirical Model (the QE Model) was also verified against EICM using the resilient modulus (M_R) values over time. The M_R values were calculated using the F_{envCF} values as input in Eq. 6.37 (M_{RCF} values). The resilient moduli values were also calculated using the F_{env} values as input in Eq. 3.4 (M_R values). The resilient moduli values were also calculated using the measured in-situ F_{env} values as input in Eq. 3.4 (the measured in-situ M_R values). The M_{RCF} values and the M_R values were compared to the measured in-situ M_R values. This analysis was conducted to verify the suitability of volumetric water contents predicted using the QE Model and EICM for use in calculating the impact of climatic factors on the measured in-situ resilient moduli of subgrades;

The analyses of data presented in Figure 7.24 and Figure 7.25 show that volumetric water contents predicted using the QE Model are more suitable for calculating in-situ resilient moduli of subgrades than volumetric water contents predicted using EICM. The data also show that EICM overpredicts the in-situ resilient modulus of the subgrade.

Comparing the Quantitative Empirical Model to EICM Using the Calculated M_R for Site C: 1998

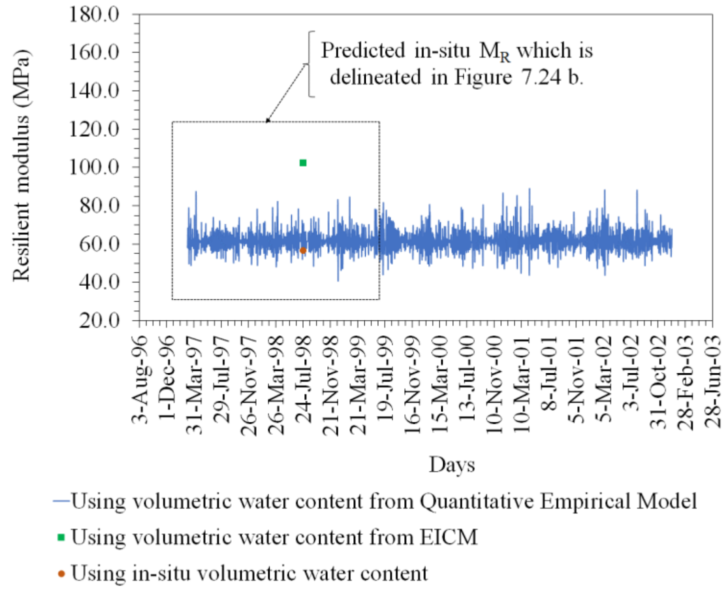

(a)

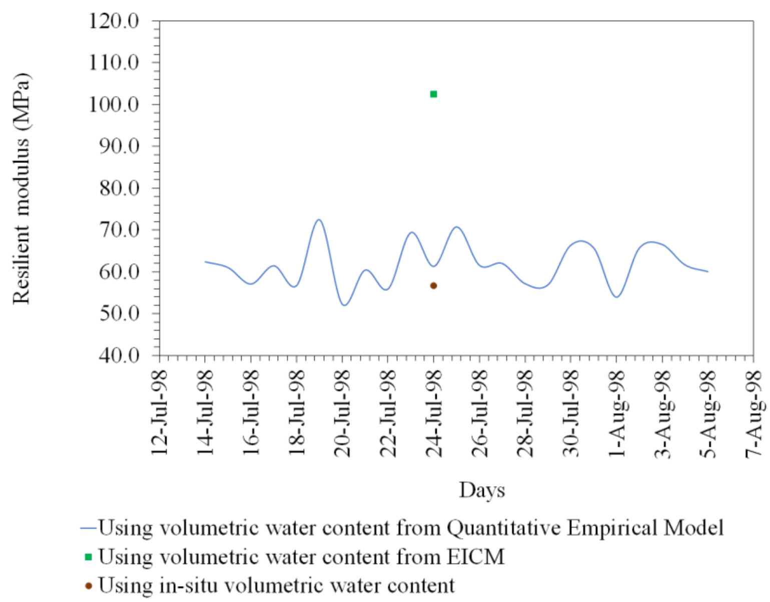

(b)

Figure 7.24: Calculated M_R vs M_R calculated using predicted in-situ volumetric water contents obtained using the QE Model and EICM.

Comparing the Quantitative Empirical Model to EICM Using the Calculated M_R for Site D: 1999

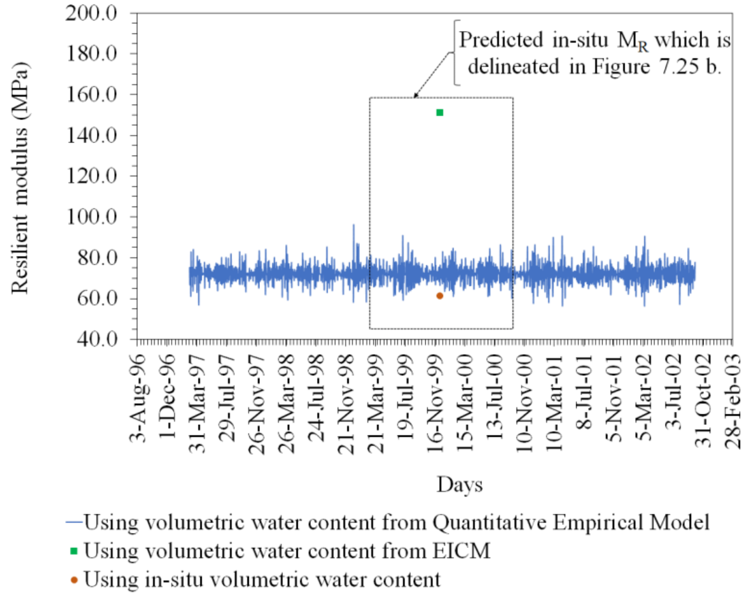

(a)

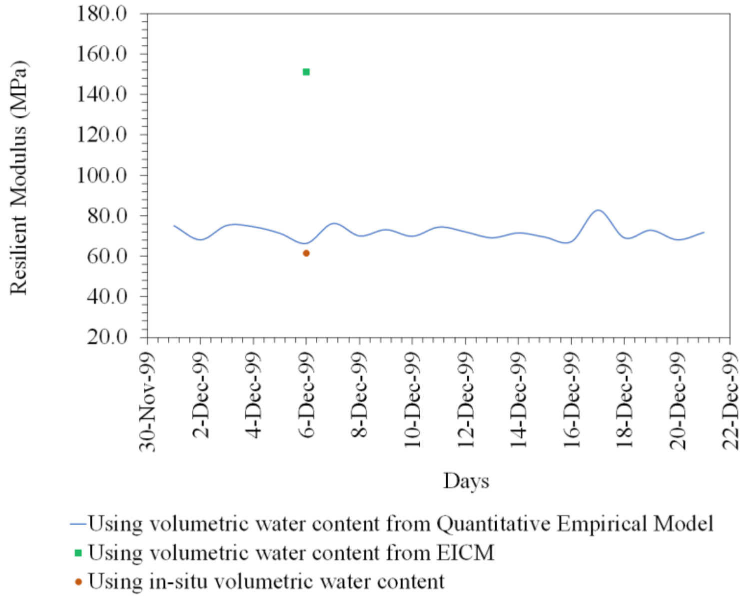

(b)

Figure 7.25: Calculated in-situ M_R vs M_R calculated using predicted in-situ volumetric water contents obtained using the QE Model and EICM.

7.5.9 Task I: Evaluating General Trends in the Predicted Cumulative Changes in In-situ Volumetric Water Contents

The cumulative changes in in-situ volumetric water contents predicted using the Quantitative Empirical Model (the QE Model) were calculated and were presented in Figure 7.26 to Figure 7.29. The analyses of data presented in Figure 7.26 to Figure 7.29 show continual fluctuations in the predicted cumulative changes in in-situ volumetric water contents within subgrades due to changes in climatic factors. Fluctuations in the predicted cumulative changes in in-situ volumetric water contents were observed up to the end of the analysis period. The data also show positive values in the cumulative changes in in-situ volumetric water contents at the end of the analysis period for the three sites.

The analyses of data presented in Figure 7.26 to Figure 7.29 also show that the predicted cumulative changes in in-situ volumetric water contents are generally lower for the pavement section at Site B relative to the predicted cumulative changes in in-situ volumetric water contents at Site A, Site C and Site D. This observation indicates that the subgrade at Site B (clayey Gravel with sand classified as A-6) has a lower water storage capacity and a higher rate of desaturation relative to the subgrade at Site A, Site C and Site D (silty Clay classified as A-7-6, A-6 and A-6 respectively). These analyses also indicated that the subgrade at Site A generally has the highest predicted cumulative changes in in-situ volumetric water contents. This observation indicates that subgrades consisting of finer materials have a higher water storage capacity and a lower rate of desaturation. Site C and Site D consist of the same climatic factors and similar subgrade characteristics. The similarity in climatic factors and subgrades at Site C and Site D are reflected in similar predicted cumulative changes in in-situ volumetric water contents within their respective subgrade.

Analysis of Predicted Cumulative Changes in in-situ volumetric water contents within the Subgrade: Site A

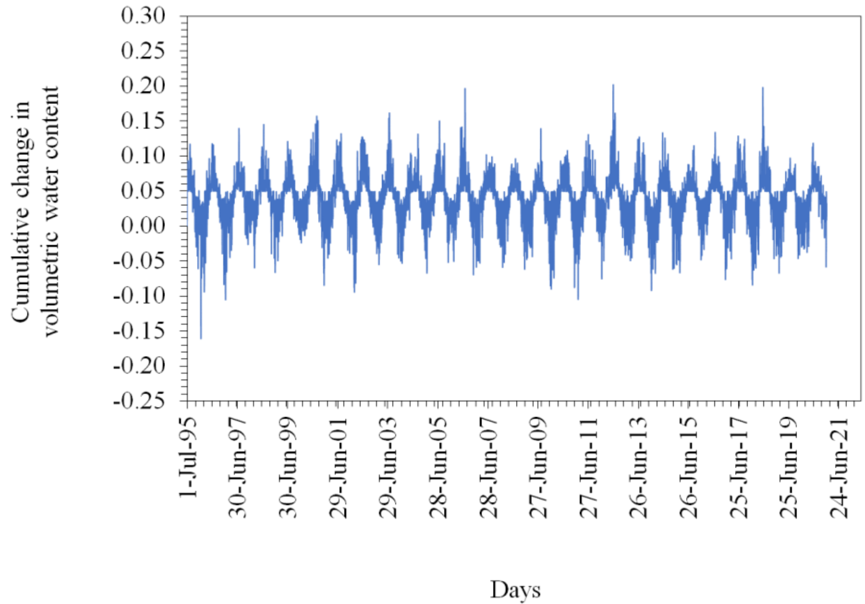

Figure 7.26: Predicted cumulative change in in-situ volumetric water contents using the QE Model

Analysis of Predicted Cumulative Changes in in-situ volumetric water contents within the Subgrade: Site B

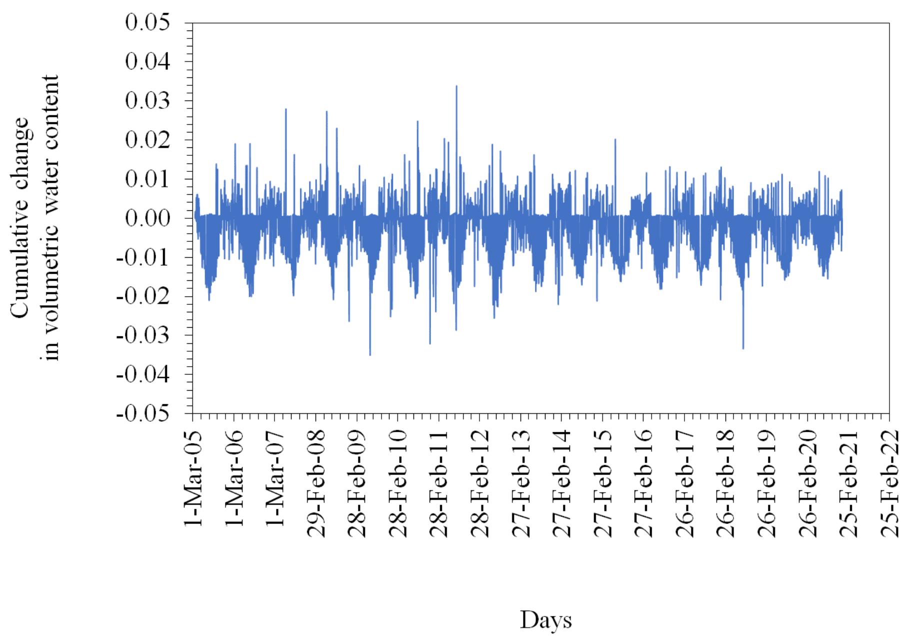

Figure 7.27: Predicted cumulative change in in-situ volumetric water contents using the QE Model

Analysis of Predicted Cumulative Changes in in-situ volumetric water contents within the Subgrade: Site C

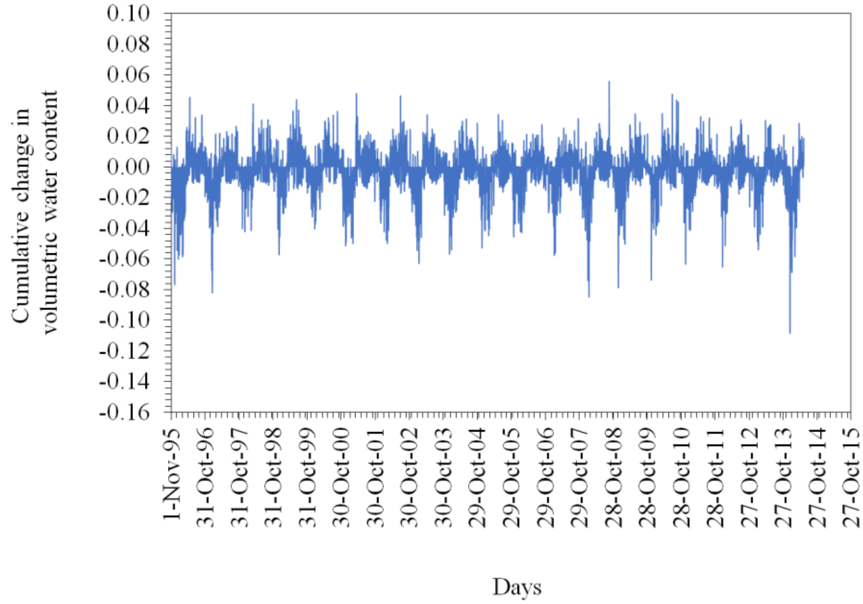

Figure 7.28: Predicted cumulative change in in-situ volumetric water contents using the QE Model

Analysis of Predicted Cumulative Changes in in-situ volumetric water contents within the Subgrade: Site D

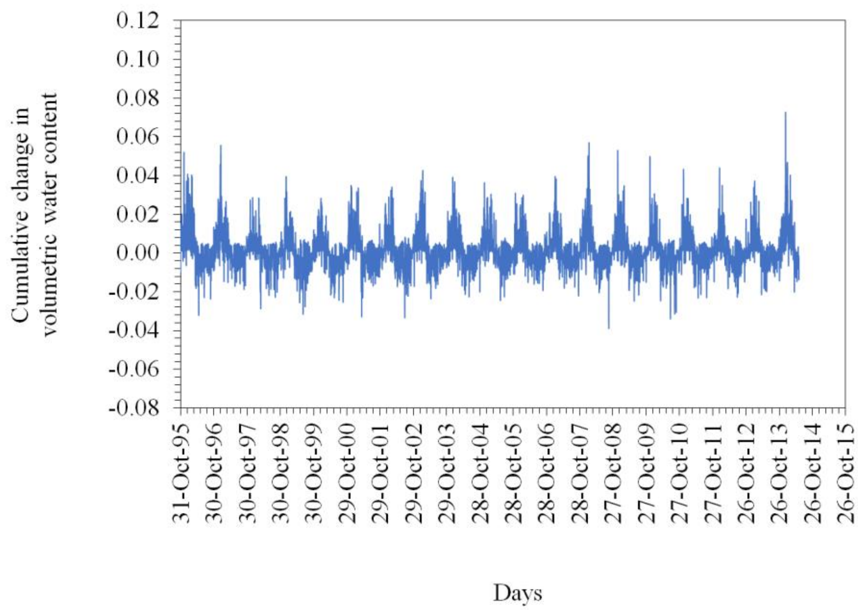

Figure 7.29: Predicted cumulative change in in-situ volumetric water contents using the QE Model

7.5.10 Task J: Determine the accuracy of the Quantitative Empirical Model and EICM in predicting in-situ volumetric water contents using Statistical Analyses

Correlation of determination (R^2) analyses were conducted to verify the Quantitative Empirical Model (the QE Model). The R^2 analyses were conducted between changes in measured in-situ volumetric water contents (the independent variable) and changes in in-situ volumetric water contents predicted using the QE Model (the dependent variable). The R^2 analyses presented in Section 5.3.2 show a strong statistical correlation between the measured and predicted in-situ volumetric water contents within subgrades. This strong statistical correlation between the measured and predicted in-situ volumetric water contents indicates that the QE Model accurately predicts the impact of climatic factors on changes in in-situ volumetric water contents within subgrades.

Two-tailed F-test statistics were also conducted to evaluate the accuracy of the QE Model and EICM in predicting in-situ volumetric water contents for use in calculating F_{env} and M_R values. The analyses of the Two-tailed F-test presented in Section 5.4.5 show that the QE Model is more accurate than EICM in predicting in-situ volumetric water contents for use in calculating the F_{env} and in-situ M_R of subgrades.

7.5.11 Summary of the Evaluation and Verification of the Quantitative Empirical Model

The long-term analysis of the water and heat transfer within subgrades presented in this Chapter indicated seasonal fluctuations in volumetric water contents in response to changes in climatic factors. However, the delineated analysis of the water and heat transfer over a short-term period indicated daily and continual fluctuations in volumetric water contents within subgrades in response to daily changes in climatic factors. The exception being minimal fluctuations in the water and heat transfer during winter months. These analyses also indicated that changes in the water and heat transfer within subgrades are primarily climate dependent.

The analyses of data presented in this Chapter also indicated that the QE Model mitigates the primary limitations in EICM. These include the QE Model accounts for the impact of climatic factors on the water and heat transfer within subgrades. The QE Model also accounts for fluctuations in volumetric water contents due to changes in climatic factors which are neglected by EICM. The QE Model also accounts for the influence of land climate interaction (LCI) on vegetated and bare ground areas adjacent to pavement structures on the water and heat transfer within subgrades. EICM also neglects the LCI on vegetated and bare ground areas adjacent to pavement structures. Unlike EICM, the QE Model accurately predicts in-situ volumetric water contents within subgrades in wet freeze and wet no-freeze climates without site-specific calibration.

These analyses also indicated that the in-situ volumetric water contents within subgrades predicted using the QE Model may be used to calculate the unfrozen F_{env} and in-situ M_R of subgrades. Hence, the QE Model may be incorporated into EICM and MEPDG to account for the impact of climatic factors on the water and heat transfer and resilient moduli of subgrades. Incorporating the QE Model into EICM and MEPDG would facilitate EICM and MEPDG accounting for the impact of climatic factors on pavement performance and service life. This would facilitate the design and construction of more economical pavement structures.

Chapter 8 Conclusion

8.1 Introduction

Chapter 8 provides background details of the literature review conducted to delineate limitations in EICM in predicting the in-situ water and heat transfer within subgrades. The Chapter provides a brief summary of the study's problem statement, research objectives, and research methodology used for conducting the FEA modeling and the development of the Quantitative Empirical Model (the QE Model). The Chapter also provides a summary of the methodology used for the verification of the QE Model.

Chapter 8 also provides a summary of tasks conducted for verifying the accuracy of the QE Model in predicting in-situ water and heat transfer within subgrades due to climatic factors. The Chapter also provides a summary of tasks conducted for verifying the accuracy of the QE Model vs the accuracy of EICM in predicting in-situ water and heat transfer and in-situ resilient moduli of subgrades.

The Chapter provides a conclusion which includes the potential for incorporating the QE Model into EICM and MEPDG. The conclusion includes the contribution of the QE Model in improving EICM and MEPDG for the design and construction of more economical pavement structures. The conclusion also includes the primary research findings, the primary features of and accuracy of the QE Model in predicting the impact of climatic factors on the in-situ water and heat transfer within subgrades. The conclusion also provides a summary of the primary limitations in EICM which are mitigated by the QE Model.

The Chapter also provides recommendations for further research to investigate the impact of climatic factors on the in-situ water and heat transfer within different types of subgrades and in different climates. Chapter 8 also provides recommendation for improving the water contents prediction model used in EICM.

8.2 Literature Review of Limitations in EICM which Form Part of Problem Statements

A comprehensive literature review was conducted to delineate the computational framework of and limitations in EICM in predicting water and heat transfer within subgrades. The literature review highlighted limitations in the climatic boundary conditions used in EICM incorporated into MEPDG (EICM). EICM accounts for only infiltration through cracks on the pavement surface, neglects the influence of land climate interaction (LCI) on vegetated and bare ground areas adjacent to pavement structures and neglects evapotranspiration. EICM only accounts for liquid water transfer and neglects water vapour transfer. EICM assumes a constant and uniform subgrade temperature, only accounts for water transfer influence by depth of shallow groundwater table and neglects the influence of the water table at significant depth. EICM also neglects the influence of climatic factors on fluctuations in the in-situ water and heat transfer within subgrades. These limitations in EICM result in inaccuracies in predicting in-situ volumetric water contents within subgrades and inaccurate prediction of in-situ resilient moduli of subgrades. These inaccuracies in predicting the in-situ water and heat transfer and in-situ resilient moduli of unbound materials result in inaccuracies in predicting the pavement distress. Hence, these limitations in EICM result in inaccurate prediction of the pavement performance and service life. These limitations also result in the design and construction of uneconomical pavement structures. These limitations form the basis of the problem statement for this study.

The primary objective of this study is to investigate the influence of climatic factors on the in-situ water and heat transfer, and on volumetric water contents within subgrades. The investigation focuses on the impact of LCI on the in-situ water and heat transfer within subgrades. The specific objective was achieved by developing a Quantitative Empirical Model (the QE Model) to account for the influence of climatic factors and LCI on in-situ volumetric water contents and on in-situ resilient moduli of subgrades. It is intended that the QE Model facilitates improvements in EICM and MEPDG to account for climatic factors and to produce more economical pavement structures.

One-dimensional (1-D) and two-dimensional (2-D) water and heat transfer finite element analyses (FEA) modeling were conducted using two rigid pavement sections in a wet freeze climate. Nonlinear regression analyses were conducted using climatic factors, measured in-situ volumetric water contents, and 2-D FEA volumetric water contents output to develop correlation functions. Mathematical computations were used to incorporate liquid water and water vapour properties, initial degree of saturation and hydraulic properties of subgrades and wearing courses in developing the QE Model. Integrals were also conducted to develop the QE Model.

The QE Model and EICM were verified using four independent pavement sections in wet freeze and wet no-freeze climates. The QE Model and EICM were verified by comparing in-situ volumetric water contents predicted using the QE Model and EICM to the measured in-situ volumetric water contents. The predicted and measured in-situ volumetric water contents were obtained at a depth of 150.0 mm below the subgrade surface and on the same days. The QE Model was also verified using unfrozen composite environmental adjacent factor (F_{env}) values and resilient moduli (M_R) values. F_{env} values calculated using in-situ volumetric water contents which were predicted using the QE Model (F_{envCF}) and EICM (F_{env}) were compared to F_{env} values which were calculated using measured in-situ volumetric water contents (the measured F_{env}). M_R values calculated using F_{envCF} values and using F_{env} values were compared to the M_R values calculated using the measured F_{env} values. The predicted and measured in-situ volumetric water contents used for calculating F_{env} values were obtained at a depth of 150.0 mm below the subgrade surface and on the same days. The QE Model and EICM were also verified using the coefficient of determination

(R^2) analyses. The R^2 analyses were conducted between in-situ volumetric water contents predicted using the QE Model and EICM, and the measured in-situ volumetric water contents.

8.3 Conclusion

The water and heat transfer within subgrades is impacted by climatic factors and by the land climate interaction (LCI) on vegetated and bare ground areas adjacent to pavement structures. The water transfer within subgrades is influenced by transient water and heat transfer, saturated/unsaturated conditions, heat conduction and forced convection with water transfer. Volumetric water contents within subgrades fluctuate continually due to changes in climatic factors. The water contents within subgrades are also impacted by the elevation of the water table. Shallow water tables (less than 10.0 m below the subgrade surface) cause a higher contribution of liquid water transfer within subgrades due to capillary rise. Deep water tables (at least 10.0 m below the subgrade surface) facilitate increased contribution of water vapour transfer within subgrades. The rate of water vapour transfer within subgrades is higher while subgrades are desaturating and are in the residual water content condition.

The Quantitative Empirical Model (the QE Model) developed as part of this study represents an in-situ soil water characteristic curve (the in-situ SWCC). The in-situ SWCC accounts for the influenced of climatic factors (the energy state) on volumetric water contents within fine-grained and coarse-grained subgrades in wet freeze and wet no-freeze climates (the climate-induced SWCC). The climate-induced SWCC represents the relationship between changes in volumetric water contents as a nonlinear function of changes in climatic factors. The climate-induced SWCC also accounts for hysteresis in water contents due to changes in the energy state. The QE Model also represents a model for predicting the site-specific net evapotranspiration which applies the Penman-Monteith method and incorporates the impact of climatic factors on the net evapotranspiration.

The QE Model facilitates improving the design, construction, and performance evaluation of pavement structures subjected to climatic factors. The QE Model accounts for the influence of climatic factors and LCI on water and heat transfer within subgrades. The QE Model accurately predicts the influence of climatic factors on fluctuations in in-situ volumetric water contents within subgrades in wet freeze and wet no-freeze climates by incorporating a climate-induced water balance approach. The QE Model has a higher accuracy than EICM in predicting the in-situ water and heat transfer within subgrades.

The QE Model may be incorporated into EICM and MEPDG to improve predicting the influence of climatic factors on in-situ volumetric water contents within subgrades (the climate-induced in-situ volumetric water contents). The climate-induced in-situ volumetric water contents may be used to predict the in-situ degree of saturation within subgrades (the climate-induced in-situ degree of saturation). The climate-induced in-situ degree of saturation may be incorporated into EICM to predict the unfrozen environmental adjustment factor (F_U) which is used as an input for calculating F_{env} and resilient moduli of subgrades. Hence, incorporating the QE Model into EICM would result in EICM accounting for the impact of climatic factors on resilient moduli of subgrades. Incorporating the QE Model into EICM would also result in the design and construction of more economical pavement structures.

The QE Model mitigates limitations in EICM in predicting in-situ water and heat transfer and limitations in predicting in-situ resilient moduli of subgrades. The mitigating features which are incorporated into the QE Model include the following:

- The QE Model accounts for the impact of climatic factors on the water and heat transfer within subgrades. The QE Model accounts for fluctuations in in-situ volumetric water contents due to climatic factors. However, EICM neglects the impact of climatic factors on fluctuations in in-situ volumetric water contents;
- The QE Model also accounts for the influence of LCI (on vegetated and bare ground areas adjacent to the pavement structure) on the water and heat transfer within subgrades (which is applicable for unpaved roads). The QE Model also incorporates the impact of LCI on water and heat transfer for cases where the wearing courses on traffic lanes and shoulders are assessed as impervious (which is applicable for new and rehabilitated pavement structures). However, EICM neglects the impact of LCI on the water and heat transfer;
- The QE Model accounts for liquid water transfer and water vapour transfer within subgrades. However, EICM accounts only for liquid water transfer and neglects water vapour transfer;
- The QE Model accounts for variations in subgrade temperatures. However, EICM assumes a constant subgrade temperature;
- The QE Model accounts for evapotranspiration which is neglected by EICM;
- Unlike EICM, the QE Model accurately predicts in-situ volumetric water contents within subgrades without the need for site-specific calibration;
- The QE Model is more suitable than EICM for predicting in-situ volumetric water contents which are used for calculating the unfrozen composite environmental adjustment factor (F_{env}) and resilient moduli of subgrades;
- The QE Model may be incorporated into EICM and MEPDG to account for the impact of climatic factors on in-situ water and heat transfer and resilient moduli of subgrade; and
- Incorporating the QE Model into EICM and MEPDG would result in incorporating the impact of climatic factors in the design and construction of more economical pavement structures.

Further research should be conducted to investigate the influence of changes in climatic factors on the in-situ water and heat transfer within different types of subgrades in different climatic zones. The recommended research includes investigating guidelines for improving the current EICM and MEPDG.

This study was conducted using fine-grained subgrades on sites in a wet freeze climatic zone. The QE Model was evaluated and verified using fine-grain and coarse-grain subgrades in wet freeze and wet no-freeze climatic zones. Further research should be undertaken for sites in other climatic zones with fine-grain and course-grain subgrades.

The water contents prediction model used in EICM (the Fredlund, and Xing 1994 model) should be replaced with a model which accounts for the impact of climatic factors and LCI on water and heat transfer (such as the QE Model developed as part of this study). The replacement model should also account for liquid water and water vapour transfer, and should mitigate the above-mentioned limitations in EICM and MEPDG.

References

Abu-Hamdeh, N. H. 2003. Thermal properties of soils as affected by density and water content. In Journal of Biosystems Engineering, 86 (1), pp. 97-102.

Addinsoft. 2022. XLSTAT statistical and data analysis solution. New York, USA.

Ahmed, Z., Marukic, I., Zaghloul, S., and Vitillo, N. 2005. Validation of Enhanced Integrated Climatic Model predictions with New Jersey seasonal monitoring data. Transportation Research Record, Journal of the Transportation Research Board. Vol. 1913 (1). pp. 148-161.

Alexander, L. T., and Haring, M. 1936. Vapor pressure-water content relations for certain typical soil colloids. The Journal of Physical Chemistry 1936 40 (2), pp. 195-205.

Allen, R. G., Pereira, L. S., Raes, D. and Smith, M. 1998. Crop evapotranspiration guidelines for computing crop water requirements. FAO Irrigation, and drainage paper No. 56. CLIM 029, LSI 007. Food and Agriculture Organization, Rome.

Alonso, E. E., and Delage, P. 1995. Editors. Unsaturated soils. Proceedings of the first international conference on unsaturated soils, UNSAT95. Paris, France, 6-8 september 1995, Vol. 3. p. 713. Balkema, Paris.

American Association of State Highway and Transportation officials (AASHTO). 2020. Mechanistic Empirical Pavement Design Guide: A manual of practice. 3rd Edition. AASHTO. pp. 245.

American Association of State Highway and Transportation Officials (AASHTO). 2011. Technical Assistance to NCHRP and NCHRP Project 1-40A: Versions 0.9 and 1.0 of the M-E Pavement Design Software

American Association of State Highway and Transportation Officials (AASHTO). 2010. Guide for the Local Calibration of the Mechanistic Empirical Pavement Design Guide, AASHTO.

American Association of State Highway and Transportation Officials (AASHTO). 2008. Mechanistic Empirical Pavement Design Guide: A Manual of Practice. AASHTO, United States:

American Association of State Highway and Transportation Officials (AASHTO). 1998. AASHTO LRFD bridge design specifications. SI Units, Second Edition, AASHTO, National Corporative Highway Research Program, Washington, DC.

American Association of State Highway and Transportation officials (AASHTO). 1993. AASHTO Guide for design of pavement structures. AASHTO, National Corporative Highway Research Program, Washington, DC.

Anapalli, S. S., Ma, L., Nielsen, D. C., Vigil, M. F., and Ahuja, L. R. 2005. Simulating planting date effects on corn production using RZWQM and CERES-Maize models. American Society of Agronomy, In Journal of Agronomy, 97(1).

Applied Research Associates Inc., ERES Consultants Division (ARA). 2004. Guide for Mechanistic Empirical Design of new and rehabilitated pavement structures. Final Report, Part 2: Design Inputs: Chapter 2: Material Characterization. NCHRP Project 1-37A. National Corporative Highway Research Program. Transportation Research Board. https://web.archive.org/web/20171017193725/http://onlinepubs.trb.org/onlinepubs/archive/mepdg/guide.htm

Applied Research Associates Inc., ERES Consultants Division (ARA). 2004. Guide for the Mechanistic Empirical Design of new and rehabilitated pavement structures, Final report, Part 2: Design Inputs: Chapter 3: Environmental Effects. NCHRP 1-37A. Transportation Research Board of the National Academies, Washington, DC. https://web.archive.org/web/20171017193725/http://onlinepubs.trb.org/onlinepubs/archive/mepdg/guide.htm

Applied Research Associates Inc., ERES Consultants Division (ARA). 2004. Guide for Mechanistic Empirical Design of new and rehabilitated pavement structures. Final Document, Appendix RR: Finite Element Procedures for Flexible Pavement Analyses. National Cooperative Highway Research Program (NCHRP), Transportation Research Board, National Research Council. Washington, DC. https://web.archive.org/web/20171017193725/http://onlinepubs.trb.org/onlinepubs/archive/mepdg/guide.htm

Arunkumar, S. 2021. Soil Water Movement-Saturated and Unsaturated flow. In AgriCos e-Newsletter, Open Access Multidisciplinary Monthly Online Magazine, Article No: 10, 02(11).

Asphalt Institute. 2014. MS-2 Asphalt Mix Design Methods. 7th Edition, USA

Asres, E.; Ghebrab, T.; and Ekwaro-Osire, S. 2022. Framework for design of sustainable flexible pavement. In Journal of Infrastructures 2022, 7, 6. Ed García-Segura., T.

Back, L. E., and Bretherton, C. S. 2005. The relationship between wind speed and precipitation in the Pacific ITCZ, In Journal of Climate. 18(20), 4317-4328.

Badeli, S., Carter, A., and Doré, G. 2018. Effect of laboratory compaction on the viscoelastic characteristics of an asphalt mix before and after rapid freeze-thaw cycles. In Journal of Cold Regions Science and Technology, 146, pp. 98-109.

Banks, J. H. 2002. Introduction to Transportation Engineering. McGraw-Hill.

Basma, A. A., and Al-Suleiman, T. I. 1991. Climatic considerations in new AASHTO flexible pavement design. American Society of Civil Engineers, Journal of Transportation Engineering, Vol. 117 (2), 1991, pp. 210-223.

Bayomy, F., and Salem, H. 2005. Monitoring and modeling subgrade soil moisture for pavement design and rehabilitation in Idaho. Phase III: Data collection and Analysis. Final Report, NIATT Project No. KLK 459, ITD Project No. SPR-0010 (27) 124. Idaho Transportation Department, pp. 234.

Bear, J. 1979. Hydraulics of Groundwater, McGraw-Hill series in water resources and environmental engineering. McGraw-Hill, New York.

Benson, C. H. and Othman, M. A. 1993. Hydraulic conductivity of compacted clay frozen and thawed in situ. Journal of Geotechnical Engineering, 119 (2): pp. 276-294.

Birgisson, B., and Roberson, R. 2000. Drainage of pavement base material: Design and construction issues. Transportation Research Record., Journal of the Transportation Research Board. Vol. 1709 (1). pp. 11-18.

Birgisson, B., Ovik, J., and Newcomb, D. E. 2000. Analytical predictions of seasonal variations in flexible pavements. Transportation Research Record, Journal of the Transportation Research Board, vol. 1730 (1). pp. 81-90.

Blow, M. 2021. Understanding pavement distress in asphalt overlays. In Asphalt Magazine, 36(1), The Asphalt Institute, pp. 23-29.

Bowden, S. T., and Jones, W. J. 1947. Latent heat of vaporization, temperature and density of liquids In Journal of the Society of Chemical Industry, 66(10), pp. 342-343.

Braga, A., Horst, M., and Traver, R. G. 2007. Temperature effects on the infiltration rate through an infiltration basin BMP. In Journal of Irrigation and Drainage Engineering, American Society for Civil Engineers (ASCE). Vol. 133 (6).

Briaud, J-L., Zhang, X., and Moon, S. 2003. Shrink test-water content method for shrink and swell predictions. American Society of Civil Engineers, Journal of Geotechnical and Geoenvironmental Engineering, vol. 129 (7), pp. 590-600.

Brooks, R. H., and Corey., A. T. 1964. Hydraulic properties of porous media. Hydrology Paper No. 3. Editors: Corey, A. T., Dils, R. E., and Yevdjevich, V. M. Fort Collins, Colorado State University, Hydrology and Water Resources Program. pp. 37.

Brooks, R. H., and Corey., A. T. 1964. Hydraulic properties of porous media and their relation to drainage design. American Society of Agricultural and Biological Engineers, Journal of Transactions of the American Society of Agricultural and Biological Engineers, vol 7 (1). pp. 26-0028.

Brown, S. F., Darter, M. M., Larson, G., Witczak, M., and El-Basyouny, M. 2006. Independent review of the Mechanistic Empirical Pavement Design Guide and software. Research result digest 307. Transportation Research Board, National Cooperative Highway Research Program (NCHRP), Scott Wilson Pavement Engineering Ltd., Applied Research Associates Inc., Arizona State University.

Bryce, J., Chattopadhyay, A., Esmaeilpour, M., and Ihnat, Z. E. 2021. Detailing an improved heat transfer model for pavements. Transportation Research Record, Journal of the Transportation Research Board, vol. 2675 (7). pp. 153-165.

Bulut, R., and Javid A. H. 2019. Developing implementable climatic input data and moisture boundary conditions for pavement analysis and design. Final Report, August 2019. Tran-SET Project No. 18POKS03. Transportation Consortium of South-Central States. pp. 49.

Bulut, R., Yue, E., Chen, L., Muraleetharan, K. K., Zaman, M., Soltani, H., and Hossain, Z. 2014. Evaluation of the Enhanced Integrated Climate Model for specification of subgrade soil in Oklahoma. Final Report-FHWA-OK-14-05. ODOT SP&R ITEM NUMBER 2160. Oklahoma Department of Transportation. pp. 121.

Bulut, R., Yue, E., Chen, L., Muraleetharan, K. K., Zaman, M., Soltani, H., and Hossain, Z. 2013. Evaluation of the Enhanced Integrated Climatic Model for modulus-based construction specification for Oklahoma pavements. Report No. OTCREOS11.1-10-F, Department of Transportation University Transportation Centers Program, Oklahoma Transportation Center. pp. 46.

Chaurasia A., and Harel, O. 2014. Partial F-tests with multiply imputed data in the linear regression framework via coefficient of determination. In Journal of Statistics in Medicine, 34(3), pp. 432-443.

Chen, X., and Hu, Q. 2004. Groundwater influences on soil moisture and surface evaporation. In Journal of Journal of Hydrology, 297 (1-4). pp. 285-300.

Cheng, R. R., Chen, Q. W., Zhang, J. G., Shi, W. Y., Li, G., and Du, S. 2020. Soil moisture variations in response to precipitation in different vegetation types: A multi-year study in the loess hilly region in China. In Journal of Ecohydrology 13 (3), e2196.

Chiu, M., Clayton, C., and Millen, G. 2017. Geometric Design Guide for Canadian Roads: Chapter 3 - Alignment and Lane Configuration. Transportation Association of Canada (TAC).

Darter, M. I., Titus-Glover, L., and Von Quintus, H. L. 2009. Implementation of the Mechanistic Empirical Pavement Design Guide in Utah: Validation, calibration, and development of the UDOT MEPDG user's guide. Report No. UT-09.11. Utah Department of Transportation. pp. 210.

Darter, M. I., Mallela, J., Titus-Glover, L., Rao, C., Larson, G., Gotlif, A., Von Quintus, H., Khazanovich, L., Witczak, M., El-Basyouny, M., El-Badawy, S., Zborowski, A., and Zapata, C. .2006. Changes to the Mechanistic Empirical Pavement Design software through version 0.900, July 2006. Research

Results Digest 308. Transportation Research Board. National Cooperative Highway Research Program. pp. 24.

de Vries, D. A. 1975. Heat transfer in soils. Heat and Mass Transfer in the Biosphere. Editors. De Vries, D. A., and Afgan, N. H. Scripta Book Co., Washington. pp. 5-28.

De Wit, C. T., and Arens, P. L. 1950. Moisture content and density of some clay minerals and some remarks on the hydration pattern of clay. In Fourth International Congress of Soil Science Transactions (Vol. 2, pp. 59– 62). Groningen, Netherlands: Hoitesema Brothers.

Dempsey, B. J., Herlache, W. A., and Patel, A. J. 1986. Climatic Materials Structural pavement analysis program. Transportation Research Record. Journal of the Transportation Research Board, issue (1095), pp. 111-123.

Dempsey, B. J., Herlache, W. A., and Patel, J. 1985. The Climatic-Materials-Structural pavement analysis program: User's manual, Publication No. FHWA-RD-84-115, Final Report Vol. 3. Federal Highway Administration. pp. 84-115.

Dempsey, B. J., and Robnett, Q. L. 1979. Influence of precipitation, joints, and scaling on pavements drainage. Journal of Transportation Research Records. No. 705. Transportation Research Board, National Academy of Sciences. Washington, D.C.

Dempsey, B. J. 1970. A heat transfer model for evaluating frost action and temperature related effects in multilayered pavement systems. Journal of Highway Research Record, issue (342). pp. 39-56.

Ding, W. B., Wang, F., Dong, Y. Y., Jin, K., Cong, C. Y., Han, J. Q., and Ge, W. Y. 2021. Effects of rainwater harvesting system on soil moisture in rain-fed orchards on the Chinese Loess Plateau. In Journal of Agricultural Water Management. volume 243, 106496.

Dinpashoh Y, Jhajharia D, Fakheri-Fard A, Singh V. P., and Kahya, E. 2011. Trends in reference crop evapotranspiration over Iran. J Hydrology, vol. 399 (3). P. 422-433.

Domitrović, J., Rukavina, T., and Lenart, S. 2019. Effect of freeze-thaw cycles on the resilient moduli and permanent deformation of RAP/natural aggregate unbound base mixtures. In Journal of Transportation Geotechnics, Volume 18, pp. 83-91.

Dong, Q., Chen, X., Dong, S., and Zhang, J. 2021. Classification of pavement climatic regions through unsupervised and supervised machine learnings. Journal of Infrastructure Preservation and Resilience. Vol. 2 (5). pp. 1-15.

Dong X., Peng, B., Sieckenius, S., Raman, R., Conley, M. M., and Leskovar, D. I. 2021. Leaf water potential of field crops estimated using NDVI in ground-based remote sensing-opportunities to Increase prediction precision. In Peer Review Journal. 9.

Drumm, C. E., and Meier, R. 2003. LTPP Data Analysis: Daily and seasonal variations in in-situ material properties. NCHRP Web Document 60 (Project 20-50[7/12]): Contractor's Final Report, National Cooperative Highway Research Program, Transportation Research Board, Washington, D. C, 707 pp.

Drumm, E. C., Reeves, J. S., Madgett, M. R. and Trolinger, W. D. 1997. Subgrade resilient modulus correction for saturation effects. In Journal of Geotechnical and Geoenvironmental Engineering, ASCE, Vol. 123, No. 7, pp. 663-670.

Dzotepe, G. A., and Ksaibati, K. 2010. Implementation of the Mechanistic Empirical Pavement Design Guide (MEPDG). MPC Report No. 10-225A. Wyoming Technology Transfer Center. pp. 92.

El Howayek, A., Muschett, D., Nantung, T., Lee, J., Santagata, M., and Bobet, A. 2016. Verification of the Enhanced Integrated Climatic Module soil subgrade input parameters in the MEPDG (Joint Transportation Research Program Publication No. FHWA/IN/JTRP-2016/08). West Lafayette, IN: Purdue University.

Evans, R., Cassel, D., and Sneed, R. E. 1996. Soil, water and crop characteristics important to irrigation scheduling. In NC State Extension Publication. North Carolina State University.

Evett, S. R. 2003b. Soil water measurement by time domain reflectometry. In Encyclopedia of Water Science, eds. B.A. Stewart and T.A. Howell, 894-898. New York, NY: Marcel Dekker, Inc.

Evett, S. R. 2000. Some aspects of time domain reflectometry (TDR), neutron scattering (NS), and capacitance methods of soil water content measurement. In Journal of International Atomic Energy Agency Symposium 59(1137): 5-49. Vienna, Austria: International Atomic Energy Agency.

Farhat, N. 2018. Effect of relative humidity on evaporation rates in Nabatieh Region. In Lebanese Science Journal, Volume 19 (1).

Farouki, O. T. 1981. Thermal properties of soils. CRREL Monograph 81-1. U.S. Army Corps of Engineers, Cold Regions Research and Engineering Laboratory, Hanover, New Hampshire.

Feddes, R. A., Hoff, H., Bruen, M., Dawson, T. de Rosnay, P., Dirmeyer, P., Jackson, R. B., Kabat, P., Kleidon, A., Lilly, A., and Pitman, A. J. 2001. Modeling root water uptake in hydrological and climate models. Bulletin of the Americal Meteorological Society, vol. 82 (12): pp. 2797-2809.

Feddes, R. A., Kowalik, P. J., and Zaradny, H. 1978. Simulation of field water use and crop yield, Simulation Monographs, Pudoc, Wageningen, 195 p.

Feki, M., Ravazzani, G., Ceppi, A., and Mancini, M. 2018. Influence of soil hydraulic variability on soil moisture simulations and irrigation scheduling in a maize field. In Journal of Agricultural Water Management. volume 202, pp. 183-194.

Franke, O. L., Reilly, T. E., and Bennett, G. D. 1987. Definition of boundary and initial conditions in the analysis of saturated groundwater flow systems: An Introduction. Techniques of Water Resources Investigations of the U.S. Geological Survey. Book 3, Chapter B5. US Government Publishing office (US G.P.O), Washington.

Fredlund, D. G. 2006. Unsaturated soil mechanics in engineering practice. American Society of Civil Engineers, Journal of Geotechnical and Geoenvironmental Engineering. Vol. 132 (3), pp. 286-321.

Fredlund, D. G., and Gitirana Jr., G. F. N. 2005. Unsaturated soil mechanics as a series of partial differential equations. In Proceedings of International Conference on Problematic Soils. Vol. 25, GEOPROB 2005. Eastern Mediterranean University, Famagusta, N, Cyprus. pp. 27.

Fredlund, D., and Hung, V. 2001. Prediction of volume change in an expansive soil as a result of vegetation and environmental changes. American Society of Civil Engineers, Proceedings of the ASCE Conference on Expansive Clay Soils and Vegetative Influences on Shallow Foundations, Geotechnical Special Publication, Houston, Texas, Reston. October 10-13, Vol. 115. pp. 24-43.

Fredlund, D. G., and Xing, A. 1994. Equations for the soil water characteristic curve. Canadian Geotechnical Journal, vol. 31 (3), pp. 521-532.

Fredlund, D. G., Bergan, A. T. and Sauer, E. K. 1975. Deformation characterization of subgrade soils for highways and runways in northern environments. In Canadian Geotechnical Journal, 12(2): 213-223.

Fredlund, D. G. 1967. Comparison of soil suction and one-dimensional consolidation characteristics of a highly plastic clay. Canada. Technical Report No. 245, Division of Building Research, National Research Council, Ottawa, Ontario, July 1967.

Gardner, W. 1958. Some steady state solutions of the unsaturated moisture flow equation with application to evaporation from a water table. Soil Science Journal, vol. 85 (4). pp. 228-232.

Gaspard, K., Martinez, M., Zhang, Z., and Wu, Z. 2007. Impact of Hurricane Katrina on roadways in the New Orleans Area. Technical Assistance Report No. 07-2TA, LTRC Pavement Research Group, Louisiana Department of Transportation and Development, Louisiana Transportation Research Center, Louisiana, USA.

Gautam, S., He, S., and Yu, X. 2019. Stabilization of expansive soil using injection of liquid ionic soil stabilizer: a case study between field and laboratory treatment. In GeoCongress 2019: Soil Improvement (pp. 335-343). American Society of Civil Engineers Reston, VA.

Gavin, H. P. 2022. The Levenberg-Marquardt algorithm for nonlinear least squares curve-fitting problems. Department of Civil and Environmental Engineering, Duke University.

GeoSlope International Ltd. (GeoSlope) 2020. Heat and mass transfer modeling with GeoStudio 2020, 1st Edition. Updated, July 2020; First Published August 2017. GeoSlope International Ltd, Calgary, Alberta, Canada.

GeoSlope International Ltd. (GeoSlope). 2015. Seepage modeling with SEEP/W: An Engineering Methodology. 2015 Edition

GeoSlope International Ltd. (GeoSlope). 2012. Seepage modeling with SEEP/W. An engineering methodology. July 2012 Edition. GeoSlope International Ltd., Calgary, AB, Canada.

Gitirana Jr, G., Fredlund, M. D., and Fredlund, D. G. 2005. Infiltration-runoff boundary conditions in seepage analysis, Proceedings of the Fifty-Eighth Canadian Geotechnical Conference, GeoSask 2005 , and Sixth Joint IAH-CNC and CGS Groundwater Speciality Conferences, Saskatoon, SK. pp. 516-523.

Gitirana Jr, G., Fredlund, M. D., and Fredlund, D. G. 2006. Numerical modeling of soil-atmosphere interaction for unsaturated surfaces. American Society of Civil Engineers. Proceedings of the Fourth International Conference on Unsaturated Soils, Carefree, Arizona, vol. 1. pp. 658–669.

Goldbaum, J. 2022. Colorado Department of Transpiration Pavement M-E Design. Online August 2022.

Gong, Y., Cao, Q., and Sun, Z. 2003. The effects of soil bulk density, clay content and temperature on soil water content measurement using time-domain reflectometry. Journal of Hydrological Processes 17: pp. 3601-3614

Guan, X., Huang, J., Guo, N., Bi, J., and Wang, G. 2009. Variability of soil moisture and its relationship with surface albedo and soil thermal parameters over the loess plateau. In Journal of Advances In Atmospheric Sciences, Vol. 26, No. 4, 2009, pp. 692-700.

Gudipudi, P. P., Underwood, B. S., and Zalghout, A. 2017. Impact of climate change on pavement structural performance in the United States. Journal of Transportation Research Part D, Transport and Environment, vol. 57 (1). pp. 172-184.

Gulliver, J., Ahmed, F., Nieber, J. L., and Horwatich, J. 2014. Infiltration into a roadside grassed swale. In 13th International Conference on Urban Drainage, Sarawak, Malaysia, 7□12 September 2014

Guymon, G. L., Berg, R. L., and Johnston, T. C. 1986. Mathematical model of frost heave and thaw settlement in pavements. CRREL Report 93-2. U. S. Army Cold Regions Research and Engineering Laboratory.

Guyer, J. P. 2018. An introduction to the principles of pavement drainage. Independently Published. p. 28.

Hall, K. D., Dennis, N. D., Qazi, A., and Chang, X. 2013. Permeability and drainage of superpave. Final Report TRC0203. Transportation Research Committee. Arkansas State Highway and Transportation Department. US Department of Transportation Federal Highway Administration.

Han, Z., Vanapalli, S. K., and Zou, W. 2016. Integrated approaches for predicting soil water characteristic curve and resilient modulus of compacted fine-grained subgrade soils. Canadian Geotechnical Journal, vol. 54 (5). pp. 646-663.

Han, Z., and Vanapalli, S. K. 2015. Model for predicting resilient modulus of unsaturated subgrade soil using soil-water characteristic curve. In Canadian Geotechnical Journal, 52(10), pp. 1605-1619.

Hartmann, K., Krois, J., Waske, B. 2018: E-Learning Project SOGA: Statistics and Geospatial Data Analysis. Department of Earth Sciences, Freie Universitaet, Berlin.

Hein, D. K., and Jung, F. W. 1994. Seasonal variations in pavement strength. Presented at 4th International Conference on the Bearing Capacity of Roads and Airfields, 1994, Vol. 1, pp. 661– 682.

Heitor, A., Parkinson, J., and Kotzur, T. 2021. The role of soil stabilisation in mitigating the impact of climate change in transport infrastructure with reference to wetting processes. In Journal of Applied Science, 11, 1080.

Henry, K. S., Olson, J. P., Farrington, S. P., and Lens, J. 2005. Improved performance of unpaved roads during spring thaw. Engineer Research and Development Center. Cold Regions Research and Engineering Laboratory, United State.

Herb, W., Marasteanu, M., and Stefan, H. G. 2006. Simulation and characterization of asphalt pavement temperatures. Project Report No. 480. Minnesota Department of Transportation (MNDOT). St. Anthony Falls Laboratory.

Holsten, A., Vetter, T., Vohland, K., and Krysanova., V. 2009. Impact of climate change on soil moisture dynamics in Brandenburg with a focus on nature conservation areas. In Journal of Ecology Modelling. volume 220 (17). pp. 2076-2087.

Hou, X., Vanapalli, S. K., and Li, T. 2019. Water flow in unsaturated soils subjected to multiple infiltration events. In Canadian Geotechnical Journal. cgj-2018-0566.R3.

Houston, W. N., Mirza, M. W., and Zapata C. E. 2006. Environmental effects in pavement mix and structural design systems, Calibration, and validation of the ICM version 2.6. Preliminary Draft Final Report Part 2. NCHRP 9-23 Project, Copy No.1. National Cooperative Highway Research Program. Transportation Research Board, National Research Council, Washington DC., pp. 333.

Hsiao, T. C., Heng, L., Steduto, P., Rojas-Lara, B., Raes, D., and Fereres, E. 2009. AquaCrop-The FAO crop model to simulate yield response to water:III. Parameterization and testing for maize. In Journal of Agronomy. 101(3), pp. 448-459

Huang, B., Gong, H., and Shu, X. 2016. Local Calibration of Mechanistic-Empirical Pavement Design Guide in Tennessee (No. RES2013-33). Tennessee. Department of Transportation.

Huang, M., Barbour, S. L. and Carey, S. K. 2015. The impact of reclamation cover depth on the performance of reclaimed shale overburden at an oil-sands mine in Northern Alberta, Canada. Journal of Hydrological Processes, vol. 29 (12). John Wiley & Sons. pp. 2840-2854.

Incropera, F. P., DeWitt, D. P., Bergman, T. L. and Lavine, A. S. 2007. Fundamentals of heat and mass transfer, 6th Edition. John Wiley and Sons Inc. New Jersey, USA.

Intergovernmental Panel on Climate Change (IPCC). 2013. Climate change 2013: The physical science basis. Working-Group I contribution to the Fifth Assessment Report of the IPCC. Cambridge, United Kingdom: Cambridge University Press.

Intergovernmental Panel on Climate Change (IPCC). 2007. Climate Change 2007: The Physical Science Basis. Contribution of Working Group I to the Fourth Assessment Report of the Intergovernmental Panel on Climate Change. (eds) Solomon, S., Qin, D., Manning, M., Chen, Z., Marquis, M., Avery, K. B., Tignor, L. M., and Miller, H. L Cambridge University Press, Cambridge, United Kingdom and New York, NY, USA, 996 p.

Intergovernmental Panel on Climate Change (IPCC). 2007. Climate Change 2007: Impacts, Adaptation and Vulnerability. Contribution of Working Group II to the Fourth Assessment Report of the Intergovernmental Panel on Climate Change, (eds) Parry, M. L., Canziani, O. F., Palutikof, J. P., van der Linden, P. J., and Hanson, C. E. Cambridge University Press, Cambridge, UK, 976 p.

Intergovernmental Panel on Climate Change (IPCC). 2001: Climate Change 2001: The Scientific Basis. Contribution of Working Group I to the Third Assessment Report of the Intergovernmental Panel on Climate Change [Houghton, J.T., Y. Ding, D.J. Griggs, M. Noguer, P.J. van der Linden, X. Dai, K. Maskell, and C.A. Johnson (eds.)]. Cambridge University Press, Cambridge, United Kingdom and New York, NY, USA, 881 pp.

Jamshidian, M., Jennrich, R. I., and Liu, W. 2007. A study of Partial F-tests for multiple linear regression models. In Journal of Computational Statistics and Data Analysis, 51(12). pp. 6269-6284.

Jia, X. X., Shao, M. A., Zhu, Y. J., and Luo, Y. 2017. Soil moisture decline due to afforestation across the Loess Plateau, China. In Journal of Hydrology, volume 546. pp. 113-122.

Jiji, L. M. 2009. Heat convection. 2nd Edition. Springer Science and Business Media. Berlin pp. 543.

Johanneck, L., Tompkins, D., Clyne, T., and Khazanovich, L. 2011. Minnesota Roads research data for evaluation and local calibration the Mechanistic Empirical Pavement Design Guide's Enhanced Integrated Climate Model. Transportation Research Records, Journal of the Transportation Research Board, Washington, DC, Vol. 2226. pp. 30-40.

Johansen, O. 1975. Thermal conductivity of soils. Draft Translation 637, ADA044002US Army Cold Regions Research and Engineering Laboratory, Hanover, New Hampshire.

Kasubuchi, T. 1975. The effect of soil moisture on thermal properties in some typical Japanese upland soils. Journal of Soil Science and Plant Nutrition, vol. 21 (2). pp. 107-112.

Khoury, C. N., Khoury, N. N., and Miller, G. A. 2011. Effect of cyclic suction history (hydraulic hysteresis) on resilient modulus of unsaturated fine-grained soil. Transportation Research Record: Journal of the Transportation Research Board, 2232, (1) (December 1, 2011): p. 68-75.

Khoury, C. N., Miller, G. A., and Abousleiman, Y. N. 2010. Effects of suction hysteresis on resilient modulus of fine-grained cohesionless soil. Report No. OTCREOS7.1-27-F. Oklahoma Transportation Center, Oklahoma.

Khoury, C. N., and Miller, G. A. 2010. Effect of suction hysteresis on the shear strength of unsaturated soil interfaces. 1st Edition, Editors, Alonso, E. E., and Gens, A. Proceedings of Fifth International Conference on Unsaturated Soils. September 2010, Barcelona, Spain, in press, vol. 1. pp. 5. CRC Press, London.

Kim, Y. R., Jadoun, F. M., Hou, T., and Muthadi, N. 2011. Local calibration of the MEPDG for flexible pavement design. Final Report No. FHWA\NC\2007-07. North Carolina Department of Transportation. pp. 528.

Kim, D., and Siddiki, N. Z. 2006. Simplification of resilient modulus testing for subgrades. Joint Transportation Research Program, 265. Final Report, FHWA/IN/JTRP-2005/23, Project No. C-36-52S, File No. 6-20-18, SPR- 2633

Kosmas, C., Danalatos, N. G., Poesen, J., and Van Wesemael, B. 1998. The effect of water vapour adsorption on soil moisture content under Mediterranean climatic conditions. In Journal of Agricultural Water Management, 36(2), pp. 157-168.

Kousari, M. R., and Ahani, H. 2012. An investigation on reference crop evapotranspiration trend from 1975 to 2005 in Iran. International Journal of Climatology vol. 32 (15), p. 2387-2402.

Laloui, L. 2013. Mechanics of unsaturated geomaterials. Wiley and Sons, London.

Larson, G., and Dempsey, B. J. 2003. Enhanced Integrated Climatic Model Version 3.0. Applied Research Associates/ ERES Division Staff, for upgrade with results from NCHRP 1- 37 A, the 2002 Guide Development.

Larson, G., and Dempsey, B. J. 1997. Integrated Climate Model, Version 2.0. Newmark Civil Engineering Laboratory, University of Illinois, at Urbana-Champaign, IL. Report No. DTFA MN/DOT 72114.

Lary, J. A., and Mahoney, J. P. 1984. Seasonal effects on the strength of pavement structures. Transportation Research Record, Journal of the Transportation Research Record, issue 954. pp. 88-94.

Lazarovitch, N., Simunek, J, and Shani, U. 2005. System-dependent boundary condition for water flow from subsurface source. In Journal of Soil Science Society of America. 69(1), pp. 46-50.

Lee, W., Bohra, N. C., Altschaeffl, A. G. and White, T. D. 1995. Resilient modulus of cohesive soils and the effect of freeze-thaw. In Canadian Geotechnical Journal, 32(4): 559-568.

Li, D. and Seilg, E. T. 1994. Resilient Modulus for Fine-Grained Subgrade Soils. Journal of Geotechnical Engineering, Vol. 120 (6) 1994.

Li, P., Li, T. L., and Vanapalli, S. K. 2016. Influence of environmental factors on the wetting front depth: A case study in the Loess Plateau. In Journal of Engineering Geology, 214: 1-10.

Li, Q., Mills, L., and McNeil, S. 2011. The implication of climate change on pavement performance and design. UDUTC Final report. University of Delaware, University Transportation Center.

Li, Q., Xiao, D. X., Wang, K. C. P., Hall, K. D., and Qui, Y. 2011, Mechanistic Empirical Pavement Design Guide (MEPDG); A bird's-eye view. Journal of Modern Transportation, Vol. 19. pp. 114-133.

Liang, H. S., and Lytton, R. L. 1989. Rainfall estimation for pavement analysis and design. Transportation Research Record, Proceedings of the 88th Annual Meeting, Transportation Research Board, issue 1252. pp. 42-49.

Lin, C., Greenwald, D., and Banin, A. 2003. Temperature dependence of infiltration rate during large scale water recharge into soil. In Soil Science Society of American Journal, 67, pp. 487-493.

Liu, L., Fei, L., Zhu, H., Hao., K., and Li., J. 2021. Effects of Water Temperature on Soil Water Infiltration Characteristics Under Film-Mulched Drip Irrigation. In Journal of Soil Science and Plant Nutrition 21, pp. 2837-2846 (2021).

Liu, S. J., and Lytton, R. L. 1985. Environmental effects on pavement drainage. Report FHWA-DTFH-61-87-C-00057, Vol. 4, Federal Highway Administration, Department of Transportation, Washington, D.C.

Liuzzo, L., Viola, F., and Noto, L. V. 2016. Wind speed and temperature trends impacts on reference evapotranspiration in Southern Italy. Journal of Theoretical and Applied Climatology, vol. 123, p. 43-62.

Lofgren, B. M., Hunter, T. S., and Wilbarger, J. 2011. Effects of using air temperature as a proxy for potential evapotranspiration in climate change scenarios of Great Lakes basin hydrology. In Journal of Great Lakes Research, volume 37(4). pp. 744-752.

Long-term Pavement Performance and Seasonal Monitoring (LTPP and SMP). 2020. Program Database. Online 2020.

Lourakis, M. A. 2005. A brief description of the Levenberg-Marquardt algorithm implemented by levmar, Technical Report, Institute of Computer Science, Foundation for Research and Technology- Hellas.

Luo, S., Bai, T., Guo, M., Wei, Y., and Ma, W. 2022. Impact of freeze-thaw cycles on the long-term performance of concrete pavement and related improvement measures: A Review. In Journal of Materials, 15(13):4568.

Lytton, R. L., Pufahl, D. E., Michalak, C. H., Liang, H. S., and Dempsey, B. J. 1993. An integrated Model of the climatic effects on pavements. Federal Highway Administration Final Report No. FHWA-RD-90-033, McLean, Virginia,

Lytton, R. L., Uzan, J., Fernando, E. G., Rogue, R., Hiltunen, D., and Stoffels, S. M. 1993. Development and validation of performance prediction models and specifications for asphalt binders and paving mixes. Report No. SHRP-A-357. Strategic Highway Research Program, National Research Council, Washington, DC.

Lytton, R. L., Pufahl, D. E., Michalak, C. H., Liang, H. S., and Dempsey, B. J. 1989. An integrated model of climatic effects on pavement. Report No. FHWA-RD-90-033. Federal Highway Administration, U.S. Department of Transportation. McLean, VA.

Malik, M. S., Shukla, J. P., and Mishra, S. N. 2021. Effect of groundwater level on soil moisture, soil temperature and surface temperature. In Journal of the Indian Society of Remote Sensing, 49(9), pp. 2143-2161.

Marquardt, D. W. 1965. An algorithm for least-squares estimation of nonlinear parameters, In Journal of the Society for Industrial and Applied Mathematics, 11(2): pp. 431-441.

Marr, S. A., Gilbert, R. B., and Rauch, A. F. 2004. A practical method for predicting expansive soil behavior. Proceedings of Geotechnical Engineering for Transportation Projects, Geo-Trans 2004. American Society of Civil Engineers, Geotechnical Special Publication, vol 1 (126), ASCE. Virginia.

Mahoney, J. P, Lee, S.W., Jackson, N. C., and Newcomb, D. E. 1988. Mechanistic-based overlay design procedure for Washington state flexible pavements. Final Report WA-RD 170.1. Washington State Department of Transportation, Washington.

McCartney, J. S., and Khosravi, A. 2013. Field monitoring system for suction and temperature profiles under pavements. American Society of Civil Engineers, Journal of Performance of Constructed Facilities, Vol. 27 (6). pp. 818-825.

McCartney, J. S., Selvam, R. P., King, J., and Khosravi, A. 2010. Evaluation of the Enhanced Integrated Climatic Model for the Arkansas State Highway and Transportation Department. Final Report TRC0902. Transportation Research Committee.

Memon, R. A., Leung, D. Y. C., and Chunho, L. 2008. A review on the generation, determination, and mitigation of urban heat island. In Journal of Environmental science, vol. 20 (1). pp. 120-128.

Miller, G. A., Khoury, C. N., Muraleetharan, K. K., Liu, C., and Kibbey, T. C. G. 2008. Effects of Solid Deformations on Hysteretic Soil Water Characteristic Curves: Experiments and simulations In Journal of Water Resources, Research Journal, 44 (6).

Ministry of Transportation Ontario (MTO). 2013. Pavement design and rehabilitation manual. Second Edition. Materials Engineering and Research Office. Ministry of Transportation Ontario, Ontario, Canada.

Modeste, K. G., Falls, L. C., and Park, P. Y. 2015. Performance of permeable pavements under low volume traffic loads. Transportation Research Records, Proceedings of Transportation Research Board, 94th

Mohammad, A. 2021. Studying the effects of roads geometry and design parameters on the pavement drainage system. In Journal of Civil Engineering. 7, pp. 49-58

Monteith, J. L. 1981. Evaporation and surface temperature. Quarterly Journal of the Royal Meteorological Society, vol. 107 (451). pp. 1-27.

Mu, F., Vandenbossche, J. M., Gatti, K. A., and Sherwood, J. A. 2012. An evaluation of JPCP faulting and transverse cracking models of the mechanistic-empirical pavement design guide, Road Materials and Pavement Design, 13:1, 128-141.

Mullan, D. J., and Reynolds, M. P. 2010. Quantifying genetic effects of ground cover on soil water evaporation using digital imaging. In Journal of Functional Plant Biology, 37: 703–712.

National Aeronautics and Space Administration (NASA). 2022. Climate. Online August 2022.

National Centers for Environmental Information (NCEI). 2022. U.S Climate Normals. National Oceanic and Atmospheric Administration. Online October 2022.

National Institute of Standards (NIST)/SEMATECH. 2022. E-handbook of statistical methods. U.S Department of Commerce. Online 2022.

National Oceanic and Atmospheric Administration (NOAA). 2022. U.S Climate Normals. National Centers for Environmental Information, Online October 2022.

National Research Council (NRC). 2008. Potential impacts of climate change on U.S. transportation: Special Report 290. National Research Council, Committee on Climate Change and U.S. Transportation, Transportation Research Board, Washington, D.C.

Neuman, S. P., Feddes, R. A., and Bresler, E. 1974. Finite element simulation of flow in saturated-unsaturated soils considering water uptake by plants. 3rd Annual Report, Project No. A10-SWC-77. Hydraulic Engineering Laboratory, Technion Research and Development Foundation, Haifa, Israel.

Newman, G. P. 1995. Heat and mass transfer in unsaturated soils during freezing. Thesis, Faculty of Graduate Studies and Research, Department of Civil Engineering, University of Saskatchewan, Saskatoon, Canada.

Nielsen, D., Miceli-Garcia, J. J., and Lyon, D. J. 2012. Canopy cover and leaf area index relationships for wheat, triticale, and corn. In Journal of Agronomy, 104 (6).

Nimmo, J. R. 2005. Unsaturated zone flow processes. Editors, Anderson, M., G., and Bear, J., Encyclopedia of Hydrological Sciences: Part 13-Groundwater: Chichester, UK, Wiley, vol. 4, p. 2299-2322.

Nimmo, J. R., and Miller, E. E. 1986. The temperature dependence of isothermal moisture vs. potential characteristics of soils. Soil Science Society of America Journal, vol. 50 (5). pp. 1105-1113.

O'Donnell, J., A, Romanovsky, V., E, Harden, J., W, and McGuire, A., D. 2009. The effect of moisture content on the thermal conductivity of moss and organic soil horizons from black spruce ecosystems in interior Alaska. Soil Science Society of America Journal, vol. 174 (12). pp. 646-651.

Oloo, S. Y., Fredlund, D. G., Gan, J. K-M. 1997. Bearing capacity of unpaved roads. Canadian In Geotechnical Journal, 34, pp. 398-407.

Ott, R. L., and Longnecker, M. 2016. An introduction to statistical methods and data analysis Seventh ed. Cengage Learning, Boston, MA.

Overton, D. D., Chao, K. C., and Nelson, J. D. 2006. Time rate of heave prediction for expansive soils. Editors, DeGroot, D. J., DeJong, J. T., Frost, D., and Baise, L. G. Proceedings of GeoCongress 2006: American Society of Civil Engineers, Geotechnical Engineering in the Information Technology Age, Atlanta, Georgia. pp. 1-6.

Ovik, J. M., Birgisson, B., and Newcomb, D. E. 2000. Characterizing seasonal variations in flexible pavement material properties for Use in Mechanistic Empirical design procedures. Report No. MN/RC-2000-35. Final Report 1996-2000. Transportation Research Records, Journal of the Transportation Research Board, Washington, D.C., vol. 1684 (1). pp. 1-7.

Ovik, J. M., Birgisson, B., and Newcomb, D. E. 1999. Characterizing seasonal variations in flexible pavement material properties. Transportation Research Record, Journal of the Transportation Research Board, vol. 1684 (1). pp. 1-7.

Pahud, D. 2002. Geothermal Energy and Heat Storage. Laboratorio di Energia, Ecologia ed Economia, Canobbio.

Papanikolaou, C. D., and Sakellariou-Makrantonaki, M. A. 2020. Estimation of corn leaf area index and ground cover with vegetation indices as a result of irrigation dose. Published by Canadian Center of Science and Education. In Journal of Agricultural Science; Vol. 12, No. 12; 2020.

Pellicer, J., Garcıa-Morales, V., Guanter, L., Hernandez, M. J., and Dolz, M. 2002. On the experimental values of the water surface tension used in some textbooks. In American Journal of Physics, 70(7), pp 705-709.

Perera, R. W., and Kohn, S. D. 2001. LTPP Data analysis: Factors affecting pavement smoothness. NCHRP Web Document 40 (Project 20-50[8/13]): Contractor's Final Report.

Perez-Garcia, N., Fredlund, D., Garnica-Anguas, P., and Mestas-Martinez, N. 2016. A model to predict changes in resilient modulus resulting from wetting and drying. Revista Infraestructura Vial/LanammeUCR/ISSN: 2215-3705/Volumen 17/Número 30/Diciembre. p.p. 23-30.

Philip, J. R. 1998. Water movement in unsaturated soils. In Journal of Encyclopedia of Hydrology and Lakes. Encyclopedia of Earth Science. Springer, Dordrecht.

Philip, J. R., 1958. Physics of water movement in porous solids: Highway Research Board, Proceedings of the 37th Annual Meeting of the Highway Research Board, National Research Council, vol. 629 (40). p 147-163.

Philip, J. R. 1957b. Transient fluid motions in saturated porous media. Australia Journal of Physics, vol. 10. pp. 43-53.

Philip, J. R. 1957h. The theory of infiltration: Soil Science Journal, vol. 84. pp. 163-178.

Pk, S., Bashir, R., and Beddoe, R. 2021. Effect of climate change on earthen embankments in Southern Ontario, Canada. In Journal of Environmental Geotechnics 8 (2). pp. 148-169.

Price, M. A., Low, R. G., and McCann, C. 2000. Mechanisms of water storage and flow in the unsaturated zone of the chalk aquifer. Journal of Hydrology, vol. 233. pp. 54-71.

Pufahl, D. E., and Lytton, R. L. 1991. Temperature and suction profiles beneath highway pavements: computed and measured. Transportation Research Records, Journal of Transportation Research Board, issue 1307. pp. 268-276.

Puri, A. N., Crowther, E. M., and Keen, B. A. 1925. The relation between the vapour pressure and water content of soils. The Journal of Agricultural Science. 15 (1), pp. 68-88.

Qin, Y., and Hiller, J., E. 2013. Ways of formulating wind speed in heat convection significantly influencing pavement temperature prediction. Journal of Heat and Mass Transfer, vol. 49 (5). pp. 745-752.

Quintero, N. 2007. Validation of the Enhanced Integrated Climatic Model (EICM) for the Ohio SHRP Test Road at U.S. 23. M.S. Thesis submitted to the Russ College of Engineering and Technology of Ohio University.

Rada, G. R., Elkins, G. E., Henderson, B., and Lopez Jr, A. 1995. LTPP seasonal monitoring program: Instrumentation installation and data collection guidelines (No. FHWA-RD-94-110). United States. Federal Highway Administration. Office of Engineering Research and Development.

Ramirez-Garcia, J., Almendros, P., and Quemada, M. 2012. Ground cover and leaf area index relationship in a grass, legume and crucifer crop. In Journal of Plant Soil Environment., 58, (8): pp. 385-390

Ravichandran, N., and Krishnapillai, S. H. 2011. A flexible model for moisture-suction relationship for unsaturated soils and its application. Scientific Research, International Journal of Geosciences, vol. 2 (3). pp. 204-213.

Raymond, D. J., Raga, G. B., Bretherton, C. S., Molinar, J., Lopez-Carillo, C., and Fuchs, Z. 2003. Convective forcing in the intertropical convergence zone of the east Pacific. In Journal of the Atmospheric Science, 60, 2064-2082.

Ridgeway, H. H. 1976. Infiltration of water through the pavement surface (abridgement). Transpiration Research Board, Journal Of The Transportation Research Record. Issue 616. pp 98-100.

Rivera-Hernandez, X. A., Ellithy, G., and vahedifard, F. 2019. Integrating field monitoring and numerical modeling to evaluate performance of a levee under climatic and tidal variations. American Society of Civil Engineers, Journal of Geotechnical and Geoenvironmental Engineering, vol. 145 (10). 05019009.

Robbins, C. W. 1977. Hydraulic conductivity and moisture retention characteristics of southern idaho's silt loam soils. Idaho Agricultural Experiment Station. Research Bulletin No. 99.

Robinson, D. A., Jones, S. B., Wraith, J. M., Or, D., and Friedman, S. P. 2003. A review of advances in dielectric and electrical conductivity measurements in soils using time domain reflectometry. Vadose Zone Journal 2: 444-475.

Romero-Morales, E. E. 1999. Characterisation and thermo-mechanical behaviour of unsaturated Boom clay: An experimental study, PhD thesis, UPC, Barcelona, Spain.

Rosenbalm, D. C., and Zapata, C. 2013. Incorporation of the soil-water characteristic curve hysteresis in pavement design. In Proceedings of the 1st Pan-Am Conference on Unsaturated Soils, Cartagena de Indias, Colombia., pp. 461-467.

Roxy, M., S, Sumithranand, V. B., and Renuka, G. 2014. Estimation of soil moisture and its effect on soil thermal characteristics at Astronomical Observatory, Thiruvananthapuram, south Kerala. Journal of Earth System Science, vol. 123 (8). pp. 1793-1807.

Saadeldin, R., and Henni, A. A. 2016. A novel modeling approach for the simulation of soil-water interaction in a highly plastic clay. In journal of Geomechanics and Geophysics for Geo-Energy and Geo-Resources.

Scaife, C. I., Singh, N. K., Emanuel, R. E., Miniat, C. F., and Band, L. E. 2020. Non-linear quick-flow response as indicators of runoff generation mechanisms. In Journal of Hydrological Processes, volume 34. pp. 2949-2964.

Schmidli, J., and Rotunno, R. 2010. Mechanisms of along-valley winds and heat exchange over mountainous terrain. In Journal of Atmospheric Science, vol. 67 (9). pp. 3033-3047.

Soliman, H., and Shalaby, A. 2010. Sensitivity of subgrade resilient modulus to moisture variation. In Development of New Technologies for Classification of Materials Session of the 2010 Annual Conference of the Transportation Association of Canada, Halifax, Nova Scotia

Shrestha, A. K., Thapa, A., and Gautam, H. 2019. Solar radiation, air temperature, relative humidity, and dew Point study: Damak, Jhapa, Nepal. International Journal of Photoenergy, vol. 2019. P 7.

Sillers, W. S. 1997. The mathematical representation of the soil-water characteristic curve. MSc thesis, University of Saskatchewan.

Simonsen, E., Janoo, V. C., and Isacsson, U. 2002. Resilient properties of unbound road materials during seasonal frost conditions. In Journal of Cold Regions Engineering, 16(1): 28-50.

Snedecor, G. W., and Cochran, W. G. 1989. Statistical methods, 8th Edition, Iowa State University Press.

Song, X., Yan, M., and Li, H. 2013. The development of a one parameter model for the soil-water characteristic curve in the loess gully region, In Journal of Food, Agriculture & Environment, vol. 11, pp. 1546-1549.

Stéfanon, M., Drobinski, P., D'Andrea, F., Lebeaupin-Brossier, C., and Bastin, S. 2014. Soil moisture–temperature feedbacks at meso-scale during summer heat waves over Western Europe. In Journal of Climate Dynamics. Volume 42 (5-6). Pp. 1309-1324.

Su, B. Q., and Shangguan, Z. P. 2018. Decline in soil moisture due to vegetation restoration on the Loess Plateau of China. In Journal of Land Degradation and Development, 30(3). pp. 290-299.

Sultana, M. 2017. Assessment and modelling deterioration of flood affected pavements. PhD Thesis. Griffith University, Griffith School of Engineering, Queensland, Australia.

Sultana, M., Chai, G., Martin, T., and Chowdhury, S. 2014. A review of the structural performance of flooded pavements. Proceedings of 26th ARRB Conference-Research driving efficiency, issue 5.1, Sydney, New South Wales.

Suseela, V., Conant, R. T., Wallenstein, M. D., and Dukes, J. S. 2012. Effects of soil moisture on the temperature sensitivity of heterotrophic respiration vary seasonally in an old-field climate change experiment. In Journal of Global Climate Biology, volume 18 (1). pp. 336-348.

Tang, A. M., Hughes, P. N., Dijkstra, T. A., Askarinejad, A., Brencič, M., Cui. Y. J., Diez, J. J., Firgi, T., Gajewska, B., Gentile, F., Grossi, G., Jommi, C., Kehagia, F., Koda, C., ter Maat, H. W., Lenart, S., Lourenco, S., Oliveira, M., Osinski, P., Springman, S. M., Stirling, R., Toll, D. G., and Van Beek, V. .2017. Atmosphere–vegetation–soil interactions in a climate change context; impact of changing conditions on engineered transport infrastructure slopes in Europe. In Quarterly Journal of Engineering Geology and Hydrogeology. COST Action TU1202- Impact of climate change on engineered slopes for infrastructure. vol. 51, pp 156-168.

Tardif, R. 2002. Notes on soil moisture sensor calibration and temperature correction. NCAR/RAP.

Thiam, P. M., Dore, G., and Bilodeau, J., P. 2013. Effect of the future increases of precipitation on the long-term performance of roads. Proceedings of 9th International Conference on the Bearing Capacity of Roads, Railways and Airfields, vol. 2. Trondheim, Norway, June 2013.

Thode, R., and Gitiriana, G. 2008. SvFlux theory manual. Soilvision Systems Ltd. Saskatchewan, Canada.

Thornthwaite, C. W. 1948. An Approach toward a rational classification of climate. Journal of Geographical Review, vol. 38 (1). pp. 55-94.

Thorup-Kristensen K., Cortasa, M. S., and Loges, R. 2009. Winter wheat roots grow twice as deep as spring wheat roots, is this important for N uptake and N leaching losses. Journal of Plant and Soil. 322: pp. 101–114.

Farashah, K. M., Salehiashani, S., Varamini, S., and Tighe, L. S. 2021. Best practices in measuring rutting and shoving on asphalt pavements. In Innovations in Pavement Management, Engineering and Technologies Session, 2021 TAC Conference and Exhibition.

Todd, L. 2014. Evaluating transportation economic development impacts: Understanding how transport policy and planning decisions affect employment, incomes, productivity, competitiveness, property values and tax revenues. Victoria Transport Policy Institute. In The International Transportation Economic Development Conference, 2014 in Dallas, Texas.

Transportation Association of Canada (TAC). 2014. Primer: Pavement asset design and management. Transportation Association of Canada, Ottawa, Canada.

Transportation Association of Canada (TAC). 1997. Pavement design and management guide, edt. Hass, R. C. G. . Transportation Association of Canada. p. 389.

Tuller, M., and Or, D. 2002. Unsaturated hydraulic conductivity of structured porous media: A review of liquid configuration based models. Vadose Zone Journal, vol. 1 (1). pp. 14-37.

United Nations Economic Commission For Europe. 2013. Climate change impacts and adaptation for international transport networks. Expert Group Report. United Nations, New York, 2013.

United States Department of Agriculture. 2017. Corn for grain in Minnesota counties: Map 4. Minnesota Department of Agriculture, United States Department of Agriculture – 2017 Census of agriculture.

University of Arkansas. 2022. Pavement management planning tool for local agencies. Center for Training Transportation Professionals. Online 2022.

Uzan, J. 1985. Characterization of granular material. Transportation Research Record No. 1022, National Research Council, Transportation Research Board, Washington, DC, pp. 52-59.

van den Honert, T. H. 1948. Water transport in plants as a catenary process. Discussion of the Faraday Society Journal. vol. 3. pp. 146-153.

Van Genuchten, M., Th. 1980. A closed form equation for predicting the hydraulic conductivity of unsaturated soils. Soil Science Society of America Journal, vol. 44 (5), pp. 892-898.

Hou, X., Vanapalli, S. K., and Li, T. 2019. Water flow in unsaturated soils subjected to multiple infiltration events. In Canadian Geotechnical Journal. cgj-2018-0566.R3.

Vanapalli, S. K., and Han, Z. 2014. Application of the unsaturated soil mechanics in the design of pavements. In Proceedings of the 6th International Conference on Unsaturated Soils, Sydney, Australia, pp. 1799-1805).

Vanapalli, S. K., and Oh, W. T. 2011. Simple techniques for the estimation of suction in compacted soils in the range of 0 to 60,000 kPa. Geotechnical Testing Journal, vol. 34 (6): pp. 765-774.

Vanapalli, S. K. 2009. Shear strength of unsaturated soils and its applications in geotechnical engineering practice. Proceedings of the 4th Asia-Pacific Conference on Unsaturated Soils, vol. 2. pp. 579-598, New Castle, Australia.

Vanapalli, S. K., Fredlund, D. G., and Pufahl, D. E. 1999. The influence of soil structure and stress history on the soil-water characteristics of a compacted till. Geotechnique, vol. 49 (2). pp. 143-159.

Vanapalli, S. K., Sillers, W. S., and Fredlund, M. D., 1998. The meaning and relevance of residual state to unsaturated soils. Proceedings of the 51st Canadian Geotechnical Conference, 4-7 October 1998, Edmonton, Alberta, vol. 1. pp. 101-108.

Vanapalli, S. K., Fredlund, D. G., Pufahl, D. E., and Clifton, A. W. 1996. Model for the prediction of shear strength with respect to soil suction. In Canadian Geotechnical Journal . 33: pp. 379-392.

Vanek, F. M., Angenent, L. T., Banks, J. H., Daziano, R. A., and Turnquist, M. A. 2014. Geometric design. Chap. D. In Sustainable Transportation Systems Engineering. 1st ed. New York: McGraw-Hill Education.

Viessman, Jr. W., and Lewis, G. L. 2003. Introduction to hydrology, 5th edn. Prentice Hall, Upper Saddle River, NJ, p 612.

Vinnikov, K. Y.; Robock, A.; Qiu, S. Entin, J. K.; Owe, M.; Choudhury, B. J.; Hollinger, S. E.; and Njoku, E. G. 1999. Satellite remote sensing of soil moisture in Illinois, USA. In Journal of Geophysical Research, vol. 104 (D4). pp. 4145-4168.

Wang, S., Fu, B., Gao, G., Liu, Y., and Zhou, J. 2013. Responses of soil moisture in different land cover types to rainfall events in a re-vegetation catchment area of the Loess Plateau, China. In Journal of Soil Science, Hydrology and Geomorphology. CATENA, Volume 101. Pp. 122-128.

Wang, G., Li, Y., Hu, H., and Wang, Y. 2008. Synergistic effect of vegetation and air temperature changes on soil water content in alpine frost meadow soil in the permafrost region of Qinghai-Tibet. In Journal of Hydrology Process. Volume 22 (17), pp. 3310-3320.

Wang, K., and Dickinson, R. E. 2013. Contribution of solar radiation to decadal temperature variability over land. Vol. 110 (37). p. 14877-14882.

Wang, D-Y., Ma, W., Niu, Y-H., Chang, X-X. and Wen, Z. 2007. Effects of cyclic freezing and thawing on mechanical properties of Qinghai–Tibet clay. In Journal of Cold Regions Science and Technology, 48(1): 34-43.

Wang, Y. 2005. Improving pavements with long-term pavement performance: Products for today and tomorrow. Paper 5. Development of a pavement climate map based on LTPP Data. Report No. FHWA-RD-03-049. Federal Highway Administration.

Weisbrod, G., and Reno, A. 2009. Economic impact of public transportation investment. Transit Cooperative Research Program (TCRP) Project J-11, Task 7. American Public Transportation Association, Economic Development Research Group and Cambridge Systematics.

Wesseling, J. G. 1991. Meerjarige simulatie van grondwaterstroming voor verschillende bodemprofielen, grondwatertrappen en gewassen met het model SWATRE. DLO-Staring Centrum, Wageningen. Rapport / DLO-Staring Centrum no. 152 p.

Wesseling, J. G. 1961. Principles of the unsaturated flow and their application to the penetration of moisture into the soil. Technical Bulletin 23. In Journal of the Institute for Land and Water Management Research, Wageningen, The Netherlands.

Williams, P. J., and Smith, M. W. 1989. The frozen earth - Fundamentals of geocryology. Cambridge University Press, Oxford.

Witczak M. W., El-Basyouny M., and El-Badawy S. 2007. Incorporation of the new (2005) E* predictive model in the MEPDG. NCHRP 1-40D Project, Final Report Addendum, National Cooperative Highway Research Program.

Witczak, M. W., Andrei, D., and Houston, W. N. 2000. Resilient modulus as function of soil moisture: Summary of predictive models, Development of the 2002 guide for the development of new and rehabilitated pavement structures. NCHRP 1-37 A, Inter Team Technical Report (Seasonal 1), Tempe, Arizona.

Witczak, M. W., Houston, W. N., and Andrei, D. 2000. A study of the expected changes in resilient modulus of the unbound layers with changes in moisture for 10 LTPP sites. Development of the 2002 Guide for the Development of New and Rehabilitated Pavement Structures, NCHRP 1-37 A, an Inter Team Technical Report. vol. 2.

Witczak, M. W., Houston, W. N., Zapata, C. E., Richter, C., Larson, G. and Walsh, K. 2000. Improvement of the Integrated Climatic Model for moisture content predictions. Development of the 2002 Guide for the Development of New and Rehabilitated Pavement Structures. Inter Team Technical Report

(Seasonal 4), NCHRP 1-37 A Project, National Cooperative Highway Research Program (NCHRP), Tempe, Arizona.

Wohl, E., Barros, A., Brunsell, N. A., Chappell, N. A., Coe, M. T., Giambelluca, T., Goldsmith, S. T., Harmon, R. S., Hendrickx, J. M. H., Juvik, J., McDonnell, J., and Ogden, F. L. 2012. The hydrology of the humid tropics. In Journal of Natural Climate Change 2, pp. 655-662.

World Meteorological Organization. 2014. Guide to Meteorological Instruments and Methods of Observation, WMO No. 8; Geneva.

Wösten, J. H. M., Lilly, A., Nemes, A., and Le Bas, C. 1999. Development and use of a database of hydraulic properties of European soils. Geoderma 90(3-4): pp. 169-185.

Wu, J., Zhang, R., Gui., S. 1999. Modeling soil water movement with water uptake by roots. In Journal of Plant and Soil. 215. pp. 7-17.

Xue, J., and Gavin, K. 2007. Effect of rainfall intensity on infiltration into partly saturated slopes. In Journal of Geotechnical and Geological Engineering, vol. 26(2). pp. 199-209.

Yang, D. Q., Rahardjo, H., Leong, E., and Choa, V. 1998. Coupled model for heat, moisture, air flow and deformation problems in unsaturated soils. American Society of Civil Engineers, Journal of Engineering Mechanics, Vol. 124 (12). pp, 1331-1338.

Yuan, X-X., and Nemtsov, L. 2018. Local calibration of the MEPDG distress and performance models for Ontario's flexible roads: Overview, Impacts, and Reflection. In Journal of the Transportation Research Record, Vol. 2672 (40) 207-216, National Academy of Sciences, Transportation Research Board.

Yuan, X-X., and Nemtsov, L. 2017. Ontario's Local calibration of the MEPDG distress and performance models for flexible roads: A Summary. In the 2017 Conference of the Transportation Association of Canada (TAC), St. John's, NL.

Yut, I., Mahoney, J., and Zinke, S. 2014. Preparation of the Implementation Plan of AASHTO Mechanistic Empirical Pavement Design Guide (M-E PDG) in Connecticut. Report No. CAPLAB XX-2014. Connecticut Department of Transportation.

Zaghloul, S., Ayed, A., Halim, A. A. E., Vitillo, N., and Sauber, R. 2006. Investigations of Environmental and Traffic Impacts on Mechanistic-Empirical Pavement Design Guide predictions. Transportation Research Record, Journal of Transportation Research board. Issue No. 1967. pp. 148-159.

Zapata, C. E., Perera, Y. Y., and Houston, W. N. 2009. Matric suction prediction model in new AASHTO Mechanistic Empirical Pavement Design Guide. Transportation Research Record, Journal of Transportation Research Board, vol. 2101(1). pp. 53-62.

Zapata C. E., and Houston W. N. 2008. Calibration and validation of the Enhanced Integrated Climatic Model for pavement design. NCHRP Report 602, 9-23 Project, American Association of State Highway and Transportation officials, National Cooperative Highway Research Program, Transportation Research Board. vol. 602.

Zapata, C. E., Witczak, M. W., Houston, W. N., and Andrei, D. 2007. Incorporation of Environmental Effects in Pavement Design. Journal of Road Materials and Pavement Design, vol. 8 (4), p. 667-693.

Zapata, C. E., Houston, W. N., Houston, S. L., and Walsh, K. D. 1999. Soil water Characteristic curve variability. Geotechnical special publication, Proceedings of Sessions of Geo-Denver 2000, Advances in Unsaturated Geotechnics, GSP 99, vol. 287 (99). pp. 84-124.

Zhang, C., and Lu, N. 2018. What is the range of soil water density? Critical reviews with a unified model. Reviews of Geophysics (IF 24.946), 56(3), pp 532-562.

Zhang, C-L., Li, T-L., and Li, P. 2014. Rainfall infiltration in Chinese loess by in situ observation. In Journal of Hydrologic Engineering, 19(9): 06014002.

Zhang, Q., Wang, S., Wang, S., Zhao, Y., and Wen, X. S. 2016. Influence factors and variation characteristics of water vapor absorption by soil in semi-arid region. In Journal of Science China Earth Sci. 59, pp. 2240–2251.

Zhou, A-H. N., Shengy, D., and Cartery, J. P. 2012. Modelling the effect of initial density on soil-water characteristic curves. In Journal of Geotechnique 62 (8), pp 669-680.

Zollinger, D., Lee, S., Puccinelli, J., and Jackson, N. 2008. Long term pavement performance computed parameter: Moisture content (Rep. No. FHWA-HRT-08-035). Washington, DC: Federal Highway Administration, U.S. Department of Transportation.